Phase Diagrams and Thermodynamic Properties of Binary and Ternary Systems Based on Nitroaromatic Compounds

James Sangster

Sangster Research Laboratories, Suite 402, 3475 de la Montagne, Montreal, Quebec, Canada H3G 2A4

Received January 31, 1996; revised manuscript received November 1, 1996

The phase diagram data of 226 binary organic systems based on nitroaromatic compounds were critically evaluated with the aid of a computer-coupled thermodynamic/phase diagram analysis. The results of this analysis include the excess Gibbs energies of all solution phases as well as the Gibbs energies of fusion and formation of intermediate compounds. These quantities were used to calculate a *best* phase diagram for each system. The phase diagrams of seven ternary systems were calculated from the evaluated thermodynamic data of the binary subsystems with the use of the Kohler interpolative model and compared with the experimental diagrams. © *1997 American Institute of Physics and American Chemical Society.* [S0047-2689(97)00202-X]

Key words: phase diagram; thermodynamic properties.

Contents

List of Tables

List of Figures

1. Introduction

The interaction of two unlike organic liquids may lie anywhere along a continuum between insolubility ("negative interaction") to chemical reaction, where two new species appear. Between these extremes one finds cases of weak interaction (dispersion forces) giving ideal or near-ideal thermodynamic behavior. There are also some interactions which, short of chemical reaction, lead to the formation of association complexes of various kinds. These may result from, e.g., dipole–dipole, hydrogen-bond, or charge-transfer interactions.[1] In a previous publication,[2] the solid–liquid phase behavior of systems having potential hydrogen-bond interactions were evaluated; a large fraction of these dis-

played the formation of stable complexes of simple stoichiometry (1:1, 1:2, etc.). In the present case, the same type of evaluation is performed on binary and ternary systems having potential charge-transfer interactions of sufficient strength to form similar complexes.[3,4]

The binary systems studied here are of the general type aromatic compound+nitro-substituted aromatic compound. Either or both components may have a second substituent other than the nitro group. The solid–liquid phase behavior between neutral organic molecules is of practical interest from the point of view of materials science, including the solid compatibility of pharmaceutical products.[1,5] One compound in particular (2,4,7-trifluoren-9-one) was used extensively[6–8] to identify synthesized organic compounds, since it formed stable and colored addition products with characteristic melting points.

The phase diagrams of the ternary systems studied here are of the conventional type, showing liquidus isotherm contours on the Gibbs composition triangle. The binary edge systems of all the ternary systems are evaluated in the present work; this is a prerequisite for the evaluation procedure. Accordingly, the binary systems are treated first in their entirety.

2. Evaluation of Binary Systems

The principles, method, and criteria here are similar to those used previously.[2] They are delineated here again for the sake of convenience. A few additional considerations are included, occasioned by particular substances and systems.

2.1. Critique of Experimental Methods

The binary phase diagrams considered in this article were originally investigated by five techniques. Their main features are given here and implications for phase diagram evaluation are discussed in Sec. 2.4.2.

2.1.1. Thermal Analysis

In this classical method, gram quantities of mixtures were used and temperature–time curves (both heating and cooling modes) were recorded. The sample was stirred and temperature indicated by a thermometer graduated in 0.1°. Both eutectic and liquidus temperatures were detected. Although thermal analysis with organic mixtures frequently encounters serious experimental difficulty (see next section), it was found in the present work that results from this technique were of equal or better quality than data derived from other methods. When necessary precautions are taken, thermal analysis carefully done is the preferred method for best results.[9,10]

2.1.2. Thaw–Melt Method

This method was developed as an alternative to thermal analysis which, when applied to organic substances, displayed several inconveniences.[11] Chief among these is severe supercooling, which may amount to 10° for unstirred samples.[12] This is aggravated by the low thermal conductivity of the sample, which sometimes can be quite viscous. The thaw–melt method is a refinement of the procedure used by organic chemists to determine melting points of synthesized compounds.[13–15] The mixture is first premelted, cooled, and ground to a fine powder in a mortar. A milligram quantity is inserted into a thin-bore melting point tube and, if necessary, protected from the atmosphere is some way. The tube is attached to a mercury thermometer, usually calibrated in 0.1°, and immersed is a liquid bath, the temperature of which is slowly raised. Phase changes and the corresponding temperatures are noted visually. The temperature of first appearance of liquid in the sample is the eutectic temperature (thaw); the temperature at which the last solid disappears is taken as the liquidus temperature (melt).

This method is both simpler and faster than thermal analysis and requires only a small quantity of material. There are, however, some weaknesses. Phase changes are detected only visually, and only the heating mode is used. Under these circumstances, the eutectic temperature is usually more accurately determined than the liquidus temperature. This is because the first appearance of the liquid phase is readily detected from a completely solidified melt. Once the eutectic temperature has been passed, there is greater uncertainty in detecting the disappearance of the solid, for a number of reasons. The two-phase mixture may become cloudy, due perhaps to the presence of impurities; since there is no stirring, the residual solid sinks to the bottom of the narrow column of liquid and there may no longer be equilibrium between solid and liquid.[14] This uncertainty is magnified when the composition being studied is situated on a steep portion of the liquidus (thermal analysis is also less dependable in this case).

2.1.3. Visual-Polythermal Method

In this procedure, a milligram quantity of sample is heated by direct contact with an electrical resistance. The primary phase change is observed through a microscope (the apparatus is also called a "hot-stage microscope"). Only the liquidus temperature is observed in this method.

2.1.4. Microthermal Method

This may be considered as a variation of the thaw–melt procedure. The small quantity of sample is placed between microscope slides, slowly heated, and observed through a microscope. The technique was developed and used extensively by Kofler and Kofler,[16] who called it a *microthermal method.* Only the liquidus temperature is detected in this method.

2.1.5. Conventional Melting Point Determination

The classical technique, when applied to mixtures, may yield good-quality data if sufficient care is taken in sample

preparation, cooling and heating rates, and temperature measurement. It is similar to the thaw–melt method, but only the liquidus temperature is recorded.

In a few investigations, the liquidus was studied below 0 °C (thermal analysis, visual-polythermal method). In these cases, the liquid sample may become very viscous and strongly supercooled; sometimes seeding is required. The lowest recorded temperatures (near the eutectic temperature) may thus be suspect.

2.2. Computer-Coupled Thermodynamic/Phase Diagram Analysis

This technique is based upon well-known principles of calculation of phase diagrams from the thermodynamic properties of the phases. Such an analysis provides a set of self-consistent thermodynamic equations, which simultaneously reproduce the the thermodynamic properties and the phase diagram of the system. It also yields a thermodynamically correct smoothing of experimental data and thereby a more reliable estimate of error limits.

The principles and general procedure of this type of analysis are the same as those detailed previously.[2] Both optimization of binary phase diagram data and calculation of binary and ternary phase diagrams were performed with interactive computer programs[17] which are available on-line or on microcomputer diskette. In the present article, the same approach is used, with minor differences occasioned by the nature of the systems studied. These are discussed further in this section.

2.2.1. Thermodynamics

The pertinent thermodynamic relationships were outlined previously.[2] In the present work, the excess Gibbs energy of the liquid phase was represented by a simple polynomial in mole fractions

$$G^{E}=x_{A}x_{B}(g_{0}+g_{1}x_{B}+g_{2}x_{B}^{2}+\cdots) \qquad (1)$$

for the binary system A+B. The parameters g_0, g_1, etc., are empirical coefficients. Various other representations for G^E could have been used such as the Redlich–Kister expansion, Legendre polynomials, the quasichemical model, etc. It was found that the simple expression, Eq. (1), was entirely adequate, with one or two coefficients (most often) or three or four (more rarely).

It is implicitly assumed, therefore, that the liquid phase is not highly structured and there are no liquid miscibility gaps.

In all systems studied, G^E was taken to be independent of temperature. This assumption was justified in the present work, for two reasons: (a) the temperature range represented by the liquidus was small, and data scatter was often severe; (b) there have been no independent measurements of the heat of mixing in these systems (e.g., by calorimetry) which would enable a separation of the H^E and S^E terms in the relation $G^E=H^E-TS^E$.

2.2.2. Limiting Slopes of Liquidus Lines and Solid Solubility

This consideration proved to be of some importance in the critical evaluation of the experimental phase diagram data and so is treated in some detail here. From purely thermodynamic principles, a relation can be derived between the slopes of the liquidus at the composition extremes ($x_B=0$, $x_B=1$) and the extent of solid solution at these compositions. For example, in the limiting case $x_B\rightarrow 1$ (pure B), both liquid and solid phases become Henrian and the excess Gibbs energies approach zero. The Gibbs energy of fusion of B at temperature T is well approximated by the expression $\Delta_{fus}H_B^0(1-T/T_{fus})$, where $\Delta_{fus}H_B^0$ is the heat of fusion at the melting point T_{fus}. In this case it can be derived thermodynamically[18] that

$$(dx_B/dT)_l-(dx_B/dT)_s=\Delta_{fus}H_B^0/RT_{fus}^2, \qquad (2)$$

where dx_B/dT is the slope of the liquidus or solidus at $x_B=1$. The expression on the right-hand side (RHS) of Eq. (2) is simply the reciprocal of the well-known freezing point depression constant and depends only on properties of the solvent (B in this case). A similar equation may be written for component A.

As a general rule, the crystal structures of unlike organic compounds are quite incompatible and there are usually no solid solutions. Similarly, intermediate compounds are generally strictly stoichiometric. In those phase diagram measurements where eutectic data were reported, the eutectic temperature generally remains constant as far as the compositions studied approached the pure substances (usually up to with 0–10 mol %). Thus the assumption of zero solid solubility is justified (for example, in the case of benzene-cyclohexane,[19] it was was about 3 mol %). If then the solidus term in Eq. (2) is set to zero,

$$(dx_B/dT)_l=\Delta_{fus}H_B^0/RT_{fus}^2. \qquad (3)$$

In the present evaluations, Eq. (3) was used extensively in weighting experimental liquidus data near the composition extremes. In all the calculated phase diagrams (Figs. 1–226) the limiting liquidus slopes conform to this requirement.

Notwithstanding these general observations, it sometimes occurred, in the course of evaluation, that solid solubility posited by the original investigators turned out to be unnecessary for reproducing the phase diagram by calculation. (Evidently some temperature arrests, perhaps due to faulty sample preparation, too rapid a cooling rate, etc., were misinterpreted as evidence of a "solidus.")

2.2.3. Optimization Procedure

The actual steps followed in an optimization of phase diagram data varied somewhat from system to system, but some generalizations can be made.[18]

Data for the A- and B-side liquidi yielded, through a least-squares optimization, an expression for the excess Gibbs energy of the liquid. This calculation was supplemented—if the system contained intermediate compound(s)—by a similar optimization using liquidus data of the compound(s). The

derived thermodynamic data were then used to generate the calculated phase diagram. Weighting of the phase diagram data and fine tuning of the optimized thermodynamic expressions are described in the next section.

2.3. Principles of Evaluation Procedure

In the original publications not all phase diagram data were tabulated; any untabulated data were read off the published phase diagrams. All experimental points—eutectic and liquidus—appear in the calculated phase diagrams.

2.3.1. Weighting of Phase Diagram Data

As a consequence of strengths and weaknesses among experimental methods (Sec. 2.1) as well as limiting liquidus slope considerations (Sec. 2.2.2), reported phase diagram data both within and among investigators were sometimes weighted differently in the optimization step (Sec. 2.2.3). In particular, where some liquidus data were found to be inconsistent with better-defined eutectic data, the following classification was used:

(a) Data given greater weight: eutectic temperatures and compositions; melting points of congruently melting intermediate compounds.

(b) Data given less weight: other liquidus data.

In those few cases where this weighting was overridden, reasons are given in the evaluations. In some cases, the liquidus was better defined in one report than in another, e.g., by a greater number of compositions. Unless otherwise stated, however, all chosen liquidus data were weighted equally in the optimization step.

2.3.2. Status of the Calculated Results

The final calculated phase diagrams, shown in Figs. 1–226 as well as the calculated excess Gibbs energies of of the liquid (Table 28) and Gibbs energies of fusion and formation of intermediate compounds (Table 30), represent the *best* results for the systems under consideration, based upon available experimental data and evaluative criteria discussed in Sec. 2.3. For each system a *probable maximum inaccuracy* of the evaluated phase diagram is offered; this simply reflects experimental data scatter, as well as possible bias in experimental method.

Information in parentheses in Tables 28 and 30 indicates data of possibly considerable uncertainty, but which were used in calculating the recommended phase diagrams. Such data are consistent with all other evaluated data in each system.

In the evaluations and in Tables 1 and 30 the large number of significant figures given for thermodynamic properties does not indicate high precision; they are included for accurate reproduction of the calculated phase boundaries.

In those systems in which a nitroaromatic compound is one component, it is placed uniformly on the right-hand side of the diagram. This facilitates comparison of phase diagram features among related systems.

2.4. Properties of the Pure Substances

For an evaluation of the present type, the quality of the recommended data depends upon the quality of the thermodynamic data of the pure components used in the calculations. A number of recent compilations of melting points and heats of fusion are useful.[20–31] Of these, the collections of Domalski and co-workers[21,23] are particularly valuable because an effort was made to evaluate and rank data from different sources. Acree's two compilations[25,26] are practically identical. The work of Donnelly *et al.*[24] reports the results of original differential scanning calorimetry (DSC) measurements and comparison is neither made nor commented upon. The choice of data used in the present calculations (Table 1) is discussed briefly here. All experimental heats of fusion mentioned were determined by DTA (differential thermal analysis) or DSC. All temperatures are quoted to the nearest 0.1°, irrespective of source, since the precision of experimental phase diagram data does not warrant citation of hundredths of a degree. Wherever possible, the quality ratings of Domalski *et al.*[21,23] were given preference.

Experimentally measured heats of fusion of eleven compounds were not available, and so these quantities were estimated by various methods. These methods, and their probable accuracy, are presented in Sec. 2.4.1. It should be mentioned here that, though the uncertainty in estimated heats of fusion is greater than that of experimental data, the resultant uncertainty in the recommended phase diagram is incremental in nature; the general aspects of the phase diagram remain the same.

In the evaluation of the present phase diagram data, as well as earlier similar work,[2] it was found that a perceived inaccuracy in melting points of the end components was not necessarily associated with a corresponding inaccuracy in the melting behavior of mixtures. In other words, the effect of a possible impurity was sometimes—though not invariably—"diluted" at intermediate compositions.

Benzene. Reported melting points[21,23,25] lie in the range 5.4–5.9 °C, and heats of fusion[21,23,25] in the range 8950–9951 J mol^{-1}.

Naphthalene. The melting point[21,23,25,32–37] is 78.2–80.9 °C, and the heat of fusion[23,25,34–37] 18 785–19 654 J mol^{-1}.

Biphenyl. From the collections[21,23,25] this melts at 68.3–70.9 °C and the heat of fusion[21,23,25] is 18 575–19 900 J mol^{-1}.

Acenaphthene. The melting point is[21,24,25,36] 88.9–94.6 °C and the heat of fusion (same sources) is 10 960–25 000 J mol^{-1}.

Fluorene. The melting range is[21,25,34,36] 113.8–115.8 °C and heat of fusion (same sources) 18 745–19 870 J mol^{-1}.

Diphenylmethane. The melting range is[25,33–36,38] 24.4–26.2 °C and heat of fusion (same sources) 14 784–19 246 J mol^{-1}.

Anthracene. The melting range[21,25,33–36,38] is 215.8–219.5 °C and the heat of fusion[21,25,32,34–36,38] 27 950–29 370 J mol^{-1}.

Phenanthrene. The melting point is[21,25,34] 98.1–100.0 °C and the heat of fusion[23–25,32,36,37,39] 15 890–18 627 J mol^{-1}.

Pyrene. The melting point is[21,25,34] 150.7–152.2 °C and heat of fusion (same sources) 17 111–17 364 J mol^{-1}.

Fluoranthene. The melting point is[21,25] 107.8 or 110.2 °C and the heat of fusion (same sources) 18 728 or 18 871 J mol^{-1}.

Triphenylmethane. There is apparently good agreement for both melting point[21] (92.1–92.4 °C) and heat of fusion (same source) 18 200–21 980 J mol^{-1}.

Nitrobenzene. There is good agreement for both[21,25] melting point (5.6 or 5.7 °C) and heat of fusion (10 815–12 121 J mol^{-1}).

1,2-Dinitrobenzene. The reported range of the melting point[21,23,25,28] is 114.5–122.9 °C and heat of fusion (same sources) 22 180–22 845 J mol^{-1}.

1,3-Dinitrobenzene. Although some individual phase diagram measurements[40–42] give high values 91.0–94.8 °C, collections[21,23,24] suggest lower: 89.7–90.1 °C. In this case the rated data[21,23] were not of preferred quality. There is good agreement,[21,23,28] however, on the heat of fusion: 17 350–17 570 J mol^{-1}.

1,4-Dinitrobenzene. The single melting point mentioned[21,23,25] is 173.5 °C, which is the same as that used on the phase diagram.[43] There is apparent excellent agreement[21,23,25] for the heat of fusion (28 100–28 128 J mol^{-1}).

1,3,5-Trinitrobenzene. There was perhaps some confusion in early work[44] about the melting point, since this compound has one or more transitions (or metastable states) at[21,45] 97, 107, and 110 °C. The true melting point is in the range[8,21,28] 121.0–125.2 °C. There is not good agreement for the heat of fusion[8,21,25,45] 15 000–22 600 J mol^{-1}, but the lower value is probably correct.[21]

1,2,3,5-Tetranitrobenzene. The melting point[20] is 126.0 °C. The heat of fusion is not known from calorimetric experiment, and hence it was estimated (see Sec. 2.4.1).

2-Nitrotoluene. The melting point[46] is given as −2.9 or −9.5 °C, depending upon the crystalline form. The chosen value (−10.4 °C) was taken from the phase diagram[47,48] (thermal analysis, carefully done). The heat of fusion is not known from calorimetric experiment, and hence was estimated.

4-Nitrotoluene. The melting point[21,28] is 48.7–51.6 °C. The reported heat of fusion is given[21,28] as 16 811, 18 410, or 69 802 J mol^{-1}. The high value is evidently erroneous, because this quantity estimated from phase diagrams[48] is ≈16 800 J mol^{-1}.

3,4-Dinitrotoluene. The melting point[20,28,46] 56.3–61.0 °C. The chosen value is close to the phase diagram datum.[44,49] There is only one value for the heat of fusion.[28]

2,6-Dinitrobenzene. The melting point is given as[28] 54.3 or[20,46] 66.0 °C. Again, the chosen value is close to the phase diagram datum.[44,49] There is only one value for the heat of fusion.[28]

2,4-Dinitrotoluene. The melting point is given as[21,25,26] 67.6–72.0 °C. The chosen value is close to those reported on the phase diagrams evaluated in the present work. The heat of fusion[21,23,28] is 20 119–22 180 J mol^{-1}.

2,4,6-Trinitrotoluene. The melting point[25,28,50,51] is 79.0–81.9 °C, and the heat of fusion[25,28] is 21 230 or 23 430 J mol^{-1}.

2,4,6-Trinitro-m-xylene. The melting point[46,50–53] is 181.9–184.0 °C. The chosen value was determined by careful thermal analysis.[53] There is only one datum for the heat of fusion.[52]

2-Nitrophenol. The melting point[23,24,37,54] is 45.2, 45.5, or 44.8 °C, the heat of fusion (same sources) is 17 446–17 900 J mol^{-1}.

3-Nitrophenol. The melting point[23,25,54,55] is 96.8 or 97.4 °C; the heat of fusion[23,25,54] is 19 200 or 20 500 J/mol^{-1}.

4-Nitrophenol. Melting points lie in the interval[23–25,54,55] 113.0–114.1 °C and heats of fusion[23–25,54] 17 330–30 118 J mol^{-1}. By comparison with the other nitrophenols and from phase diagrams, a lower heat of fusion is more correct.

2-Nitroaniline. The melting point[21,25] is given as 69.3 or 71.2 °C, but phase diagram studies[56] indicate a slightly higher value. There is only one reported datum for the heat of fusion.[21,25]

3-Nitroaniline. The melting point[21,23,25] is 111.8–114.0 °C. The chosen value was taken from the phase diagram.[57] The heat of fusion[21,23] is 23 600 or 23 680 J mol^{-1}.

4-Nitroaniline. The melting point is[21,23,25,56] 146.2–147.8 °C and the phase diagram value[58] was chosen. There is good agreement[21,23,25] about the heat of fusion: 21 090 and 21 150 J mol^{-1}.

3-Nitrobenzoic acid. The melting point is[21] 141.0 °C. The heat of fusion lies in the range[21,25,39,59] 19 292–21 730 J mol^{-1}.

2,4-Dinitrophenol. Two sources[23,25] agree both about the melting point (114.8 °C) and the heat of fusion (24 174 J mol^{-1}).

2,4-Dinitroaniline. The melting point[20,46] of 180.0 °C is in good agreement with the phase diagram value.[41] The heat of fusion is not known from calorimetry and was estimated.

Picric acid (2,4,6-trinitrophenol). The melting point[23,51,60,61] is 120.9–123.0 °C. Reported heats of fusion[23,32,60] vary from 17 100 to 33 885 J mol^{-1}, but the true value is closer to the low value.[23]

Picryl chloride (1-chloro-2,4,6-trinitrobenzene). The melting point range[20,46,50] is 81.0–85.0 °C. There are no calorimetric data for the heat of fusion, which was estimated.

2,4,6-Trinitroanisole. The melting point[46] is 68.5–69.0 °C, and this agrees well with phase diagram data.[43,62] There is no calorimetric datum for the heat of fusion and hence it was estimated.

2.4.7-Trinitrofluoren-9-one. The melting point[6–8,34] is 175.0–177.0 °C, and the heat of fusion[8,34] is 23 012 or 23 500 J mol^{-1}. There is a transition[8,34] at 155.3 or 157.0 °C (heat of transition, from the same sources, 4200 or 2900 J mol^{-1}). This transition is omitted from the phase diagrams[34,63] but is included in present calculations. It ap-

pears either above or below the eutectic temperature,[34,63] but since the heat of transition is much less than the heat of fusion, the exact value is relatively unimportant for the calculation of the liquidus in these systems.

Aniline. The melting point[21,23,25] is −6.4 to −5.9 °C, and the heat of fusion[21,25] is 10 556–10 920 J mol^{-1}.

1,2-Diaminobenzene. The melting point lies in the range[64–66] 100.7–102.0 °C, and there is one value for the heat of fusion.[64]

1,3-Diaminobenzene. The melting point is[23,64,66] 62.3–65.9 °C and the heat of fusion[23,64] is 15 400 or 15 570 J mol^{-1}.

4-Methylaniline. The reported melting point[23,25,67] is well defined at 42.4–43.4 °C. The heat of fusion[23,25,26,32,67] is 17 280–18 222 J mol^{-1}.

4,4′-Dipyridine. For this compound, a high value[22,46] (171.0–172.0 °C) and a low value[20,68,69] (111.0–114.0 °C) are given. The phase diagram[57] indicates the lower temperature. The heat of fusion is not known from calorimetry and hence was estimated.

1-Aminonaphthalene. The given melting point[25] of 50.0 °C is very close to experimental values[31,37,70] 49.0–49.8 °C. The heat of fusion[25,37] is 13 300 or 14 492 J mol^{-1}.

2-Aminonaphthalene. The melting point is[25,31] 113.0 °C and there is one value[25] for the heat of fusion.

Carbazole. The melting point is given as[21,25,34–36,38] 243.0–248.0 °C and the heat of fusion[21,25,34,35,38] 21 170–29 419 J mol^{-1}. There is a transition[38] at 147.0 °C with heat change (same source) of 275 J mol^{-1}. This transition—assuming it is real—would probably not have been detected in most studies because of the small magnitude of the heat effect. For the sake of completeness, this transition is included in all calculated phase diagrams containing carbazole.

N-Isopropylcarbazole. The melting point and heat of fusion[25,63] are given as 122.0 °C and 17 730 J mol^{-1}.

Phenol. The melting point[21,23,25] lies in the range 39.5–40.9 °C and the heat of fusion (same sources) is 10 580–11 514 J mol^{-1}.

Hydroquinone (1,4-dihydroxybenzene). The melting point is in the range[25,64,71–73] 171.8–174.0 °C and the heat of fusion[21,28,64] lies in the range 21 090–27 110 J mol^{-1}.

1-Naphthol. The melting point lies in the range[21,24,25,65,73] 94.0–96.0 °C and the heat of fusion[21,24,25,32,37,74] is 22 800–23 332 J mol^{-1}.

2-Naphthol. The melting point is in the range[21,25,63,73,75] 120.0–123.9 °C and the heat of fusion[21,25,74] is 17 510–21 940 J mol^{-1}.

2-Hydroxybiphenyl. The melting point is[21,23,25,76] 57.4–57.6 °C and the heat of fusion is either[24,25] 13 460 J mol^{-1} or[21,76] 16 210 J mol^{-1}.

4-Hydroxybiphenyl. The melting point is given as[20,22,72] 164.0–167.0 °C. The heat of fusion is not known from calorimetric measurements, and so an estimated value was used.

Dimethylacetamide. The melting point is[46,77,78] between −20.0 and −23.5 °C. There is no calorimetric value for the heat of fusion; an estimated datum was used.

Benzoic acid. The melting point is[21,25,79] at 122.0 or 122.4 °C and the heat of fusion[21,25,37,79,80] is in the range 16 230–18 060 J mol^{-1}.

Benzamide. The melting point is[25,81] 129.1 or 130.0 °C and there is only one datum for the heat of fusion.[25]

3-Hydroxybenzaldehyde. The melting point is[20,22] 108.0 °C. Since no calorimetric heat of fusion is available, it was estimated.

Salicylic acid. The melting point is in the range[82–85] 158.3–160.0 °C. For the heat of fusion, an estimated value of 25 710 J/mol was used. After submission of the manuscript, an experimental value of 18 200 J/mol was found.[85]

4-Aminobenzoic acid. The melting point is in the range[21,25,86] 187.3–188.5 °C. The heat of fusion (same sources) is 20 920 or 24 016 J mol^{-1}.

Acetophenone. The melting point is[46] 20.5 °C. There is no calorimetric heat of fusion available, so a value was estimated.

Cinnamic acid. The melting point is[23] at 133.0 °C and the heat of fusion is given as[23,60] 22 626 or 34 374 J mol^{-1}. The lower value is more consistent with the phase diagram.[60]

Camphor. This is an optically active molecule and exists in *D*, *L*, and *DL* forms.[46] Phase diagram reports[87,88] make no mention of this fact; presumably the sample used was a racemic mixture. The melting points of the three forms[46] all lie within 1.2°, observed melting points of the racemic mixture[21,46,37,86] lie in the range 175.0–178.8 °C, a high value[24,25] of 189.2 °C is erroneous. Camphor has an unusually low heat and entropy of melting. The heat of fusion[21,37,86] is 4400–6820 J mol^{-1}; the high value[24,25] of 15 730 J mol^{-1} was disregarded. There is apparently[21] more than one transition below 0 °C, but these are not included in calculated phase diagrams.

Dibenzothiophene. The melting point is in the range[23,25,34,89] 97.8–99.2 °C. The heat of fusion[23,25,34] is 15 300, 21 580, or 22 350 J mol^{-1}.

Benzophenone. The melting point is in the range[23,90] 47.7–48.0 °C. The heat of fusion[23] is 17 670 or 18 194 J mol^{-1}.

2.4.1. Estimation of Heat of Fusion

Experimental heats of fusion of eleven compounds in Table 1 were not available, and so they were estimated. Four methods for this purpose were used[91–94]; they all have an additive-constitutive basis, using recognizable molecular fragments (benzene ring, nitro group, amino group, etc.). Of these, the method of Tingli[92] was difficult to use and was less accurate than the others. The method of Joback and Reid[91] was inaccurate for molecules containing more than one nitro group. Subject to these limitations, the methods were applied to all the compounds concerned, except dimethylacetamide. For dimethylacetamide, the heat of fusion was estimated from the limiting liquidus slopes of phase diagrams involving this compound,[77,78,95] excluding of course the phase diagrams under study in the present work. In addition to these methods, another—of the author's own devising—was used as a check. It can be called an "entropy of fusion" method. It is based on the assumption that the entropy of fusion of a compound may be estimated from the entropy of fusion of

closely related species (homologously, structurally or chemically similar, etc.). For example, $\Delta_{fus}S$ of 4,4′-dipyridine may be estimated by considering the known entropies of fusion of the following compounds: benzene, pyridine, and biphenyl. The different estimation methods gave results which agreed within 20%, and a mean value was used in the calculations (Table 1).

2.4.2. Experimental Melting Points of Pure Substances

As a general rule, in only relatively recent phase diagram reports was mention made of purification of starting substances. Fractional or recrystallization was most often used. Other methods were distillation or sublimation. In two studies[40,96] the substances were "purified." The remaining reports included no information concerning purification.

2.5. The Evaluations

The same convention is used throughout this paper for identifying the left- and right-hand components of binary systems. For example, in the case of PY (A)+1,3-DNB (B) the left-hand component is always component A and the right-hand component is B. This corresponds to the layout in all binary phase diagrams and also identifies A and B components in the expression for the excess Gibbs energy of the liquid, Eq. (1). In the same manner it identifies the stoichiometry of intermediate compounds, e.g., in the above-mentioned binary system the designation 1:2 refers to the compound of mole ratio AB_2.

In the evaluations, where there are more than one eutectic (E) in the system studied, these are identified as E_1, E_2, etc. Peritectics are indicated by "P." In all cases, the temperatures and compositions indicated in Figs. 1–226 are the calculated (evaluated) data.

2.5.1. Systems Based on Nitrobenzene

BZ (A)+NB (B)

Data were obtained[97] both by thermal analysis (with stirring) and the visual-polythermal method. The reported eutectic[97] is −25 °C, x_B=0.49. All the liquidus data were used in the optimization, and the phase diagram (Fig. 1) was calculated with the use of Eq. (4),

$$G^E(l)=951x_Bx_Ax_B \text{ J mol}^{-1} \quad (4)$$

and the calculated eutectic is −25.5 °C, x_B=0.470. The probable maximum inaccuracy in the calculated diagram is ±1°.

NA (A)+NB (B)

Data were obtained by thermal analysis.[98] The reported eutectic[98] is −6.8 °C, x_B=0.86. Since the experimental[98] melting point of nitrobenzene is inaccurate, only the LHS liquidus data were optimized, and the phase diagram (Fig. 2) was calculated with the use of Eq. (5),

$$G^E(l)=2x_Ax_B \text{ J mol}^{-1}. \quad (5)$$

The calculated eutectic is −2.4 °C, x_B=0.862, reflecting the correct melting point for component B. The probable maximum inaccuracy in the calculated diagram is ±1°.

AN (A)+NB (B)

Data were obtained by thermal analysis,[98] and the reported eutectic[98] is −29.8 °C, x_B=0.41. Since the experimental[98] melting point of nitrobenzene was low, only data in the range $0<x_B<0.63$ were optimized to give

$$G^E(l)=639x_Ax_B \text{ J mol}^{-1}. \quad (6)$$

The phase diagram calculated with the use of Eq. (6) is shown in Fig. 3 and the calculated eutectic is −31.1 °C, x_B=0.423. The probable maximum inaccuracy in the calculated diagram is ±4°.

2.5.2. Systems Based on 1,2-Dinitrobenzene

BZ (A)+1,2-DNB (B)

Data were obtained by thermal analysis.[44] There is no reported eutectic,[44] but it evidently is very close to the melting point of benzene. All liquidus data were optimized to give

$$G^E(l)=x_Ax_B(3757-5848x_B+6355x_B^2) \text{ J mol}^{-1}. \quad (7)$$

The phase diagram (Fig. 4) was calculated with the use of Eq. (7) and the calculated eutectic is 4.7 °C, x_B=0.013. The probable maximum inaccuracy in the calculated diagram is ±2°.

FLN (A)+1,2-DNB (B)

Data were obtained by thermal analysis,[99] and the reported eutectic[99] is 77.0 °C, x_B=0.47. (The eutectic temperature is not well defined experimentally.) Data in the range $0.2<x_B<1$ were optimized with the result

$$G^E(l)=-78x_Ax_B \text{ J mol}^{-1} \quad (8)$$

and the calculated phase diagram (Fig. 5) based on Eq. (8) shows a calculated eutectic of 78.0 °C, x_B=0.469. The probable maximum inaccuracy in the calculated diagram is ±2°.

ANTH (A)+1,2-DNB (B)

Data were obtained by thermal analysis,[100] and the reported eutectic[100] is 110.0 °C, x_B=0.88. Liquidus data in the range $0.35<x_B<1$ were optimized, with the result

$$G^E(l)=547x_Ax_B \text{ J mol}^{-1}. \quad (9)$$

The phase diagram (Fig. 6) was calculated with the use of Eq. (9), and the calculated eutectic is 109.7 °C, x_B=0.881. The probable maximum inaccuracy in the calculated diagram is ±3°.

PH (A)+1,2-DNB (B)

Data were obtained by thermal analysis[44] and there is no reported eutectic. The experimental[44] melting point of phenanthrene is about 4° too high; the LHS liquidus data had little effect in the optimization, and the result

$$G^E(l)=1028x_Ax_B \text{ J mol}^{-1} \quad (10)$$

followed from the RHS liquidus data. The phase diagram, Fig. 7, was calculated with the use of Eq. (10), and the cal-

TABLE 1. Gibbs energies of fusion (fus) or transition (trs) of pure compounds $\Delta G = \Delta H - T\Delta S$ J mol^{-1}

Substance	Abbreviation	Temperature (°C)	trs or fus	ΔH	ΔS
		Aromatichydrocarbons			
Benzene	BZ	5.5	fus	9 866	35.406
Naphtalene	NA	80.3	fus	19 046	53.886
Biphenyl	BP	69.0	fus	18 800	54.947
Acenaphthene	ACN	93.4	fus	21 600	58.928
Fluorene	FLN	114.8	fus	19 670	50.702
Diphenylmethane	DPM	25.3	fus	18 950	63.495
Anthracene	ANTH	218.1	fus	28 810	58.646
Phenanthrene	PH	99.2	fus	17 440	46.838
Pyrene	PY	151.2	fus	17 250	40.650
Fluoranthene	FTHN	109.0	fus	18 800	49.195
Triphenylmethane	TPM	92.3	fus	20 350	55.685
		Nitroaromatic compounds			
Nitrobenzene	NB	5.7	fus	11 500	41.241
1,2-Dinitrobenzene	1,2-DNB	16.5	fus	22 600	58.000
1,3-Dinitrobenzene	1,3-DNB	90.3	fus	17 400	47.874
1,4-Dinitrobenzene	1,4-DNB	173.5	fus	28 120	62.958
1,3,5-Trinitrobenzene	TNB	125.2	fus	15 000	37.655
1,2,3,5-Tetranitrobenzene	TENB	126.0	fus	(33 500)[a]	(83.928)
2-Nitroluene	2-NT	−10.4	fus	(13 700)	(52.141)
4-Nitroluene	4-NT	51.6	fus	16 810	51.763
3,4 Dinitrotoluene	3,4-DNT	59.0	fus	18 830	56.691
2,6-Dinotrotoluene	2,6-DNT	66.0	fus	23 850	70.323
2,4-Dinitrotoluene	2,4-DNT	70.5	fus	21 000	61.109
2,4,6-trinitrotoluene	TNT	80.8	fus	22 330	63.088
2,4,6-Trinitro-*m*-xylene	TNX	182.2	fus	38 490	84.528
		Substituted nitroaromatic compounds			
2-Nitrophenol	2-NP	44.8	fus	17 446	54.862
3-Nitrophenol	3-NP	96.8	fus	19 196	51.881
4-Nitrophenol	4-NP	113.8	fus	18 254	47.168
2-Nitroaniline	2-NA	72.0	fus	16 110	46.675
3-Nitroaniline	3-NA	113.5	fus	23 600	61.037
4-Nitroaniline	4-NA	147.5	fus	21 120	50.208
3-Nitrobenzoic acid	NBA	141.1	fus	21 730	52.445
2,4-Dinitrophenol	DNP	114.8	fus	24 174	62.304
2,4-Dinitroaniline	DNA	180.0	fus	(29 680)	(65.497)
Picric acid	PA	122.5	fus	18 560	46.910
Picryl chloride	PC	83.0	fus	(25 000)	(70.195)
2,4,6-Trinitroanisole	TNA	68.0	fus	(20 920)	(61.322)
2,4,7-Trinitrofluoren-9-one	TNF	156.0	trs	3 550	8.2722
		175.8	fus	23 250	51.787
		Amino aromatic compounds			
Aniline	AN	−6.3	fus	10 650	39.910
1,2-Diaminobenzene	1,2-DAB	103.0	fus	23 100	61.404
1,3-Diaminobenzene	1,3-DAB	63.8	fus	15 570	46.202
4-Methylaniline	MA	43.3	fus	17 750	56.091
4,4′-Dipyridine	DP	114.0	fus	(19 380)	(51.220)
1-Aminonaphthalene	1-AN	49.8	fus	13 900	61.404
2-Aminonaphthalene	2-AN	113.0	fus	23 610	61.142
Carbazole	CAR	147.0	trs	275	0.6545
		246.1	fus	26 380	50.804
N-Isopropylcarbazole	ICAR	122.0	fus	17 730	44.869
		Hydroxyaromatic compounds			
Phenol	P	40.9	fus	11 514	36.657
Hydroquinone	HQ	172.3	fus	27 110	60.853
1-Napthol	1-N	95.5	fus	23 182	62.875
2-Naphthol	2-N	123.5	fus	18 790	47.366
2-Hydroxybiphenyl	2-HBP	57.5	fus	16 210	49.025
4-Hydroxybiphenyl	4-HBP	166.0	fus	(21 000)	(47.820)
Other compounds					
Dimethylacetamide	DMA	−22.5	fus	(6 008)	(23.970)
Benzoic acid	BA	122.4	fus	17 580	44.439
Benzamide	BENZ	130.0	fus	18 490	45.858

TABLE 1. Gibbs energies of fusion (fus) or transition (trs) of pure compounds $\Delta G=\Delta H-T\Delta S$ J mol^{-1}—(Continued)

Substance	Abbreviation	Temperature (°C)	trs or fus	ΔH	ΔS
3-Hydroxybenzaldehyde	HB	108.0	fus	(20 100)	(52.735)
Salicyclic acid	SA	158.3	fus	(25 710)	(59.590)
4-Aminobenzoic acid	ABA	188.2	fus	22 450	48.662
Acetophenone	ACP	20.5	fus	(13 000)	(44.270)
Cinnamic acid	CA	133.0	fus	22 626	55.708
Camphor	CAM	178.3	fus	5 680	12.582
Dibenzothiophene	DBT	98.2	fus	21 580	58.112
Benzophenone	BZP	47.9	fus	18 194	56.670

[a]Data in parentheses have been estimated.

culated eutectic is 73.9 °C, $x_B=0.368$. The probable maximum inaccuracy in the calculated diagram is ±2°.

MA (A)+1,2-DNB (B)

Data were obtained by thermal analysis[101] and the reported eutectic is 31.5 °C, $x_B=0.18$. All liquidus data were optimized, giving the result

$$G^E(l)=-957x_Ax_B \text{ J mol}^{-1}. \quad (11)$$

The calculated phase diagram, Fig. 8, shows a calculated eutectic 33.1 °C, $x_B=0.191$. The probable maximum inaccuracy in the calculated diagram is ±2°.

1-AN (A)+1,2-DNB (B)

Data were obtained by thermal analysis[102] and the reported eutectic is 30.2 °C, $x_B=0.23$. Upon optimization of all liquidus data, the expression

$$G^E(l)=x_Ax_B(-3025+1583x_B) \text{ J mol}^{-1} \quad (12)$$

was obtained. The phase diagram, based on Eq. (12), showed a calculated eutectic of 29.6 °C, $x_B=0.231$ (Fig. 9). The probable maximum inaccuracy in the calculated diagram is ±2°.

2-AN (A)+1,2-DNB (B)

Data were obtained by thermal analysis[102] and the reported eutectic is 73.5 °C, $x_B=0.47$; the eutectic temperature is not well defined experimentally. Data in the range $0.3<x_B<1$ were optimized, and the result

$$G^E(l)=x_Ax_B(-2889+1613x_B) \text{ J mol}^{-1} \quad (13)$$

was used to calculate the phase diagram (Fig. 10). The calculated eutectic is 72.4 °C, $x_B=0.470$. The probable maximum inaccuracy in the calculated diagram is ±2°.

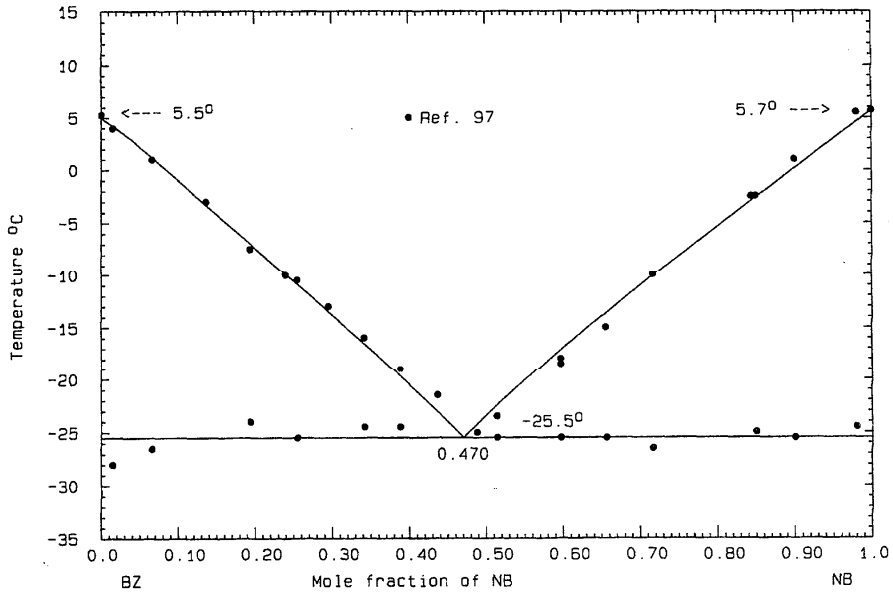

FIG. 1. The system BZ (A)+NB (B)

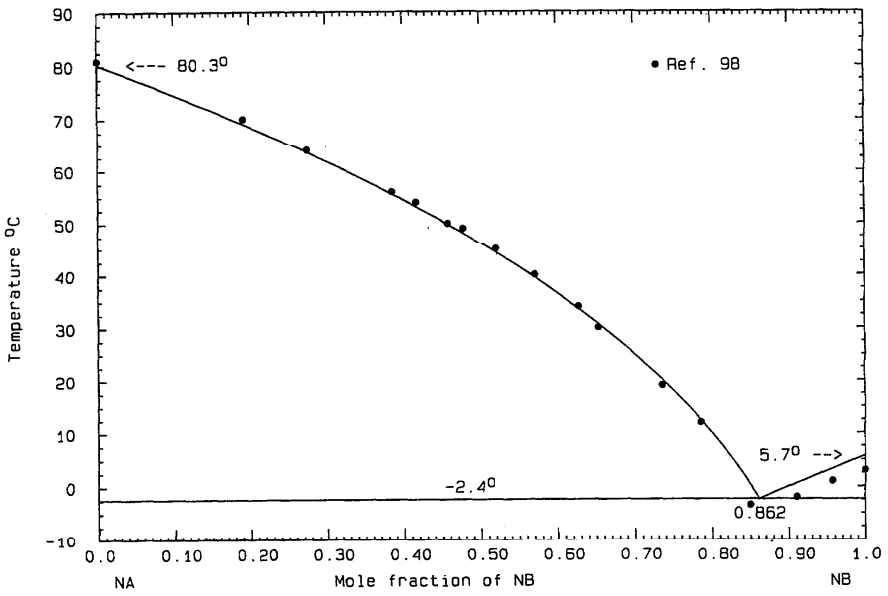

FIG. 2. The system NA (A)+NB (B)

CAR (A)+1,2-DNB (B)

Liquidus data were obtained by thermal analysis;[103] no eutectic arrests were noted. The optimization was performed on data in the range $0.3<x_B<1$, with the result

$$G^E(l) = -1061 x_A x_B \ J\ mol^{-1}. \qquad (14)$$

The phase diagram calculated from Eq. (14) is shown in Fig. 11, with a calculated eutectic of 107.9 °C, $x_B=0.860$. The carbazole transition, not reported experimentally,[103] appears on the calculated liquidus at $x_B=0.723$. The probable maximum inaccuracy in the calculated diagram is ±3°.

HB (A)+1,2-DNB (B)

Data were obtained by thermal analysis[104] and the reported eutectic is 84.0 °C, $x_B=0.35$. The RHS liquidus definitely suggests some solid solubility based on dinitrobenzene; none is indicated, however, on the LHS. More weight was given to

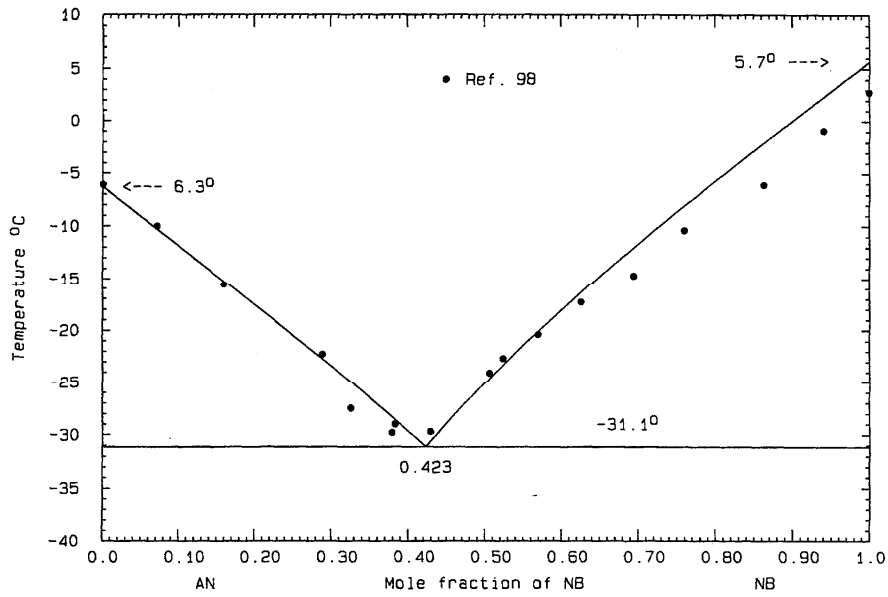

FIG. 3. The system AN (A)+NB (B)

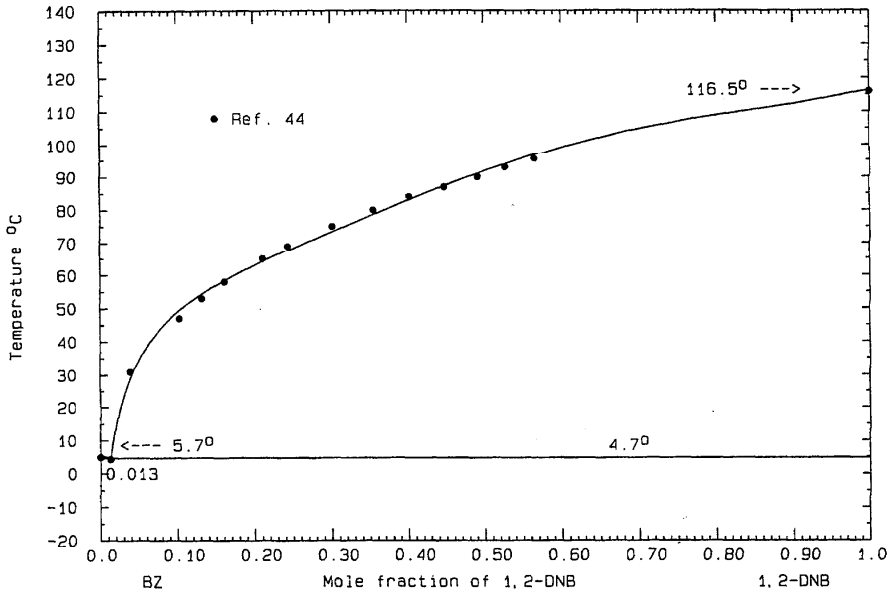

FIG. 4. The system BZ (A)+1,2-DNB (A)

the liquidus data on the RHS; the phase diagram (Fig. 12) was calculated with the use of Eq. (15),

$$G^{E}(l) = 1262 x_A x_B \text{ J mol}^{-1}, \quad (15)$$

and the solid solution was represented by a Henrian solution with a constant Henrian activity coefficient given by

$$RT \ln \gamma_A = 5500 \text{ J mol}^{-1}. \quad (16)$$

The calculated eutectic is 84.3 °C, $x_B = 0.383$ and there is 15.7 mol % solid solubility at the eutectic temperature. The probable maximum inaccuracy in the calculated diagram is ±3°.

2.5.3. Systems Based on 1,3-Dinitrobenzene

BZ (A)+1,3-DNB (B)

Data were obtained by thermal analysis[44,97] and also by the visual-polythermal method.[97] The reported eutectic[97] is

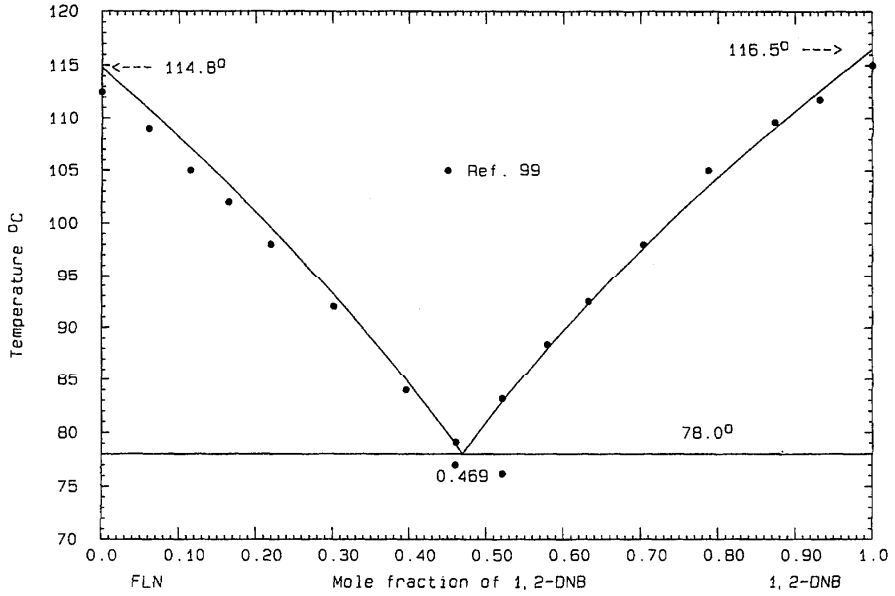

FIG. 5. The system FLN (A)+1,2-DNB (B)

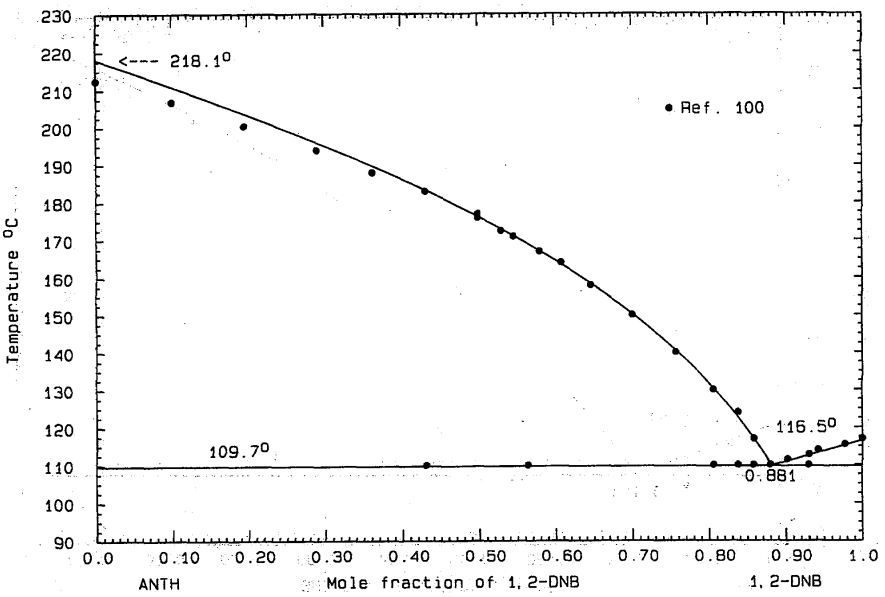

FIG. 6. The system ANTH (A)+1,2-DNB (B)

-1.0 °C, $x_B=0.093$. The agreement between the two studies[44,97] is within 3°. All liquidus data[44,97] were given equal weight in the optimization, with the result

$$G^E(l)=959x_Ax_B \text{ J mol}^{-1}. \quad (17)$$

The phase diagram, Fig. 13, was calculated with the use of Eq. (17) and the calculated eutectic is -1.1 °C, $x_B=0.103$. The probable maximum inaccuracy in the calculated diagram is ±3°.

NA (A)+1,3-DNB (B)

Data were obtained by thermal analysis[98,105–107] and the thaw–melt method.[105] A eutectic summary is given in Table 2. A comparison of the theoretical limiting liquidus slopes of both end components suggests that the LHS liquidus data of Puschin and Rikovski[107] are too low and that the RHS data of Kremann[98] are also too low. In the two studies of Puschin and co-worker[106,107] it appears that a 1:1 compound melts

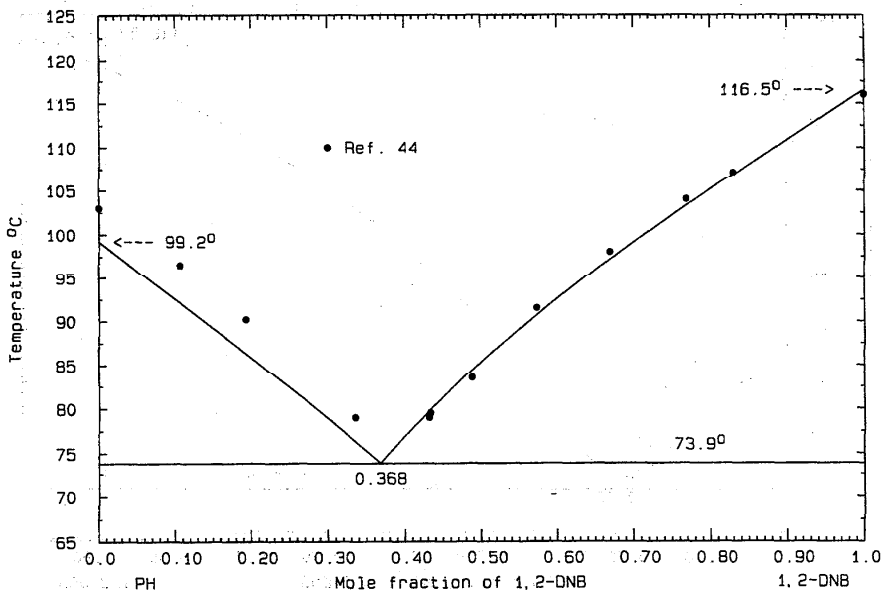

FIG. 7. The system PH (A)+1,2-DNB

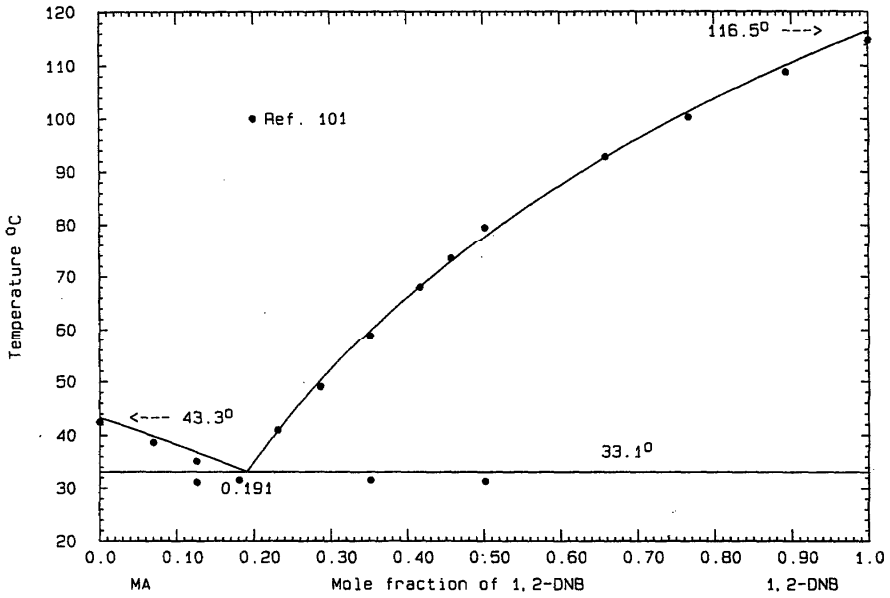

FIG. 8. The system MA (A) + 1,2-DNB (B)

incongruently at 50.5 °C; in the other reports[98,105] the compound melts congruently at 51.8 and 50.8 °C, respectively. In preliminary calculations, it was ascertained that an *incongruently* melting compound was consistent with the liquidus on the RHS. In the optimization, the chosen LHS liquidus data[98,105,106] and RHS data[105–107] were used. The result was

$$G^{E}(l)=x_A x_B(-791+1161x_B)\ \text{J mol}^{-1}. \quad (18)$$

Since the peritectic and eutectic temperatures are very close, the thermodynamic properties of the compound (AB)/2,

$$\Delta_{fus}G^0=14\,965-46.1250T\ \text{J mol}^{-1}, \quad (19)$$

$$\Delta_f G^0=-15\,018+40.3620T\ \text{J mol}^{-1}, \quad (20)$$

were assigned to reproduce the observed eutectic temperature as closely as possible. The quantity $\Delta_f G^0$ is the Gibbs energy of formation of the compound, from the pure liquids. The phase diagram, Fig. 14, was calculated with the use of Eqs. (18) and (20); the calculated data are $E=50.4$ °C $x_B=0.415$ and $P=51.3$ °C, $x_B=0.483$. The probable maximum inaccuracy in the calculated diagram is ±4°.

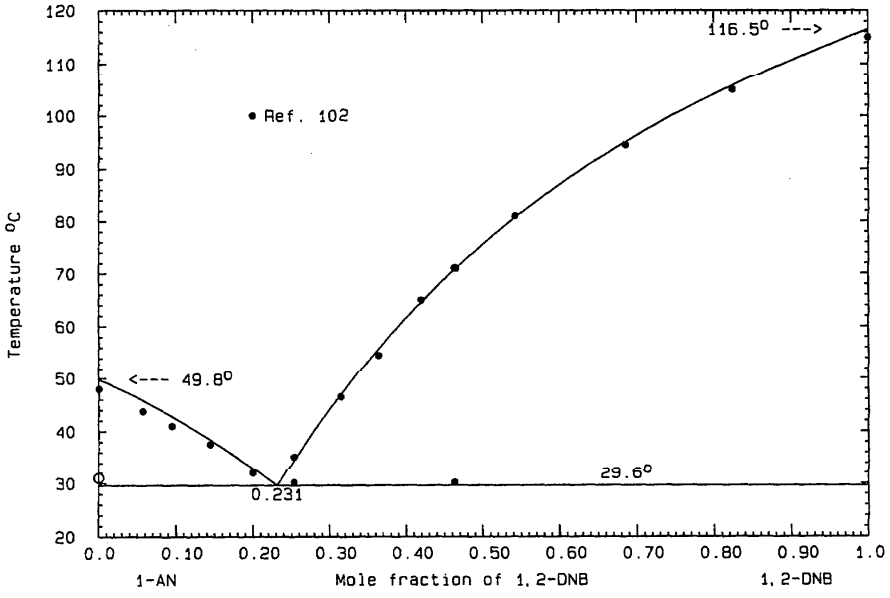

FIG. 9. The system 1-AN (A)+1,2-DNB (B)

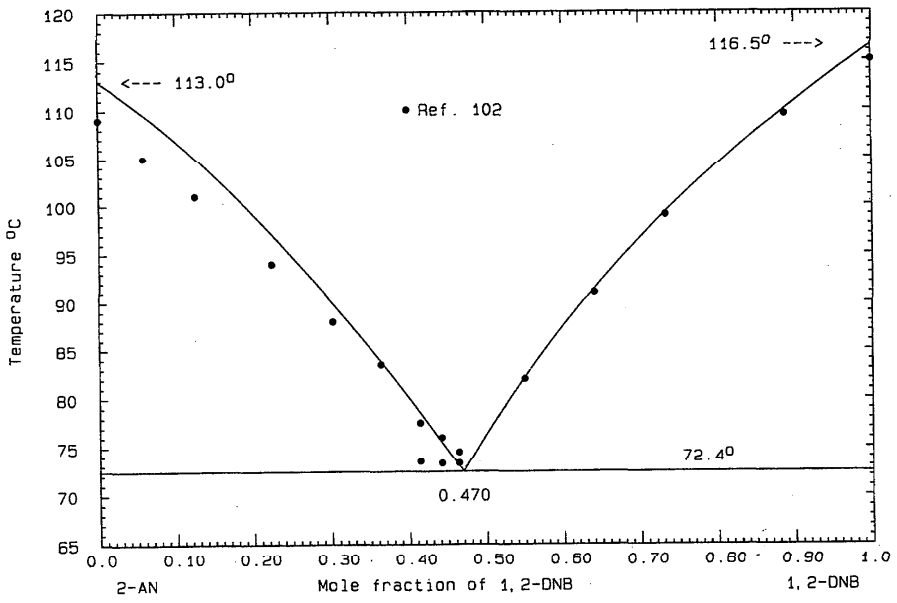

FIG. 10. The system 2-AN (A)+1,2-DNB (B)

FLN (A)+1,3-DNB (B)

Data were obtained by thermal analysis[99] and the reported eutectic is 54.0 °C, x_B=0.58. Liquidus data in the range $0.25<x_B<1$ were optimized, with the result

$$G^E(l)-x_Ax_B(-2264+696x_B)\ \text{J mol}^{-1}. \quad (21)$$

The phase diagram was calculated with the use of this equation (Fig. 15) and the calculated eutectic is 54.0 °C, x_B=0.580. The probable maximum inaccuracy in the calculated diagram is ±2°.

ANTH (A)+1,3-DNB (B)

Data were obtained by thermal analysis[100] and the reported eutectic is 84.0 °C, x_B=0.92. All the liquidus data were weighted equally in the optimization, which yielded the quantity

$$G^E(l)=x_Ax_B(1188-2425x_B)\ \text{J mol}^{-1}. \quad (22)$$

The phase diagram, Fig. 16, was calculated with the use of

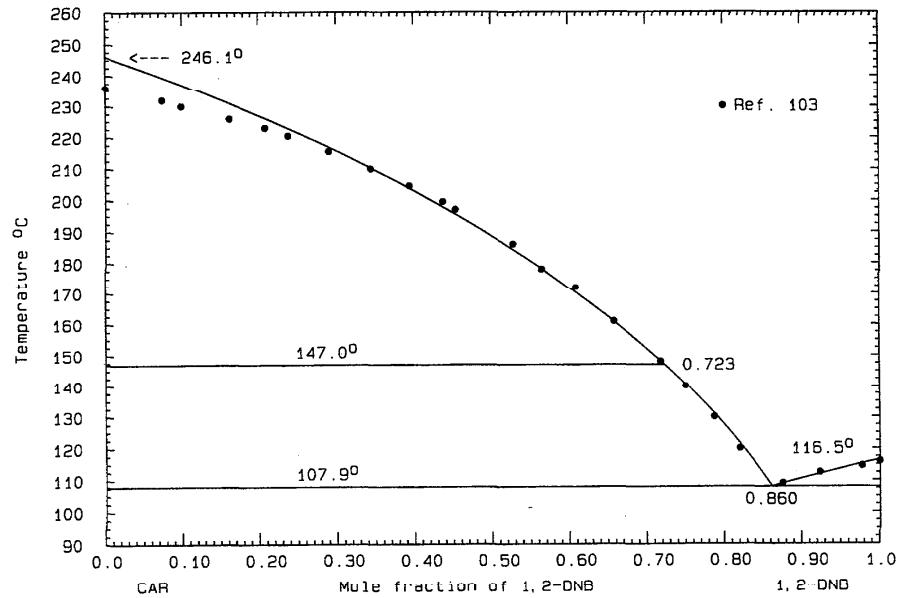

FIG. 11. The system CAR (A)+1,2-DNB (B)

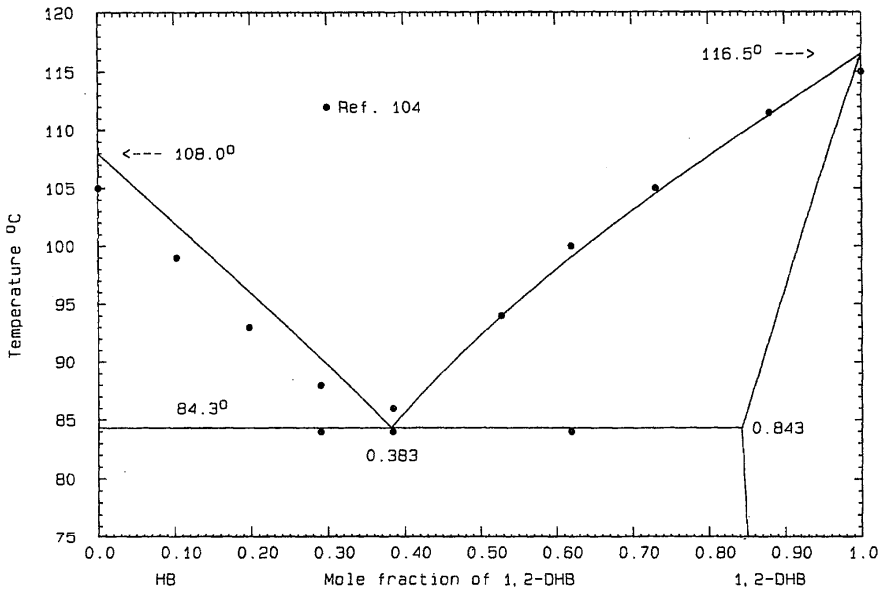

FIG. 12. The system HB (A)+1,2-DAB (B)

Eq. (22) and the calculated eutectic is 84.0 °C, x_B=0.911. The probable maximum inaccuracy in the calculated diagram is ±4°.

PH (A)+1,3-DNB (B)

Liquidus data were obtained by thermal analysis.[44] No eutectic arrests were noted, and no eutectic was reported. Data in the range $0.35<x_B<1$ were optimized with the result

$$G^E(l) = -1137 x_A x_B \text{ J mol}^{-1}. \quad (23)$$

The phase diagram was calculated (Fig. 17) with the use of Eq. (23) and the calculated eutectic is 49.3 °C, x_B=0.529. The probable maximum inaccuracy in the calculated diagram is ±2°.

PY (A)+1,3-DNB (B)

Data were obtained by the thaw–melt method.[43] A eutectic summary is given in Table 3 and there are two congruently melting compounds: 1:1 at 92.7 °C and 1:2 at 89.3 °C.

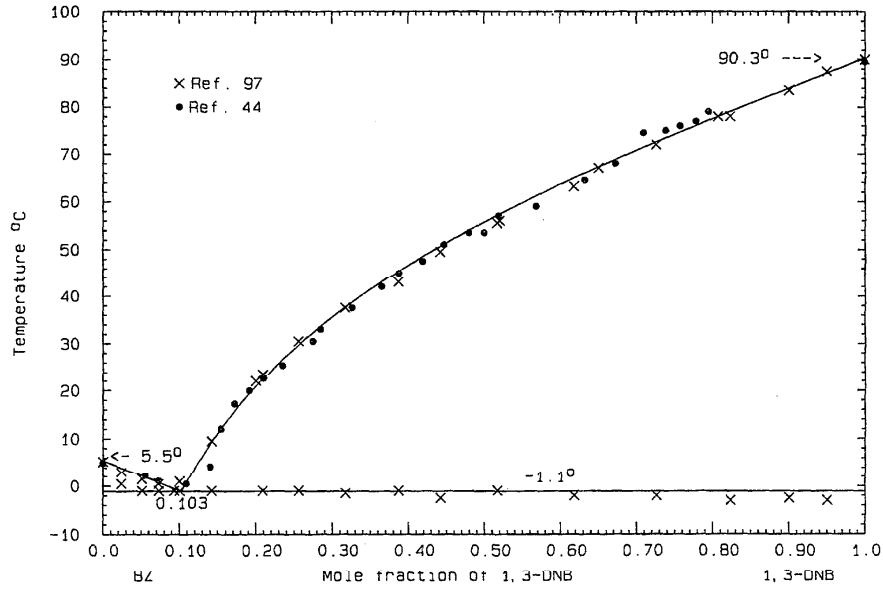

FIG. 13. The system BZ (A)+1,3-DNB (B)

TABLE 2. Reported eutectic data for the system NA (A)+1,3-DNB (B)

	°C	x_B	Ref.
E_1	50.1	0.39	105
	50.3	0.40	98
	51.0	0.44	106
	49.3	0.34	107
E_2	50.5	0.58	98
	51.1	0.52	105

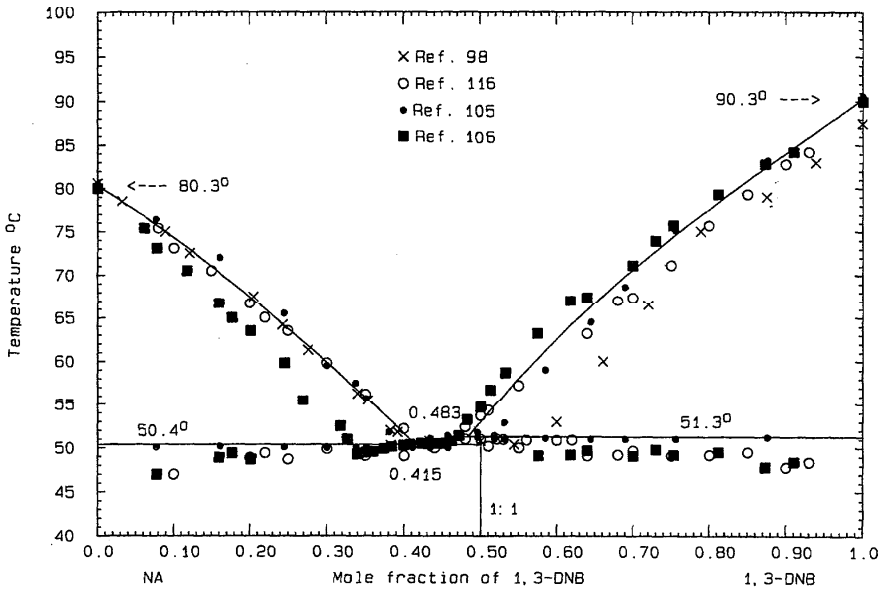

FIG. 14. The system NA (A)+1,3-DNB (B)

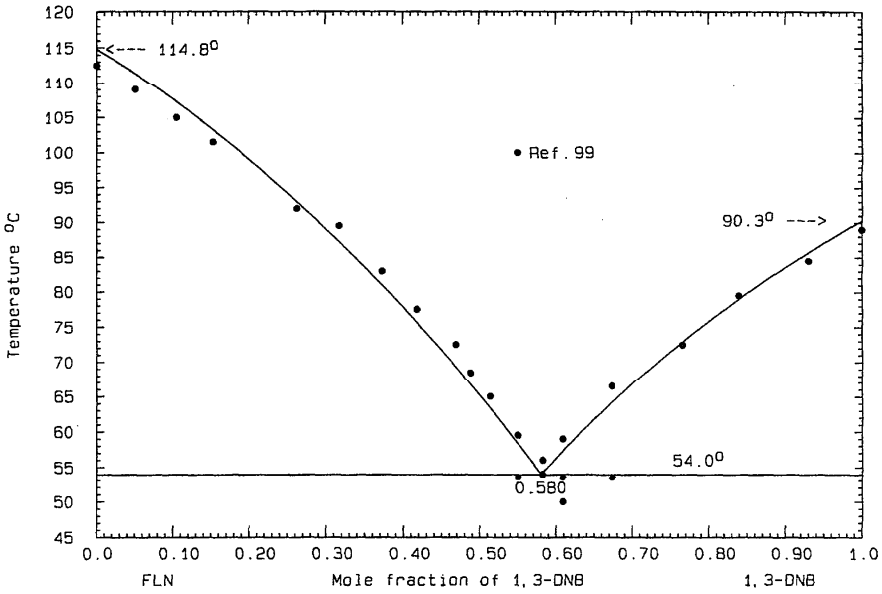

FIG. 15. The system FLN (A)+1,3-DNB (B)

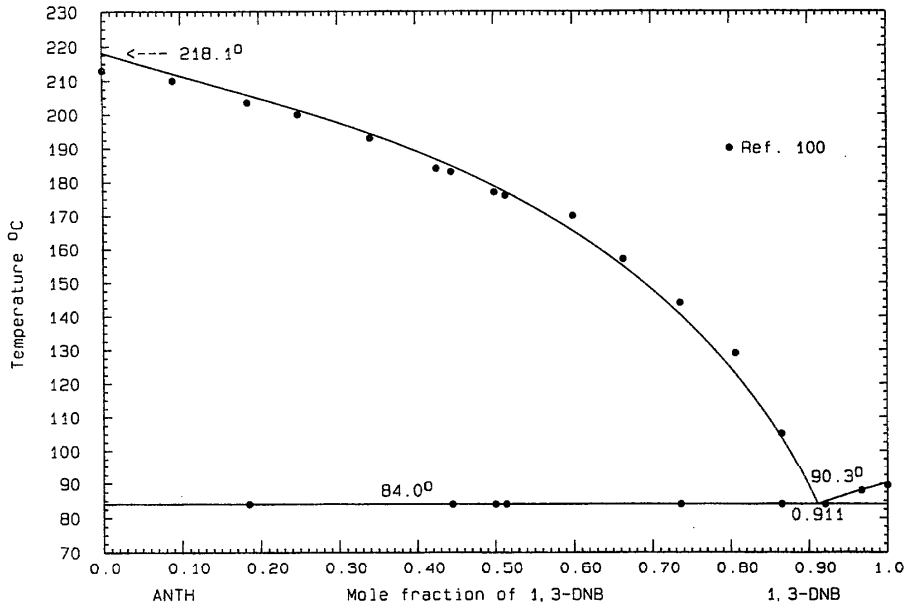

FIG. 16. The system ANTH (A)+1,3-DNB (B)

The liquidus data in the range $0.25<x_B<0.43$ were found not to be consistent with E_1 and the melting point of the 1:1 compound. The optimization yielded the result

$$G^E(l)=x_A x_B(-5136-2475x_B)\ \text{J mol}^{-1}, \quad (24)$$

and the thermodynamic properties of the compounds are, for (AB)/2,

$$\Delta_{fus}G^0=11\ 148-30.400T\ \text{J mol}^{-1}, \quad (25)$$

$$\Delta_f G^0=-12\ 741+24.7072T\ \text{J mol}^{-1}, \quad (26)$$

and for $(AB_2)/3$,

$$\Delta_{fus}G^0=26\ 189-72.2560T\ \text{J mol}^{-1}, \quad (27)$$

$$\Delta_f G^0=-27\ 697+66.9640T\ \text{J mol}^{-1}, \quad (28)$$

where AB_2 signifies a compound between A and B of stoichiometry 1:2. The phase diagram was calculated with the use of Eqs. (24), (26), and (28), Fig. 18. The calculated eutectics are E_1=90.2 °C, x_B=0.420, E_2=88.5 °C, x_B=0.600,

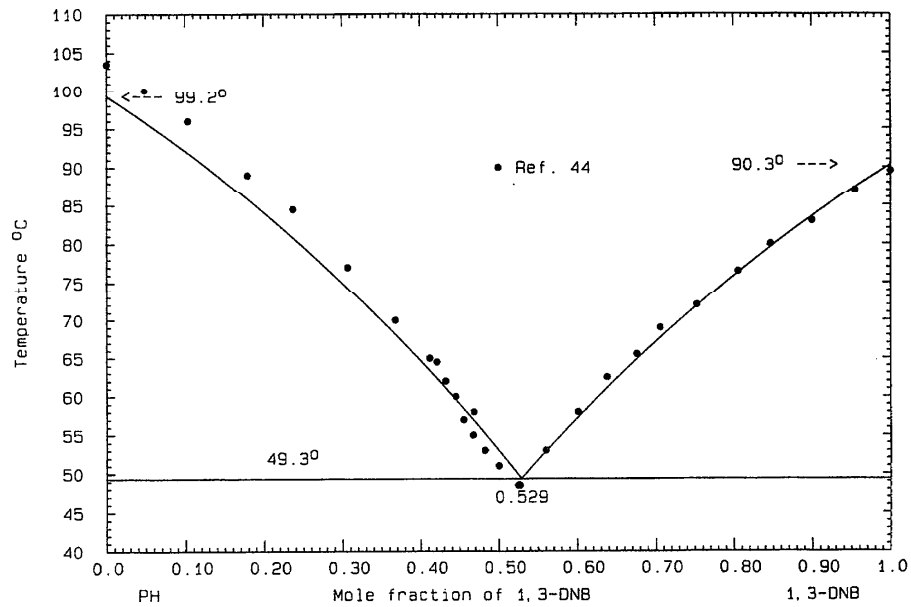

FIG. 17. The system PH (A)+1,3-DNB (B)

TABLE 3. Reported eutectic data for the system PY (A)+1,3-DNB (B)

	°C	x_B	Ref.
E_1	89.0	0.435	43
E_2	88.0	0.634	43
E_3	79.0	0.870	43

and E_3=78.7 °C, x_B=0.872. The compounds melt congruently at 92.7 and 89.3 °C. The probable maximum inaccuracy in the calculated diagram is ±2°.

FTHN (A)+1,3-DNB (B)

Data were obtained by the thaw–melt method.[43] No eutectic data were reported, but the eutectic temperatures may be deduced by inspection to be 71.0 and 68.0 °C. Liquidus data on the LHS are lacking, and so the eutectic temperatures and the congruent melting point of the 1:1 compound[43] (77.0 °C) were taken as guides for the optimization. The phase diagram, Fig. 19, was calculated with the use of Eq. (29),

$$G^E(l)=x_Ax_B(-4100+2675x_B)\ \text{J mol}^{-1}, \quad (29)$$

and the calculated thermodynamic properties of the compound (AB)/2 are

$$\Delta_{fus}G^0=11\,644-33.2510T\ \text{J mol}^{-1}, \quad (30)$$

$$\Delta_fG^0=-12\,334+27.4882T\ \text{J mol}^{-1}. \quad (31)$$

Other calculated data are E_1=71.0 °C, x_B=0.355, E_2=68.0 °C, x_B=0.695, and the 1:1 compound melts at 77.0 °C. The probable maximum inaccuracy in the calculated diagram is ±3°.

AN (A)+1,3-DNB (B)

Liquidus data were obtained by thermal analysis.[98] Although no eutectic or peritectic arrests were noted, the reported eutectic[98] is −8.0 °C, x_B=0.04, and the peritectic temperature (1:1 compound) is 40.0 °C (no composition given). Optimization yielded

$$G^E(l)=x_Ax_B(-3608+2696x_B)\ \text{J mol}^{-1} \quad (32)$$

and for the compound (AB)/2,

$$\Delta_{fus}G^0=18\,607-59.2793T\ \text{J mol}^{-1}, \quad (33)$$

$$\Delta_fG^0=19\,172+53.5181T\ \text{J mol}^{-1}. \quad (34)$$

The phase diagram (Fig. 20) was calculated with the use of Eqs. (32) and (34); other calculated data are E=−9.0 °C, x_B=0.044 and P=40.5 °C, x_B=0.456. The probable maximum inaccuracy in the calculated diagram is ±2°.

1,2-DAB (A)+1,3-DNB (B)

Data were obtained by thermal analysis[107] and the reported eutectic is 59.0 °C, x_B=0.60. In the optimization the reported eutectic temperature was given priority, with the result

$$G^E(l)=x_Ax_B(-550+66x_B)\ \text{J mol}^{-1}. \quad (35)$$

The phase diagram, Fig. 21, was calculated with the use of Eq. (35) and the calculated eutectic is 59.0 °C, x_B=0.598. The probable maximum inaccuracy in the calculated diagram is ±2°.

1,3-DAB (A)+1,3-DNB (B)

Data were obtained by thermal analysis[107] and the reported eutectic is 37.0 °C, x_B=0.35. As in the previous system, the

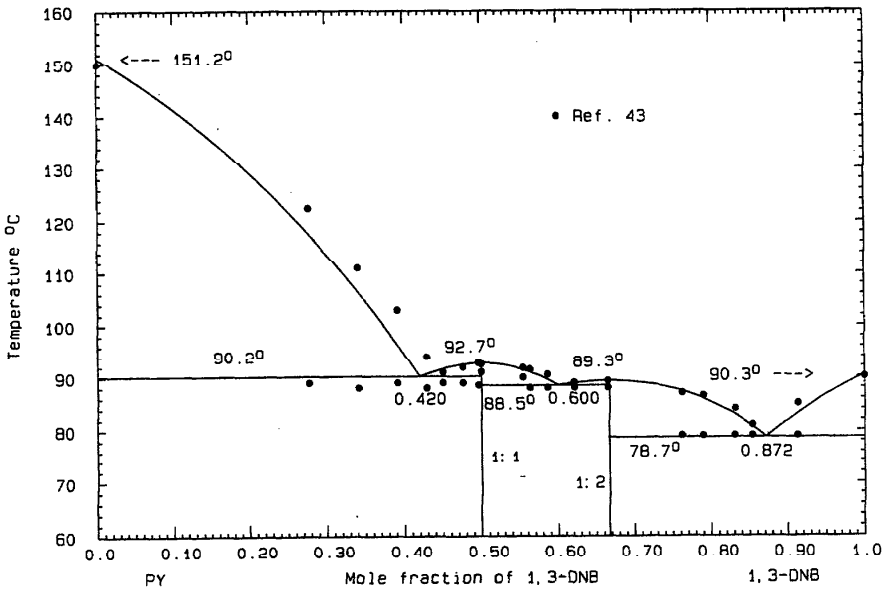

FIG. 18. The system PY (A)+1,3-DNB (B)

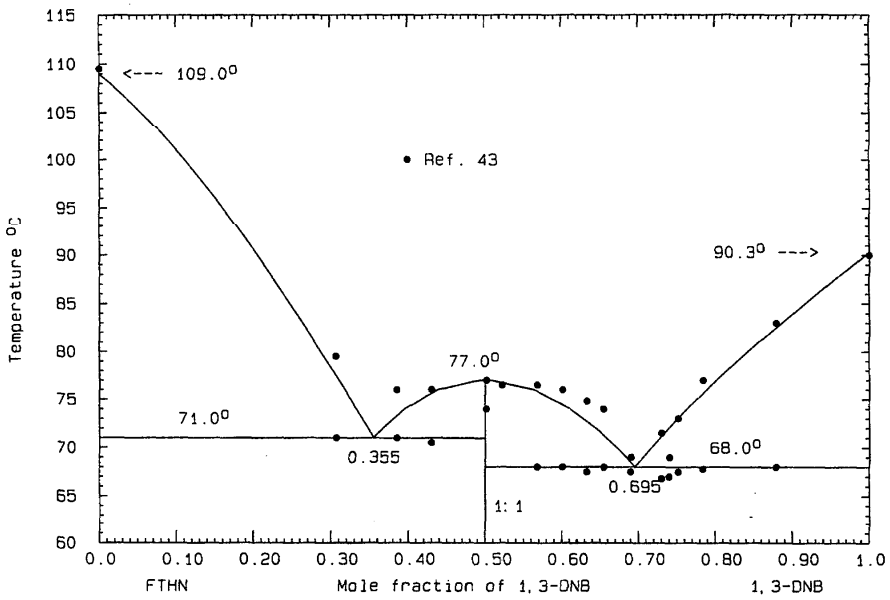

FIG. 19. The system FTHN (A)+1,3-DNB (B)

reported eutectic temperature was given priority in the optimization. The phase diagram, Fig. 22, was calculated with the use of Eq. (36)

$$G^{E}(l)=x_A x_B(-633+1427x_B)\ \text{J mol}^{-1}, \qquad (36)$$

and the calculated eutectic is 37.0 °C, $x_B=0.350$. The probable maximum inaccuracy in the calculated diagram is ±4°.

MA (A)+1,3-DNB (B)

Data were obtained by thermal analysis[101] and the reported eutectic is 16.0 °C, $x_B=0.38$. Optimization of all liquids data gave the result

$$G^{E}(l)=x_A x_B(-3391+965x_B)\ \text{J mol}^{-1}, \qquad (37)$$

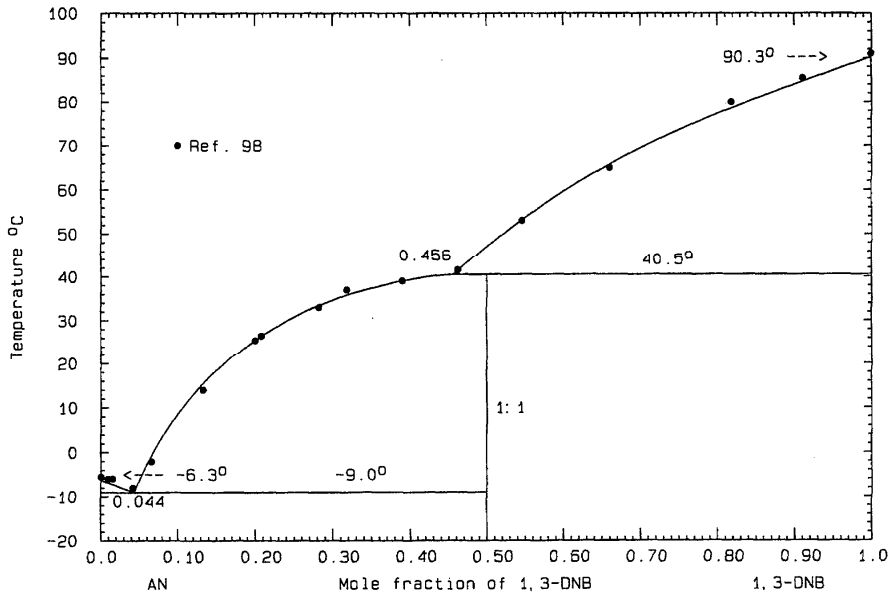

FIG. 20. The system AN (A)+1,3-DNB (B)

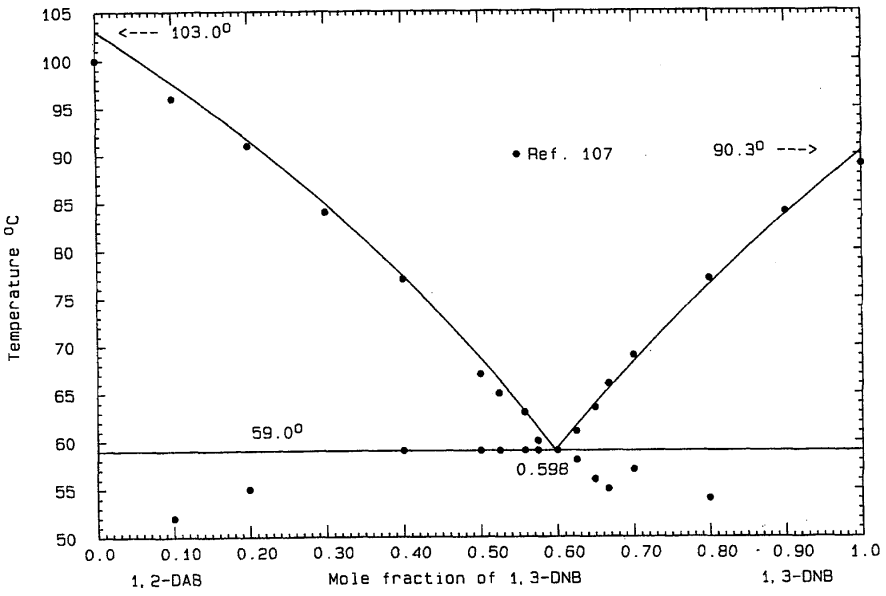

FIG. 21. The system 1,2-DAB (A)+1,3-DAB (B)

and the calculated phase diagram, Fig. 23, shows a calculated eutectic of 15.8 °C, x_B=0.359. The probable maximum inaccuracy in the calculated diagram is ±2°.

1-AN (A)+1,3-DNB (B)

Data were obtained by thermal analysis[102] and the reported eutectics are E_1=33.0 °C, x_B=0.18 and E_2=56.9 °C, x_B=0.65. The 1:1 compound melts congruently[102] at 63.8 °C. In the optimization, eutectic and compound melting temperatures were given priority, and the phase diagram (Fig. 24) was calculated with the use of Eq. (38),

$$G^E(l)=x_A x_B(-5510+1100x_B)\ \text{J mol}^{-1}. \quad (38)$$

The calculated eutectics are E_1=33.0 °C, x_B=0.183 and E_2=56.9 °C, x_B=0.662. The thermodynamic properties of the compound (AB)/2 are

$$\Delta_{fus}G^0=13\,322-39.5359T\ \text{J mol}^{-1}, \quad (39)$$

$$\Delta_f G^0=-14\,562+33.7731T\ \text{J mol}^{-1}, \quad (40)$$

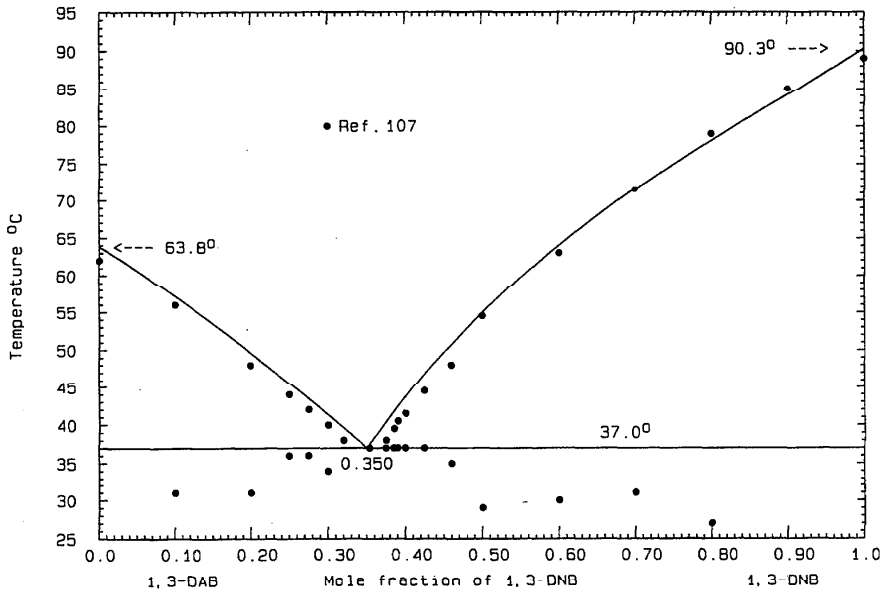

FIG. 22. The system 1,3-DAB (A)+1,3-DNB (B)

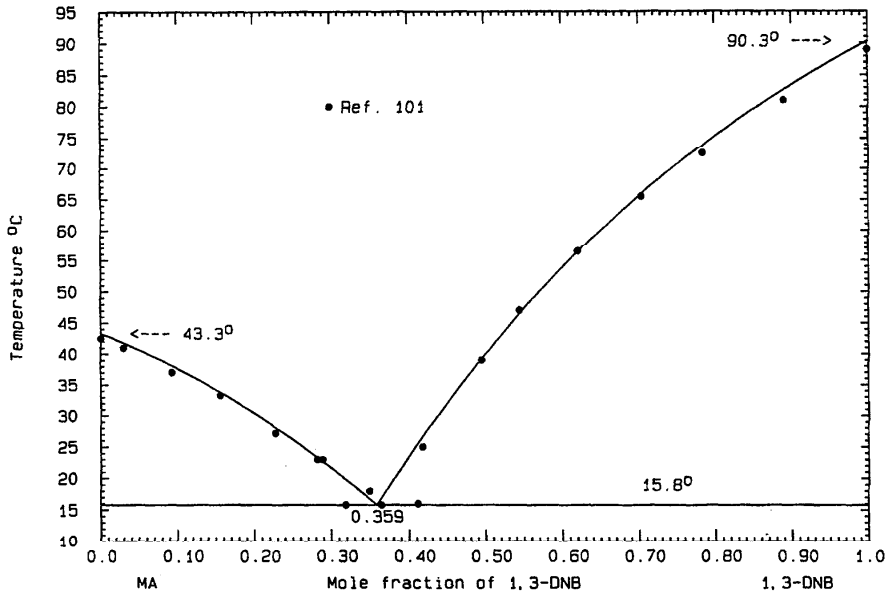

FIG. 23. The system MA (A)+1,3-DNB (B)

and its calculated melting point is 63.8 °C. The probable maximum inaccuracy in the calculated diagram is ±2°.

2-AN (A)+1,3-DNB (B)

Liquidus data were obtained by thermal analysis[102] and the reported eutectic is 51.8 °C, $x_B=0.60$. There is also a 1:1 compound melting incongruently, with peritectic 53.3 °C, $x_B=0.50$. Liquidus data in the range $0.35<x_B<1$ were optimized with the result

$$G^E(l)=x_A x_B(-5309+1816x_B)\ \text{J mol}^{-1}. \quad (41)$$

The phase diagram, Fig. 25, was calculated with the use of Eq. (41); the calculated thermodynamic properties of the compound (AB)/2 are

$$\Delta_{fus}G^0=20\,688-63.3858T\ \text{J mol}^{-1}, \quad (42)$$

$$\Delta_f G^0=-21\,789+57.6246T\ \text{J mol}^{-1}. \quad (43)$$

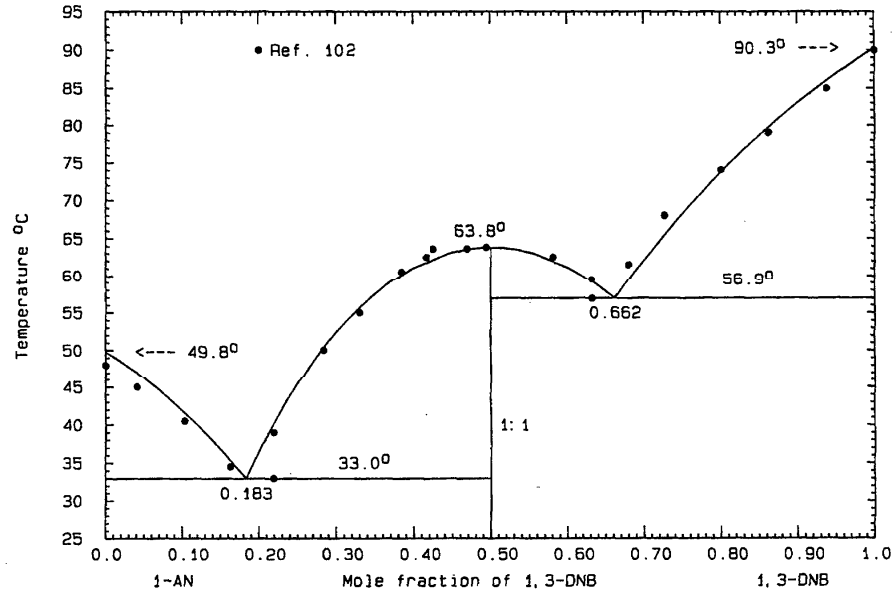

FIG. 24. The system 1-AN (A)+1,3-DNB (B)

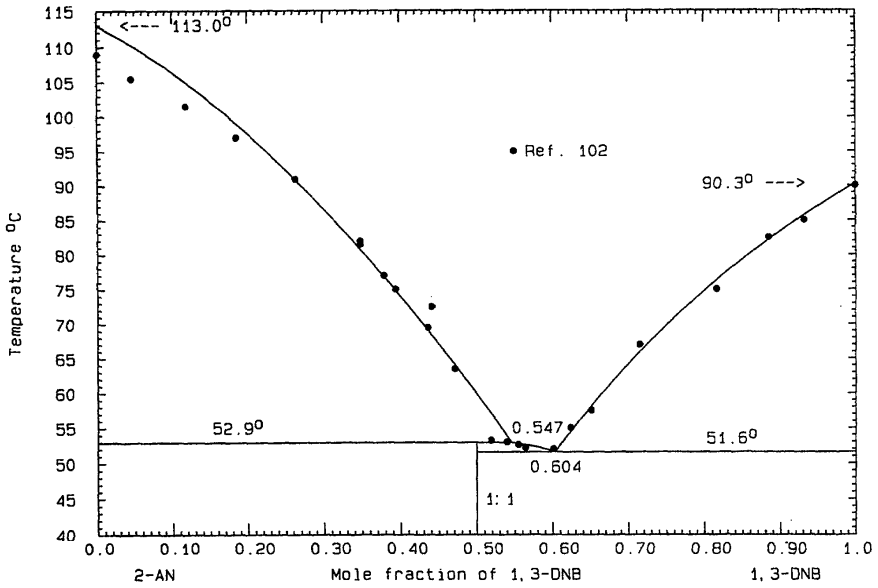

FIG. 25. The system 2-AN (A)+1,3-DNB (B)

Other calculated data are E=51.6 °C, x_B=0.604 and P 52.9 °C, x_B=0.547. The probable maximum inaccuracy in the calculated diagram is ±2°.

CAR (A)+1,3-DNB (B)

Data were obtained by thermal analysis[103] and the reported eutectic is 72.0 °C, x_B=0.87. Only liquidus data in the range $0.3<x_B<1$ were optimized, with the result

$$G^E(l)=x_A x_B(-2578-1508x_B)\ \text{J mol}^{-1}. \quad (44)$$

The experimental limiting liquidus slope at the RHS is faulty, and the extreme RHS data were ignored. The phase diagram (Fig. 26), calculated with the use of Eq. (44), shows a calculated eutectic of 79.0 °C, x_B=0.861. The carbazole transition appears on the calculated liquidus at x_B=0.656. The probable maximum inaccuracy in the calculated diagram is ±5°.

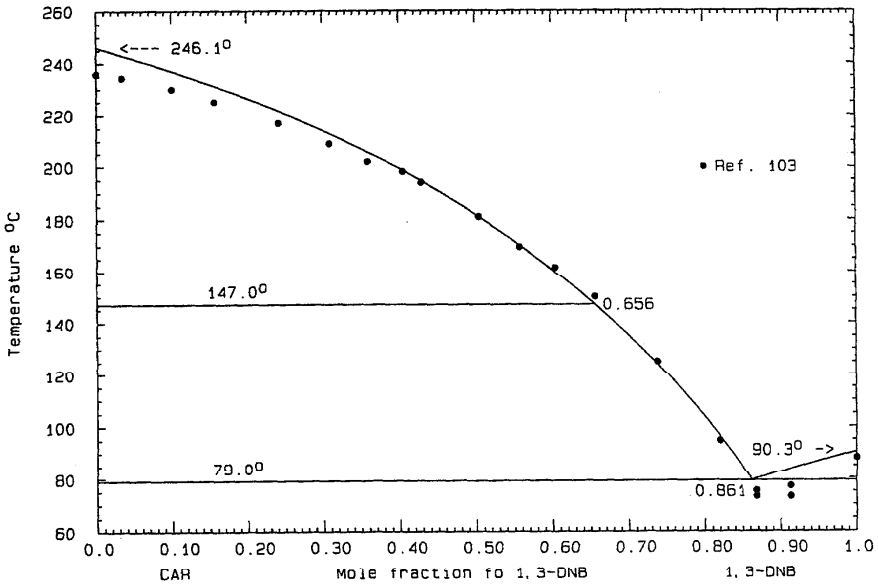

FIG. 26. The system CAR (A)+1,3-DNB (B)

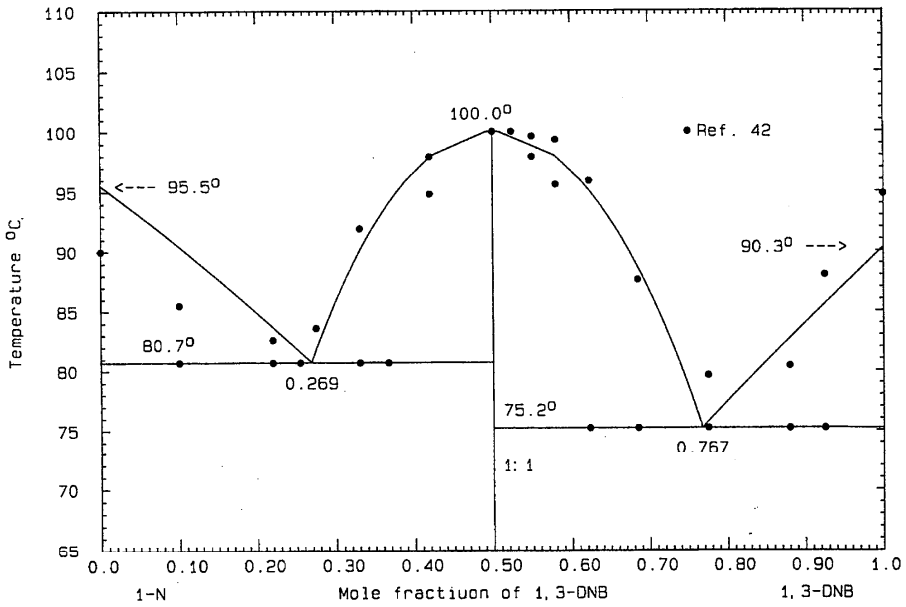

FIG. 27. The system 1-N (A)+1,3-DNB (B)

1-N (A)+1,3-DNB (B)

Data were obtained by the thaw–melt method.[42] The reported eutectics are E_1=80.7 °C, x_B=0.26 and E_2=75.2 °C, x_B=0.86.; the 1:1 compound melts congruently at 100.0 °C. Both pure component melting points[42] are quite inaccurate, and so for the optimization, the eutectic temperatures and compound melting point were taken as guides. The phase diagram, Fig. 27, was calculated with the use of Eq. (45),

$$G^E(l)=x_A x_B(90+475x_B)\ \text{J mol}^{-1}. \quad (45)$$

The calculated thermodynamic properties of the compound (AB)/2 are

$$\Delta_{fus}G^0=6715-17.9949T\ \text{J mol}^{-1}, \quad (46)$$

$$\Delta_f G^0=-6634+12.2337T\ \text{J mol}^{-1}. \quad (47)$$

Both the heat and entropy of fusion in Eq. (46) are very low, compared with those properties of the end components. This finding may be only artefactual, since if the true eutectic temperatures are 5 °C higher (say) than observed, the calculated heat and entropy of fusion would be closer to expectation. Other calculated data are E_1=80.7 °C, x_B=0.269 and E_2=75.2 °C, x_B=0.767, and the compound melts at 100.0 °C. The probable maximum inaccuracy in the calculated diagram is ±5°.

HB (A)+1,3-DNB (B)

Data were obtained by thermal analysis[104] and the reported eutectic is 63.0 °C, x_B=0.585. Since both pure component melting points[104] are faulty, the excess Gibbs energy of the liquid was obtained from the reported eutectic:

$$G^E(l)=x_A x_B(99+862x_B)\ \text{J mol}^{-1}. \quad (48)$$

The phase diagram, Fig. 28, was calculated with the use of Eq. (48). The calculated eutectic is identical to the experimental datum by deliberate choice. The probable maximum inaccuracy in the calculated diagram is ±4°.

2.5.4. Systems Based on 1,4-Dinitrobenzene

BZ (A)+1,4-DNB (B)

A few liquidus data were obtained by thermal analysis.[44] There is no reported eutectic; it is evidently very close to the melting point of benzene. Optimization of the data yielded the result

$$G^E(l)=1594x_A x_B\ \text{J mol}^{-1}, \quad (49)$$

and the phase diagram, Fig. 29, was calculated with the use of Eq. (49). The calculated eutectic is 5.2 °C, x_B=0.005. The probable maximum inaccuracy in the calculated diagram is +1°.

FLN (A)+1,4-DNB (B)

Data were obtained by thermal analysis[99] and the reported eutectic is 90.0 °C, x_B=0.28. Only liquidus data in the range $0.2<x_B<1$ were optimized, with the result

$$G^E(l)=x_A x_B(-3394+1875x_B)\ \text{J mol}^{-1}. \quad (50)$$

The phase diagram, Fig. 30, was calculated with the use of Eq. (50) and the calculated eutectic is 90.1 °C, x_B=0.268. The probable maximum inaccuracy in the calculated diagram is ±2°.

ANTH (A)+1,4-DNB (B)

Data were obtained by thermal analysis[100] and the reported eutectic is 146.0 °C, x_B=0.66. Since the experimental melting points of both end components[100] are too low, only data in the range $0.4<x_B<0.8$ were optimized with the result

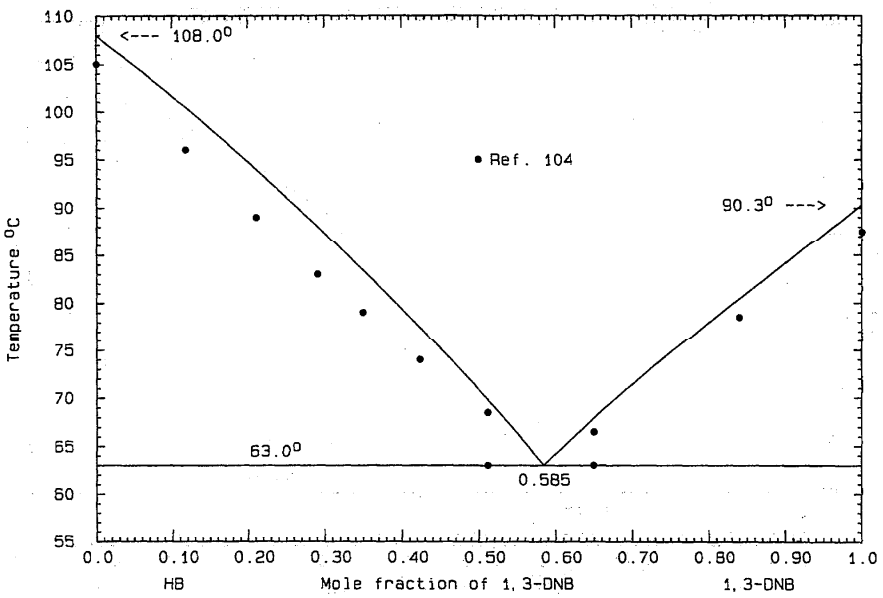

FIG. 28. The system HB (A)+1,3-DNB (B)

$$G^{E}(l) = -1487 x_A x_B \text{ J mol}^{-1}. \quad (51)$$

The calculated phase diagram, Fig. 31, shows a calculated eutectic of 146.2 °C, x_B=0.644. The probable maximum inaccuracy in the calculated diagram is ±3°.

PH (A)+1,4-DNB (B)

Data were obtained by thermal analysis[44] and there is no reported eutectic. The experimental[44] melting point of phenanthrene is high, and so only data of the RHS liquidus were optimized, with the result

$$G^{E}(l) = x_A x_B(-6683 + 3724 x_B) \text{ J mol}^{-1}. \quad (52)$$

The phase diagram calculated with the use of Eq. (52) shows a calculated eutectic of 69.5 °C, x_B=0.255. The RHS liqui-

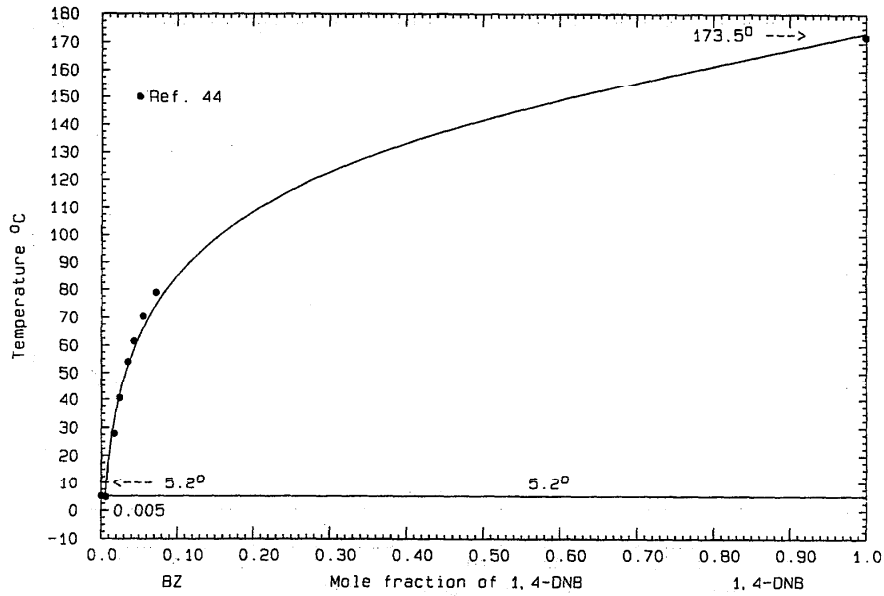

FIG. 29. The system BZ (A)+1,4-DNB (B)

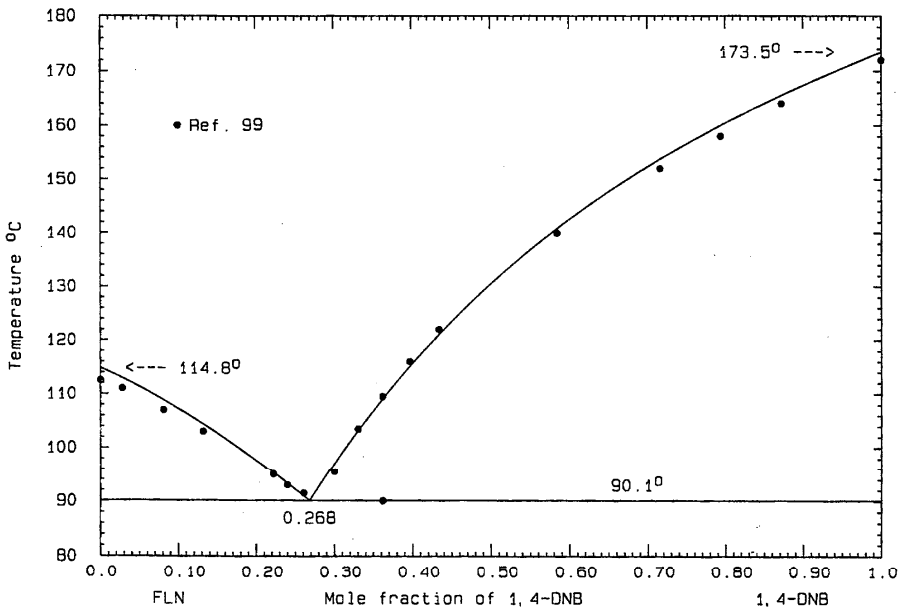

FIG. 30. The system FLN (A) 1,4-DNB (B)

dus effectively defines the complete phase diagram, Fig. 32. The probable maximum inaccuracy in the calculated diagram is ±2°.

PY (A)+1,4-DNB (B)

Data were obtained[43] by the thaw–melt method. The reported eutectic is 114.5 °C, x_B=0.48, and peritectic (1:1 compound) 107.5 °C, x_B=0.363. Optimization of the liquidus data yielded the expression

$$G^E(l)=x_A x_B(-2748-1258x_B)\ \text{J mol}^{-1}, \quad (53)$$

and the calculated properties of the compound (AB)/2 are

$$\Delta_{fus}G^0=8156-20.9873T\ \text{J mol}^{-1}, \quad (54)$$

$$\Delta_f G^0=-9004+15.2245T\ \text{J mol}^{-1}. \quad (55)$$

Both the heat and entropy of fusion of the compound, Eq. (54), are rather low in comparison with the properties of the end components. Other calculated data of the phase diagram,

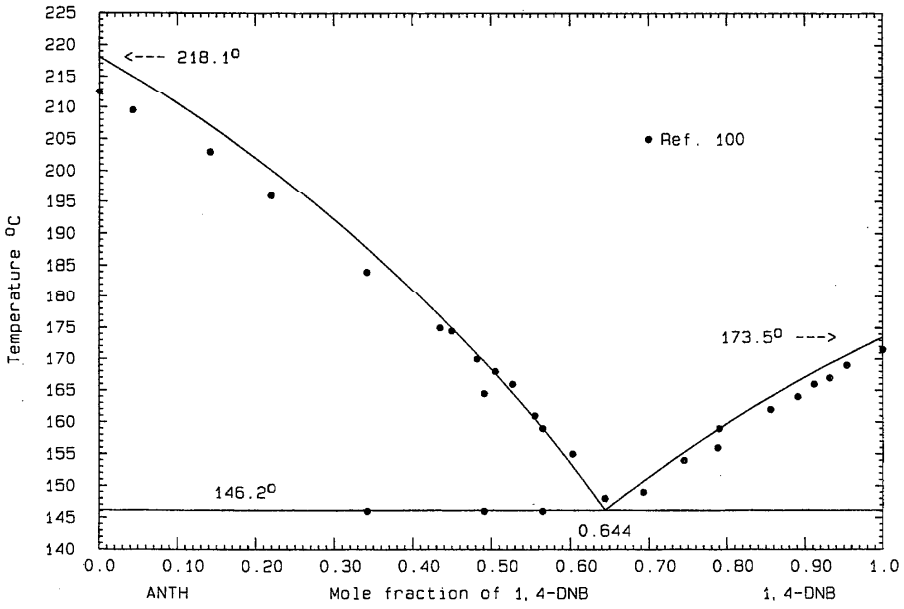

FIG. 31. The system ANTH (A)+1,4-DNB (B)

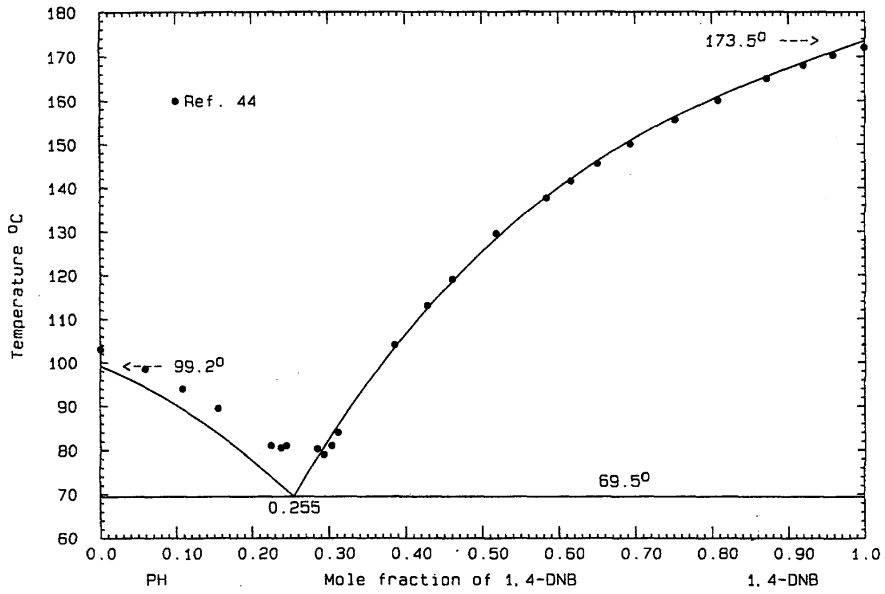

FIG. 32. The system PH (A)+1,4-DNB (B)

Fig. 33, are $E=107.5$ °C, $x_B=0.368$ and $P=114.5$ °C, $x_B=0.453$. The probable maximum inaccuracy in the calculated diagram is ±2°.

MA (A)+1,4-DNB (B)

Data were obtained by thermal analysis[101] and the reported eutectic is 36.5 °C, $x_B=0.11$. Only data in the range $0.1<x_B<0.6$ were optimized, with the result

$$G^E(l)=x_A x_B(-5253+7761x_B-6242x_B^2)\ \text{J mol}^{-1}. \quad (56)$$

The phase diagram, Fig. 34, calculated with the use of Eq. (56) shows a calculated eutectic of 35.8 °C, $x_B=0.110$. The RHS liquidus effectively defines the calculated phase diagram. The probable maximum inaccuracy in the calculated diagram is ±2°.

1-AN (A)+1,4-DNB (B)

Data were obtained by the thaw–melt method[13] and thermal analysis.[102] A critical point summary is as follows (Table 4): The two sets of liquidus data[13,102] agree to within

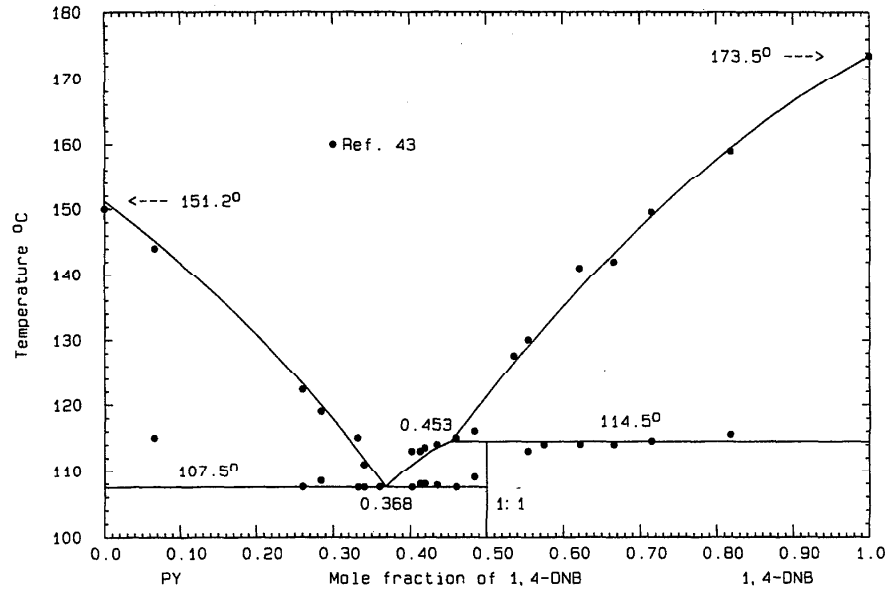

FIG. 33. The system PY (A)+1,4-DNB (B)

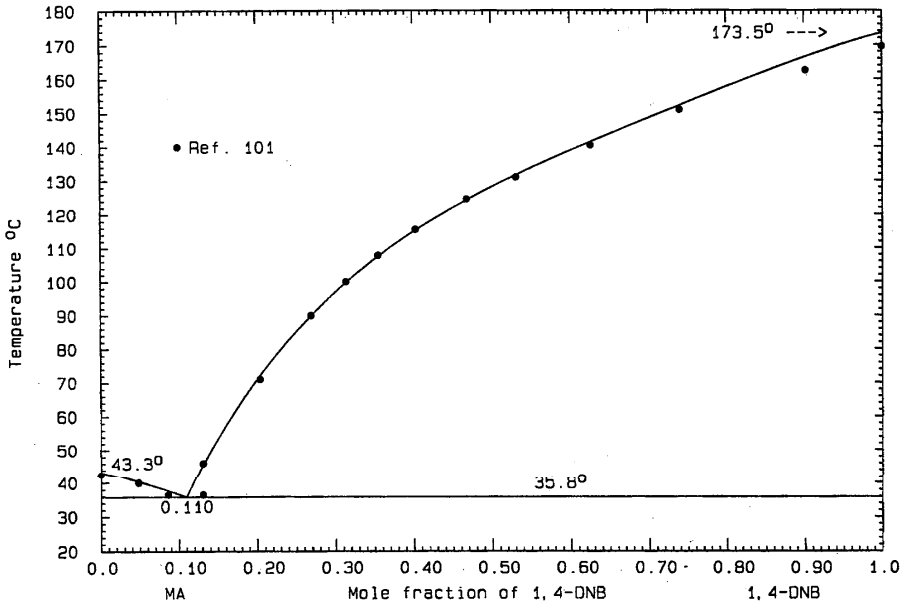

FIG. 34. The system MA (A)+1,4-DNB (B)

3°. The stoichiometry of the compound was set at[13] 1:1, while the other study[102] was noncommittal. All liquidus data were weighted equally in the optimization, with the result

$$G^{E}(l) = -5144 x_A x_B \text{ J mol}^{-1}, \quad (57)$$

and the properties of the compound (AB)/2 are

$$\Delta_{fus} G^0 = 13\,673 - 37.4535T \text{ J mol}^{-1}, \quad (58)$$

$$\Delta_f G^0 = -14\,959 + 31.6923T \text{ J mol}^{-1}. \quad (59)$$

The phase diagram, Fig. 35, was calculated with the use of Eqs. (57) and (59). Other calculated data are $E=40.7$ °C, $x_B=0.116$ and $P=81.7$ °C, $x_B=0.318$. The probable maximum inaccuracy in the calculated diagram is ±2°.

2-AN (A)+1,4-DNB (B)

Data were obtained by the thaw–melt method[13] and thermal analysis.[102] Liquidus data of the two reports agree to within 2°. A critical point summary is (Table 5) as follows. Since the experimental melting points of the pure substances were low in both studies,[13,107] only data in the range $0.2<x_B<0.6$ were optimized, with the result

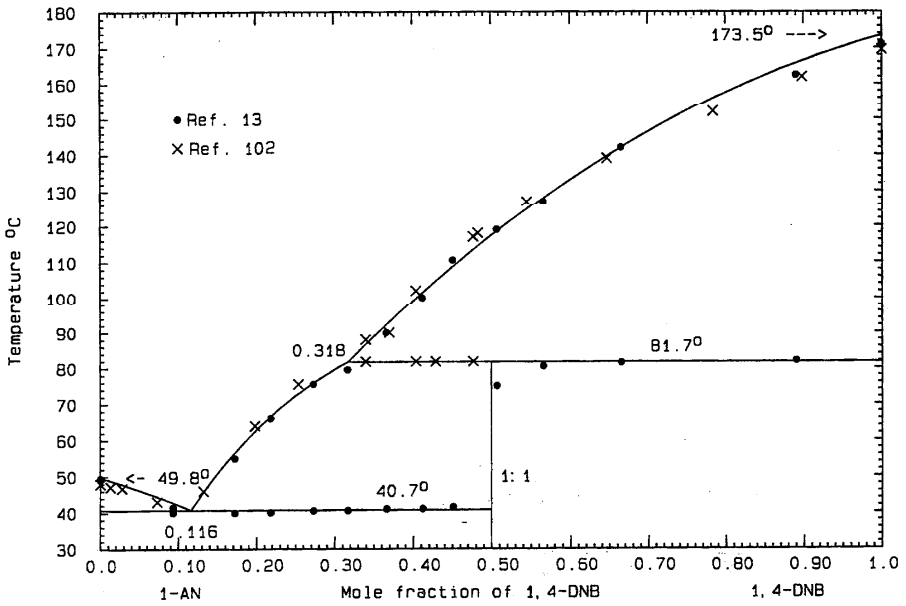

FIG. 35. The system 1-AN (A)+1,4-DNB (B)

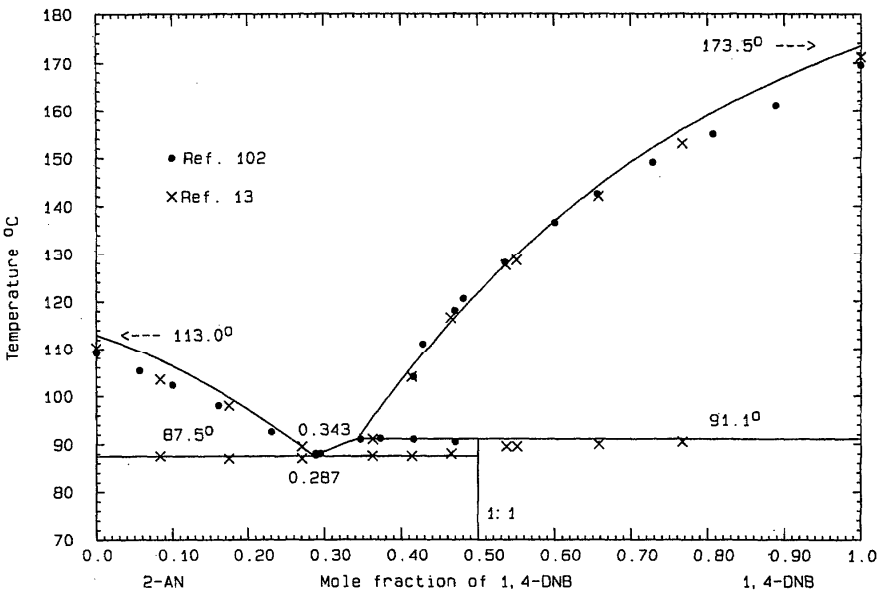

FIG. 36. The system 2-AN (A)+1,4-DNB (B)

$$G^{E}(l)=x_A x_B(-5824+1880x_B)\ \text{J mol}^{-1}. \quad (60)$$

The small interval between the peritectic and eutectic temperatures was not sufficient to calculate accurately the thermodynamic properties of the compound. Instead, the experimental eutectic and peritectic temperatures were used as guides, and the assigned properties for (AB)/2 are

$$\Delta_{fus}G^0=27\,496-74.6878T\ \text{J mol}^{-1}, \quad (61)$$

$$\Delta_f G^0=-28\,717+68.9250T\ \text{J mol}^{-1}. \quad (62)$$

With the use of Eqs. (60) and (62), the calculated phase diagram, Fig. 36, shows a calculated eutectic of 87.5 °C, $x_B=0.287$ and peritectic 91.1 °C, $x_B=0.343$. The probable maximum inaccuracy in the calculated diagram is ±2°.

CAR (A)+1,4-DNB (B)

Liquidus data were obtained by thermal analysis,[103] and the reported eutectic is 143.0 °C, $x_B=0.66$. Although the experimental melting point of carbazole is low, most of the liquidus data were accurate. Optimization yielded the result

$$G^{E}(l)=x_A x_B(-2550-2103x_B)\ \text{J mol}^{-1}, \quad (63)$$

and the phase diagram, calculated with the use of Eq. (63), is shown in Fig. 37 and indicates a calculated eutectic of 142.2 °C, $x_B=0.669$. The carbazole transition appears on the calculated liquidus at $x_B=0.651$. The probable maximum inaccuracy in the calculated diagram is ±2°.

HB (A)+1,4-DNB (B)

Data were obtained by thermal analysis[104] and the reported eutectic is 91.0 °C, $x_B=0.15$. The experimental melting point of 3-hydroxybenzaldehyde[104] is low and the limiting liquidus slope is faulty; as a result, the eutectic temperature, defined by the arrests, is probably too low. Thus only the RHS liquidus data were used in the optimization, with the result

$$G^{E}(l)=x_A x_B(1434-3447x_B+4264x_B^2)\ \text{J mol}^{-1}. \quad (64)$$

The phase diagram calculated with the use of Eq. (64) is shown in Fig. 38, indicating a calculated eutectic of 97.5 °C, $x_B=0.187$. The phase diagram has effectively been defined by the RHS liquidus. The probable maximum inaccuracy in calculated diagram is ±2°.

2.5.5. Systems Based on 1,3,5-Trinitrobenzene

BZ (A)+TNB (B)

Data were obtained by thermal analysis.[45] Reported eutectic data are $E_1=1.7$ °C, $x_B=0.02$ and $E_2=71.2$ °C, $x_B=0.50$. The data were not tabulated in the original publication,[45] and

TABLE 4. Reported critical data for the system 1-AN (A)+1,4-DNB (B)

	°C	x_B	Ref.
E	40.0	0.11	13
	40.0	0.11	102
P	81.0	0.33	13

TABLE 5. Reported critical data for the sysetm 2-AN (A)+1,4-DNB (B)

	°C	x_B	Ref.
E	88.0	0.30	102
	87.0	0.30	13
P	91.0	0.40	102
	91.2	0.40	13

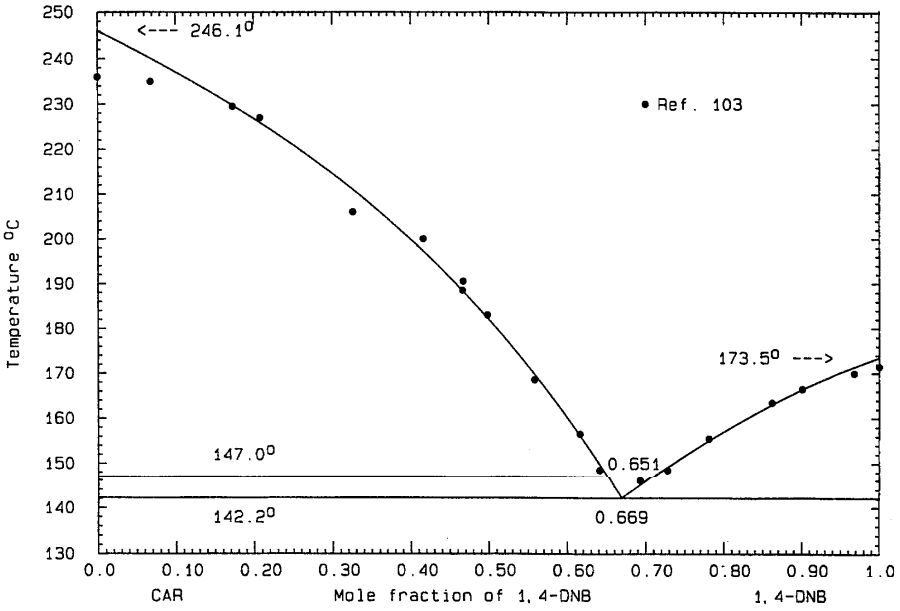

FIG. 37. The system CAR (A)+1,4-DNB (B)

the phase diagram temperature axis was distorted in two or three locations. Despite this, the data were read off the diagram and were sufficient to provide a general guide to calculations. The compound was given a 2:1 stoichiometry[45] and its heat of fusion was measured as 28 900 J mol^{-1}. In preliminary calculations, it was found that neither the observed heat of fusion nor the 2:1 stoichiometry of the compound were thermodynamically consistent with its congruent melting point (73.7 °C) and the eutectic temperatures. Liquidus data were optimized to give

$$G^{E}(l)=x_A x_B(-1987+2849x_B)\ \text{J mol}^{-1}. \quad (65)$$

For the compound, a stoichiometry 3:2 provided a better fit to the observed eutectic temperatures and thus for $(A_3B_2)/5$,

$$\Delta_{fus}G^0=8000-23.0647T\ \text{J mol}^{-1}, \quad (66)$$

$$\Delta_f G^0=-8203+17.4693T\ \text{J mol}^{-1}. \quad (67)$$

The liquidus data for the compound in the range $0.05<x_B<0.3$ proved to lie too high for thermodynamic con-

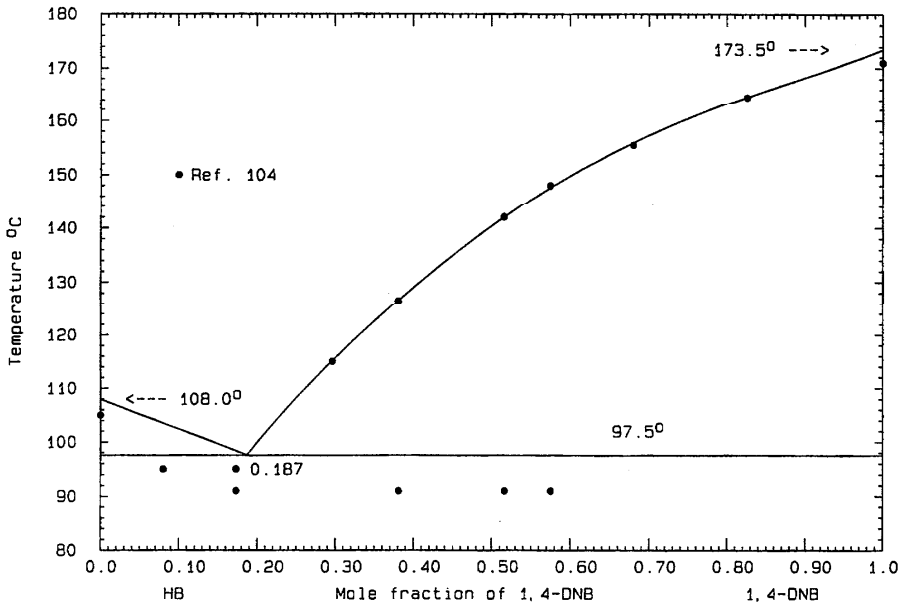

FIG. 38. The system HB (A)+1,4-DNB (B)

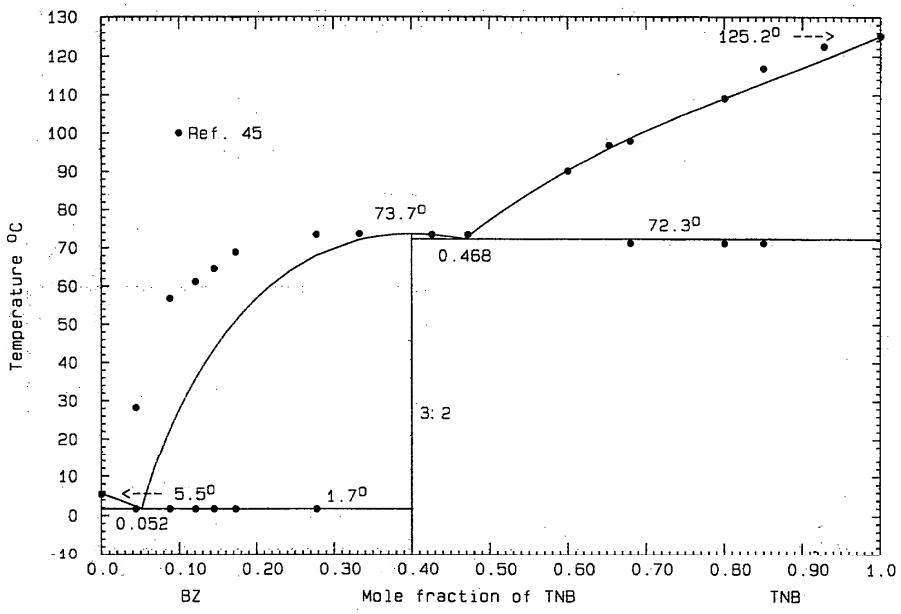

FIG. 39. The system BZ (A)+TNB (B)

istency with the rest of the phase diagram. The phase diagram, Fig. 39, was calculated with the use of Eqs. (65) and (67) and shows calculated eutectics E_1=1.7 °C, x_B=0.052, E_2=72.3 °C, x_B=0.468. The compound melts at 73.7 °C. The calculated heat and entropy of fusion of the compound, Eq. (66), are close to that of benzene, and considerable uncertainty remains concerning its properties. The probable maximum inaccuracy in the calculated diagram is ±7°.

NA (A)+TNB (B)

Data were obtained by thermal analysis.[98,108] Liquidus data of the two studies differ by up to 10° at a given composition. A eutectic summary is as follows (Table 6). A 1:1 intermediate compound has been universally reported, melting congruently at[70,98,108,109] 153.0, 157.6, 151.0, and 152.5 °C, respectively. Its heat of fusion was measured[35] as 31 900 J mol^{-1}. A transition was reported[35] at 151.3 °C with an enthalpy of transition of 1600 J mol^{-1} (another transition is also claimed[35] at −53.0 °C). The liquidus data[98,108] were optimized to give Eq. (68),

$$G^E(l)=x_A x_B(-9000+1400x_B)\ \text{J mol}^{-1}, \quad (68)$$

and all the compound liquidus data similarly yielded the properties

TABLE 6. Reported eutectic data for the system NA (A)+TNB (B)

	°C	x_B	Ref.
E_1	77.0	0.08	98
	75.3	0.05	108
	77.0	···	70
E_2	114.0	0.88	98
	113.3	0.91	108
	114.0	···	70

$$\Delta_{fus}G^0=25\,313-58.8638T\ \text{J mol}^{-1}, \quad (69)$$

$$\Delta_f G^0=-27\,388+53.1010T\ \text{J mol}^{-1} \quad (70)$$

for the compound (AB)/2. The experimental transition enthalpy[35] was used to reproduce the transition at 151.3 °C:

$$\Delta_{trs}G^0=1600-3.7696T\ \text{J mol}^{-1}, \quad (71)$$

$$\Delta_f G^0=-28\,988+56.8706T\ \text{J mol}^{-1}. \quad (72)$$

The phase diagram, Fig. 40, was calculated with the use of Eqs. (68), (70), and (72); it shows calculated eutectics E_1=78.0 °C, x_B=0.037 and E_2=113.7 °C, x_B=0.894. The calculated melting point of the compound is 156.9 °C. The probable maximum inaccuracy in calculated diagram is ±5°.

ACN (A)+TNB (B)

Liquidus data were obtained by thermal analysis[103] and the reported eutectics are E_1=87.0 °C, x_B=0.06 and E_2=115.0 °C, x_B=0.92. A 1:1 compound melts congruently[103] 161.0 °C or[109] 168.0 °C. Since the crystallization field of the compound occupies more than 80% of the composition range, the calculation of the phase diagram is somewhat insensitive to the exact value of $G^E(l)$. The value

$$G^E(l)=-4400x_A x_B\ \text{J mol}^{-1} \quad (73)$$

is approximate. The optimization of the compound liquidus data showed that the reported eutectic temperatures[103] are somewhat in error; for (AB)/2, the result is

$$\Delta_{fus}G^0=18\,538-42.5712T\ \text{J mol}^{-1}, \quad (74)$$

$$\Delta_f G^0=-19\,638+36.8100T\ \text{J mol}^{-1}. \quad (75)$$

The calculated phase diagram, Fig. 41, is based on Eqs. (73) and (75). The calculated compound melting point is

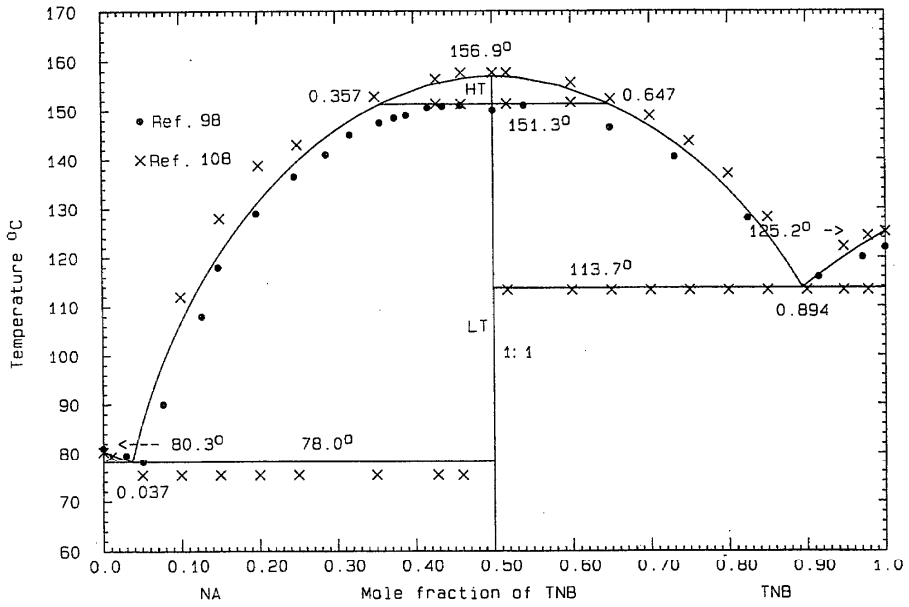

FIG. 40. The system NA (A)+TNB (B)

162.3 °C. Other calculated data are E_1=89.9 °C, x_B=0.061 and E_2=113.2 °C, x_B=0.885. The probable maximum inaccuracy in the calculated diagram is ±3°.

FLN (A)+TNB (B)

Data were obtained by thermal analysis[99] and the microthermal method.[70] A eutectic summary is given in Table 7. There is disagreement, up to 5°, between the two sets of liquidus data[70,99] and the LHS liquidus data of Kremann[99] are low. There is a congruently melting compound, whose stoichiometry is uncertain. According to two reports[70,110] the stoichiometry is 1:1 with melting point 106.0 or 105–106 °C, other reports[99,109] have 2:3 and 105.0 °C. The structure of the compound was elucidated by x-ray diffraction[110] (monoclinic: a=0.764 nm, b=0.734 nm, c=2.82 nm, β=97°). The assignment of 1:1 stoichiometry would therefore appear to be definitive, but the liquidus data in the central region are not precise enough to confirm this. The liquidus data of Kofler[70] were optimized, giving

$$G^E(l)=x_A x_B(-1989+1376x_B)\ \text{J mol}^{-1}. \quad (76)$$

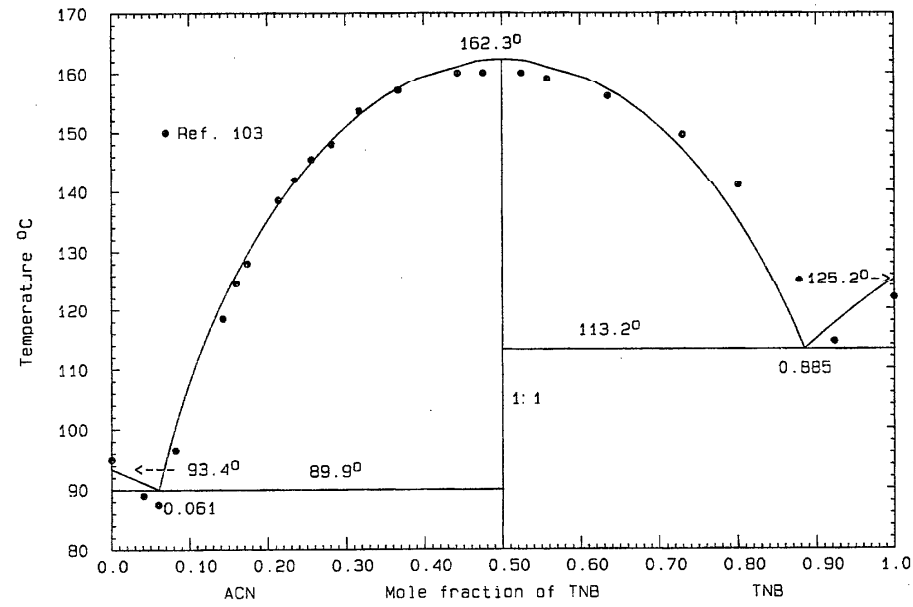

FIG. 41. The system ACN (A)+TNB (B)

TABLE 7. Reported eutectic data for the system FLN (A)+TNB (B)

	°C	x_B	Ref.
E_1	88.0	0.30	70
	86.0	0.30	99
E_2	100.0	0.73	70
	98.5	0.76	99

TABLE 8. Reported eutectic data for the system ANTH (A)+TNB (B)

	°C	x_B	Ref.
E_1	163.8	0.485	108
	162.0	0.44	100
	164.0	···	70
E_2	116.8	0.940	108
	112.0	0.95	100
	118.0	···	70

Preliminary calculations showed that the observed eutectic data[70,99] could be respected only with 2:3 stoichiometry; for the compound $(A_2B_3)/5$,

$$\Delta_{fus}G^0 = 14\,680 - 38.6990T \text{ J mol}^{-1}, \quad (77)$$

$$\Delta_f G^0 = -14\,959 + 33.1052T \text{ J mol}^{-1}, \quad (78)$$

melting at 106.2 °C. The phase diagram, Fig. 42, was calculated with the use of Eqs. (76) and (78) shows calculated eutectics of E_1=88.3 °C, x_B=0.308 and E_2=101.5 °C, x_B=0.750. The probable maximum inaccuracy in the calculated diagram is ±5°.

ANTH (A)+TNB (B)

Data were obtained by thermal analysis[100,108] and observed eutectic data are summarized in Table 8. The congruent melting point of the 1:1 compound[8,67,70,108,109] is 165.5, 165.0, 165.0, 165.4, or 164.0 °C, its heat of fusion was measured[8] as 39 750 J mol^{-1} or[35] 29 000 J mol^{-1}. The liquidus data of Kremann and Müller[100] are low, and so optimization of the later data[108] gave

$$G^E(l) = -4379x_A x_B \text{ J mol}^{-1}, \quad (79)$$

and for the compound $(AB)/2$,

$$\Delta_{fus}G^0 = 27\,537 - 62.9177T \text{ J mol}^{-1}, \quad (80)$$

$$\Delta_f G^0 = -28\,631 + 57.1565T \text{ J mol}^{-1}. \quad (81)$$

The phase diagram, Fig. 43, was calculated with the use of Eqs. (79) and (81) and shows calculated eutectics E_1=164.2 °C, x_B=0.460 and E_2=118.0 °C, x_B=0.927. The compound melts congruently at 164.5 °C. The probable maximum inaccuracy in the calculated diagram is ±5°.

PH (A)+TNB (B)

Liquids data were obtained by thermal analysis[44] and the microthermal method.[70] A summary of critical data is as follows (Table 9). The data of Kremann[44] are quite erroneous, since the 1:1 compound melts congruently at the higher temperature. Kofler[70] reports also a transition temperature for the compound at 149.0 °C. The optimization therefore used only the later data[70] with the following results for the compound $(AB)/2$:

$$\Delta_{fus}G^0 = 18\,333 - 41.9165T \text{ J mol}^{-1}, \quad (82)$$

$$\Delta_f G^0 = -19\,433 + 36.1537T \text{ J mol}^{-1}. \quad (83)$$

Similar to the system with anthracene above, the compound

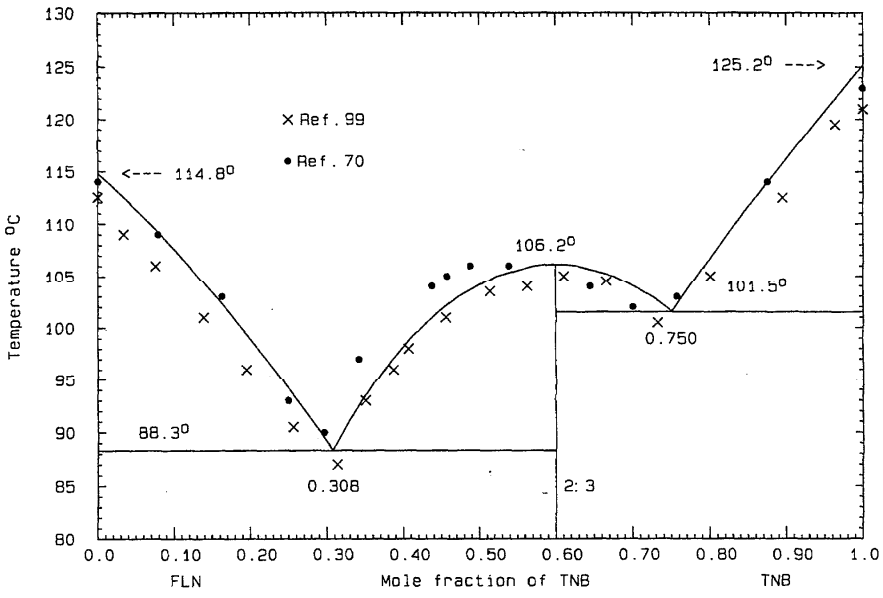

FIG. 42. The system FLN (A)+TNB (B)

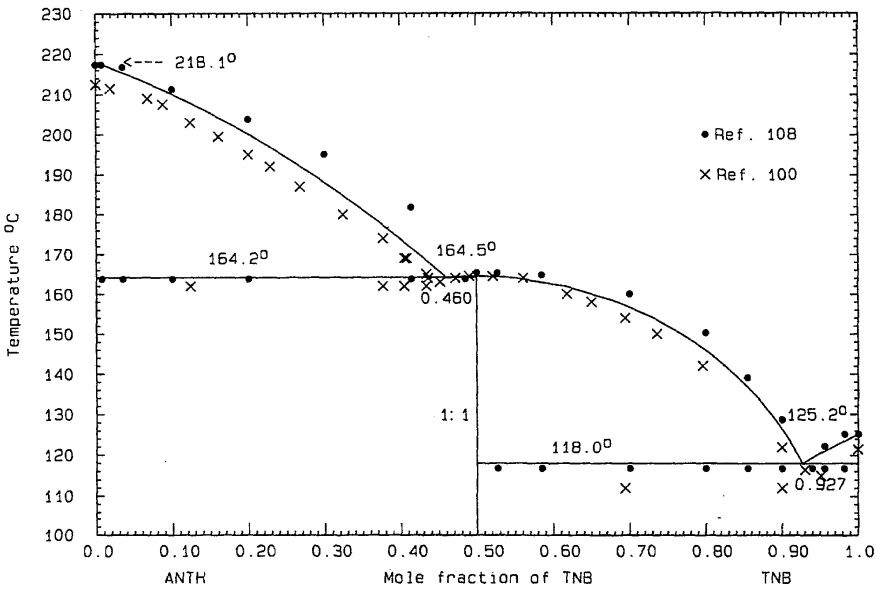

FIG. 43. The system ANTH (A)+TNB (B)

liquidus covers more than 80% of the composition range, and hence the excess Gibbs energy of the liquid was simply given an assigned value

$$G^{E}(l) = -4400 x_A x_B \text{ J mol}^{-1}. \quad (84)$$

The phase diagram, Fig. 44, was calculated with the use of Eqs. (83) and (84), and calculated eutectics are E_1=94.2 °C, x_B=0.067 and E_2=113.5 °C, x_B=0.887. The compound melts congruently at 164.2 °C. The probable maximum inaccuracy in the calculated diagram is ±3°C.

PY (A)+TNB (B)

Data were obtained by the thaw–melt method[43] and the reported eutectics are E_1=141.5 °C, x_B=0.10 and E_2=116.0 °C, x_B=0.98. The 1:1 compound melts congruently at[43] 245.5 or[8] 253.3 °C. Its heat of fusion[8] was measured as 38 500 J mol^{-1}. Like the systems with phenanthrene or anthracene above, the crystallization field of the compound occupies over 80% of the composition range and hence the quantity

$$G^{E}(l) = -4400 x_B \text{ J mol}^{-1} \quad (85)$$

was assigned to the liquid. For the compound, the eutectic temperatures and observed melting point[43] were given more weight than liquidus data, with the result for (AB)/2

$$\Delta_{fus}G^0 = 12\,325 - 23.7628T \text{ J mol}^{-1}, \quad (86)$$

$$\Delta_f G^0 = -13\,425 + 18.0000T \text{ J mol}^{-1}. \quad (87)$$

It is seen that the compound liquidus data[43] are not consistent with other measured phase diagram data. The phase diagram, Fig. 45, was calculated with the use of Eqs. (85) and (87) and the calculated eutectics are E_1=141.3 °C, x_B=0.099 and E_2=118.4 °C, x_B=0.931. The compound melts at 245.5 °C. The probable maximum inaccuracy in the calculated diagram is ±8°.

FTHN (A)+TNB(B).

Data were obtained by the thaw–melt method.[43] The reported eutectic are E_1=98.5 °C, x_B=0.132 and E_2=103.0 °C, x_B=0.96. The 1:1 compound melts congruently at 205.0 °C. The observed RHS eutectic temperature is low, and both it and the RHS liquidus arm of the compound are inconsistent with the theoretical limiting liquidus slope of trinitrobenzene. As in the systems with phenanthrene, pyrene, and anthracene above, the crystallization field of the compound covers most of the composition range, so the quantity

$$G^{E}(l) = -4400 x_A x_B \text{ J mol}^{-1} \quad (88)$$

was assigned rather than calculated. For the compound, its observed melting point[43] and the E_1 eutectic temperature were taken as guides to calculation of the properties

$$\Delta_{fus}G^0 = 8733 - 18.2628T \text{ J mol}^{-1}, \quad (89)$$

TABLE 9. Reported critical points for the system PH (A)+TNB (B)

	°C	x_B	Ref.
E_1	91.0	0.09	70
	85.5	0.155	44
E_2	114.0	0.91	70
	104.0	0.83	44
1:1	164.0	···	70
	164.0	···	109
	165.5	···	8
	125.0	···	44

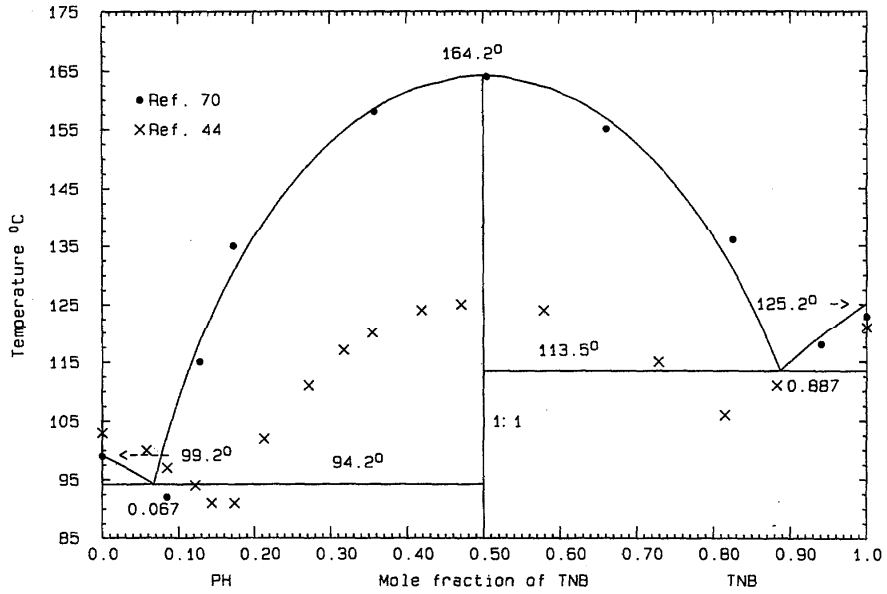

FIG. 44. The system PH (A)+TNB (B)

$$\Delta_f G^0 = -9833 + 12.50\,000T \text{ J mol}^{-1} \quad (90)$$

for (AB)/2. The phase diagram, calculated with the use of Eqs. (88) and (90), is shown in Fig. 46 and displays eutectics E_1=99.4 °C, x_B=0.123 and E_2=110.1 °C, x_B=0.860; the compound melts at 205.0 °C. The probable maximum inaccuracy in the calculated diagram is ±10°.

AN (A)+TNB (B)

Data were obtained by thermal analysis[98] and the reported eutectics are E_1=−6.0 °C, x_B=0.005 and E_2=101.0 °C, x_B=0.82. The 1:1 compound melts congruently at[98] 125.5 °C. Since the crystallization field of the compound covers 80% of the composition range, the quantity

$$G^E(l) = -5000 x_A x_B \text{ J mol}^{-1} \quad (91)$$

was assigned rather than calculated. The compound liquidus data were optimized to give, for (AB)/2,

$$\Delta_{fus} G^0 = 16\,574 - 41.3683T \text{ J mol}^{-1}, \quad (92)$$

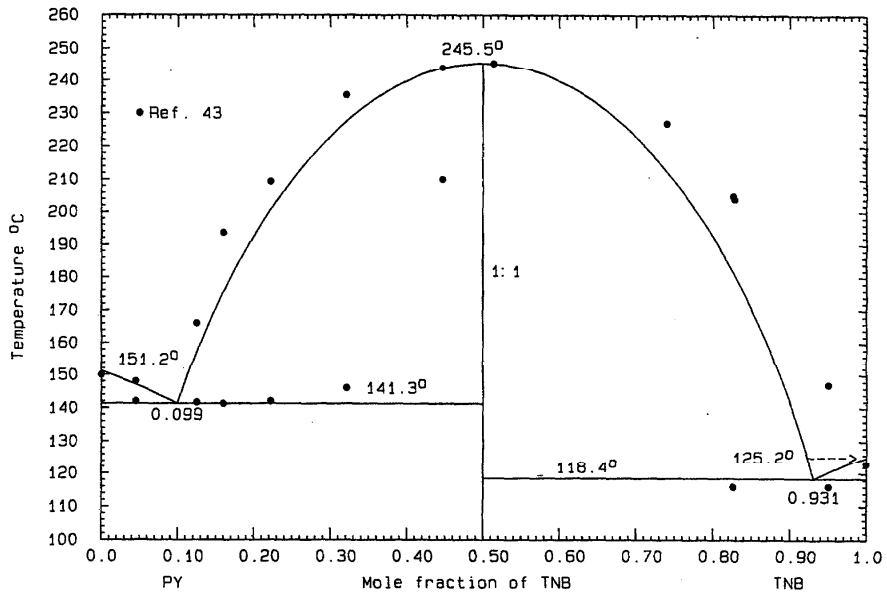

FIG. 45. The system PY (A)+TNB (B)

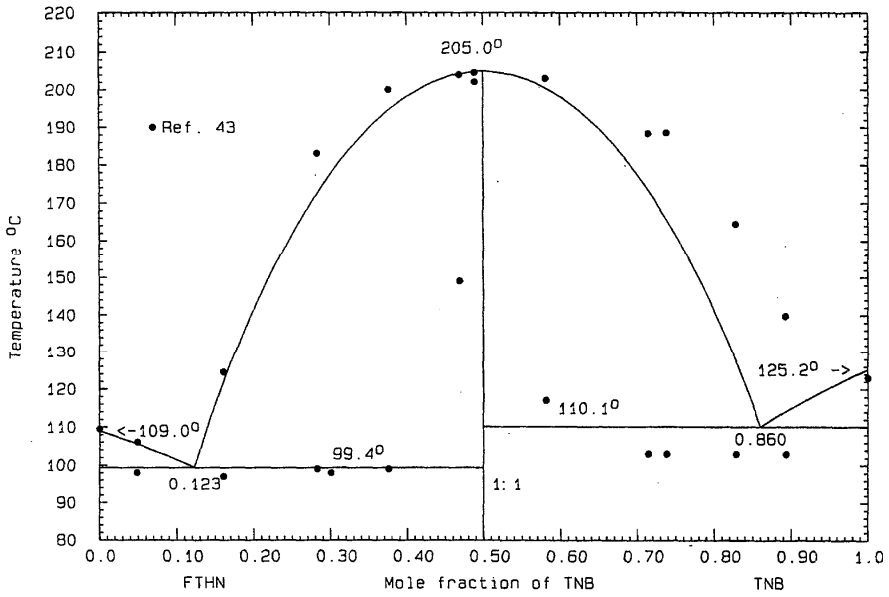

FIG. 46. The system FTHN (A)+TNB (B)

$$\Delta_f G^0 = -17\,824 + 35.6071T \text{ J mol}^{-1}. \quad (93)$$

The phase diagram, Fig. 47, was calculated with the use of Eqs. (91) and (93) and the calculated eutectics are $E_1 = -6.6$ °C, $x_B = 0.005$ and $E_2 = 100.8$ °C, $x_B = 0.796$. The compound melts at 127.5 °C. The probable maximum inaccuracy in the calculated diagram is ±2°.

DP (A)+TNB (B)

Liquidus data were obtained by the conventional melting point method[57]; no critical points were reported. Although there are few RHS and LHS liquidus data for optimization, an expression was obtained,

$$G^E(l) = x_A x_B(-11\,688 + 3134x_B) \text{ J mol}^{-1}, \quad (94)$$

which sufficed for reproducing the diagram, together with the optimized properties of the compound (AB)/2,

$$\Delta_{fus} G^0 = 32\,174 - 83.7141T \text{ J mol}^{-1}, \quad (95)$$

$$\Delta_f G^0 = -34\,704 + 77.9529T \text{ J mol}^{-1}. \quad (96)$$

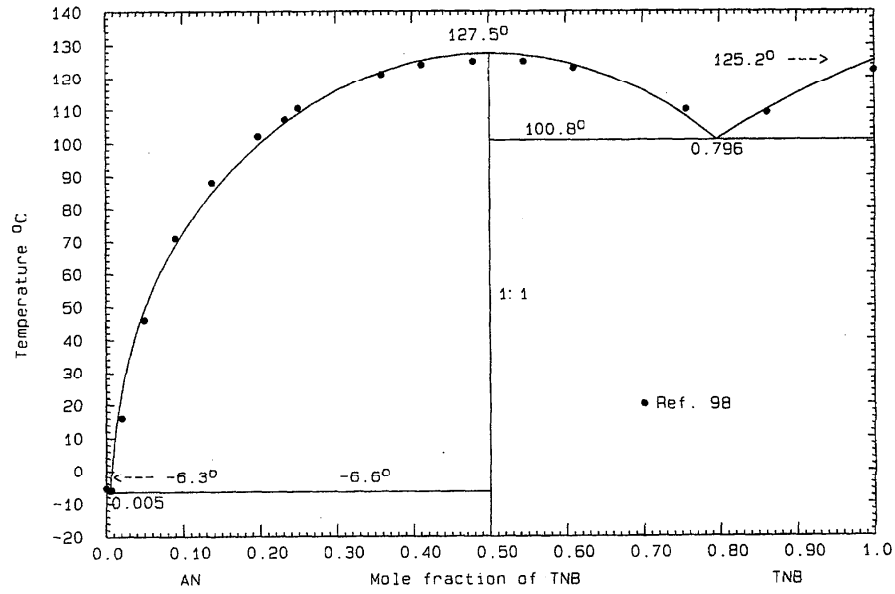

FIG. 47. The system AN (A)+TNB (B)

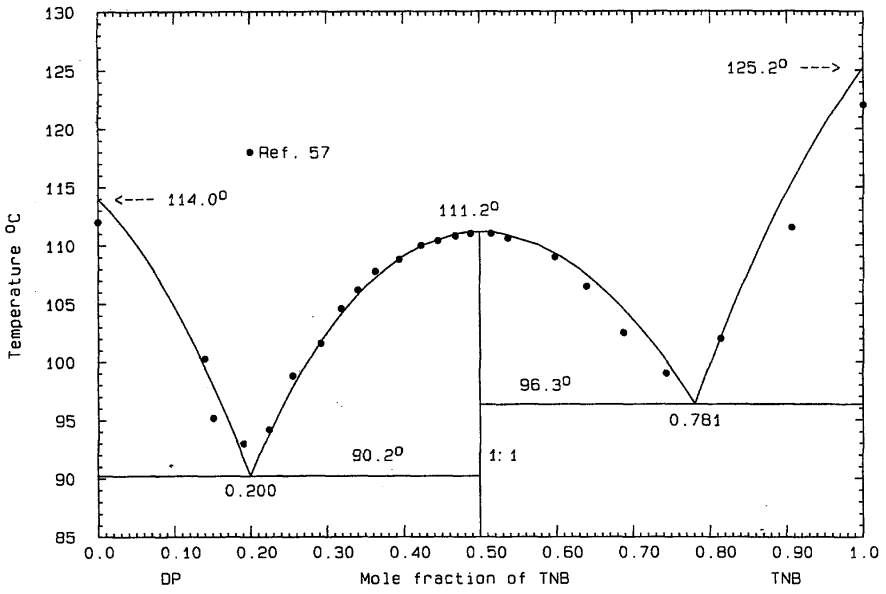

FIG. 48. The system DP (A)+TNB (B)

The calculated phase diagram, Fig. 48, shows calculated eutectics E_1=90.2 °C, x_B=0.200 and E_2=96.3 °C, x_B=0.781; the compound melts congruently at 111.2 °C. Despite the low experimental melting points of the pure substances,[57] the liquidus data are well reproduced. The probable maximum inaccuracy in the calculated diagram is ±2°.

2-AN (A)+TNB (B)

Data were obtained by the thaw-melt method[13,111] and thermal analysis.[102] Reported eutectic data are summarized in Table 10. The 1:1 compound melts congruently at[13,70,102,112] 163.0, 166.0, 161.0, and 162.0 °C. All LHS and RHS liquidus data are suspect because experimental melting points of the pure substances are low, as are the reported eutectic temperatures. An assigned quantity

$$G^E(l)=x_A x_B(-5000+2500x_B)\ \text{J mol}^{-1} \quad (97)$$

was used and the compound liquidus data were optimized, giving for (AB)/2,

$$\Delta_{fus}G^0=13\,853-31.9215T\ \text{J mol}^{-1}, \quad (98)$$

$$\Delta_f G^0=-14\,791+26.1603T\ \text{J mol}^{-1}. \quad (99)$$

The calculated phase diagram, Fig. 49, is based upon Eqs. (97) and (99) and shows calculated eutectics E_1=103.0 °C, x_B=0.141 and E_2=113.0 °C, x_B=0.870. The compound melts congruently at 160.8 °C. The probable maximum inaccuracy in the calculated diagram is ±5°.

TABLE 10. Reported eutectic data for the system 2-AN (A)+TNB (B)

	°C	x_B	Ref.
E_1	98.0	0.13	102
	100.0	0.13	13
	102.0	···	70
E_2	108.0	0.87	102
	109.0	0.87	13
	112.0	···	70

CAR (A)+TNB (B)

Data were obtained by thermal analysis[103,108] and a eutectic summary is given in Table 11. The 1:1 compound melts congruently[103,108,113] at 204.3, 203.0, or 204.0 °C, and the heat of fusion[35] is 43 700 J mol^{-1}. There is wide discrepancy between the two sets of liquidus data[103,108] and hence the quantity

$$G^E(l)=-5000x_A x_B\ \text{J mol}^{-1} \quad (100)$$

was assigned to the liquid. The compound liquidus data were used as only as a guide in the calculation, for (AB)/2,

$$\Delta_{fus}G^0=20\,384-42.7628T\ \text{J mol}^{-1}, \quad (101)$$

$$\Delta_f G^0=-21\,634+37.0000T\ \text{J mol}^{-1}. \quad (102)$$

The phase diagram, Fig. 50, calculated with the use of Eqs. (100) and (102), shows calculated eutectics E_1=197.9 °C, x_B=0.365 and E_2=119.9 °C, x_B=0.946. The calculated melting point of the compound is 203.5 °C. Thus the experimental critical data of this system have been reproduced well, although most of the liquidus data diverge widely. The probable maximum inaccuracy in the calculated diagram is ±7°.

2.5.6. Systems Based on 1,2,3,5-Tetranitrobenzene

ACN (A)+TENB (B)

Data were obtained by the thaw–melt method[43] and the reported eutectics are E_1=76.0 °C, x_B=0.190 and E_2=102.0 °C, x_B=0.642. The 1:1 compound melts congruently[43] at 110.5 °C. There are very few liquidus data for the calculation of the quantity

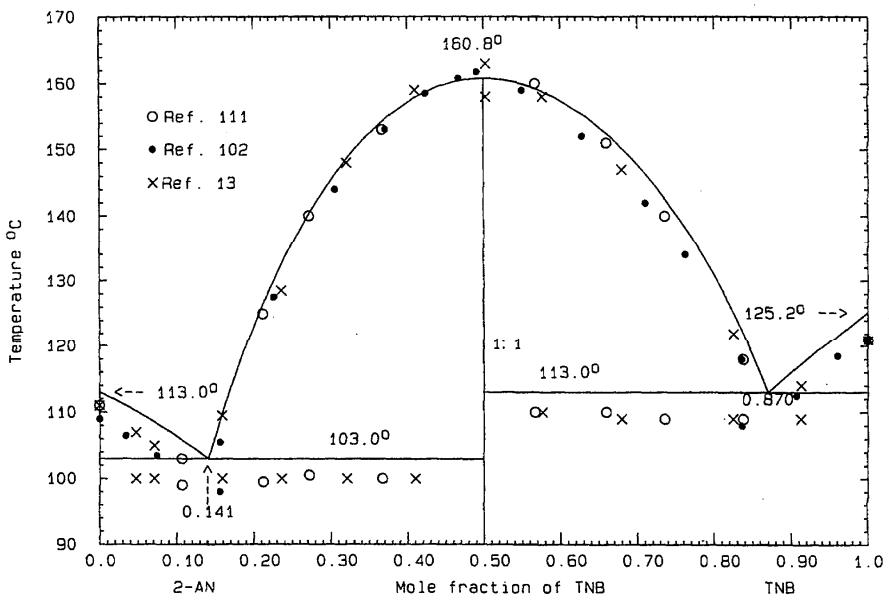

FIG. 49. The system 2-AN (A)+TNB (B)

$$G^{E}(l)=x_A x_B(-7200+1400x_B)\ \text{J mol}^{-1}. \quad (103)$$

For the compound, its melting point and the eutectic data were taken as guides for the calculation of the properties

$$\Delta_{fus}G^0=13\,721-35.7628T\ \text{J mol}^{-1}, \quad (104)$$

$$\Delta_f G^0=-15\,346+30.0000T\ \text{J mol}^{-1} \quad (105)$$

for (AB)/2. The calculated phase diagram, Fig. 51, shows eutectics E_1=76.1 °C, x_B=0.208 and E_2=102.3 °C, x_B=0.652, while the calculated compound melting point is 110.5 °C. The probable maximum inaccuracy in the calculated diagram is ±3°.

FLN (A)+TENB (B)

Data were obtained by the thaw–melt method[43] and the reported eutectics are E_1=91.0 °C, x_B=0.22 and E_2=117.5 °C, x_B=0.88. The 1:2 compound melts congruently[43] at 130.0 °C. Optimization of the LHS and RHS liquidus data gave the result

$$G^{E}(l)=x_A x_B(-7409-3268x_B)\ \text{J mol}^{-1}. \quad (106)$$

For the compound, its melting point and the eutectic temperatures were taken as guides to the calculation of the properties

$$\Delta_{fus}G^0=26\,367-65.2920T\ \text{J mol}^{-1}, \quad (107)$$

TABLE 11. Reported eutectic data for the system CAR (A)+TNB (B)

	°C	x_B	Ref.
E_1	195.0	0.38	103
	197.8	0.46	108
E_2	120.0	0.97	103
	118.3	0.97	108

$$\Delta_f G^0=-28\,498+60.0000T\ \text{J mol}^{-1} \quad (108)$$

for $(AB_2)/3$. The phase diagram, Fig. 52, was calculated with the use of Eqs. (106) and (108); calculated eutectics are E_1=91.0 °C, x_B=0.246 and E_2=117.4 °C, x_B=0.864. The compound melts at 130.7 °C. The probable maximum inaccuracy in the calculated diagram is ±5°.

ANTH (A)+TENB (B)

Data were obtained by the thaw–melt method[43] and the reported eutectics are E_1=163.0 °C, x_B=0.395 and E_2=120.5 °C, x_B=0.942. The 1:1 compound melts congruently at[43] 171.0 °C. Some liquidus data are incompatible with the reported eutectic temperatures; as before, these temperatures and the reported compound melting point were given more weight in the calculations. For the liquid,

$$G^{E}(l)=x_A x_B(-12\,400+4400x_B)\ \text{J mol}^{-1}, \quad (109)$$

and for the compound

$$\Delta_{fus}G^0=21\,880-49.2628T\ \text{J mol}^{-1}, \quad (110)$$

$$\Delta_f G^0=-24\,430+43.5000T\ \text{J mol}^{-1}. \quad (111)$$

The calculated phase diagram, Fig. 53, shows calculated eutectics of E_1=162.5 °C, x_B=0.352 and E_2=120.5 °C, x_B=0.885; the compound melting point is 171.0 °C. The probable maximum inaccuracy in the calculated diagram is ±5°.

PH (A)+TENB (B)

Data were obtained by the thaw–melt method.[43] No eutectic data were recorded, but a 2:3 compound compound melts congruently at 125.0 °C and a 1:1 compound melts incongruently (peritectic 115.0 °C, x_B=0.385). The presence of the 1:1 compound was apparently deduced[43] from "peritectic melting" at 115.0 °C. In preliminary calculations, it was

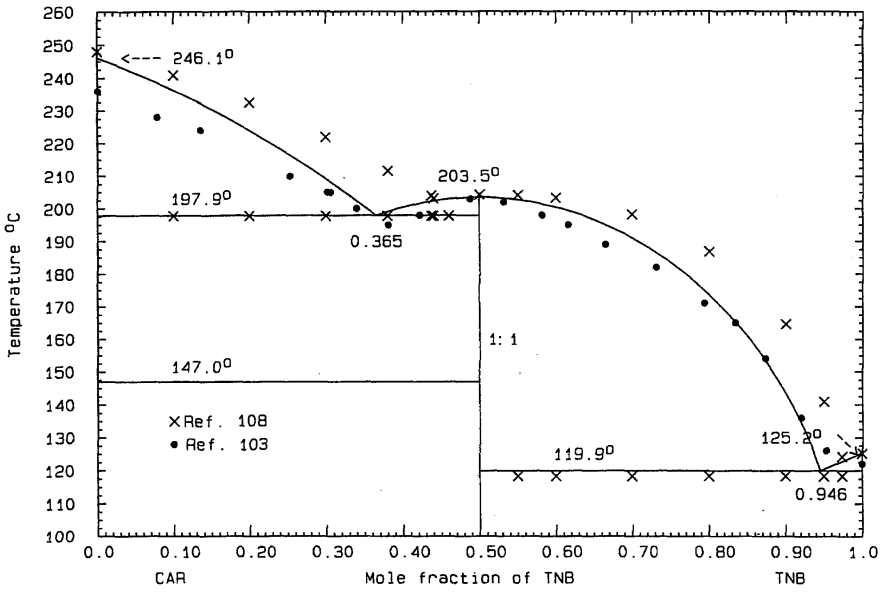

FIG. 50. The system CAR (A)+TNB (B)

found that the data could reasonably be accounted for by the 2:3 compound alone and a eutectic at 115.0 °C. Thus the liquid could be represented by

$$G^{E}(l)=x_A x_B(-12\,400+3000x_B)\ \text{J mol}^{-1} \quad (112)$$

and the compound $(A_2B_3)/5$ by

$$\Delta_{fus}G^0=31\,951-80.2459T\ \text{J mol}^{-1}. \quad (113)$$

$$\Delta_f G^0=-34\,495+74.6505T\ \text{J mol}^{-1}. \quad (114)$$

The phase diagram, Fig. 54, was calculated with the use of Eqs. (112) and (114) and shows calculated eutectics $E_1=78.8$ °C, $x_B=0.169$ and $E_2=115.0$ °C, $x_B=0.815$; the calculated melting point of A_2B_3 is 125.0 °C. The probable maximum inaccuracy in the calculated diagram is ±5°.

PY (A)+TENB (B)

Data were obtained by the thaw–melt method[43] and the reported eutectics are $E_1=125.0$ °C, $x_B=0.190$ and

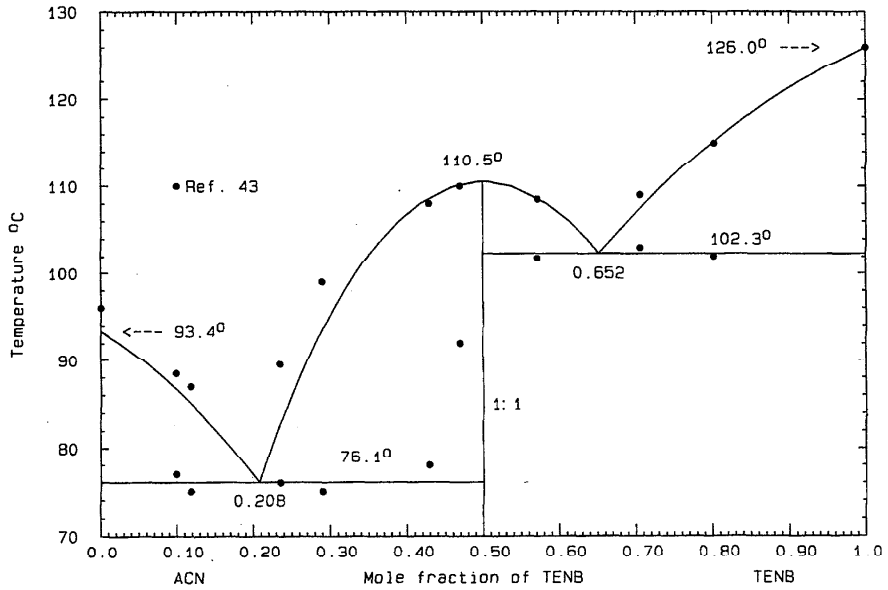

FIG. 51. The system ACN (A)+TENB (B)

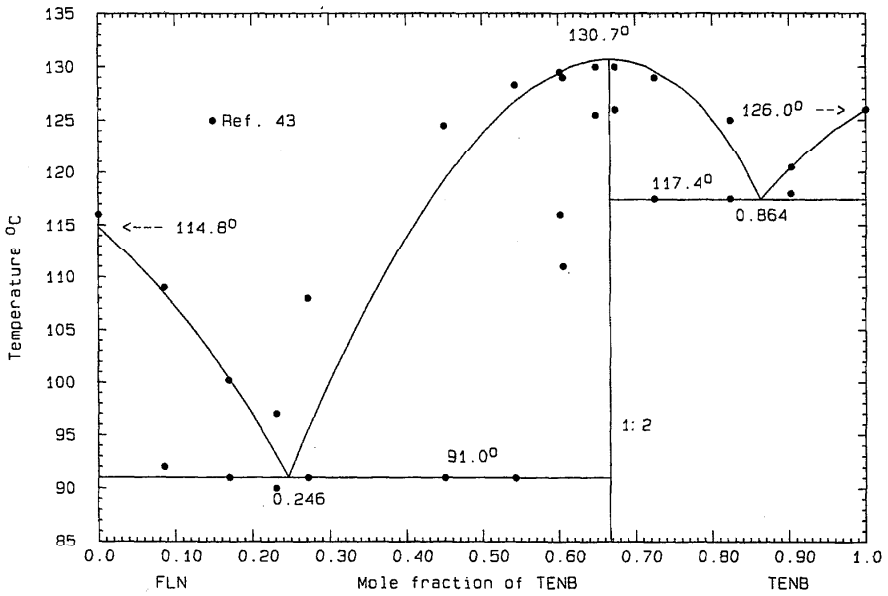

FIG. 52. The system FLN (A)+TENB (B)

E_2=122.0 °C, x_B−0.915. A 1:1 compound melts congruently[43] at 168.5 °C. The postulated high E_2 temperature is not consistent with the thermodynamic limiting liquidus slope for tetranitrobenzene. Neither is it consistent with symmetrical liquidus arms for the compound. For the liquid,

$$G^E(l) = -6072 x_A x_B \text{ J mol}^{-1} \quad (115)$$

and for the compound (AB)/2,

$$\Delta_{fus} G^0 = 13\,244 - 29.9742T \text{ J mol}^{-1}, \quad (116)$$

$$\Delta_f G^0 = -14\,762 + 24.2131T \text{ J mol}^{-1}. \quad (117)$$

The calculated phase diagram, Fig. 55, is based upon Eqs. (115) and (117) and shows calculated eutectics E_1=126.6 °C, x_B=0.203 and E_2=116.6 °C, x_B=0.828; the compound melts at 168.7 °C. The probable maximum inaccuracy in the calculated diagram is ±4°.

FTHN (A)+TENB (B)

Data were obtained by the thaw–melt method[43] and the

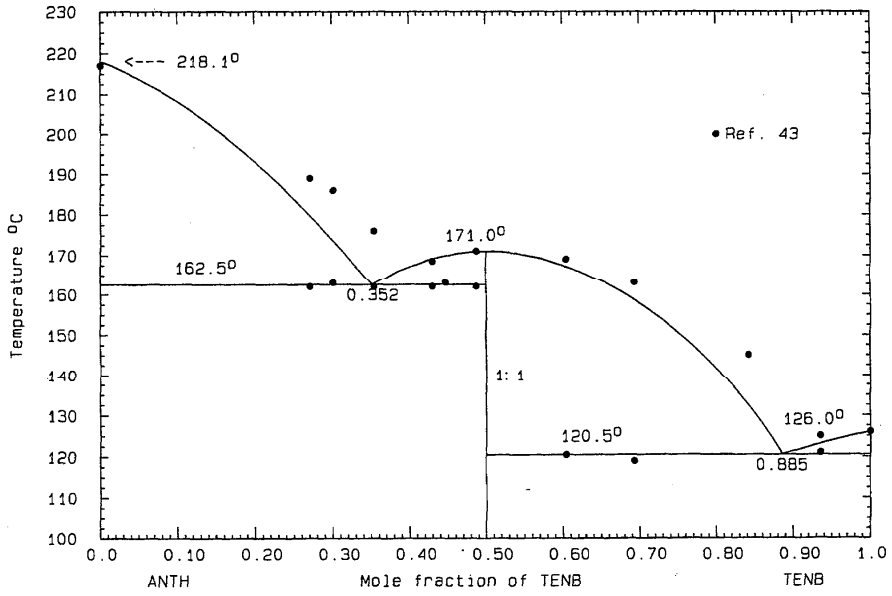

FIG. 53. The system ANTH (A)+TENB (B)

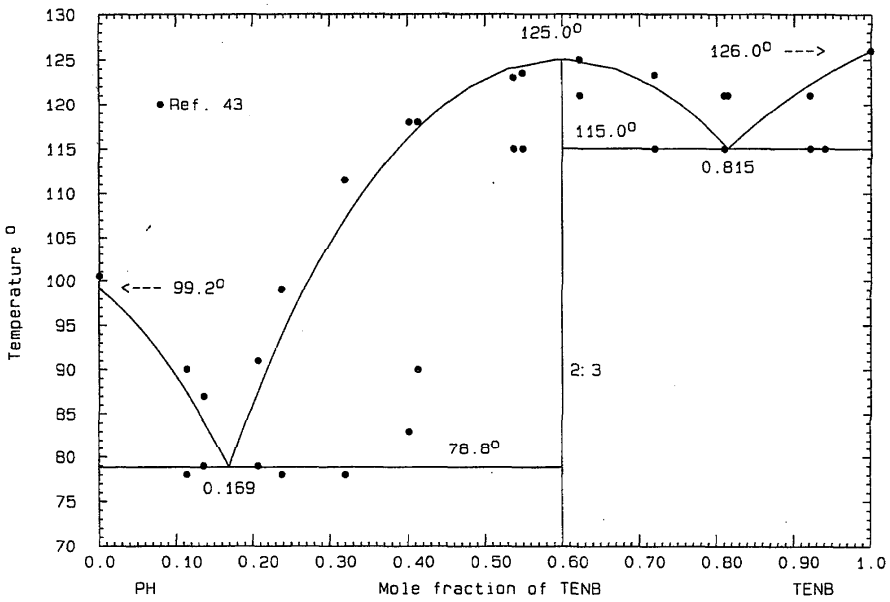

FIG. 54. The system PH (A)+TENB (B)

reported eutectics are E_1=84.0 °C, x_B=0.20 and E_2=110.0 °C, x_B=0.747. The 1:1 compound melts congruently at 134.0 °C. Optimization of LHS and RHS liquidus data gave

$$G^E(l)=x_A x_B(-13\,400+4650x_B)\ \text{J mol}^{-1} \quad (118)$$

and for the compound (AB)/2

$$\Delta_{fus}G^0=16\,555-40.6607T\ \text{J mol}^{-1}, \quad (119)$$

$$\Delta_f G^0=-19\,324+34.8988T\ \text{J mol}^{-1}. \quad (120)$$

The phase diagram, Fig. 56, was calculated with the use of Eqs. (118) and (120) and shows eutectics E_1=84.0 °C, x_B=0.192 and E_2=110.0 °C, x_B=0.747; the compound melts at 134.0 °C. The probable maximum inaccuracy in the calculated diagram is ±1°.

2.5.7. Systems Based on 2-Nitrotoluene

BZ (A)+2-NT (B)

Data were obtained by thermal analysis, with stirring,[114]

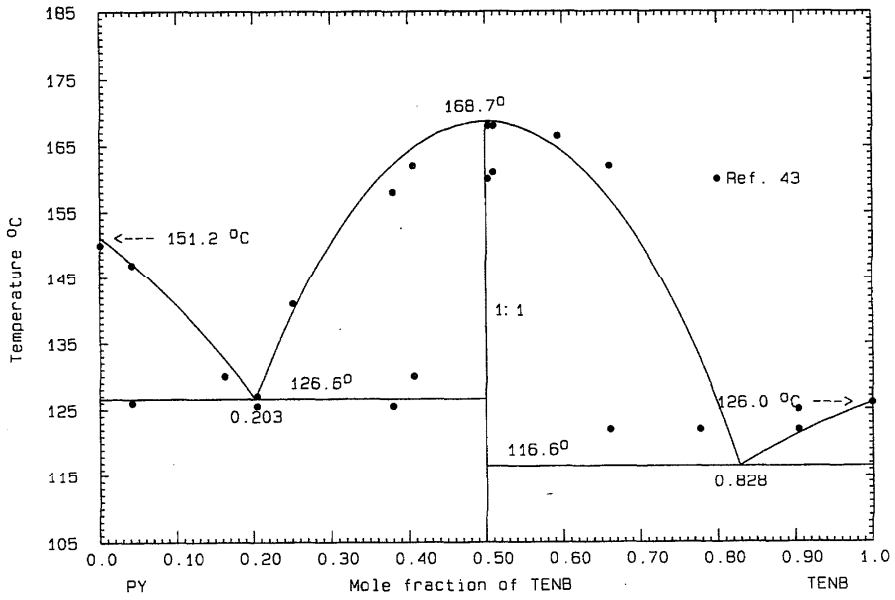

FIG. 55. The system PY (A)+TENB (B)

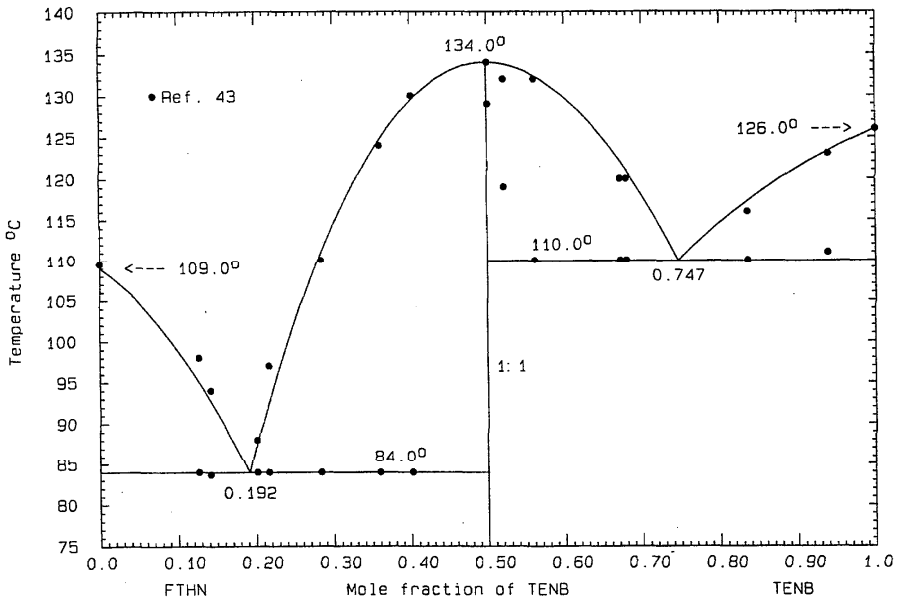

FIG. 56. The system FTHN (A)+TENB (B)

and the reported eutectic temperature is −33.3 °C (no composition given). No eutectic arrests were recorded. The data appear to be of good quality, and optimization gave the result

$$G^{E}(l)=x_A x_B(516+318x_B-1410x_B^2)\ \text{J mol}^{-1}. \quad (121)$$

The calculated phase diagram, Fig. 57, shows the eutectic −34.0 °C, $x_B=0.564$. The probable maximum inaccuracy in the calculated diagram is ±1°.

BA (A)+2-NT (B)

Data were obtained by thermal analysis with stirring[47] and there is no reported eutectic. (Tabulated eutectic arrests lay in the range −13.0 to −14.7 °C.) The data appear to be of good quality, and optimization gave the result

$$G^{E}(l)=534x_A x_B\ \text{J mol}^{-1}. \quad (122)$$

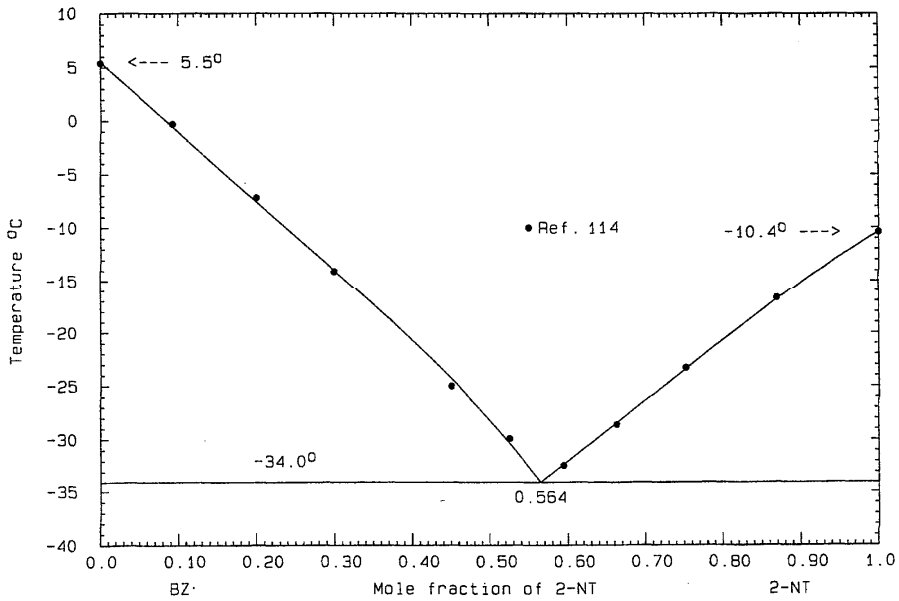

FIG. 57. The system BZ (A)+2-NT (B)

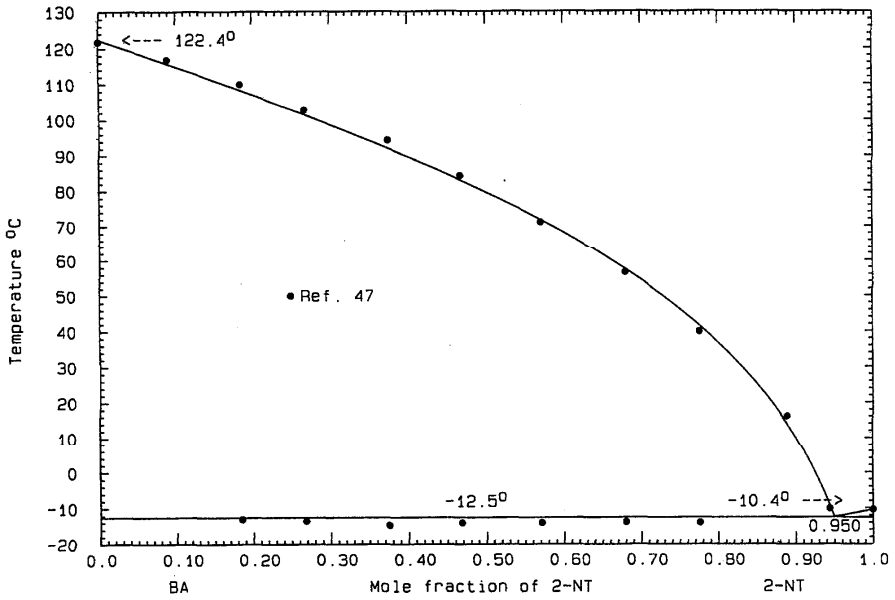

FIG. 58. The system BA (A)+2-NT (B)

The calculated phase diagram, Fig. 58, shows a calculated eutectic −12.5 °C, x_B=0.950. The probable maximum inaccuracy in the calculated diagram is ±2°.

2.5.8. Systems Based on 4-Nitrotoluene

BZ (A)+4-NT (B)

Data were obtained by thermal analysis with stirring[114] and the reported eutectic is −7.2 °C (no composition given). No eutectic arrests were recorded. The data appear to be of good quality and optimization yielded the equation

$$G^E(l)=x_A x_B(938-783x_B)\ \text{J mol}^{-1}. \quad (123)$$

The calculated phase diagram, Fig. 59, shows a calculated eutectic of −7.5 °C, x_R=0.211. The probable maximum inaccuracy in the calculated diagram is ±1°.

NA (A)+4-NT (B)

Data were obtained by the microthermal method[16] and thermal analysis.[98] The eutectic temperature is[16] 29.0 or[98] 27.0 °C, composition[98] x_B=0.62. The data of the two studies

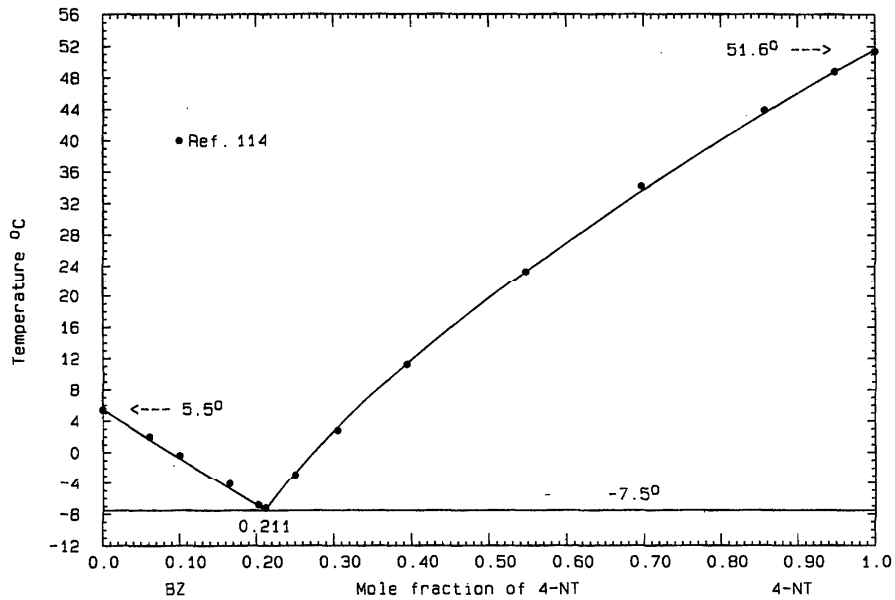

FIG. 59. The system BZ (A)+4-NT (B)

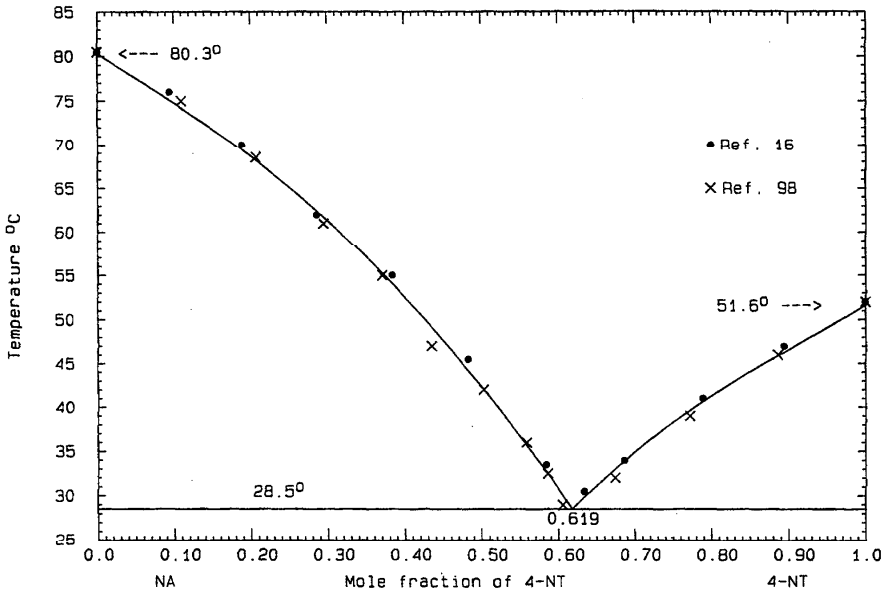

FIG. 60. The system NA (A)+4-NT (B)

agree to within 2° (no eutectic arrests were recorded). Optimization of all data yielded the result

$$G^{E}(l)=x_A x_B(-304-1915x_B+2401x_B^2)\ \text{J mol}^{-1}. \quad (124)$$

The calculated phase diagram, Fig. 60, shows a calculated eutectic 28.5 °C, $x_B=0.619$. The probable maximum inaccuracy in the calculated diagram is ±1°.

AN (A)+4-NT (B)

Data were obtained by thermal analysis[98] and the reported eutectic is −17.0 °C, $x_B=0.15$ (no eutectic arrests were recorded). The data appear to be of good quality and they were optimized to give

$$G^{E}(l)=x_A x_B(638-558x_B)\ \text{J mol}^{-1}. \quad (125)$$

The calculated phase diagram, Fig. 61, shows a calculated

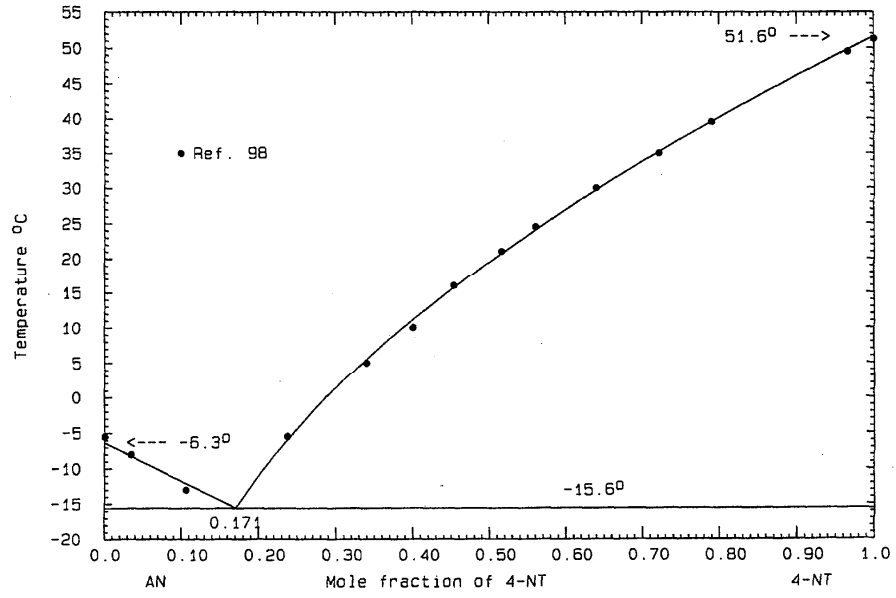

FIG. 61. The system AN (A)+4-NT (B)

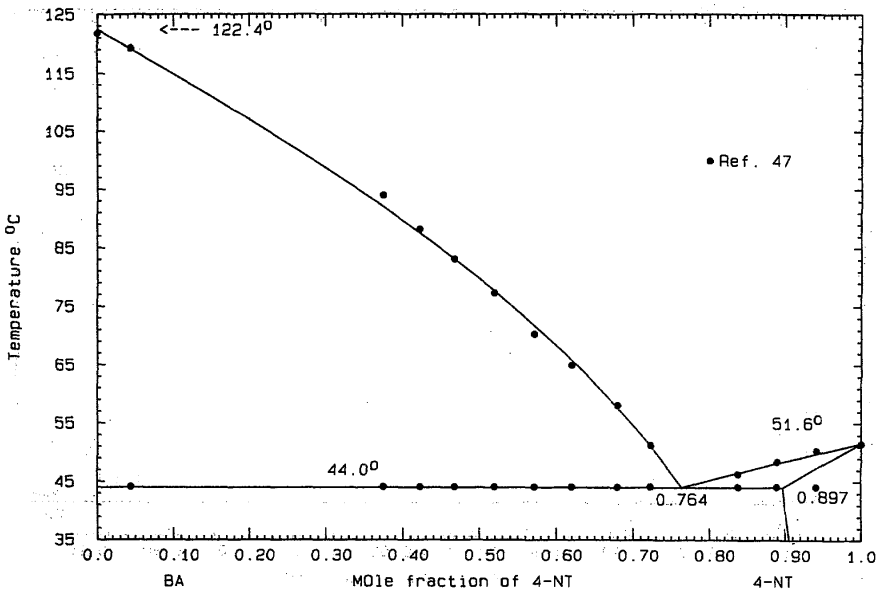

FIG. 62. The system BA (A)+4-NT (B)

eutectic −15.6 °C, x_B=0.171. The probable maximum inaccuracy in the calculated diagram is ±1°.

BA (A)+4-NT (B)

Data were obtained by thermal analysis with stirring[47] and there is no reported eutectic. The RHS liquidus definitely suggests the presence of solid solubility based on 4-nitrotoluene; the data appear to be of good quality. Optimization gave the result

$$G^E(l)=550x_Ax_B \text{ J mol}^{-1} \quad (126)$$

and the solid solution was represented by a constant Henrian activity coefficient given by

$$RT \ln \gamma_A=6000 \text{ J mol}^{-1}. \quad (127)$$

The calculated phase diagram, Fig. 62, shows a calculated eutectic 44.0 °C, x_B=0.764; there is 10.3 mol % solid solubility at the eutectic temperature. The probable maximum inaccuracy in the calculated diagram is ±1°.

SA (A)+4-NT (B)

Data were obtained by thermal analysis with stirring[83] and there is no reported eutectic (no eutectic arrests were recorded). The data appear to be of good quality; they were optimized to give the equation

$$G^E(l)=888x_Ax_B \text{ J mol}^{-1}. \quad (128)$$

The calculated phase diagram, Fig. 63, shows a calculated eutectic 48.2 °C, x_B=0.936. The probable maximum inaccuracy in the calculated diagram is ±1°.

2.5.9. Systems Based on 3,4-Dinitrotoluene

BZ (A)+3,4-DNT (B)

Liquidus data were obtained by thermal analysis[44] and the reported eutectic is −5.0 °C, x_B=0.245 (no eutectic arrests were recorded). The data appear to be of good quality; the LHS liquidus[44] definitely suggests solid solubility based on benzene. Optimization gave the equation

$$G^E(l)=x_Ax_B(-869+596x_B) \text{ J mol}^{-1}, \quad (129)$$

and the calculated phase diagram, Fig. 64, shows a calculated eutectic −5.0 °C, x_B=0.230. The solid solution was represented by a temperature-independent Henrian activity coefficient

$$RT \ln \gamma_B=4800 \text{ J mol}^{-1}. \quad (130)$$

The LHS solid solution extends to x_B=0.116 at the eutectic temperature. The probable maximum inaccuracy in the calculated diagram is ±1°.

ACN (A)+3,4-DNT (B)

Data were obtained by thermal analysis[49] and the reported eutectic is 39.0 °C, x_B=0.66. The LHS limiting liquidus slope[49] shows positive deviation from ideality, whereas the RHS shows negative deviations. This could be interpreted as some solid solubility at the LHS; however, it is probably not justifiable on this evidence alone. Optimization of data in the range $0.4<x_B<1$ gave the result

$$G^E(l)=x_Ax_B(263-1527x_B) \text{ J mol}^{-1}, \quad (131)$$

and the calculated phase diagram, Fig. 65, shows a calculated eutectic 39.0 °C, x_B=0.692. The probable maximum inaccuracy in the calculated diagram is ±2°.

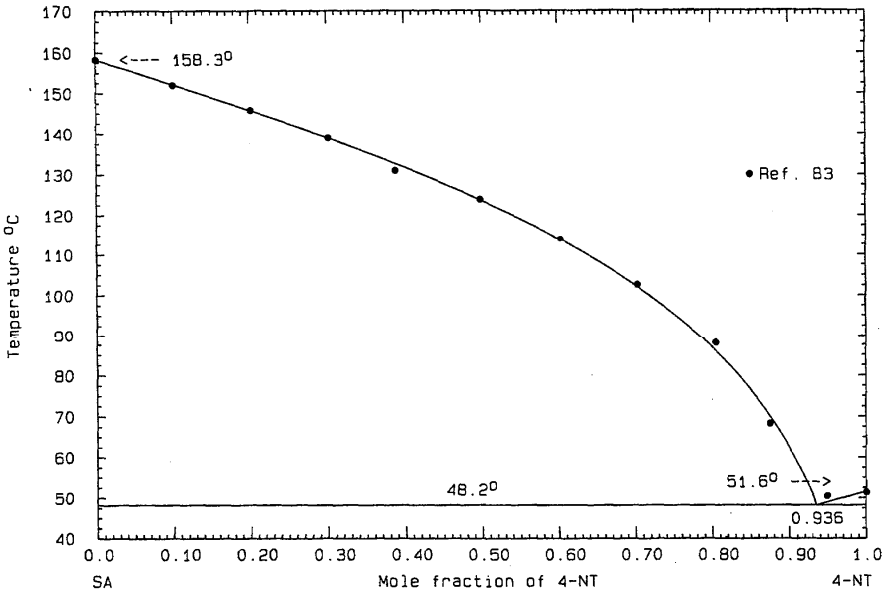

FIG. 63. The system SA (A)+4-NT (B)

FLN (A)+3,4-DNT (B)

Data were obtained by thermal analysis[49] and the reported eutectic is 37.0 °C, x_B=0.69. Data in the range $0.3<x_B<1$ were optimized, with the result

$$G^E(l)=x_A x_B(-1073-1795x_B)\ \text{J mol}^{-1}, \quad (132)$$

and the calculated phase diagram, Fig. 66, shows a eutectic 36.9 °C, x_B=0.698. The probable maximum inaccuracy in the calculated diagram is ±2°.

ANTH (A)+3,4-DNT (B)

Data were obtained by thermal analysis[49] and the reported eutectic is 55.0 °C, x_B=0.98. Only data in the range $0.3<x_B<1$ were optimized, with the result

$$G^E(l)=-1037x_A x_B\ \text{J mol}^{-1}. \quad (133)$$

The calculated phase diagram, Fig. 67, shows a calculated eutectic of 56.7 °C, x_B=0.955. The probable maximum inaccuracy in the calculated diagram is ±2°.

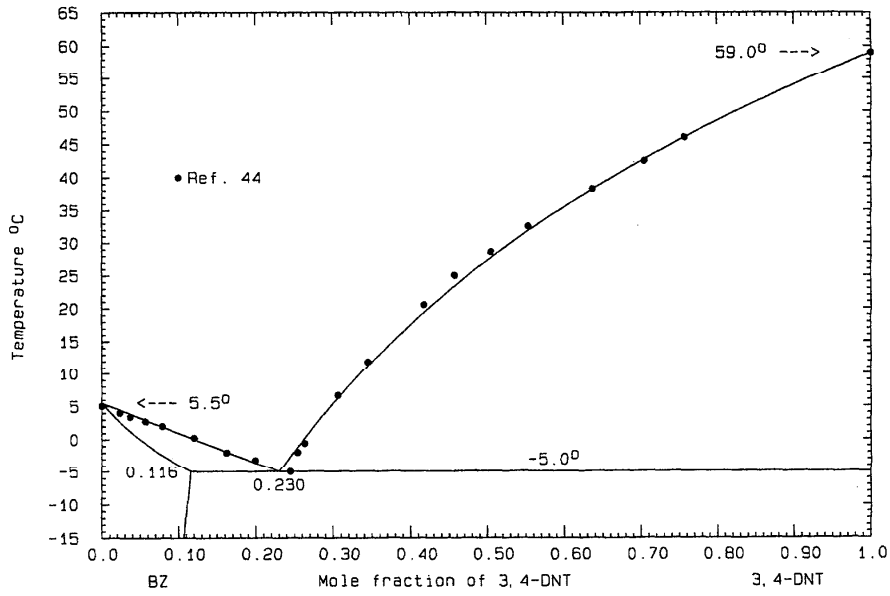

FIG. 64. The system BZ (A)+3,4-DNT (B)

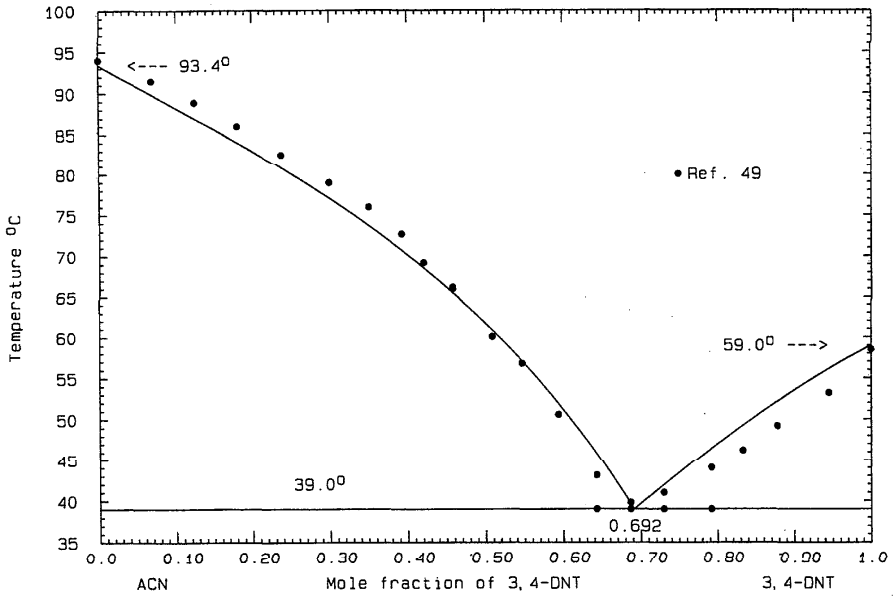

FIG. 65. The system ACN (A)+3,4-DNT (B)

PH (A)+3,4-DNT (B)

Liquidus data were obtained by thermal analysis[44] (neither eutectic arrests nor eutectic data were recorded). Data in the range $0.3<x_B<1$ were optimized to yield the equation

$$G^E(l)=x_A x_B(-155-2031x_B)\ \text{J mol}^{-1}, \quad (134)$$

and the calculated phase diagram, Fig. 68, displays a calculated eutectic 34.0 °C, $x_B=0.655$. The probable maximum inaccuracy in the calculated diagram is ±2°.

AN (A)+3,4-DNT (B)

Data were obtained by thermal analysis[49]; the reported eutectic is −17.0 °C, $x_B=0.19$. The data appear to be of fair quality, and optimization gave the result

$$G^E(l)=x_A x_B(-656-1096x_B)\ \text{J mol}^{-1}. \quad (135)$$

The calculated phase diagram, Fig. 69, shows a calculated eutectic −17.1 °C, $x_B=0.184$. The probable maximum inaccuracy in the calculated diagram is ±1°.

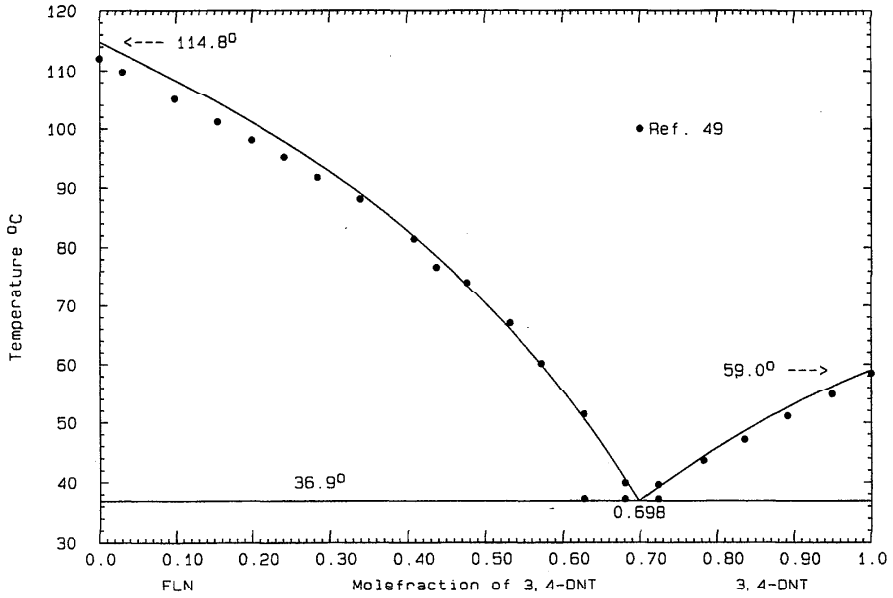

FIG. 66. The system FLN (A)+3,4-DNT (B)

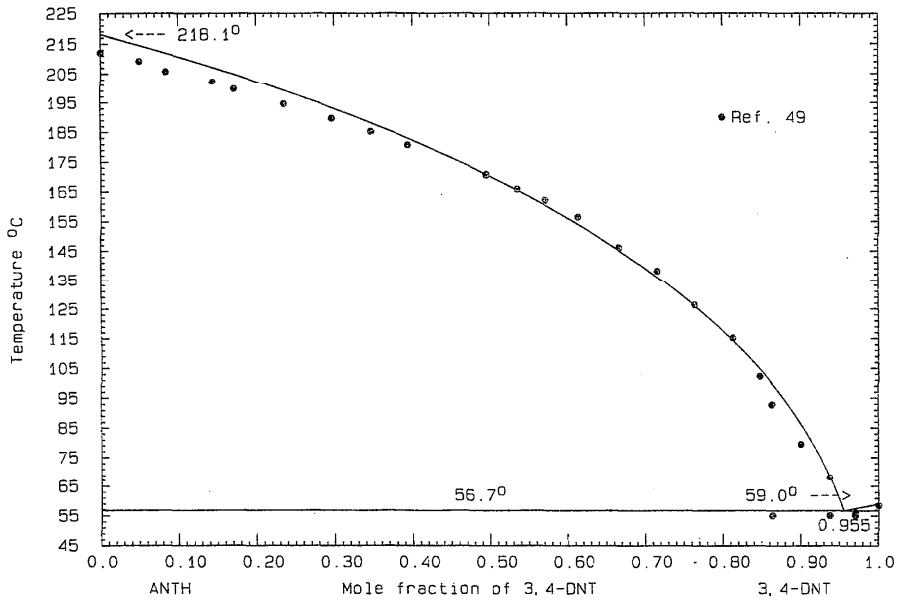

FIG. 67. The system ANTH (A)+3,4-DNT (B)

MA (A)+3,4-DNT (B)

Data were obtained by thermal analysis[49] with a reported eutectic of 11.0 °C, $x_B=0.46$. All the data were used in the optimization, which gave the result

$$G^E(l)=x_A x_B(-2150-550x_B)\ \text{J mol}^{-1}. \quad (136)$$

The calculated phase diagram, Fig. 70, shows a eutectic 11.0 °C, $x_B=0.446$. The probable maximum inaccuracy in the calculated diagram is $\pm 1°$.

1-AN (A)+3,4-DNT (B)

Data were obtained by thermal analysis[49] and the reported eutectic is −10.0 °C, $x_B=0.40$. The RHS liquidus data show a somewhat abrupt change in curvature, which may not represent true behavior. In preliminary calculations, it was found that close adherence to the low-temperature liquidus data points implied a eutectic temperature about 3° higher than observed. It was decided to deduce $G^E(l)$ directly from the reported eutectic; this gave

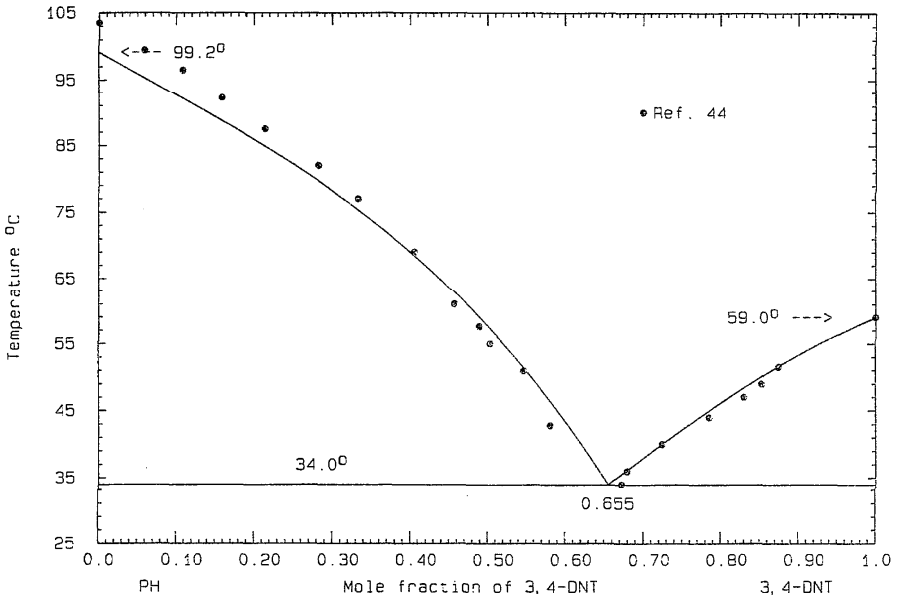

FIG. 68. The system PH (A)+3,4-DNT (B)

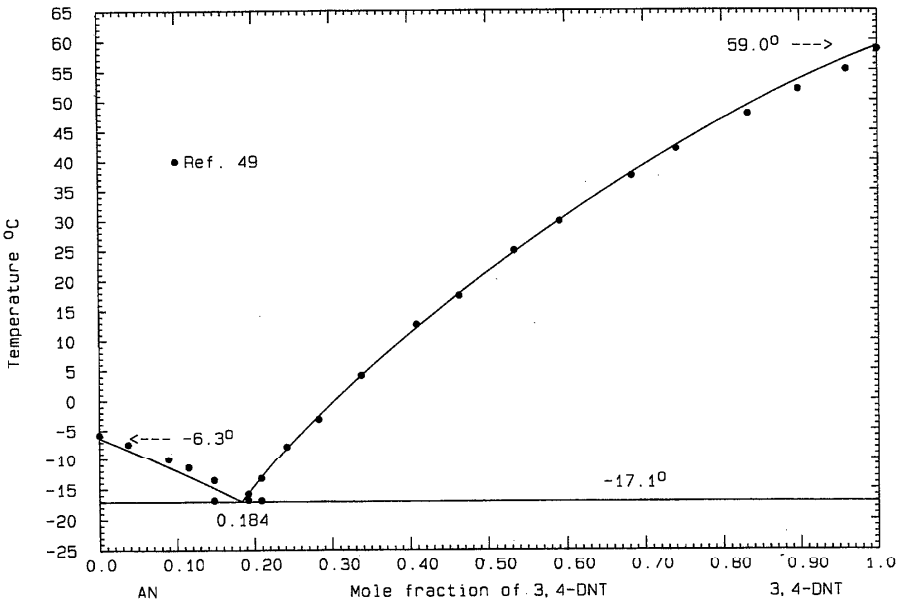

FIG. 69. The system AN (A)+3,4-DNT (B)

$$G^{E}(l)=x_A x_B(-8342+3804x_B)\ \text{J mol}^{-1}. \quad (137)$$

The calculated phase diagram, Fig. 71, therefore shows exact agreement with the reported eutectic. The probable maximum inaccuracy in the calculated diagram is ±3°.

2-AN (A)+3,4-DNB (B)

Data were obtained by thermal analysis[49] and the reported eutectic is 33.0 °C, $x_B=0.67$. Only data in the range $0.35<x_B<1$ were optimized, with the result

$$G^{E}(l)=x_A x_B(-4824+665x_B)\ \text{J mol}^{-1}. \quad (138)$$

The calculated phase diagram, Fig. 72, shows a calculated eutectic 33.3 °C, $x_B=0.669$. The probable maximum inaccuracy in the calculated diagram is ±2°.

2.5.10. Systems Based on 2,6-Dinitrotoluene

BZ (A)+2,6-DNT (B)

Liquidus data were obtained by thermal analysis[44]; neither eutectic data nor eutectic arrests were recorded. Data in the range $0<x_B<0.7$ were optimized, with the result

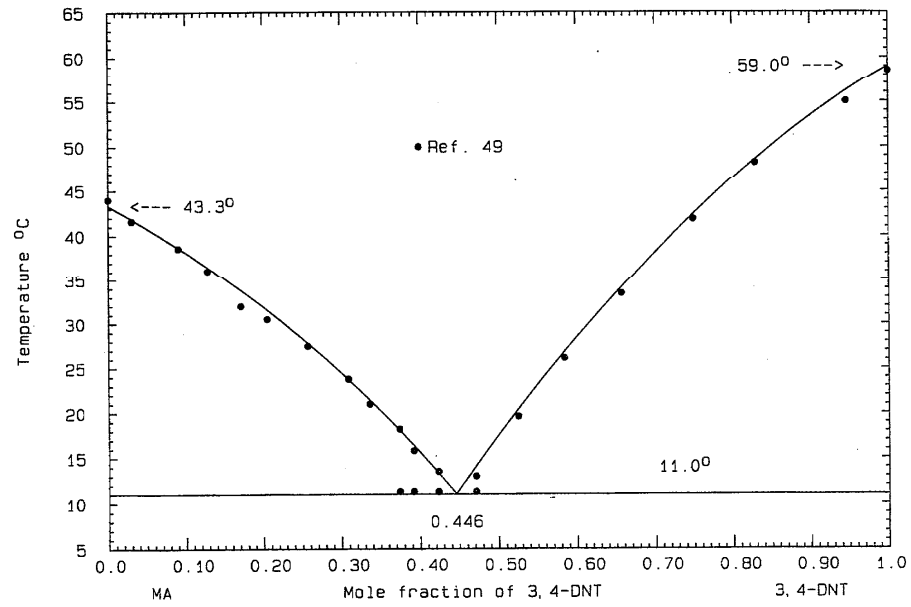

FIG. 70. The system MA (A)+3,4-DNT (B)

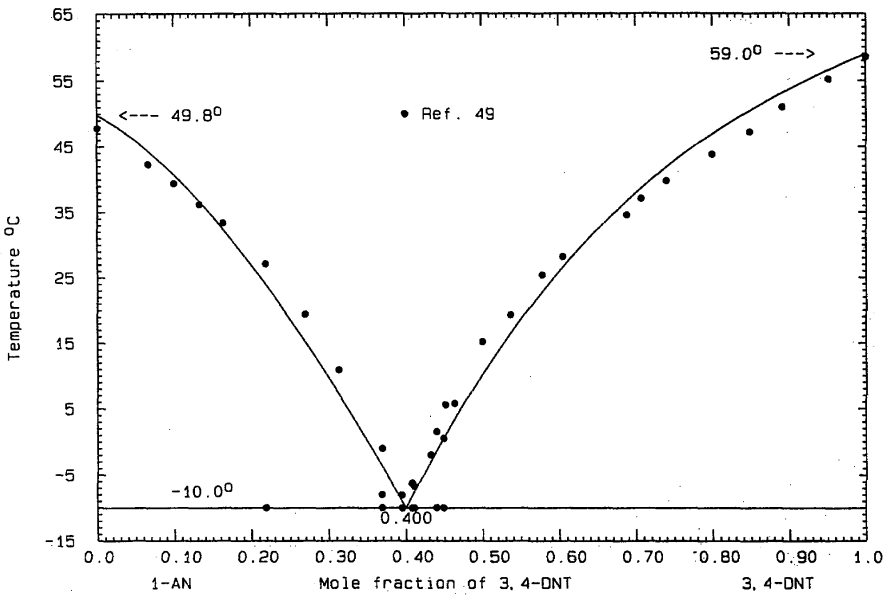

FIG. 71. The system 1-AN (A)+3,4-DNT (B)

$$G^{E}(l)=x_A x_B(1408-2779x_B)\ \text{J mol}^{-1}, \quad (139)$$

and the calculated phase diagram, Fig. 73, shows a calculated eutectic 0.1 °C, $x_B=0.094$. The probable maximum inaccuracy in the calculated diagram is ±1°.

ACN (A)+2,6-DNT (B)

Data were obtained by thermal analysis[49] and the reported eutectic is 46.0 °C, $x_B=0.70$. The RHS liquidus is evidently low; in the optimization only data in the range $0<x_B<0.7$ were used:

$$G^{E}(l)=x_A x_B(-1590+6182x_B-7494x_B^2)\ \text{J mol}^{-1}. \quad (140)$$

The calculated phase diagram, Fig. 74, shows a calculated eutectic 46.0 °C, $x_B=0.677$. The probable maximum inaccuracy in the calculated diagram is ±1°.

FLN (A)+2,6-DNT (B)

Data were obtained by thermal analysis[49] and the reported eutectic is 46.0 °C, $x_B=0.68$. The RHS liquidus is low, and preliminary calculations showed that the LHS liquidus ther-

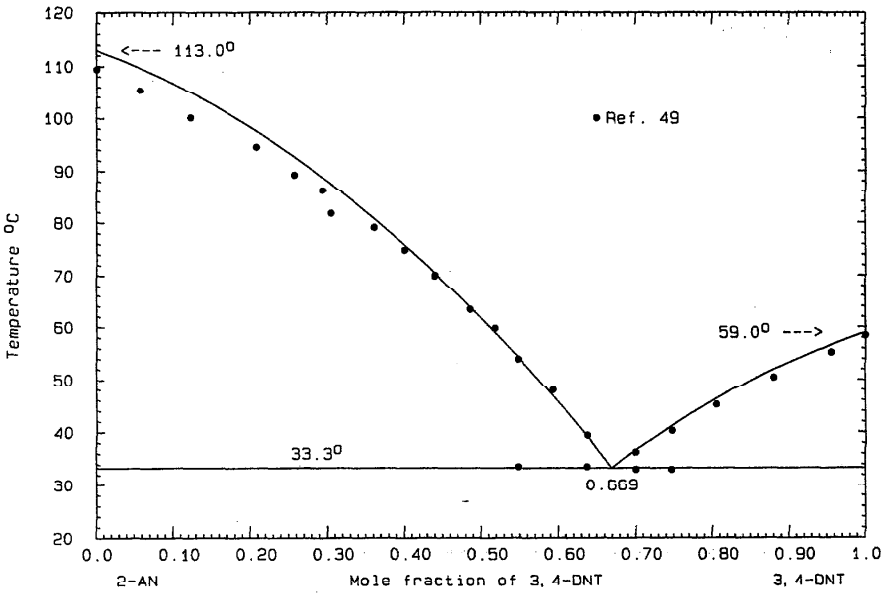

FIG. 72. The system 2-AN (A)+3,4-DNT (B)

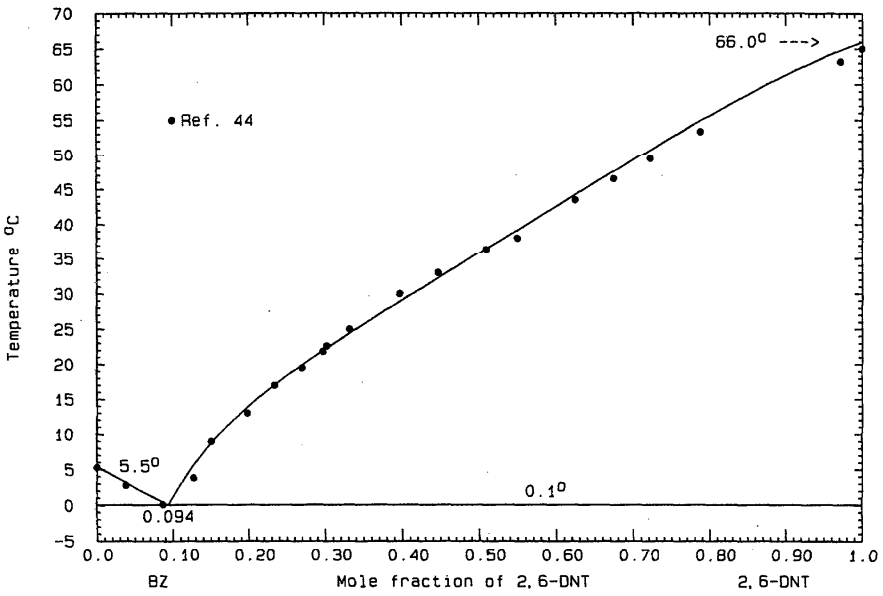

FIG. 73. The system BZ (A)+2,6-DNT (B)

modynamically implies a eutectic temperature higher than that observed. Data in the range $0.3<x_B<0.65$ were optimized and the result

$$G^E(l)=x_A x_B(-2378+4049x_B-3798x_B^2)\ \text{J mol}^{-1} \tag{141}$$

was used to calculated the phase diagram, Fig. 75. The calculated eutectic is 47.5 °C, $x_B=0.669$. The probable maximum inaccuracy in the calculated diagram is ±2°.

ANTH (A)+2,6-DNT (B)

Data were obtained by thermal analysis[49] and the reported eutectic is 54.0 °C, $x_B=0.94$. Both LHS and RHS limiting liquidus slopes[49] are faulty and both pure component melting points are low; the reported eutectic temperature was therefore disregarded in the optimization. Only data in the range $0.4<x_B<0.9$ were optimized, with the result

$$G^E(l)=-3996x_A x_B\ \text{J mol}^{-1}. \tag{142}$$

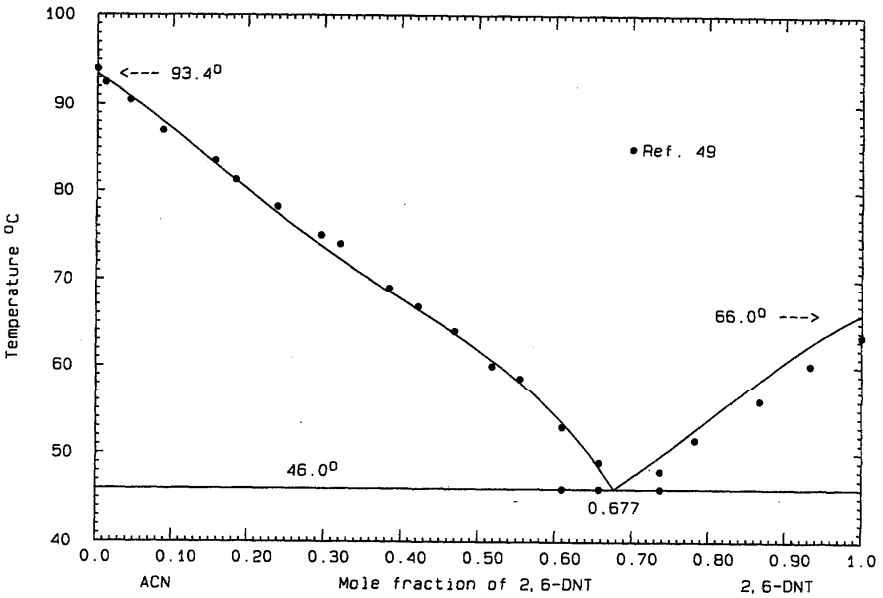

FIG. 74. The system ACN (A)+2,6-DNT (B)

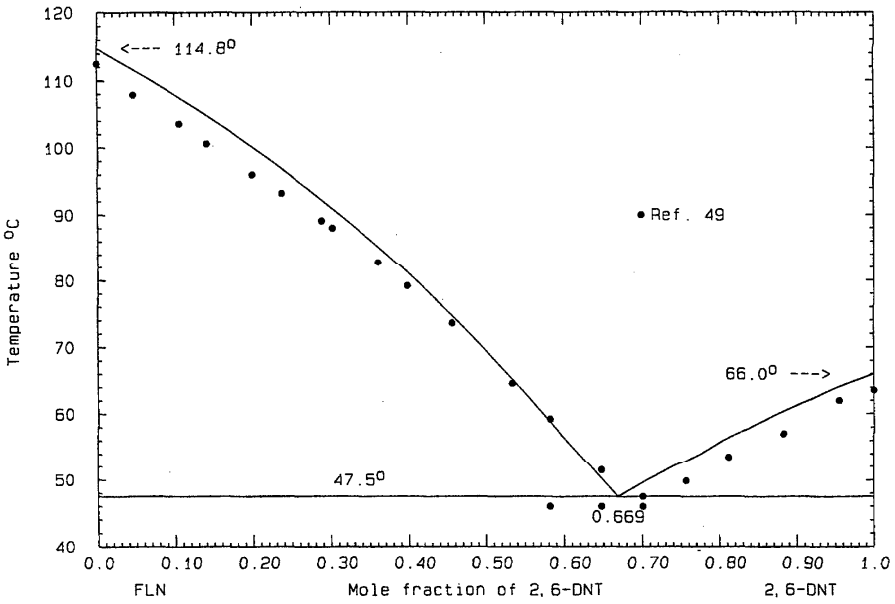

FIG. 75. The system FLN (A)+2,6-DNT (B)

The phase diagram, calculated with the use of Eq. (142), is given in Fig. 76 and shows a calculated eutectic 60.6 °C, x_B=0.888. As explained above, this eutectic temperature is considered to be more accurate than the one observed. The probable maximum inaccuracy in the calculated diagram is ±10°.

PH (A)+2,6-DNT (B)

Liquidus data were obtained from thermal analysis[44] and there are no reported eutectic data or eutectic arrests. Only data in the range $0.3<x_B<0.8$ were optimized and the result

$$G^E(l)=x_A x_B(12-2925x_B)\ \text{J mol}^{-1} \qquad (143)$$

was used to calculate the phase diagram, Fig. 77. The calculated eutectic is 40.5 °C, x_B=0.616. The probable maximum inaccuracy in the calculated diagram is ±2°.

MA (A)+2,6-DNT (B)

Data were obtained by thermal analysis[49] and the reported

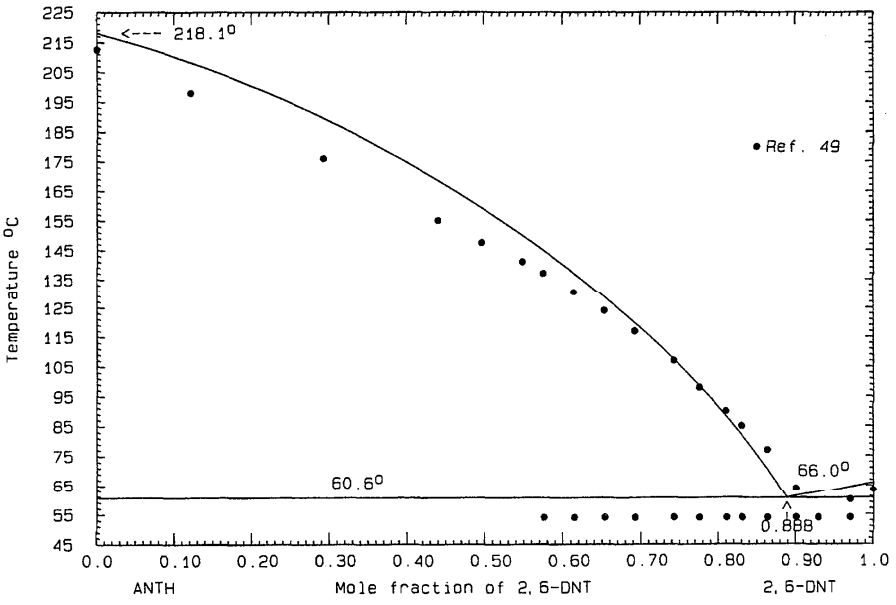

FIG. 76. The system ANTH (A)+2,6-DNT (B)

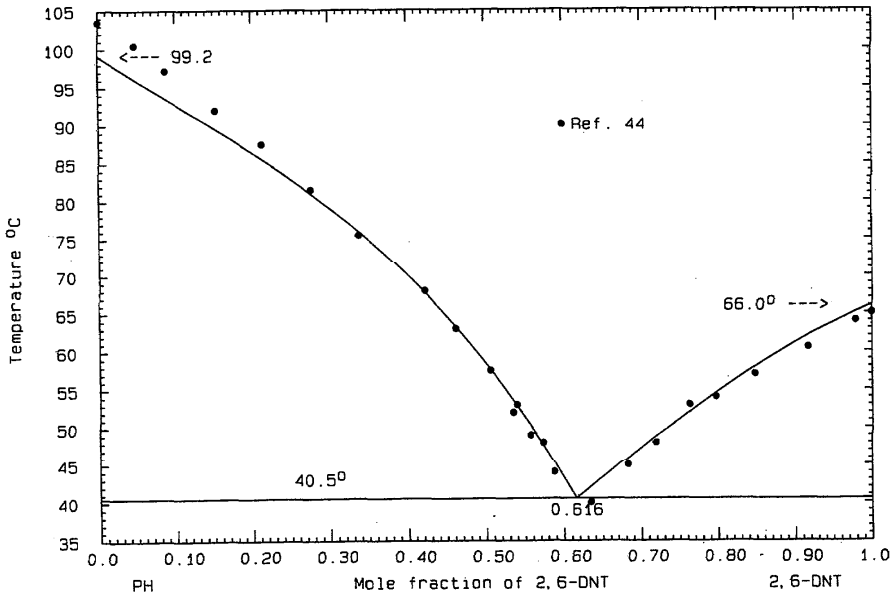

FIG. 77. The system PH (A)+2,6-DNT (B)

eutectic is 18.0 °C, x_B=0.32. All data were used in the optimization, with the result

$$G^E(l)=x_A x_B(-3060+3216x_B-3476x_B^2)\ \text{J mol}^{-1}. \quad (144)$$

The calculated phase diagram, Fig. 78, displays a calculated eutectic 18.0 °C, x_B=0.355. The probable maximum inaccuracy in the calculated diagram is ±1°.

1-AN (A)+2,6-DNT (B)

Liquidus data were obtained by thermal analysis[49] and the reported eutectic is 7.5 °C, x_B=0.32 (no eutectic arrests were recorded). Only data in the range $0<x_B<0.7$ were optimized; the result is

$$G^E(l)=x_A x_B(-6229+7737x_B-7374x_B^2)\ \text{J mol}^{-1}. \quad (145)$$

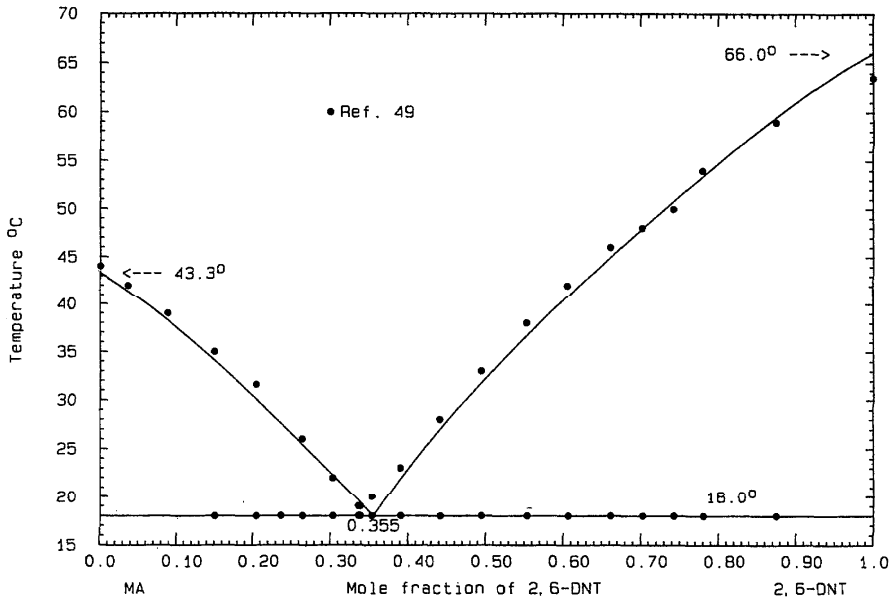

FIG. 78. The system MA (A)+2,6-DNT (B)

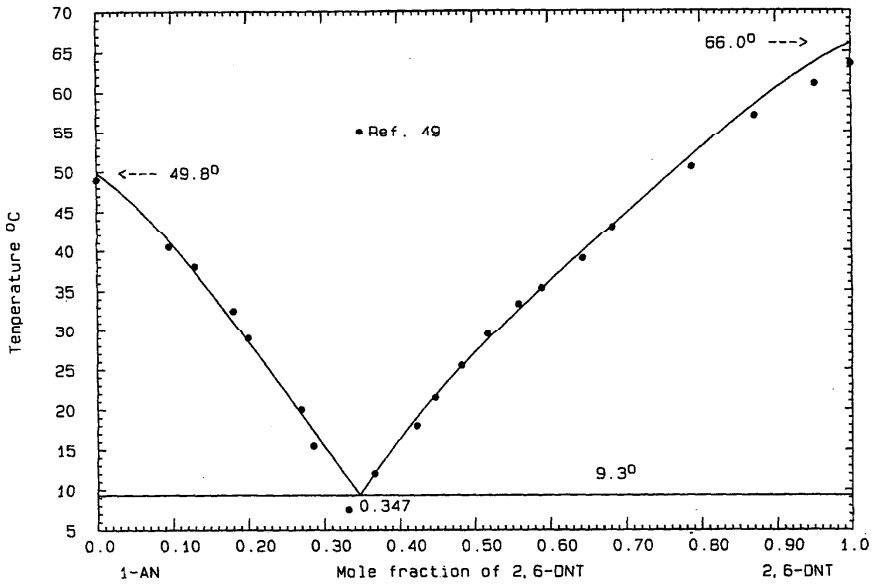

FIG. 79. The system 1-AN (A)+2,6-DNT (B)

The phase diagram, Fig. 79, was calculated with the use of Eq. (145) and the calculated eutectic is 9.3 °C, x_B=0.347. The two liquidus data points[49] near x_B=0.3 may be erroneously low, as they are noticeably out of line with the remainder of the set. The probable maximum inaccuracy in the calculated diagram is ±2°.

2-AN (A)+2,6-DNT (B)

Data were obtained by thermal analysis[49] and the reported eutectic is 45.0 °C, x_B=0.71. Both LHS and RHS component melting points are low and in preliminary calculations it was ascertained that a eutectic temperature of 45 °C was not consistent with the LHS liquidus. Data in the range $0.3<x_B<0.7$ were optimized, with the result

$$G^E(l)=x_A x_B(-4754+8345x_B-6775x_B^2)\ \text{J mol}^{-1}, \quad (146)$$

which was used to calculate the phase diagram, Fig. 80. The calculated eutectic is 47.7 °C, x_B=0.686. For reasons given above, the calculated eutectic temperature is probably more accurate than the observed. The probable maximum inaccuracy in the calculated diagram is ±2°.

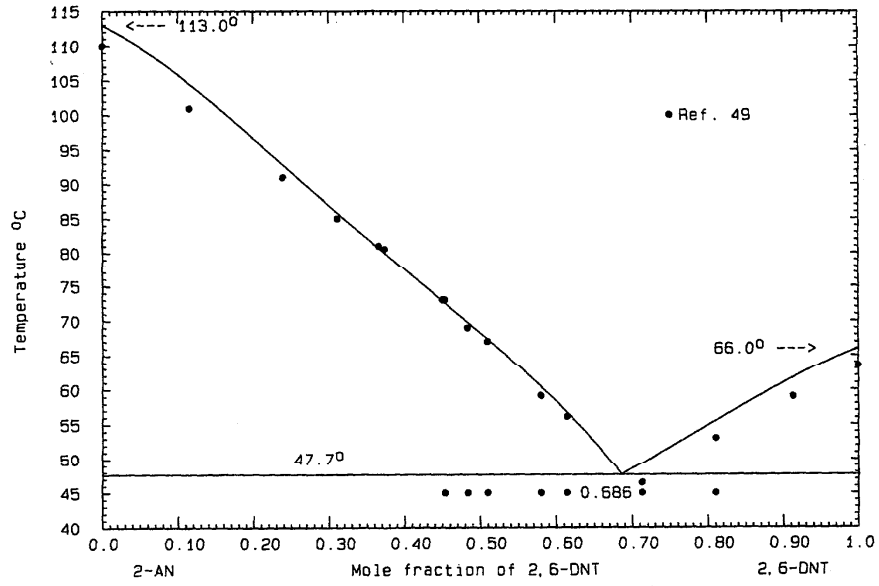

FIG. 80. The system 2-AN (A)+2,6-DNT (B)

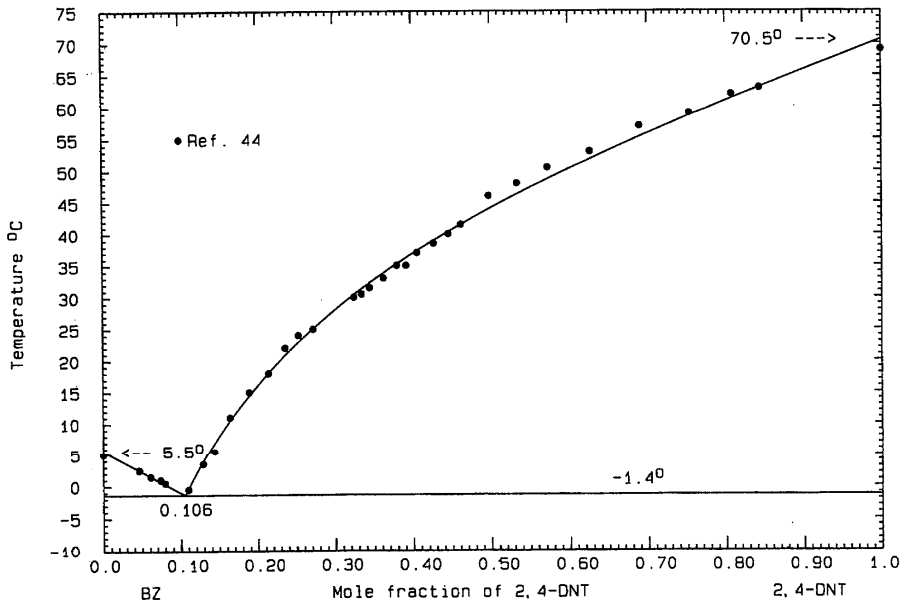

FIG. 81. The system BZ (A)+2,4-DNT (B)

2.5.11. Systems Based on 2,4-Dinitrotoluene

BZ (A)+2,4-DNT (B)

Liquidus data were obtained by thermal analysis[44]; neither eutectic arrests nor eutectic data were recorded. The data appear to be of good quality and optimization yielded the equation

$$G^{E}(l)=855x_{A}x_{B}\ \text{J mol}^{-1}. \quad (147)$$

The calculated phase diagram, Fig. 81, shows a calculated eutectic −1.4 °C, x_B=0.106. The probable maximum inaccuracy in the calculated diagram is ±1°.

NA (A)+2,4-DNT (B)

Liquidus data were obtained by thermal analysis[98] and the microthermal method.[16] A eutectic summary is given in Table 12. The 1:1 compound melts congruently[98] at 59.0 °C. The agreement between the data sets[16,98] is quite good, within 1°–2°. Optimization gave

$$G^{E}(l)=-820x_{A}x_{B}\ \text{J mol}^{-1} \quad (148)$$

and for the compound (AB)/2,

$$\Delta_{fus}G^{0}=18\,378-55.1213T\ \text{J mol}^{-1}, \quad (149)$$

$$\Delta_{f}G^{0}=-18\,583+49.3602T\ \text{J mol}^{-1}. \quad (150)$$

TABLE 12. Reported eutectic data for the system NA (A)+2,4-DNT (B)

	°C	x_B	Ref.
E_1	57.0	···	16
	56.0	0.31	98
E_2	54.0	···	16
	63.0	0.72	98

The phase diagram, Fig. 82, was calculated with the use of Eqs. (148) and (150) and shows calculated eutectics E_1=57.2 °C, x_B=0.341 and E_2=54.5 °C, x_B=0.715. The compound melts congruently at 60.2 °C. The probable maximum inaccuracy in the calculated diagram is ±1°.

FLN (A)+2,4-DNT (B)

Data were obtained by thermal analysis[99] and the reported eutectic is 44.0 °C, x_B=0.60. The limiting liquidus slope on the RHS is significantly different from thermodynamic expectation, suggesting that this part of the liquidus may lie too high. Liquidus data in the range $0.3<x_B<1$ were optimized, with the result

$$G^{E}(l)=-2858x_{A}x_{B}\ \text{J mol}^{-1}. \quad (151)$$

and the calculated phase diagram, Fig. 83, indicates a eutectic 43.1 °C, x_B=0.619. The RHS liquidus remains poorly defined experimentally and the calculated phase diagram has been effectively defined by the LHS liquidus. The probable maximum inaccuracy in the calculated diagram is ±3°.

ANTH (A)+2,4-DNT (B)

Data were obtained by thermal analysis[100] and the reported eutectic is 66.0 °C, x_B=0.91. The effect of the low experimental melting point of anthracene[100] appears to be diluted for compositions $x_B>0.3$; such data, when optimized, gave the result

$$G^{E}(l)=-1967x_{A}x_{B}\ \text{J mol}^{-1}. \quad (152)$$

The calculated phase diagram, Fig. 84, shows a calculated eutectic 66.5 °C, x_B=0.922. The probable maximum inaccuracy in the calculated diagram is ±1°.

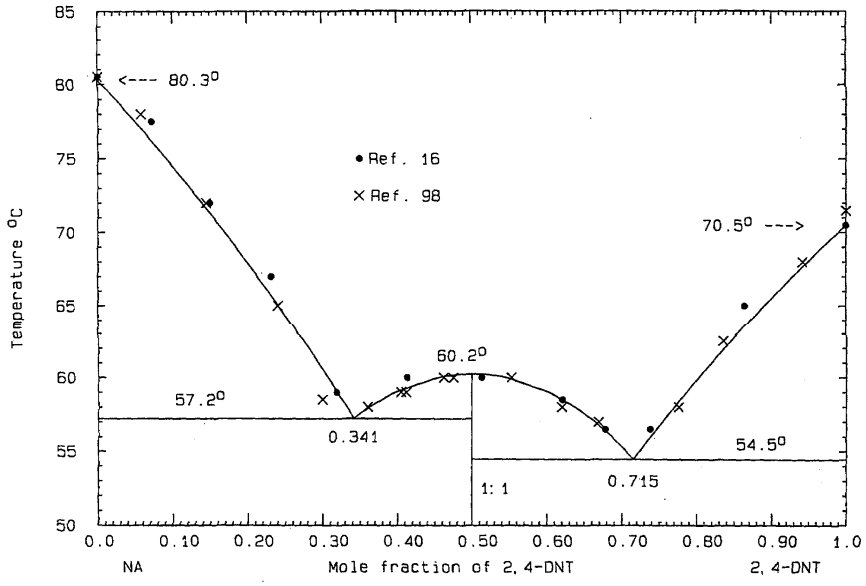

FIG. 82. The system NA (A)+2,4-DNT (B)

PH (A)+2,4-DNT (B)

Liquidus data were obtained by thermal analysis[44]; neither eutectic arrests nor eutectic data were recorded, although the data are plentiful. Data in the range $0.3<x_B<1$ were optimized, and the equation

$$G^E(l)=x_A x_B(-1063-5280x_B+4631x_B^2)\ \text{J mol}^{-1} \quad (153)$$

was used to calculate the phase diagram, Fig. 85. The calculated eutectic is 37.4 °C, $x_B=0.558$, and

$$\Delta_{fus}G^0=17\,082-48.9948T\ \text{J mol}^{-1}, \quad (158)$$

$$\Delta_f G^0=-18\,578+43.2336T\ \text{J mol}^{-1} \quad (159)$$

for the compound (AB)/2. Other calculated data are $E_1=68.0$ °C, $x_B=0.331$ and $E_2=57.0$ °C, $x_B=0.784$; the compound melts at 75.5 °C. The probable maximum inaccuracy in the calculated diagram is ±1°.

AN (A)+2,4-DNT (B)

Liquidus data were obtained by thermal analysis[98] and the

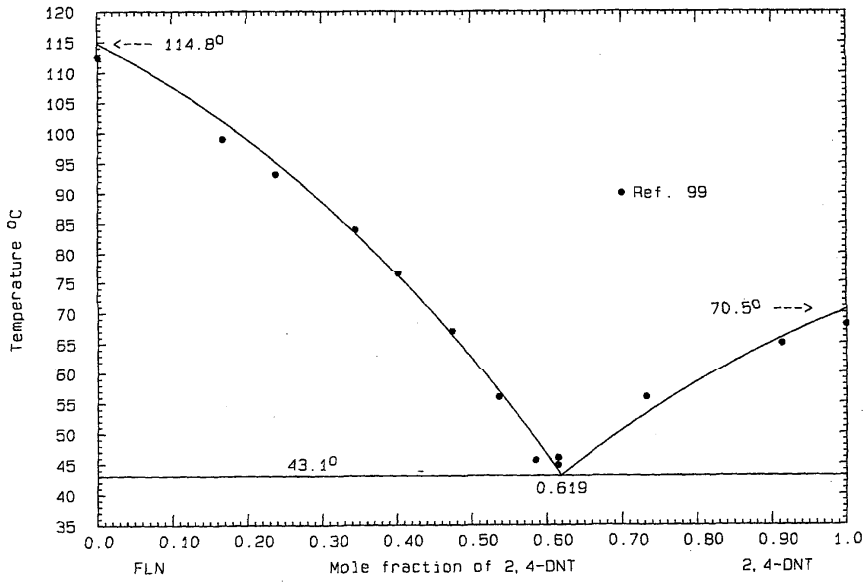

FIG. 83. The system FLN (A)+2,4-DNT (B)

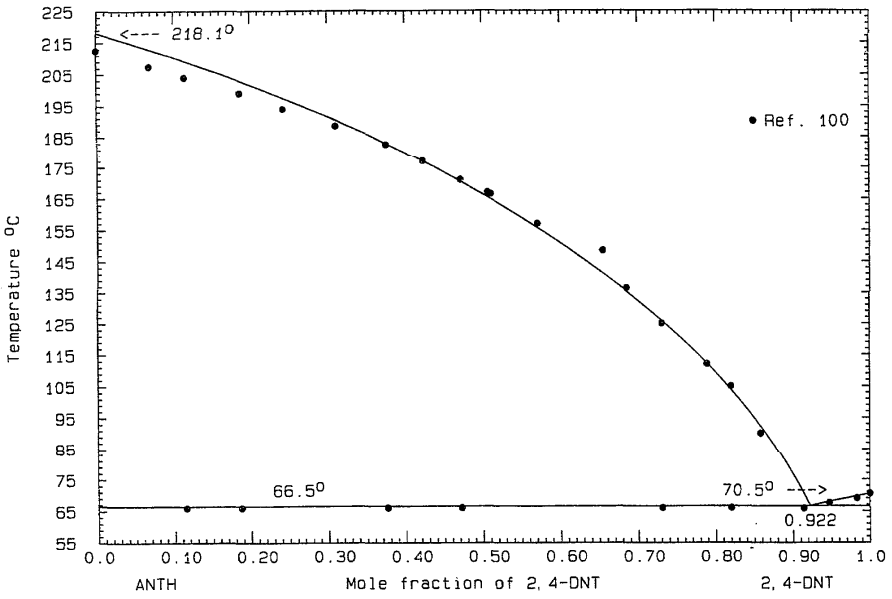

FIG. 84. The system ANTH (A)+2,4-DNT (B)

reported eutectic is −13.0 °C, x_B=0.11 (no eutectic arrests were recorded). The data appear to be of good quality, and optimization yielded the expression

$$G^E(l)=x_A x_B(-894-456x_B)\ \text{J mol}^{-1}. \quad (160)$$

The calculated phase diagram, Fig. 88, based on Eq. (160), shows a eutectic −14.0 °C, x_B=0.130. The probable maximum inaccuracy in the calculated diagram is ±1°.

MA (A)+2,4-DNT (B)

Data were obtained by Kremann and co-workers on two occasions[49,104] using thermal analysis. The reported eutectic is[101] 18.0 °C, x_B=0.38 or[49] 15.5 °C, x_B=0.37. The two sets of data are less in agreement on the RHS. In the optimization, all the data were weighted equally. The phase diagram, Fig. 89, was calculated with the use of

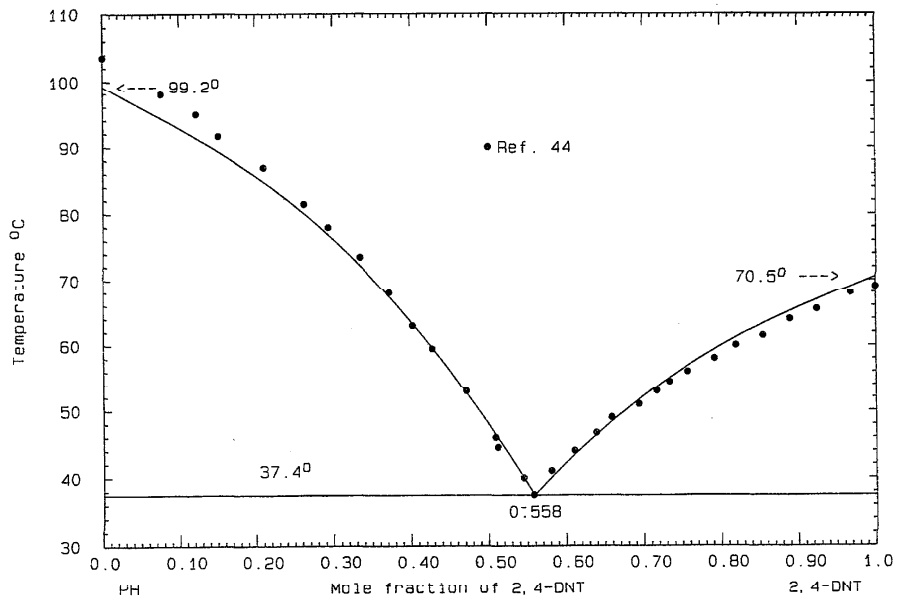

FIG. 85. The system PH (A)+2,4-DNT (B)

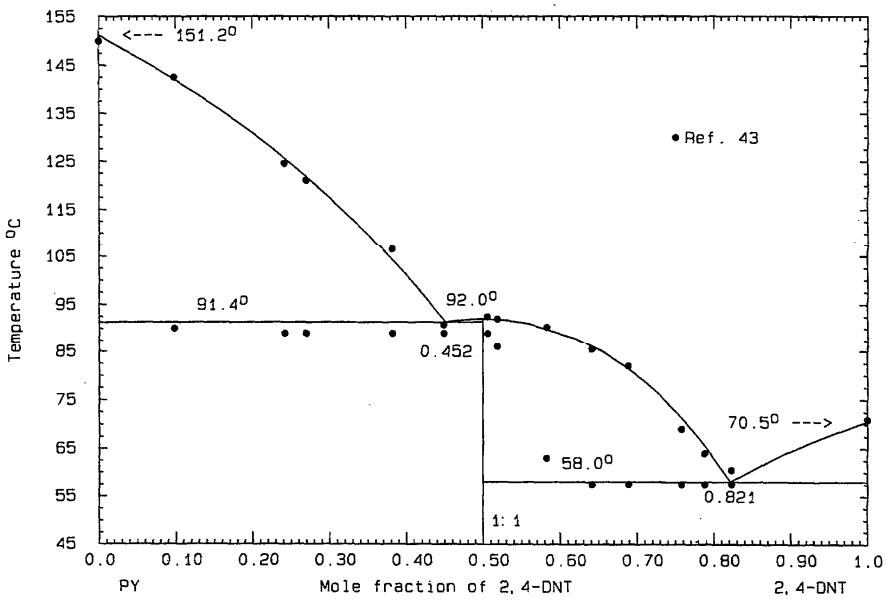

FIG. 86. The system PY (A) + 2,4-DNT (B)

$$G^{E}(l) = -2750 x_A x_B \text{ J mol}^{-1}, \quad (161)$$

and the calculated eutectic is 15.5 °C, $x_B = 0.382$. The probable maximum inaccuracy in the calculated diagram is ±2°.

1-AN (A)+2,4-DNT (B)

Liquidus data were obtained by thermal analysis[102] and the reported eutectics are $E_1 = 34.0$ °C, $x_B = 0.18$ and $E_2 = 53.0$ °C, $x_B = 0.72$. No eutectic arrests were recorded. The 1:1 compound melts congruently at 62.0 °C. The data appear to be of fair quality. All the data were used in the optimization, which yielded the expression

$$G^{E}(l) = x_A x_B(-5279 + 3000 x_B) \text{ J mol}^{-1} \quad (162)$$

for the liquid and

$$\Delta_{fus} G^0 = 13\,507 - 40.2893T \text{ J mol}^{-1}, \quad (163)$$

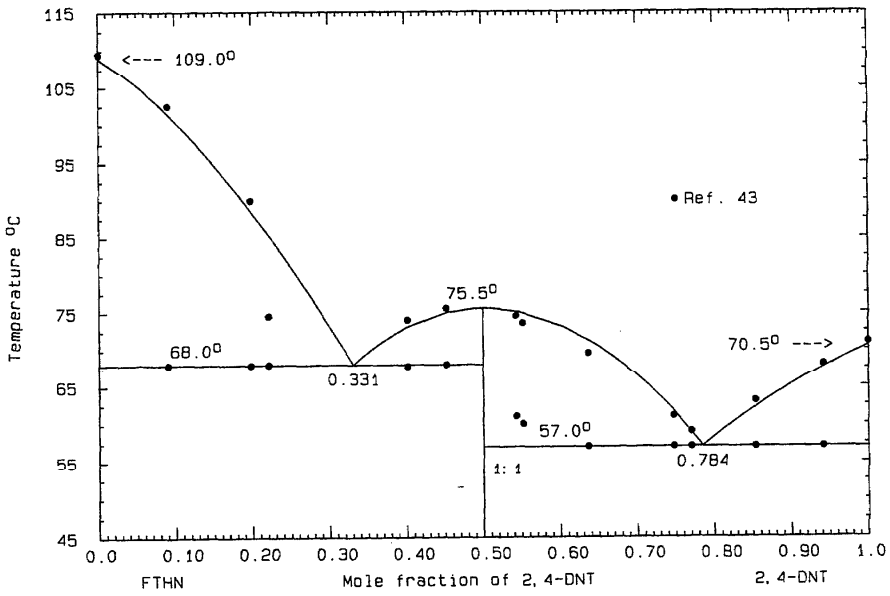

FIG. 87. The system FTHN (A)+2,4-DNT (B)

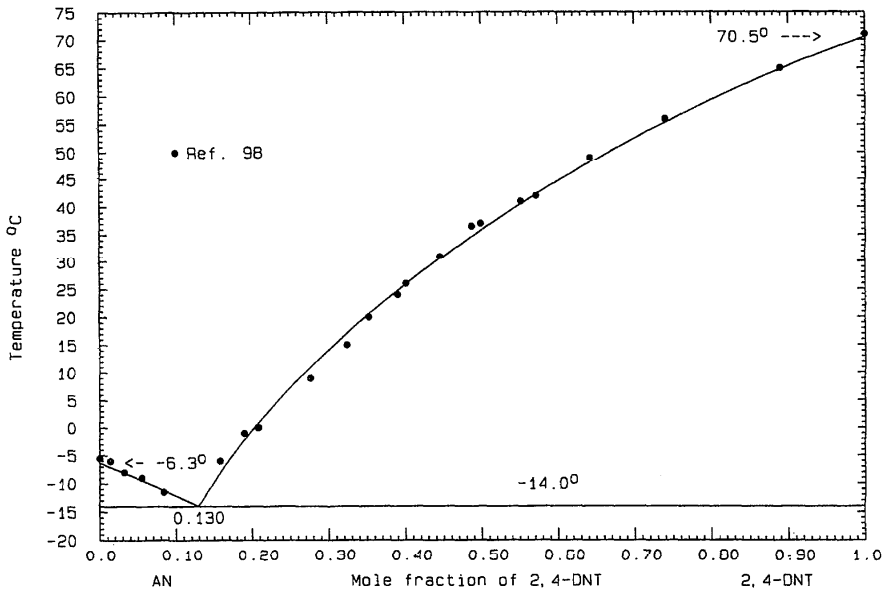

FIG. 88. The system AN (A)+2,4-DNT (B)

$$\Delta_f G^0 = -14\,608 + 34.5282T \text{ J mol}^{-1} \quad (164)$$

for the compound (AB)/2. The phase diagram, Fig. 90, was calculated with the use of Eqs. (162) and (164) and shows eutectics E_1=32.6 °C, x_B=0.185 and E_2=51.5 °C, x_B=0.710. The compound melts at 62.1 °C. The probable maximum inaccuracy in the calculated diagram is ±1°.

AN (A)+2,4-DNT (B)

Data were obtained by thermal analysis[102] and the reported eutectic is 42.0 °C, x_B=0.60. Data in the range $0.3<x_B<1$ were optimized to give

$$G^E(l) = x_A x_B(-5671 + 2399x_B) \text{ J mol}^{-1}. \quad (165)$$

The calculated phase diagram, Fig. 91, shows a eutectic 42.0 °C, x_B=0.606. The probable maximum inaccuracy in the calculated diagram is ±1°.

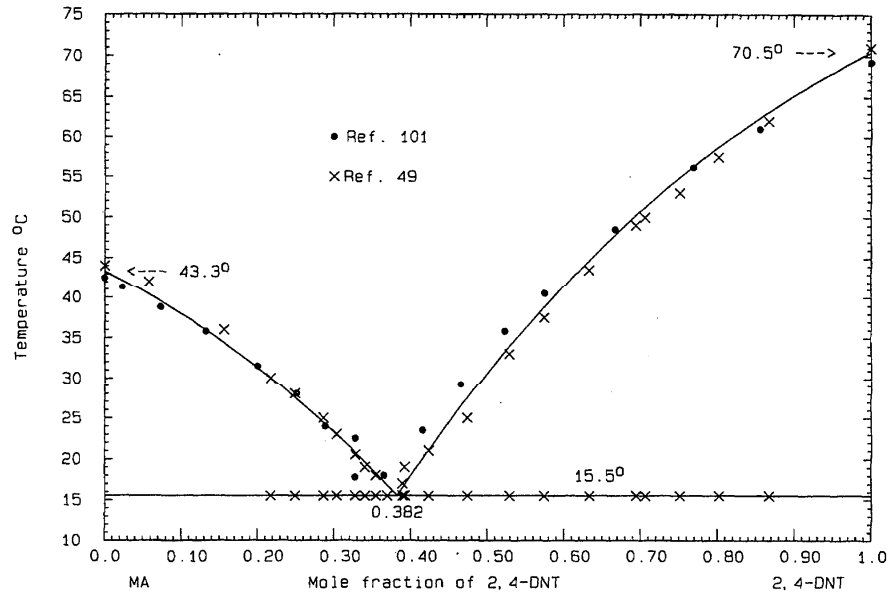

FIG. 89. The system MA (A)+2,4-DNT (B)

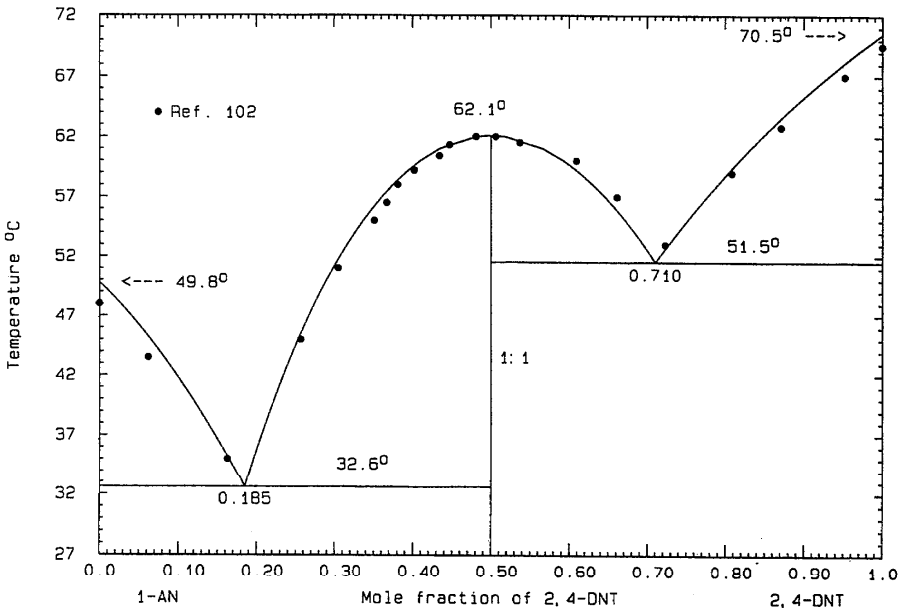

FIG. 90. The system 1-AN (A)+2,4-DNT (B)

CAR (A)+2,4-DNT (B)

Liquidus data were obtained by thermal analysis[103] and the reported eutectic is 62.0 °C, $x_B=0.88$. Data in the interval $0.2<x_B<1$ were optimized to give

$$G^E(l) = -3940 x_A x_B \text{ J mol}^{-1}, \quad (166)$$

and the calculated phase diagram, Fig. 92, shows a eutectic of 64.2 °C, $x_B=0.888$. The carbazole transition appears on the liquidus at $x_B=0.630$. The probable maximum inaccuracy in the calculated diagram is ±2°.

BA (A)+2,4-DNT (B)

Data were obtained by thermal analysis with stirring[47]; no eutectic arrests were reported, but inspection of the tabulated data[47] suggests 59 °C, $x_B=0.7$. The data appear to be of good quality, and optimization yielded the expression

$$G^E(l) = x_A x_B (1260 + 788 x_B) \text{ J mol}^{-1}. \quad (167)$$

The calculated phase diagram, Fig. 93, shows a eutectic 59.4 °C, $x_B=0.737$. The probable maximum inaccuracy in the calculated diagram is ±1°.

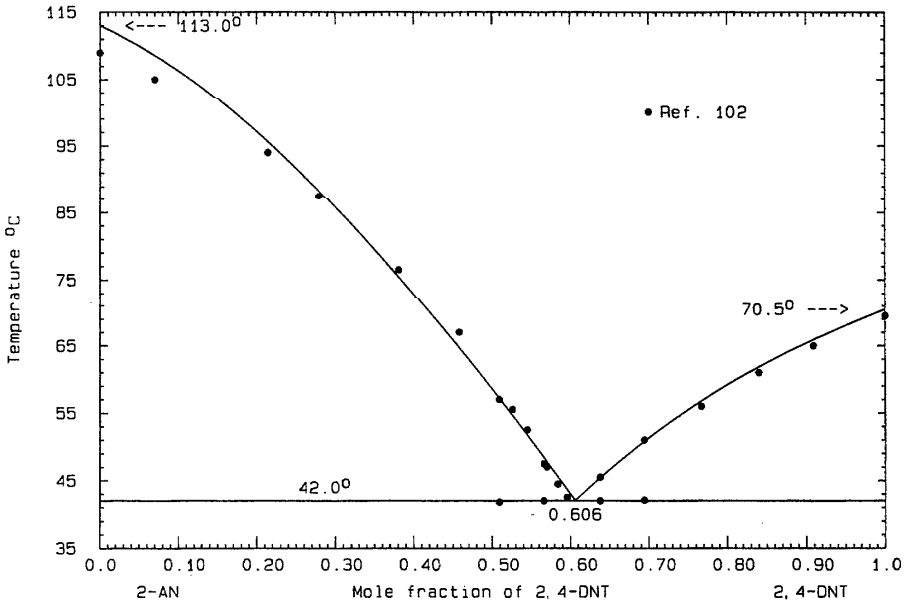

FIG. 91. The system 2-AN+2,4-DNT (B)

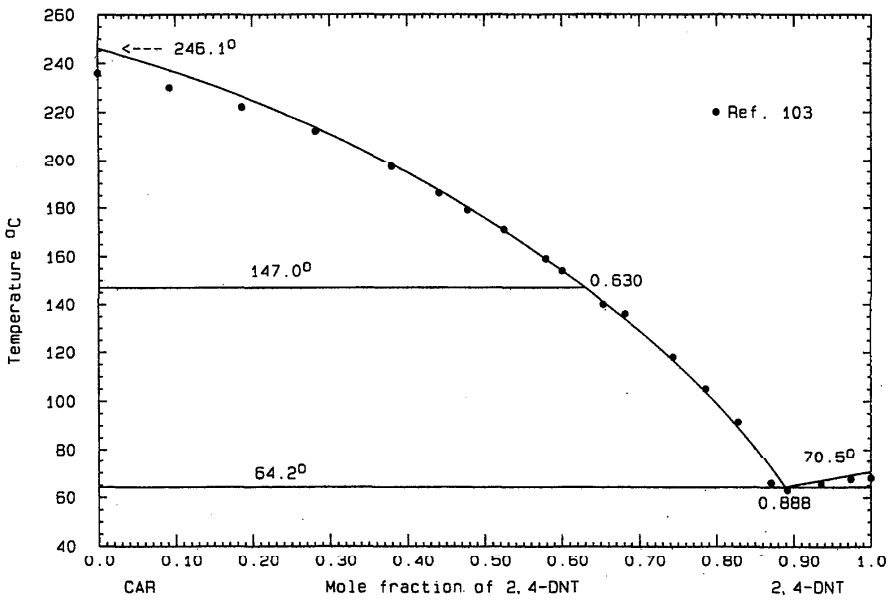

FIG. 92. The system CAR (A)+2,4-DNT (B)

HB (A)+2,4-DNT (B)

Data were obtained by thermal analysis[104] and the reported eutectic is 55.0 °C, $x_B=0.68$. Some LHS liquidus data are suspect, due to the low experimental[104] melting point of 3-hydroxybenzaldehyde; data in the interval $0.3<x_B<1$ were optimized to give

$$G^E(l)=x_Ax_B(-500+1943x_B)\ \text{J mol}^{-1}. \quad (168)$$

The calculated phase diagram, Fig. 94, shows a calculated eutectic 55.0 °C, $x_B=0.644$. The probable maximum inaccuracy in the calculated diagram is ±2°.

SA (A)+2,4-DNT (B)

Liquidus data were obtained by thermal analysis with stirring[83]; neither eutectic arrests nor eutectic data were recorded. From inspection of the tabulated data,[83] the observed eutectic would be close to 66 °C, $x_B=0.9$. The data, which appear to be of good quality, were optimized to give

$$G^E(l)=1059x_Ax_B\ \text{J mol}^{-1}, \quad (169)$$

and the calculated phase diagram, Fig. 95, shows a eutectic 65.6 °C, $x_B=0.896$. The probable maximum inaccuracy in the calculated diagram is ±2°.

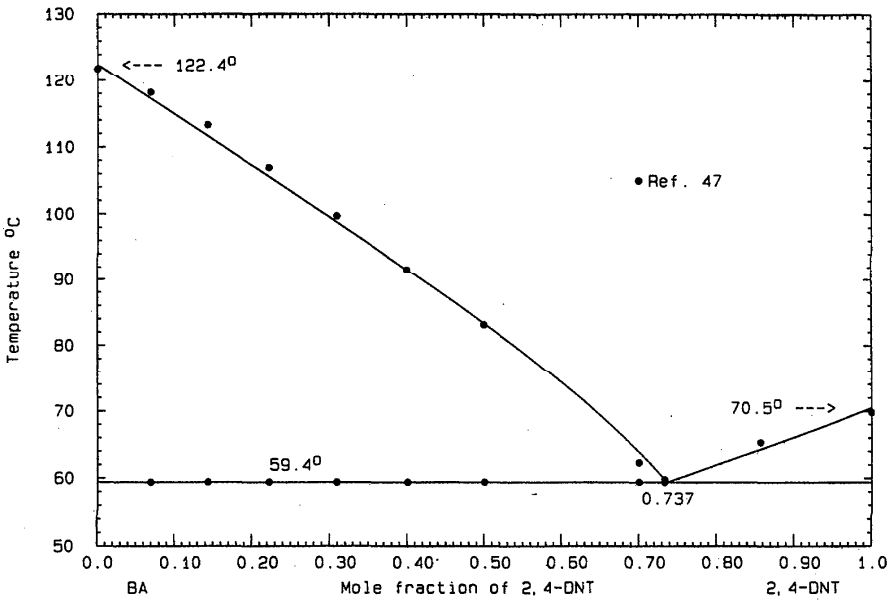

FIG. 93. The system BA (A)+2,4-DNT (B)

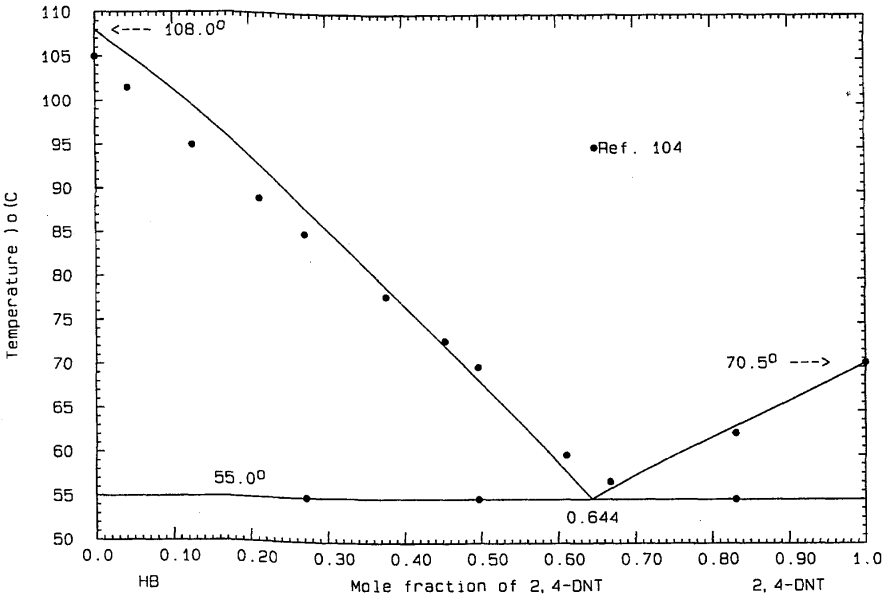

FIG. 94. The system HB (A)+2,4-DNT (B)

2.5.12. Systems Based on 2,4,6-Trinitrotoluene

NA (A)+TNT (B)

Liquidus data were obtained by thermal analysis[98] and the reported eutectics are E_1=72.0 °C, x_B=0.12 and E_2=71.0 °C, x_B=0.85 (no eutectic arrests were recorded). The 1:1 compound melts at 96.5 °C. Optimization of liquidus data yielded

$$G^E(l) = -186 x_A x_B \text{ J mol}^{-1} \quad (170)$$

for the liquid and

$$\Delta_{fus}G^0 = 18\,973 - 37.7542T \text{ J mol}^{-1}, \quad (171)$$

$$\Delta_f G^0 = -14\,019 + 31.9930T \text{ J mol}^{-1} \quad (172)$$

for the compound (AB)/2. The calculated phase diagram, Fig. 96, shows eutectics E_1=71.4 °C, x_B=0.153 and E_2=72.8 °C, x_B=0.840. The compound melts at 96.9 °C. Since the eutectic temperatures were not experimentally[98]

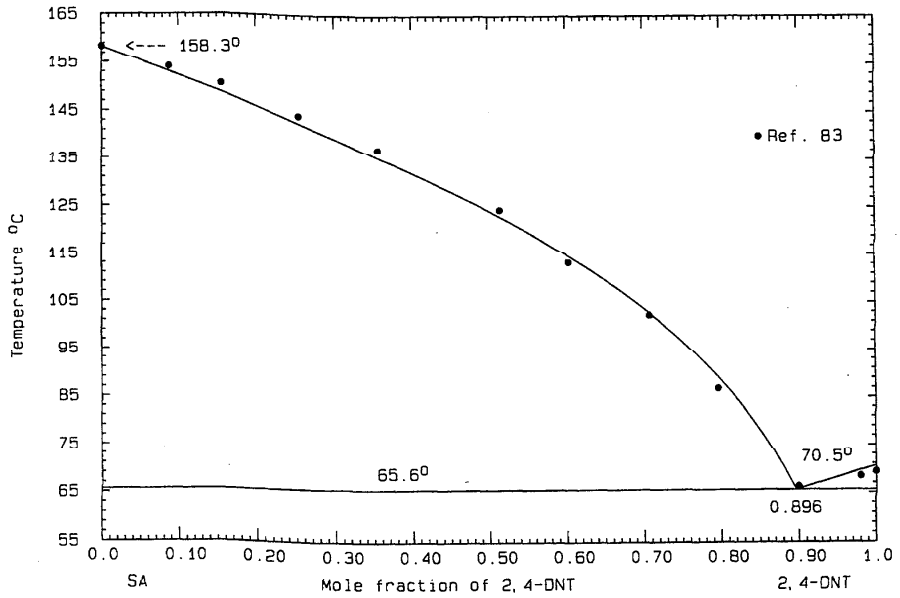

FIG. 95. The system SA (A)+2,4-DNT (B)

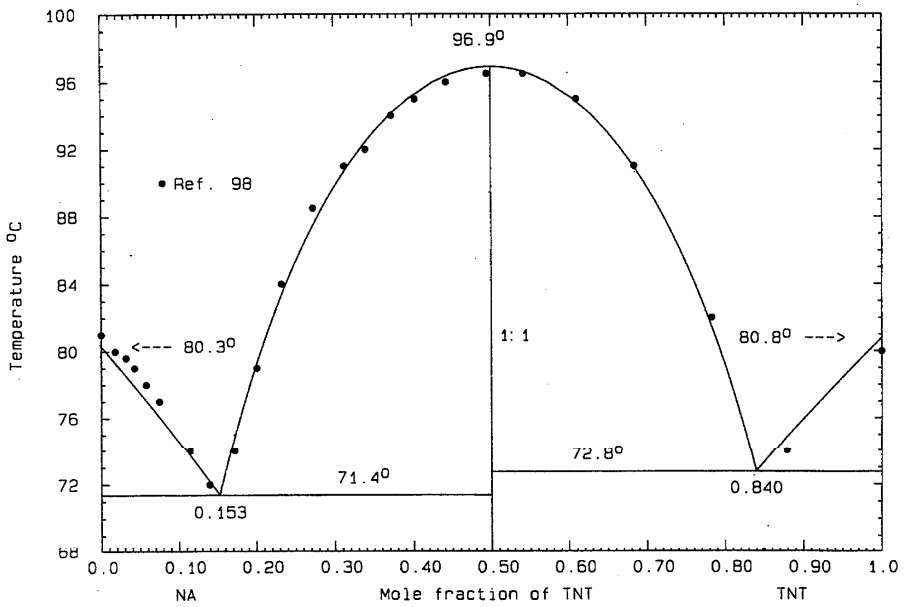

FIG. 96. The system NA (A)+TNT (B)

well defined, the calculated diagram is uncertain to this extent. The probable maximum inaccuracy in the calculated diagram is ±2°.

ACN (A)+TNT (B)

Liquidus data were obtained by thermal analysis[103] and the reported eutectics are E_1=81.0 °C, x_B=0.13 and E_2=72.0 °C, x_B=0.89. (No eutectic arrests were recorded.) The 1:1 compound melts congruently at 112.0 °C. The liquidus data for the compound are not consistent with its observed melting point and the two eutectic temperatures; it was decided to give the observed[103] eutectic temperatures more weight in the optimization. Thus for the liquid

$$G^{E}(l) = -15616 x_A x_B \text{ J mol}^{-1} \quad (173)$$

and for the compound (AB)/2

$$\Delta_{fus}G^0 = 37\,761 - 98.4569T \text{ J mol}^{-1}, \quad (174)$$

$$\Delta_f G^0 = -41\,665 + 92.6957T \text{ J mol}^{-1}. \quad (175)$$

The calculated phase diagram, Fig. 97, displays eutectics

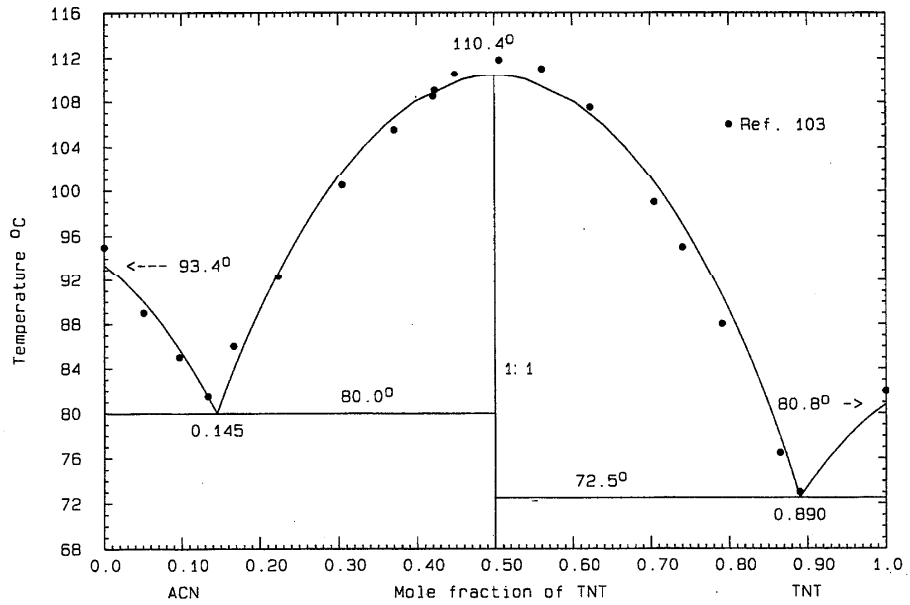

FIG. 97. The system ACN (A)+TNT (B)

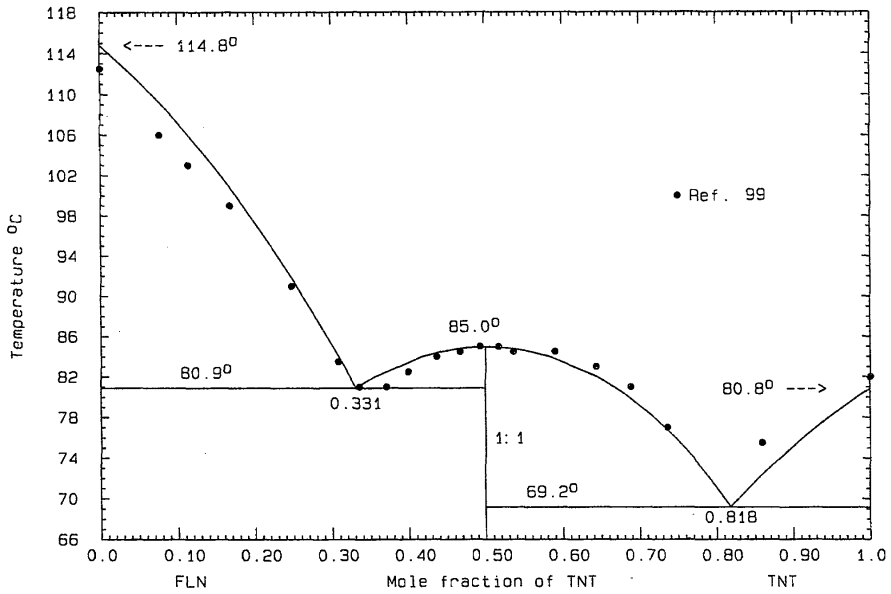

FIG. 98. The system FLN (A)+TNT (B)

E_1=80.0 °C, x_B=0.145 and E_2=72.5 °C, x_B=0.890; the compound melts at 110.4 °C. The probable maximum inaccuracy in the calculated diagram is ±2°.

FLN (A)+TNT (B)

Liquidus data were obtained by thermal analysis[99] and the reported eutectics are E_1=78.5 °C, x_B=0.35 and E_2=72.0 °C, x_B=0.78. (No eutectic arrests were recorded.) The 1:1 compound melts at 85.0 °C. The E_2 temperature is not well defined experimentally[99] and the liquidus arms of the compound are not symmetric. Under these circumstances, optimization was unable to give satisfactory results. Hence the optimization was restricted to data in the range $0.2<x_B<0.75$ with the result

$$G^E(l) = -4893 x_A x_B \text{ J mol}^{-1} \quad (176)$$

for the liquid and

$$\Delta_{fus}G^0 = 27\,978 - 78.1250T \text{ J mol}^{-1}, \quad (177)$$

$$\Delta_f G^0 = 29\,201 + 72.3638T \text{ J mol}^{-1} \quad (178)$$

for the compound (AB)/2. The calculated phase diagram, Fig. 98, shows eutectics E_1=80.9 °C, x_B=0.331 and E_2=69.2 °C, x_B=0.818; the compound melts at 85.0 °C. The probable maximum inaccuracy in the calculated diagram is ±2°.

ANTH (A)+TNT (B)

Data were obtained by thermal analysis[100] and the reported eutectic is 75.0 °C, x_B=0.93. Only data in the interval $0.3<x_B<0.9$ were used in the optimization, to give

$$G^E(l) = x_A x_B(-3437 + 1253 x_B) \text{ J mol}^{-1}. \quad (179)$$

The calculated phase diagram, Fig. 99, shows a eutectic 75.3 °C, x_B=0.891; many liquidus data are seen to be not internally consistent. The probable maximum inaccuracy in the calculated diagram is ±4°.

PH (A)+TNT (B)

Liquidus data were obtained by thermal analysis[44] and the reported eutectics are E_1=76.0 °C, x_B=0.30 and E_2=69.0 °C, x_B=0.82. No eutectic arrests were recorded in the original article.[44] The 1:1 compound melts congruently at 87.5 °C. Many liquidus data are in error. In this case, the observed eutectic temperatures[44] and compound melting point were taken as guides to optimization. The result was

$$G^E(l) = x_A x_B(-2800 + 200 x_B) \text{ J mol}^{-1} \quad (180)$$

for the liquid and

$$\Delta_{fus}G^0 = 16\,525 - 45.8180T \text{ J mol}^{-1}, \quad (181)$$

$$\Delta_f G^0 = -17\,201 + 40.0568T \text{ J mol}^{-1} \quad (182)$$

for the compound (AB)/2. The phase diagram, Fig. 100, was calculated with the use of Eqs. (180) and (182) and reproduces the chosen temperature data exactly: E_1=76.0 °C, x_B=0.263 and E_2=69.0 °C, x_B=0.798. The compound melts at 87.5 °C. The probable maximum inaccuracy in the calculated diagram is ±5°.

PY (A)+TNT (B)

Data were obtained by the thaw–melt method[43] and the reported eutectics are E_1=126.0 °C, x_B=0.188 and E_2=75.0 °C, x_B=0.952. The 1:1 compound melts congruently at 164.5 °C. Since the crystallization field of the compound occupies about 80% of the composition range, the expression for the liquid

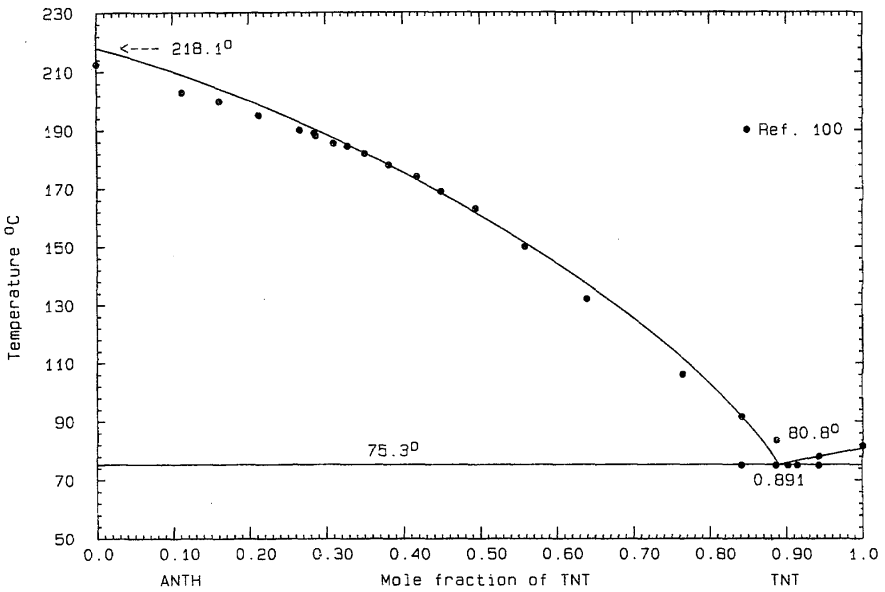

FIG. 99. The system ANTH (A)+TNT (B)

$$G^{E}(l) = -12\,000 x_A x_B \text{ J mol}^{-1} \quad (183)$$

is approximate. The E_2 temperature[43] is not consistent with the limiting liquidus slope of trinitrotoluene and the RHS compound liquidus. For the compound (AB)/2, the equations

$$\Delta_{fus}G^0 = 24\,922 - 56.9458T \text{ J mol}^{-1}, \quad (184)$$

$$\Delta_f G^0 = -27\,925 + 51.1846T \text{ J mol}^{-1} \quad (185)$$

were found from optimization. The calculated phase diagram, Fig. 101, reproduces most of the data[43] well; $E_1 = 126.4$ °C, $x_B = 0.175$ and $E_2 = 78.1$ °C, $x_B = 0.952$ and the compound melts at 164.5 °C. The probable maximum inaccuracy in the calculated diagram is ±2°.

FTHN (A)+TNT (B)

Data were obtained by the thaw–melt method[43] and the reported eutectics are $E_1 = 89.0$ °C, $x_B = 0.212$ and $E_2 = 72.5$ °C, $x_B = 0.850$. The 1:1 compound melts congruently at 133.0 °C. Most of the data could be reproduced well with the use of the equations

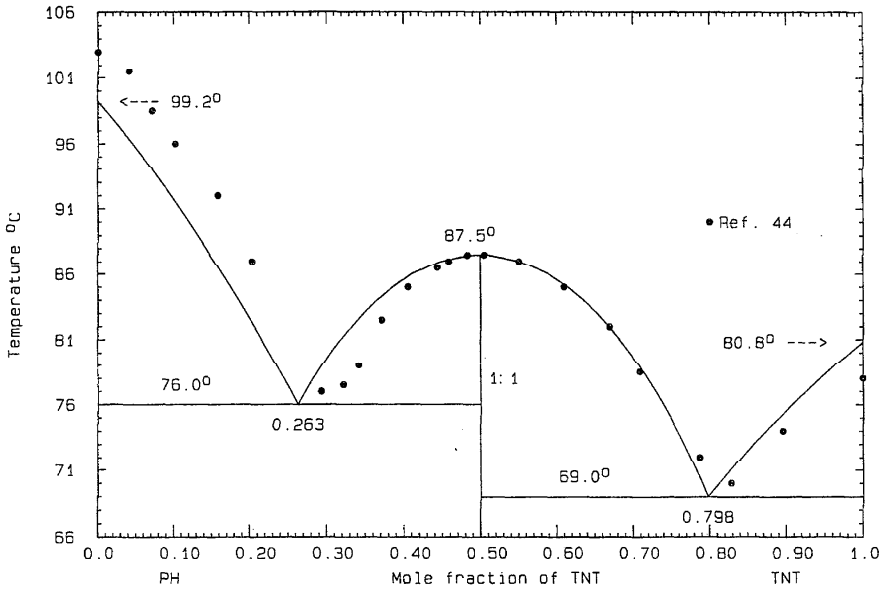

FIG. 100. The system PH (A)+TNT (B)

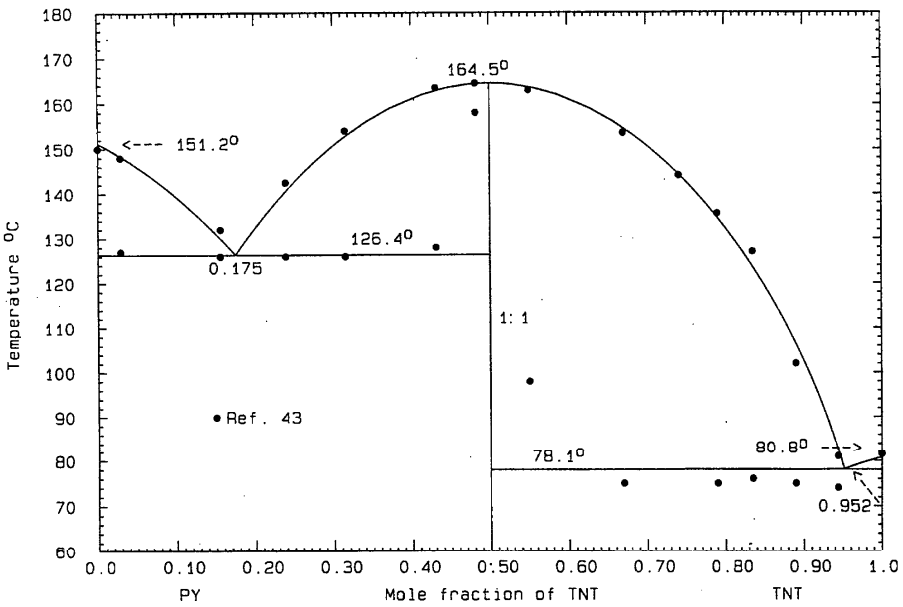

FIG. 101. The system PY (A)+TNT (B)

$$G^{E}(l)=x_A x_B(-4950+1267x_B)\ \text{J mol}^{-1} \quad (186)$$

for the liquid and

$$\Delta_{fus}G^0=9145-22.4609T\ \text{J mol}^{-1}, \quad (187)$$

$$\Delta_f G^0=-10\,226+16.6997T\ \text{J mol}^{-1} \quad (188)$$

for the compound (AB)/2. The calculated phase diagram, Fig. 102, displays eutectics E_1=89.0 °C, x_B=0.214 and E_2=72.4 °C, x_B=0.850; the compound melts at 134.0 °C. The probable maximum inaccuracy in the calculated diagram is ±2°.

AN (A)+TNT (B)

Liquidus data were obtained by thermal analysis[98] and the reported eutectics are E_1=−8.0 °C, x_B=0.015 and E_2=60.0 °C, x_B=0.85 (no eutectic arrests were recorded).

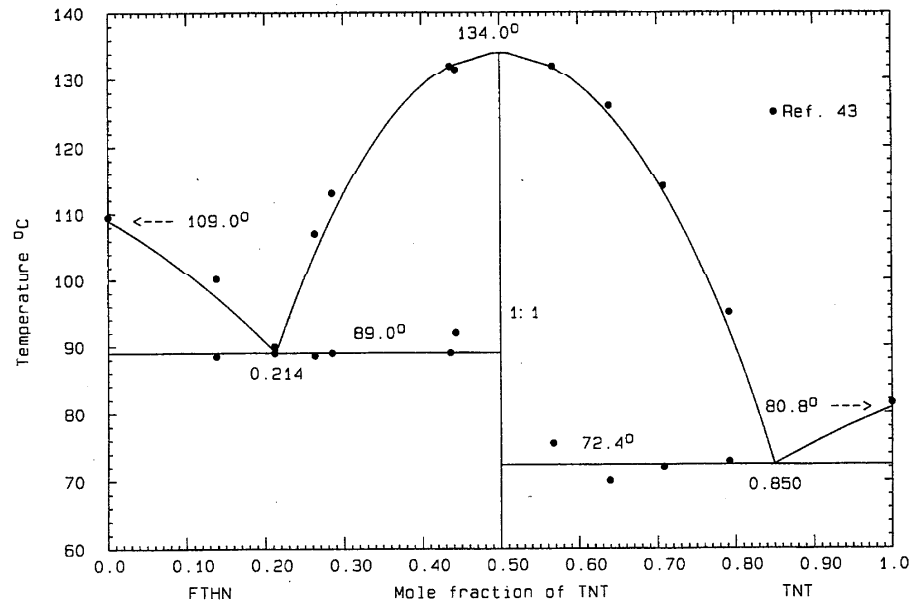

FIG. 102. The system FTHN (A)+TNT (B)

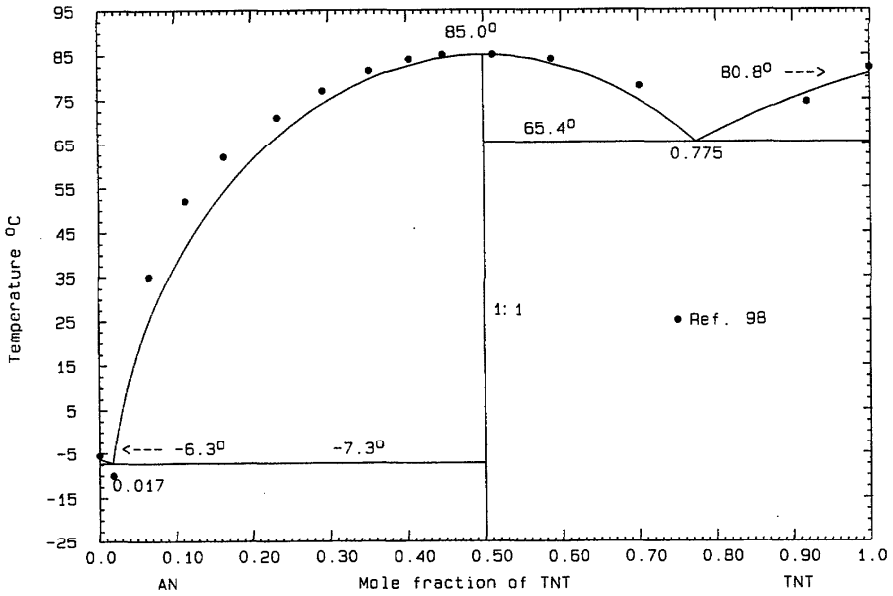

FIG. 103. The system AN (A)+TNT (B)

The 1:1 compound melts congruently at 85.0 °C. The RHS eutectic temperature is ill defined experimentally.[98] Since the crystallization field of the compound covers much of the composition range and the RHS liquidus data are so sparse, the quantity

$$G^{E}(l) = -5000 x_A x_B \text{ J mol}^{-1} \quad (189)$$

is approximate. For the compound (AB)/2, the optimization yielded

$$\Delta_{fus}G^0 = 16\,084 - 44.9084T \text{ J mol}^{-1}, \quad (190)$$

$$\Delta_f G^0 = -17\,335 + 39.1472T \text{ J mol}^{-1}. \quad (191)$$

The calculated phase diagram, Fig. 103, shows calculated eutectics $E_1 = -7.3$ °C, $x_B = 0.017$ and $E_2 = 65.4$ °C, $x_B = 0.775$. The compound melts at 85.0 °C. The probable maximum inaccuracy in the calculated diagram is ±5°.

CAR (A)+TNT (B)

Data were obtained by thermal analysis[100,113] and the thaw–melt method.[13] A critical point summary is given in Table 13. The presence of a congruently melting 2:3 compound (160 °C) was also claimed[113] but there is no supporting evidence for this. There is fair agreement between the two sets of liquidus data.[13,100] Data in the range $0.3 < x_B < 1$ were optimized to give

$$G^{E}(l) = x_A x_B(-4055 - 5000 x_B) \text{ J mol}^{-1} \quad (192)$$

for the liquid and

$$\Delta_{fus}G^0 = 20\,288 - 48.8929T \text{ J mol}^{-1}, \quad (193)$$

$$\Delta_f G^0 = -22\,062 + 43.1317T \text{ J mol}^{-1} \quad (194)$$

for the compound (AB)/2. The calculated phase diagram, Fig. 104, shows invariant points $E = 74.8$ °C, $x_B = 0.910$ and $P = 140.0$ °C, $x_B = 0.623$. The carbazole transition appears on the calculated liquidus at $x_B = 0.601$. The probable maximum inaccuracy in the calculated diagram is ±3°.

TABLE 13. Reported invariant data for the system CAR (A)+TNT (B)

	°C	x_B	Ref.
E	73.5	0.94	13
	75.0	0.93	100
P (1:1)	140.0	0.63	13
	140.0	0.62	100
	140.0	···	113

BA (A)+TNT (B)

Data were obtained by thermal analysis with stirring[47] and no eutectic data were reported. The limiting liquidus slope at the LHS[47] shows slightly positive deviation from ideality; this could be interpreted as indicating the presence of some solid solubility, but it is simpler to absorb this effect into the optimization of the liquidus data:

$$G^{E}(l) = x_A x_B(2491 - 2036 x_B) \text{ J mol}^{-1}. \quad (195)$$

The calculated phase diagram, Fig. 105, shows a eutectic 64.5 °C, $x_B = 0.702$. The probable maximum inaccuracy in the calculated diagram is ±2°.

HB (A)+TNT (B)

Data were obtained by thermal analysis[104] and the reported eutectic is 65.5 °C, $x_B = 0.68$. Data in the range $0.3 < x_B < 1$ were optimized to give

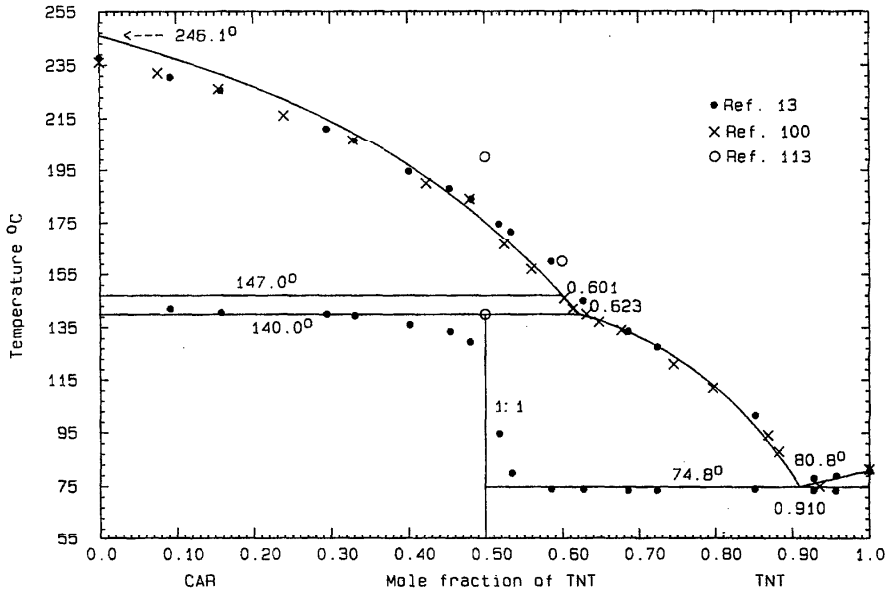

FIG. 104. The system CAR (A)+TNT (B)

$$G^{E}(l)=x_A x_B(-1000+8095x_B-5723x_B^2)\ \text{J mol}^{-1}. \quad (196)$$

The phase diagram, Fig. 106, calculated with the use of Eq. (196), displays a calculated eutectic of 65.6 °C, $x_B=0.639$. The probable maximum inaccuracy in the calculated diagram is ±2°.

SA (A)+TNT (B)

Liquidus data were obtained by thermal analysis with stirring[83] and neither eutectic arrests nor eutectic data were recorded.[83] The data appear to be of good quality. From inspection of the original tabulated data,[83] it may be concluded that the eutectic is close to 76 °C, $x_B=0.9$. All liquidus data were optimized, and the result

$$G^{E}(l)=x_A x_B(1640+670x_B)\ \text{J mol}^{-1} \quad (197)$$

was used to calculate the phase diagram, Fig. 107. The calculated eutectic is 76.3 °C, $x_B=0.898$. The probable maximum inaccuracy in the calculated diagram is ±1°.

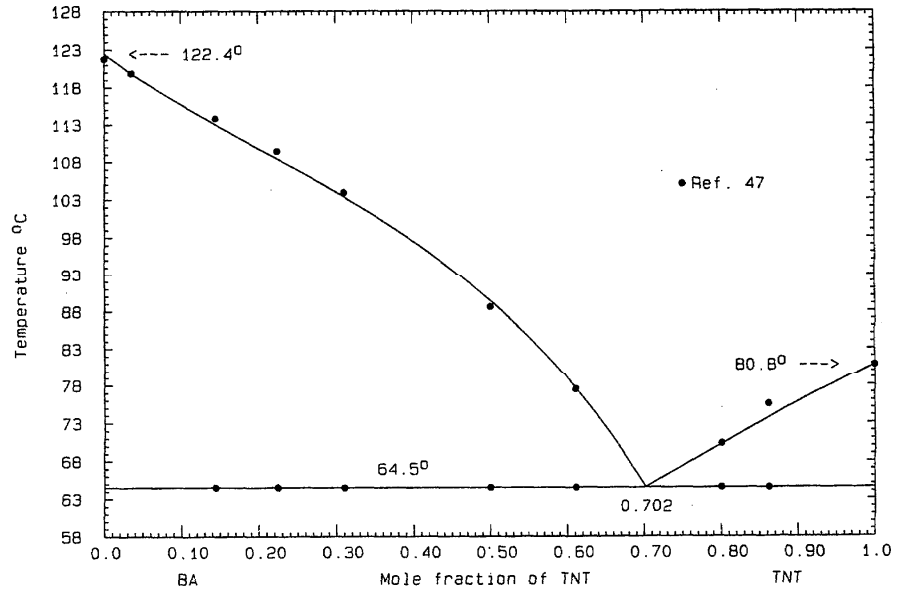

FIG. 105. The system BA (A)+TNT (B)

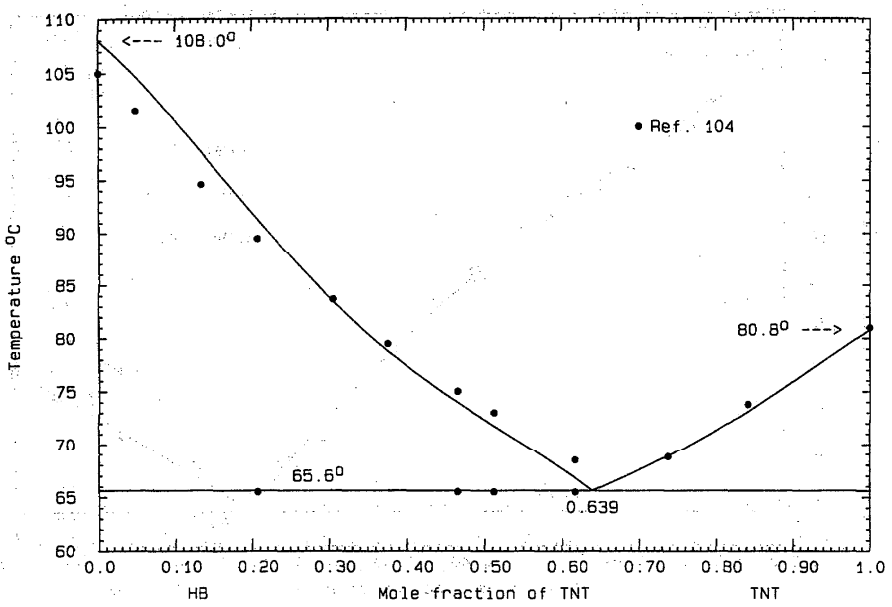

FIG. 106. The system HB (A)+TNT (B)

2.5.13. Systems Based on 2-Nitrophenol

NA (A)+2-NP (B)

Data were obtained by the thaw–melt method[37] and thermal analysis.[98,115] No eutectic arrests were recorded in the three reports. The reported eutectic data are, respectively,[37,98,115] 27.3 °C, x_B=0.675; 30.0 °C, x_B=0.70; ≈30 °C, x_B≈0.68. The agreement among the observed liquidus data is quite good, within about 2°. All liquidus data were optimized to give

$$G^E(l)=413x_Ax_B \text{ J mol}^{-1}, \quad (198)$$

and the calculated phase diagram, Fig. 108, shows a eutectic 28.8 °C, x_B=0.694. The probable maximum inaccuracy in the calculated diagram is ±2°.

BP (A)+2-NP (B)

Data were obtained by thermal analysis[116] and the reported eutectic is 28.2 °C, x_B=0.67. There is some small scatter in

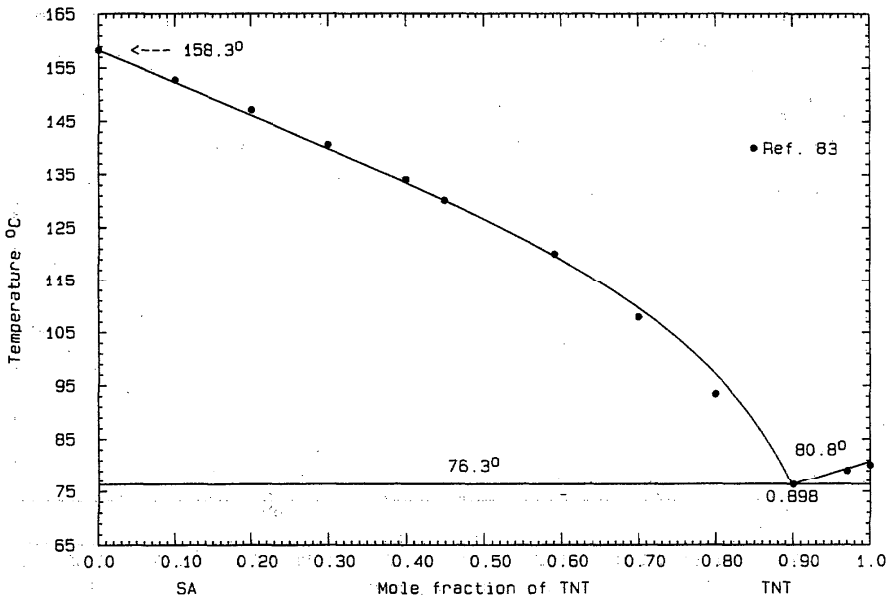

FIG. 107. The system SA (A)+TNT (B)

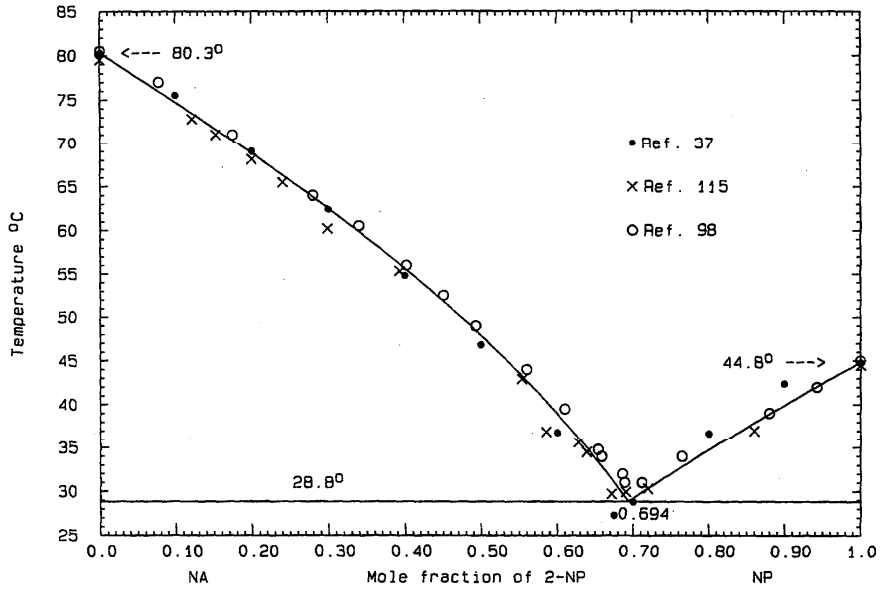

FIG. 108. The system NA (A)+2-NP (B)

the liquidus data[116] but optimization of all data yielded the expression

$$G^{E}(l)=991x_{A}x_{B}\ \text{J mol}^{-1} \qquad (199)$$

and the calculated phase diagram, Fig. 109, shows a eutectic 27.9 °C, $x_B=0.659$. The probable maximum inaccuracy in the calculated diagram is ±1°.

ANTH (A)+2-NP (B)

Data were obtained by thermal analysis[100] and the reported eutectic is 44.0 °C, $x_B=0.98$. Liquidus data in the interval $0.18<x_B<1$ were optimized and the result

$$G^{E}(l)=x_{A}x_{B}(842-793x_{B})\ \text{J mol}^{-1} \qquad (200$$

was used to calculate the phase diagram, Fig. 110. The cal

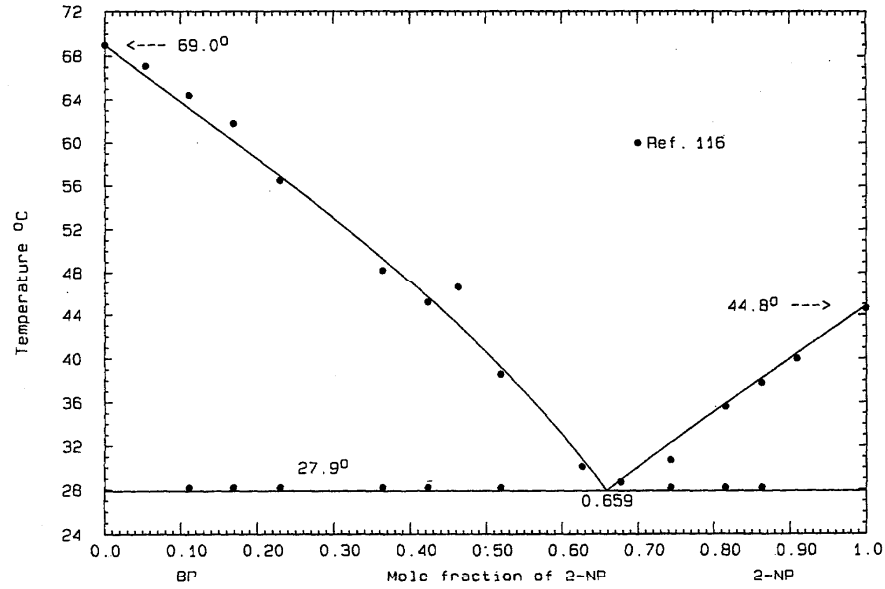

FIG. 109. The system BP (A)+2-NP (B)

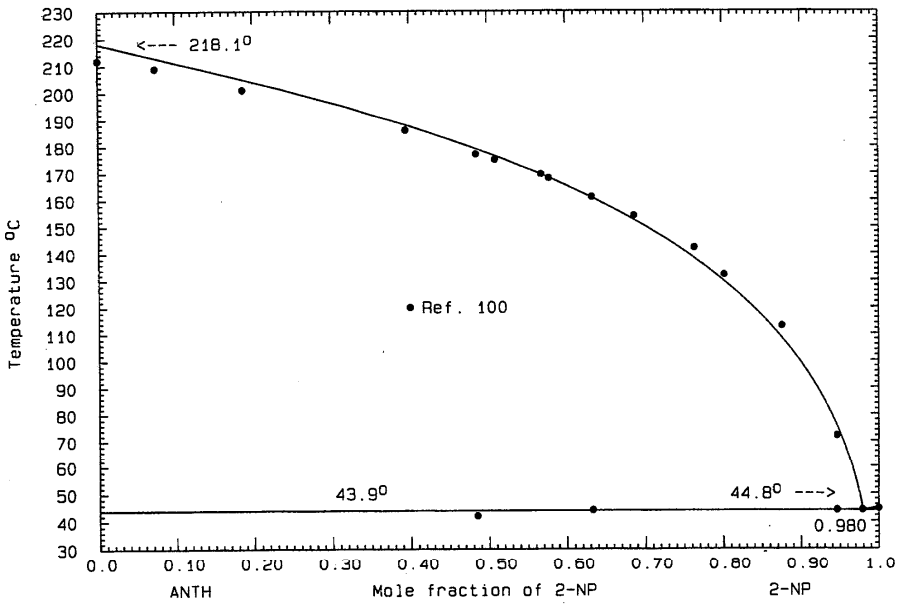

FIG. 110. The system ANTH (A)+2-NP (B)

culated eutectic is 43.9 °C, x_B=0.980. The probable maximum inaccuracy in the calculated diagram is ±2°.

TPM (A)+2-NP (B)

Data were obtained by thermal analysis[87] and the reported eutectic is 36.0 °C, x_B=0.80. The data appear to be of good quality; those in the interval $0.2<x_B<1$ were optimized, giving

$$G^E(l)=x_A x_B(1199+586x_B)\ \text{J mol}^{-1}, \qquad (201)$$

which was used to calculate the phase diagram, Fig. 111. The calculated eutectic is 35.9 °C, x_B=0.800. The probable maximum inaccuracy in the calculated diagram is ±1°.

1-AN (A)+2-NP (B)

Data were obtained by thermal analysis[102] and the reported eutectic is 14.0 °C, x_B=0.49. The experimental melting points of both pure components are about 2° lower than adopted values. Data in the interval $0.2<x_B<0.8$ were optimized, giving the result

$$G^E(l)=-116x_A x_B\ \text{J mol}^{-1}. \qquad (202)$$

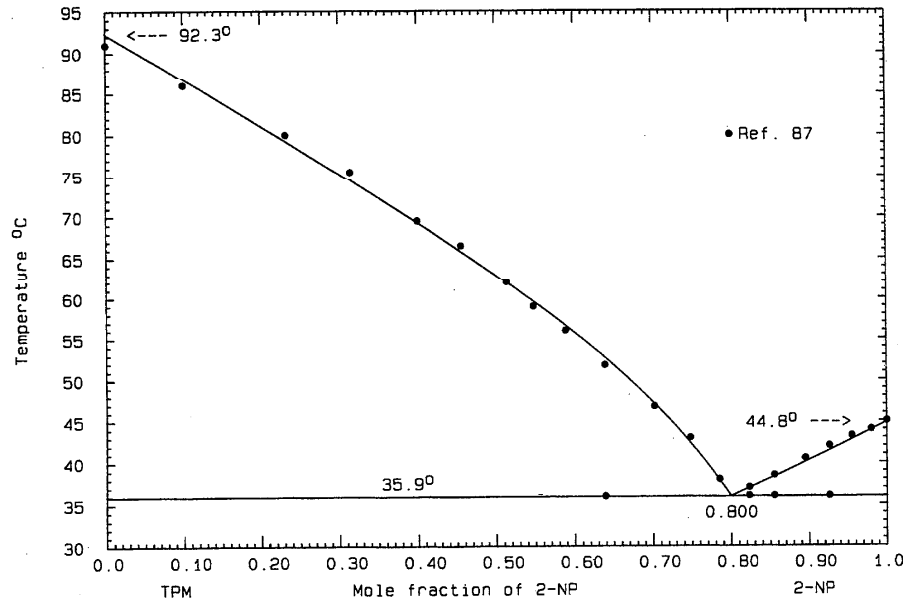

FIG. 111. The system TPM (A)+2-NP (B)

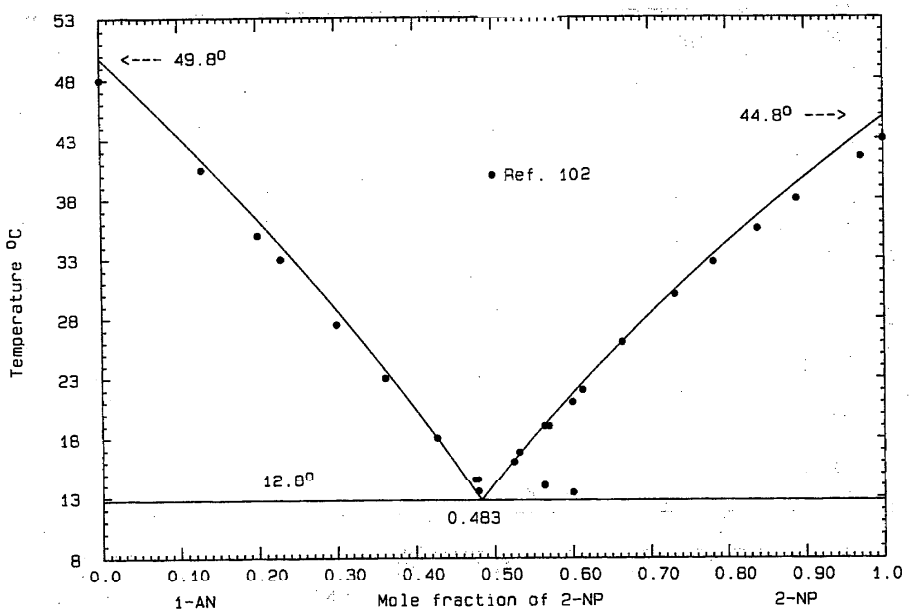

FIG. 112. The system 1-AN (A)+2-NP (B)

The calculated phase diagram, Fig. 112, shows a calculated eutectic of 12.8 °C, $x_B=0.483$. The diagram is almost symmetrical, and so the observed high eutectic temperature is not thermodynamically consistent with the experimental liquidus. The probable maximum inaccuracy in the calculated diagram is ±1°.

2-AN (A)+2-NP (B)

Data were obtained by thermal analysis[102] and the reported eutectic is 35.9 °C, $x_B=0.84$. Liquidus data in the range $0.3<x_B<1$ were optimized, giving the expression

$$G^E(l)=x_A x_B(-776+1140x_B)\ \text{J mol}^{-1}. \quad (203)$$

The calculated phase diagram, Fig. 113, shows a eutectic 36.9 °C, $x_B=0.835$. Since the eutectic composition is close to pure 2-nitrophenol, the low experimental melting point of this component[102] may be responsible for the difference be-

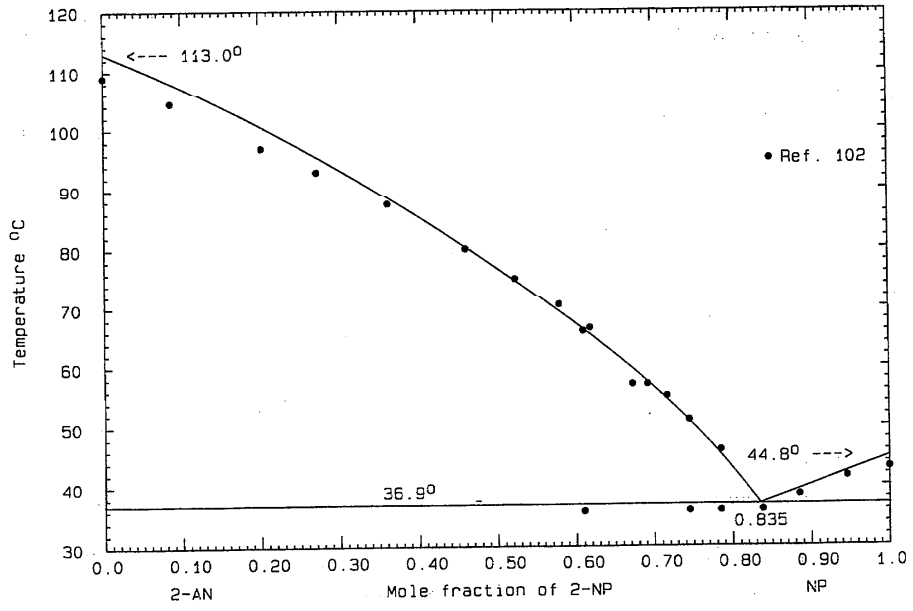

FIG. 113. The system 2-AN (A)+2-NP (B)

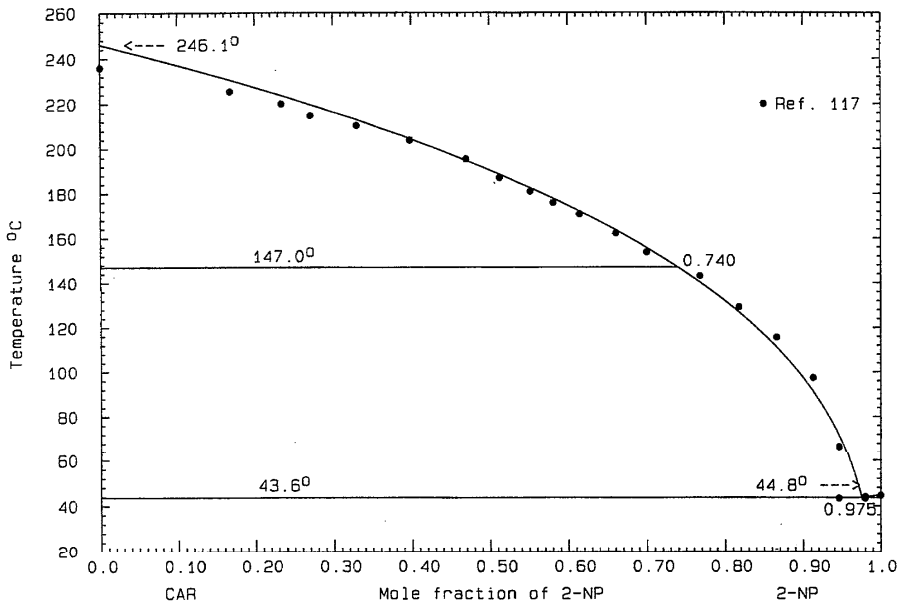

FIG. 114. The system CAR (A)+2-NP (B)

tween observed and calculated eutectic temperatures. The probable maximum inaccuracy in the calculated diagram is ±2°.

CAR (A)+2-NP (B)

Data were obtained by thermal analysis[117] and the reported eutectic is 43.5 °C, x_B=0.97. All liquidus data were optimized and the result

$$G^E(l) = -606 x_A x_B \text{ J mol}^{-1} \quad (204)$$

was used to calculate the phase diagram, Fig. 114. The calculated eutectic is 43.6 °C, x_B=0.975 and the carbazole transition appears on the calculated liquidus at x_B=0.740. The probable maximum inaccuracy in the calculated diagram is ±3°.

DMA (A)+2-NP (B)

Data were obtained by the visual-polythermal method[95] and the reported critical points are E=−36.5 °C, x_B=0.16 and P=2.5 °C, x_B=0.46 (1:1 compound). The liquidus of the compound appeared to be inconsistent with the E and P temperatures, so that in the optimization, these temperatures were given preference. For the liquid,

$$G^E(l) = -1800 x_A x_B \text{ J mol}^{-1}, \quad (205)$$

and for the compound (AB)/2,

$$\Delta_{fus} G^0 = 6571 - 23.7967T \text{ J mol}^{-1}, \quad (206)$$

$$\Delta_f G^0 = -7022 + 18.0355T \text{ J mol}^{-1}. \quad (207)$$

The calculated phase diagram is shown in Fig. 115. Other calculated data are E=−36.5 °C, x_B=0.142 and P=2.5 °C, x_B=0.457. The probable maximum inaccuracy in the calculated diagram is ±2°.

BENZ (A)+2-NP (B)

Data were obtained by the visual-polythermal method[118] and the reported eutectic is 42.0 °C, x_B=0.95. The experimental benzamide liquidus[118] may be artificially high, but the reported eutectic temperature is probably accurate. Data in the range $0.55 < x_B < 1$ were optimized, yielding the expression

$$G^E(l) = x_A x_B (2270 + 2116 x_B) \text{ J mol}^{-1}. \quad (208)$$

The calculated phase diagram, Fig. 116, shows a calculated eutectic 42.6 °C, x_B=0.948. The probable maximum inaccuracy in the calculated diagram is ±4°.

HB (A)+2-NP (B)

Data were obtained by thermal analysis[104] and the reported eutectic is 41.0 °C, x_B=0.90. The RHS liquidus[104] lies slightly higher than thermodynamic ideality whereas the LHS liquidus is low due to the low melting point of 3-hydroxybenzaldehyde. Liquidus data in the interval $0.25 < x_B < 1$ were optimized and the phase diagram, Fig. 117, calculated with the use of

$$G^E(l) = x_A x_B (-129 + 3447 x_B) \text{ J mol}^{-1} \quad (209)$$

follows the experimental liquidus data faithfully (calculated eutectic 40.3 °C, x_B=0.878). The calculated liquidus shows points of inflection that may not correspond to true behavior. The probable maximum inaccuracy in the calculated diagram is ±3°.

ACP (A)+2-NP (B)

Data were obtained by thermal analysis[119] and the reported eutectic is 2.5 °C, x_B=0.43. The data appear to be of good

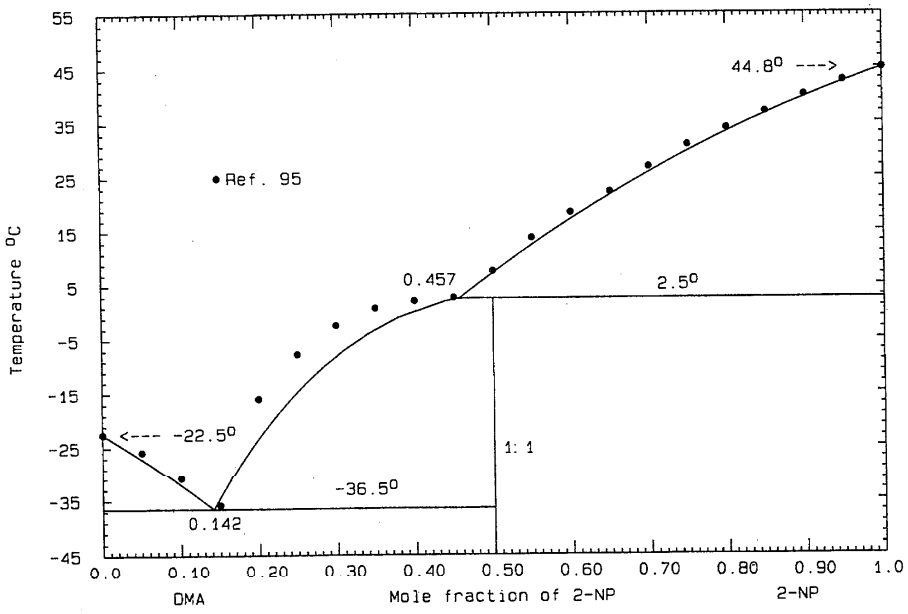

FIG. 115. The system DMA (A)+2-NP (B)

quality except for those in the interval $0.4<x_B<0.6$; these aberrant data were omitted from the optimization, which yielded the equation

$$G^E(l)=x_A x_B(1110-1590x_B)\ \text{J mol}^{-1}. \quad (210)$$

The calculated phase diagram, Fig. 118, shows a calculated eutectic 2.0 °C, $x_B=0.360$. The probable maximum inaccuracy in the calculated diagram is ±1°.

CAM (A)+2-NP (B)

Data were obtained by thermal analysis[88] and the reported eutectic is 15.0 °C, $x_B=0.48$. The data appear to be of good quality, and a good fit was obtained with the use of

$$G^E(l)=x_A x_B(-1076-675x_B+2540x_B^2)\ \text{J mol}^{-1}. \quad (211)$$

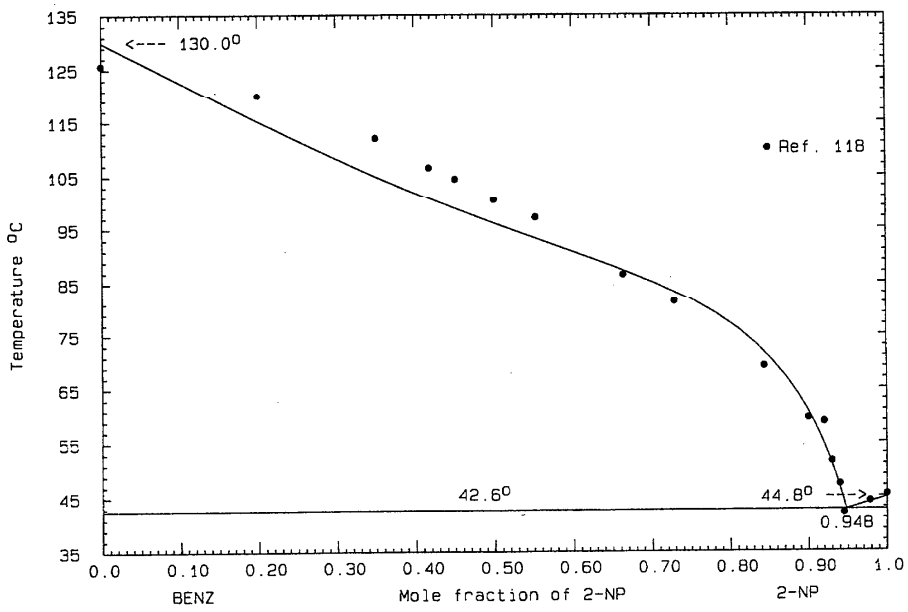

FIG. 116. The system BENZ (A)+2-NP (B)

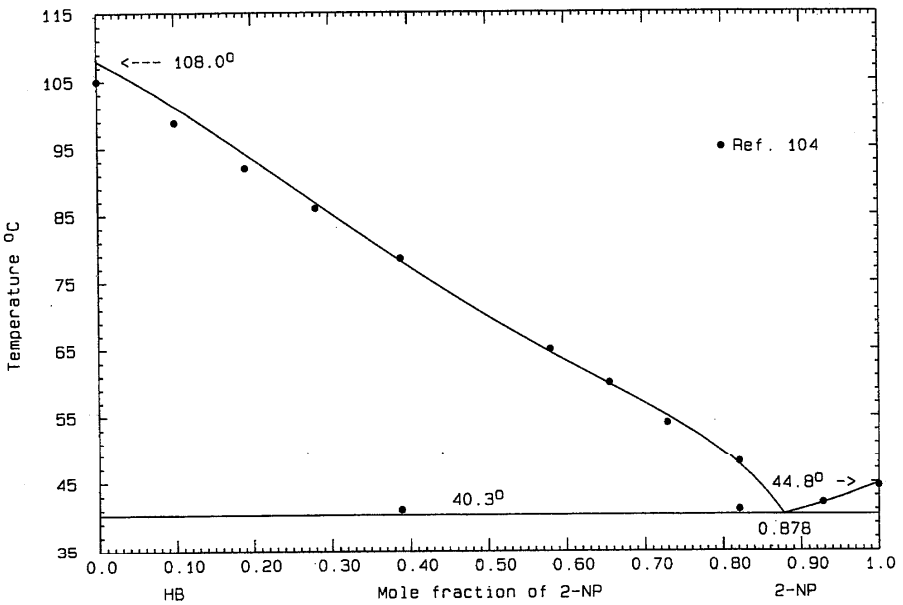

FIG. 117. The system HB (A)+2-NP (B)

The calculated phase diagram, Fig. 119, shows a calculated eutectic 14.8 °C, x_B=0.495. The probable maximum inaccuracy in calculated diagram is ±3°.

2.5.14. Systems Based on 3-Nitrophenol

BP (A)+3-NP (B)

Data were obtained by thermal analysis[116] and the reported eutectic is 62.3 °C, x_B=0.16. The presence of a compound melting incongruently is postulated[116] (P=76.1 °C, x_B=0.48, stoichiometry uncertain). No peritectic arrests were recorded, however. The observed change in the slope of the RHS liquids near x_B=0.5 may also be accounted for by a slight tendency toward liquid immiscibility between a polar molecule (3-nitrophenol) and a nonpolar one. Liquidus data in the range $0<x_B<0.8$ were optimized to give the expression

$$G^E(l)=x_A x_B(4950-1421x_B)\ \text{J mol}^{-1}. \quad (212)$$

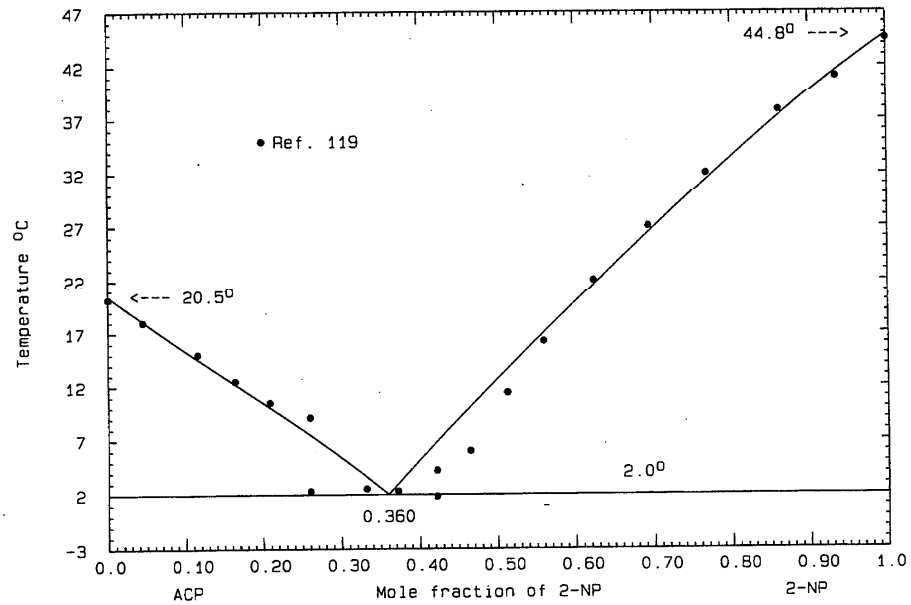

FIG. 118. The system ACP (A)+2-NP (B)

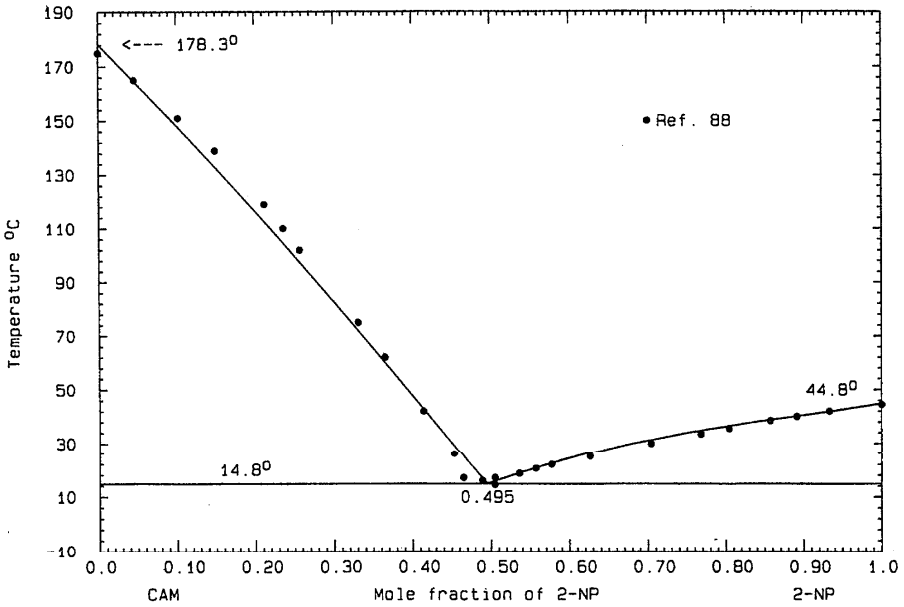

FIG. 119. The system CAM (A)+2-NP (B)

The calculated phase diagram, Fig. 120, shows a calculated eutectic 62.3 °C, x_B=0.181. The probable maximum inaccuracy in the calculated diagram is ±2°.

DPM (A)+3-NP (B)

Data were obtained by thermal analysis[120] and the reported eutectic is 22.0 °C, x_B=0.036. The observed eutectic temperature is not consistent with the theoretical limiting liquidus slope for diphenylmethane. Liquidus data in the interval $0<x_B<0.8$ were optimized to give

$$G^E(l)=x_A x_B(4601-338x_B)\ \text{J mol}^{-1} \quad (213)$$

with which the phase diagram, Fig. 121, was calculated. The calculated eutectic is 23.9 °C, x_B=0.039. The probable maximum inaccuracy in the calculated diagram is ±1°.

ANTH (A)+3-NP (B)

Data were obtained by thermal analysis[100] and the reported eutectics are E_1=186.0 °C, x_B=0.47 and E_2=93.0 °C, x_B=0.98. The 1:1 compound melts congruently at 187.0 °C.

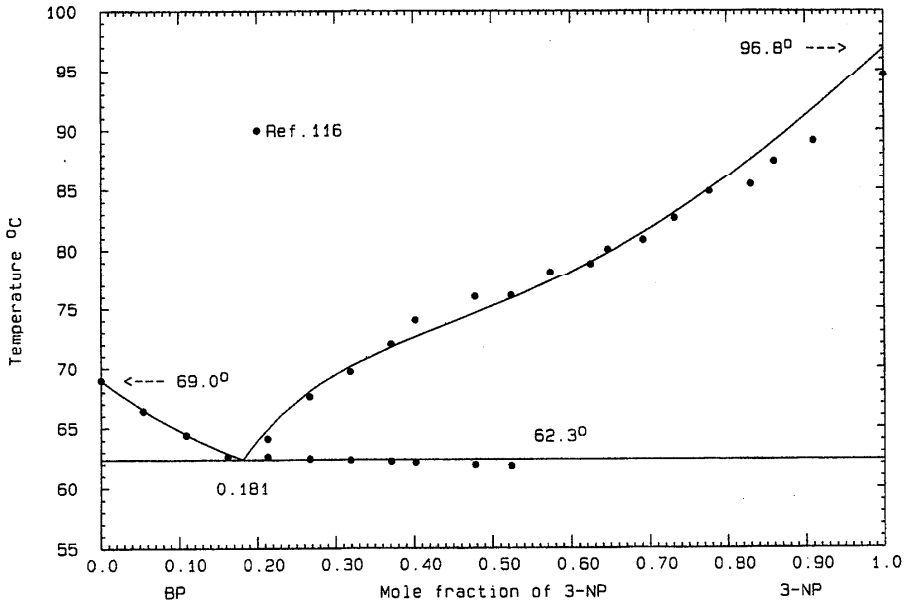

FIG. 120. The system BP (A)+3-NP (B)

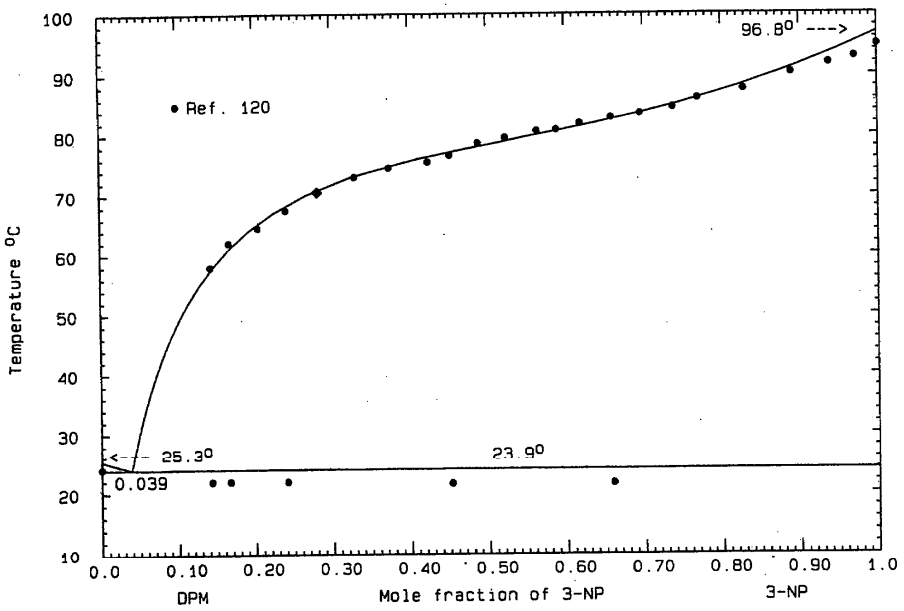

FIG. 121. The system DPM (A)+3-NP (B)

The E_1 and compound melting temperatures are very close but there is no suggestion of a peritectic. The observed shape of the RHS liquidus arm of the compound is not thermodynamically consistent with the rest of the phase diagram. The expression

$$G^{E}(l)=x_A x_B(4601-338x_B)\ \text{J mol}^{-1} \qquad (214)$$

was found by optimization of the LHS liquidus data; for the compound (AB)/2

$$\Delta_{fus}G^0=16\,232-35.3345T\ \text{J mol}^{-1}, \qquad (215)$$

$$\Delta_f G^0=-15\,825+29.5717T\ \text{J mol}^{-1}. \qquad (216)$$

The phase diagram, Fig. 122, was calculated with the use of Eqs. (214) and (216), showing calculated eutectics E_1=186.1 °C, x_B=0.473 and E_2=95.0 °C, x_B=0.969; the compound melts at 186.2 °C. The calculated E_2 temperature—higher than the observed[100]—reflects the cor-

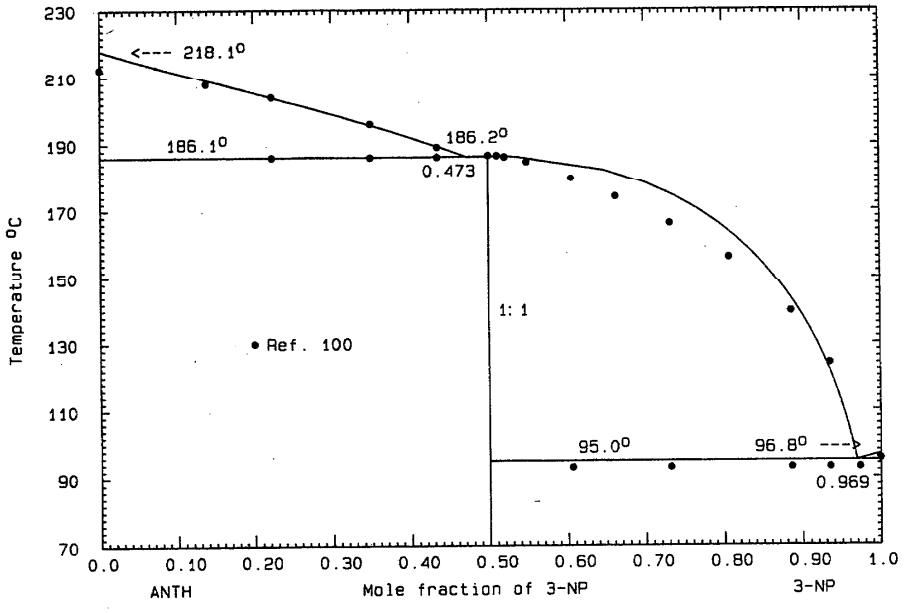

FIG. 122. The system ANTH (A)+3-NP (N)

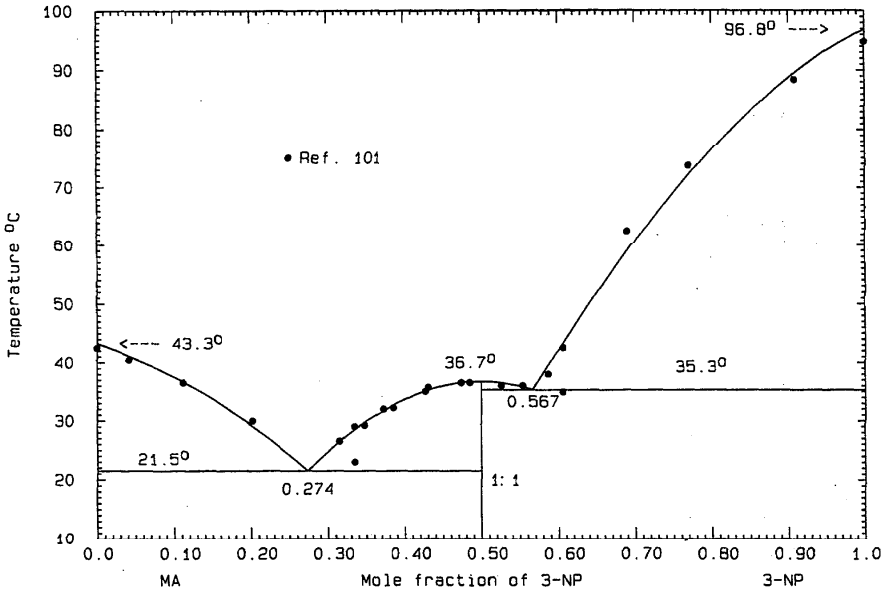

FIG. 123. The system MA (A)+3-NP (B)

rected melting point of 3-nitrophenol. The probable maximum inaccuracy in the calculated diagram is ±2°.

MA (A)+3-NP (B)

Data were obtained by thermal analysis[101] and the the reported eutectics are E_1=23.0 °C, x_B=0.29 and E_2=35.0 °C, x_B=0.58. The 1:1 compound melts congruently at 36.5 °C. The data appear to be of good quality. There were only two eutectic arrests recorded.[101] Data in the range $0<x_B<0.7$ were optimized, and the result was

$$G^E(l)=x_A x_B(-6853-2106x_B)\ \text{J mol}^{-1}. \quad (217)$$

For the compound (AB/2), the calculated properties are

$$\Delta_{fus}G^0=12\,925-41.7099T\ \text{J mol}^{-1}, \quad (218)$$

$$\Delta_f G^0=-14\,901+35.9487T\ \text{J mol}^{-1}. \quad (219)$$

The calculated phase diagram, Fig. 123, shows eutectics E_1=21.5 °C, x_B=0.274 and E_2=35.3 °C, x_B=0.567. The compound melts at 36.7 °C. The probable maximum inaccuracy in the calculated diagram is ±1°.

1-AN (A)+3-NP (B)

Data were obtained by thermal analysis[102] and there is one reported eutectic: 51.0 °C (sic), x_B=0.53; a 1:1 compound melts congruently at 56.3 °C. Very few eutectic arrests were recorded, and as a result the exact nature of the phase diagram around x_B=0.5 is ill defined experimentally.[107] In preliminary calculations it was ascertained that either a congruently melting 1:1 or incongruently melting 1:2 compound would be thermodynamically consistent with the rest of the phase diagram. The 1:1 stoichiometry was chosen because the compound liquidus data ($0.2<x_B<0.5$) were reproduced more precisely. For the liquid,

$$G^E(l)=-1711x_A x_B\ \text{J mol}^{-1}, \quad (220)$$

and for the compound (AB)/2

$$\Delta_{fus}G^0=11\,387-34.5597T\ \text{J mol}^{-1}, \quad (221)$$

$$\Delta_f G^0=-11\,815+28.7985T\ \text{J mol}^{-1}. \quad (222)$$

The phase diagram, Fig. 124, was calculated with the use of Eqs. (220) and (222). Other calculated data are E_1=35.1 °C, x_B=0.198 and E_2=56.1 °C, x_B=0.530. The compound melts at 56.3 °C. The probable maximum inaccuracy in the calculated diagram is ±1°.

2-AN (A)+3-NP (B)

Data were obtained by thermal analysis[102] and reported invariant points are E=61.0 °C, x_B=0.62 and P=63.5 °C (1:1 compound, no peritectic composition recorded). In preliminary calculations, it was found that the LHS liquidus is consistently low and that the RHS liquidus is more accurate. Optimization of these data gave the result

$$G^E(l)=x_A x_B(-3784+1291x_B)\ \text{J mol}^{-1}. \quad (223)$$

The experimental data[102] defining the compound liquidus were not accurate enough for optimization and hence for the compound (AB)/2 the properties

$$\Delta_{fus}G^0=11\,768-35.0000T\ \text{J mol}^{-1}, \quad (224)$$

$$\Delta_f G^0=-12\,553+29.2372T\ \text{J mol}^{-1} \quad (225)$$

were assigned. The phase diagram, Fig. 125, shows the calculated data E=61.1 °C, x_B=0.589 and P=63.0 °C, x_B=0.520. The probable maximum inaccuracy in the calculated diagram is ±2°.

CAR (A)+3-NP (B)

Data were obtained by thermal analysis[117] and the reported eutectic is 92.0 °C, x_B=0.96. The experimental melting point

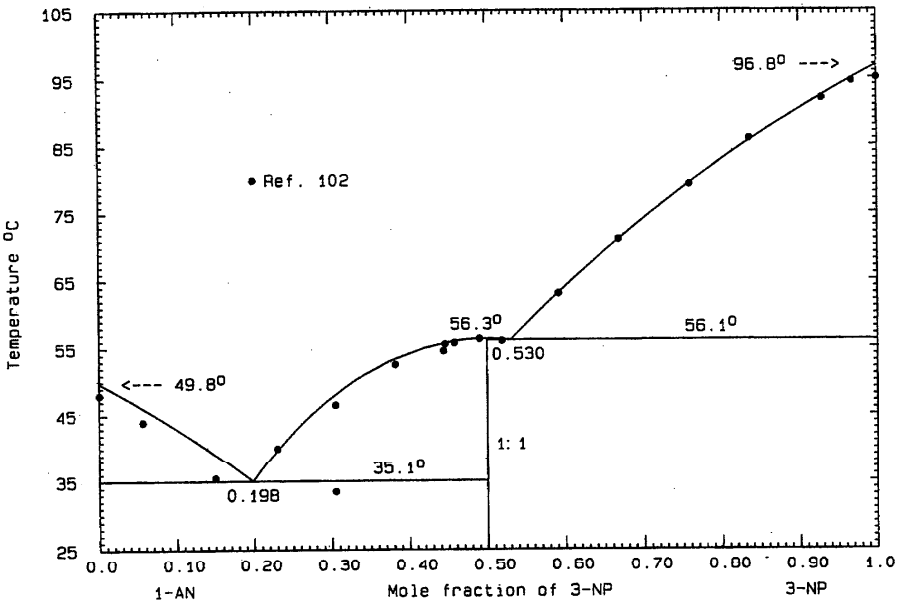

FIG. 124. The system 1-AN (A)+3-NP (B)

of 3-nitrophenol is low, and since the eutectic is very close to this composition, the observed eutectic temperature is probably too low. Data in the interval $0.39<x_B<1$ were optimized to give the result

$$G^E(l)=x_A x_B(-52+2545x_B)\ \text{J mol}^{-1}. \quad (226)$$

The calculated phase diagram, Fig. 126, shows a calculated eutectic 94.6 °C, $x_B=0.960$, and the carbazole transition appears on the calculated liquidus at $x_B=0.828$. The probable maximum inaccuracy in the calculated diagram is ±3°.

DMA (A)+3-NP (B)

Liquidus data were obtained by the visual-poythermal method[95] and the reported eutectics are $E_1=-58.0$ °C, $x_B=0.26$ (approximate data) and $E_2=7.0$ °C, $x_B=0.58$. The 1:1 compound melts congruently at 15.0 °C. Preliminary calculations showed that the RHS liquidus is not thermodynamically consistent with the observed E_2 temperature. The eutectic and compound melting temperatures were taken as guides to calculations. The quantity

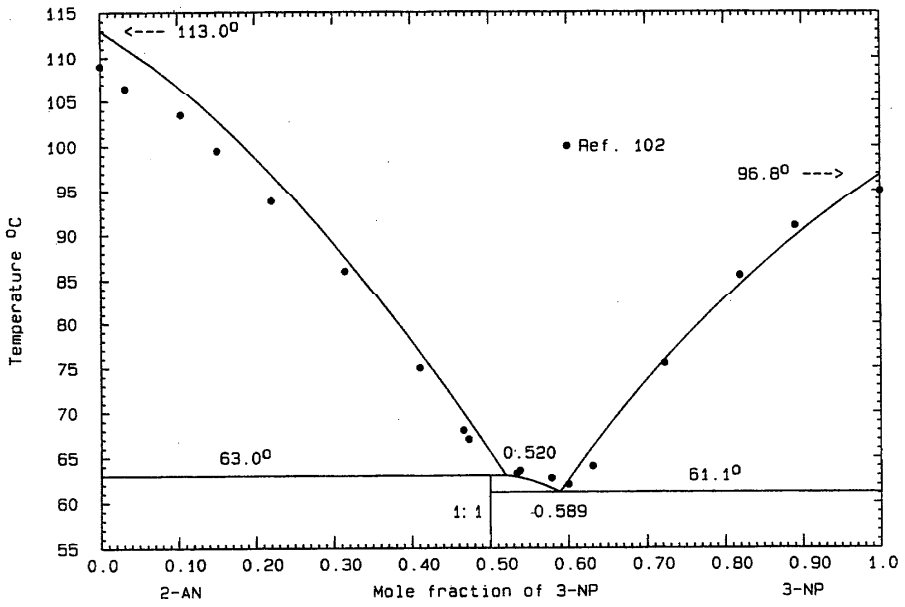

FIG. 125. The system 2-AN (A)+3-NP (B)

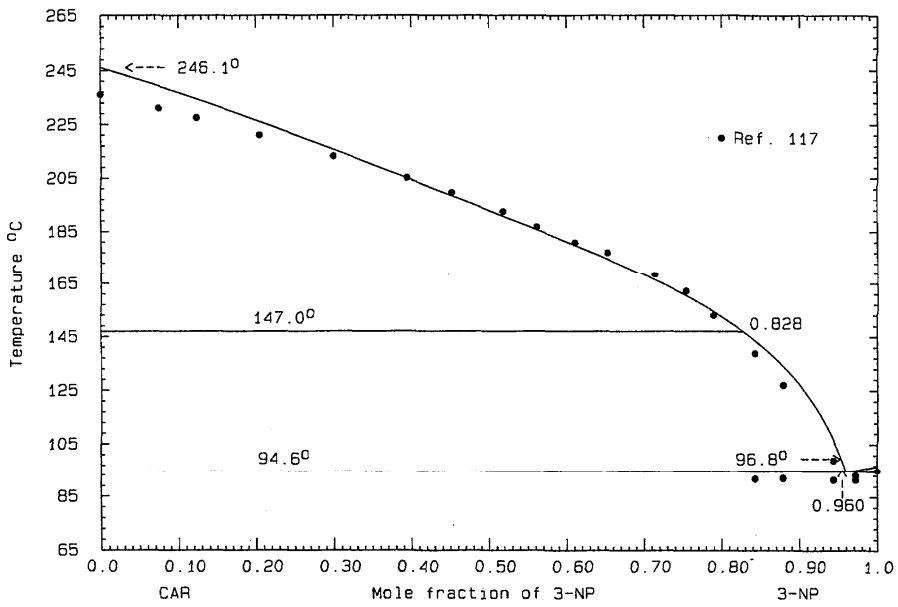

FIG. 126. The system CAR (A)+3-NP (B)

$$G^{E}(l)=x_A x_B(-15\,650-4400x_B)\ \text{J mol}^{-1} \quad (227)$$

was found to support a calculated phase diagram reasonably similar to the experimental. For the compound (AB)/2, the calculated properties are

$$\Delta_{fus}G^0=7415-25.7341T\ \text{J mol}^{-1}, \quad (228)$$

$$\Delta_f G^0=-11\,879+19.9730T\ \text{J mol}^{-1}. \quad (229)$$

The calculated phase diagram, Fig. 127, shows eutectics $E_1=-58.0$ °C, $x_B=0.191$ and $E_2=7.0$ °C, $x_B=0.594$; the compound melts at 15.0 °C. The eutectic temperatures remain experimentally ill defined, however. The probable maximum inaccuracy in the calculated diagram is ±5°.

BENZ (A)+3-NP (B)

Data were obtained by thermal analysis[107] and the visual-polythermal method.[118] The liquidus data of the two studies[107,118] are in quite good agreement (about 2°–3°). The

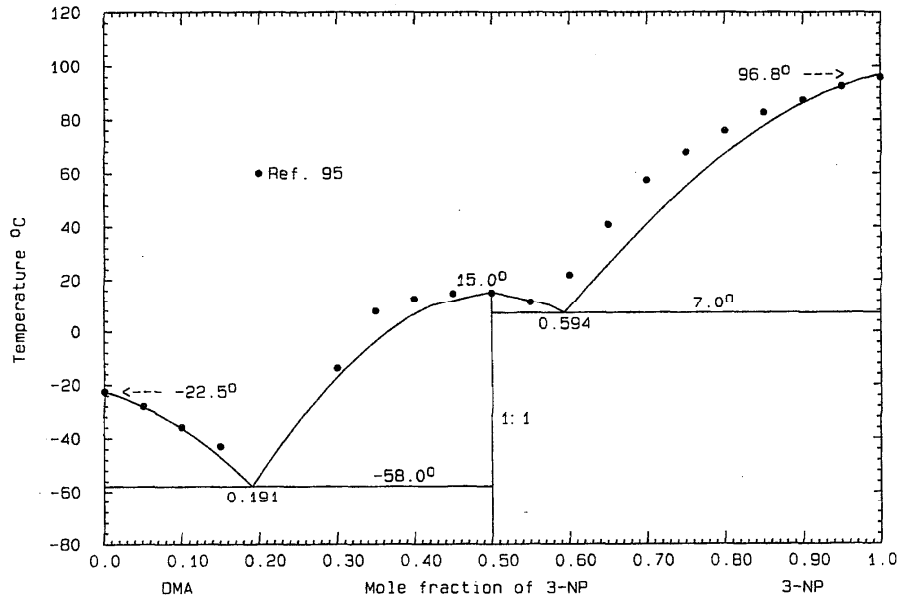

FIG. 127. The system DMA (A)+3-NP (B)

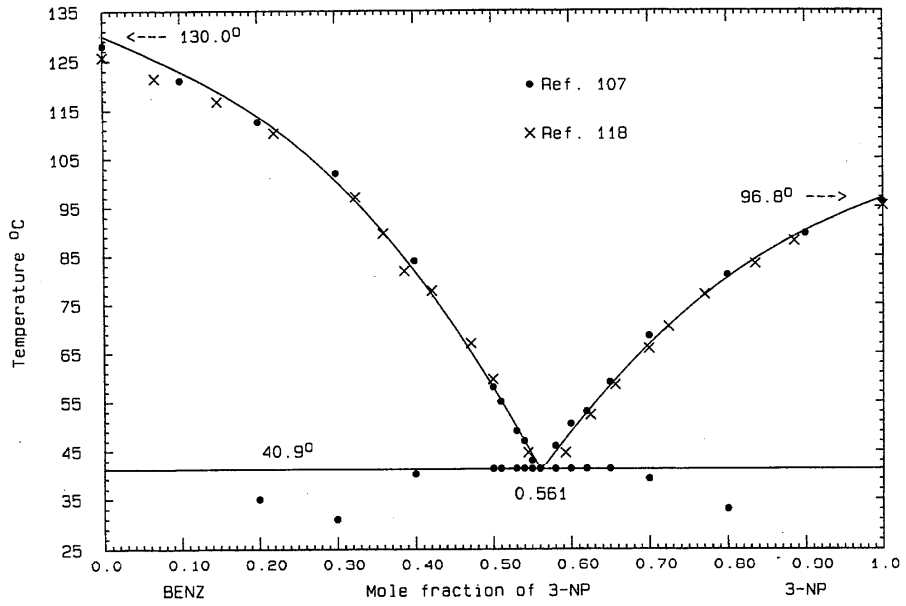

FIG. 128. The system BENZ (A)+3-NP (B)

observed eutectic[107,118] is 41.0 °C, x_B=0.56 or 39.0 °C, x_B=0.56. The combined liquidus data were optimized to give

$$G^E(l)=x_A x_B(-3993-8283x_B+639x_B^2)\ \text{J mol}^{-1}, \quad (230)$$

and the calculated phase diagram, Fig. 128, shows a eutectic 40.9 °C, x_B=0.561. The probable maximum inaccuracy in the calculated diagram is ±2°.

ACP (A)+3-NP (B)

Liquidus data were obtained by thermal analysis[119] and the reported eutectic is −16.0 °C, x_B=0.38 (no eutectic arrests were recorded). Optimization of the liquidus data gave the result

$$G^E(l)=x_A x_B(-3435-1502x_B+14\,635x_B^2)\ \text{J mol}^{-1}. \quad (231)$$

Equation (231) indicates that the excess Gibbs energy goes from negative (at the LHS) to rather strongly positive on the RHS; this unusual behavior was necessary to reproduce both arms of the liquidus simultaneously. The calculated phase diagram, Fig. 129, shows a eutectic −13.2 °C, x_B=0.360. The probable maximum inaccuracy in the calculated diagram is ±3°.

CAM (A)+3-NP (B)

Liquidus data were obtained by thermal analysis[88] and neither eutectic data nor eutectic arrests were recorded. It was found that only an expression with three coefficients

$$G^E(l)=x_A x_B(-9423-761x_B+9583x_B^2)\ \text{J mol}^{-1} \quad (232)$$

could enable the liquidus to be reproduced satisfactorily. The calculated phase diagram, Fig. 130, shows a calculated eutectic −6.1 °C, x_B=0.337. The probable maximum inaccuracy in the calculated diagram is ±2°.

2.5.15. Systems Based on 4-Nitrophenol

NA (A)+4-NP (B)

Data were obtained by thermal analysis[98] and the thaw–melt method[13] and both studies report the same eutectic: 73.0 °C, x_B=0.23. The liquidus data of the two studies are in good agreement, within 1°. The LHS limiting liquidus slope[13,98] definitely suggests solid solubility based on naphthalene. Optimization of the combined liquidus data yielded the expression

$$G^E(l)=x_A x_B(4276-1077x_B)\ \text{J mol}^{-1}. \quad (233)$$

The phase diagram, Fig. 131, was calculated with the use of Eq. (233) for the liquid and the solid solution was represented by a temperature independent Henrian activity coefficient

$$RT\ \ln\ \gamma_B=9200\ \text{J mol}^{-1}. \quad (234)$$

The calculated eutectic is 73.0 °C, x_B=0.242 and there is a 4.1 mol % solid solution at the eutectic temperature. The probable maximum inaccuracy in the calculated diagram is ±1°.

BP (A)+4-NP (B)

Data were obtained by thermal analysis[116] and the reported eutectics are E_1=64.2 °C, x_B=0.11 and E_2=62.4 °C, x_B=0.87. The 1:1 compound melts congruently at 79.0 °C. Preliminary calculations showed that most of the data at x_B>0.5 are erroneous and hence were ignored in further con-

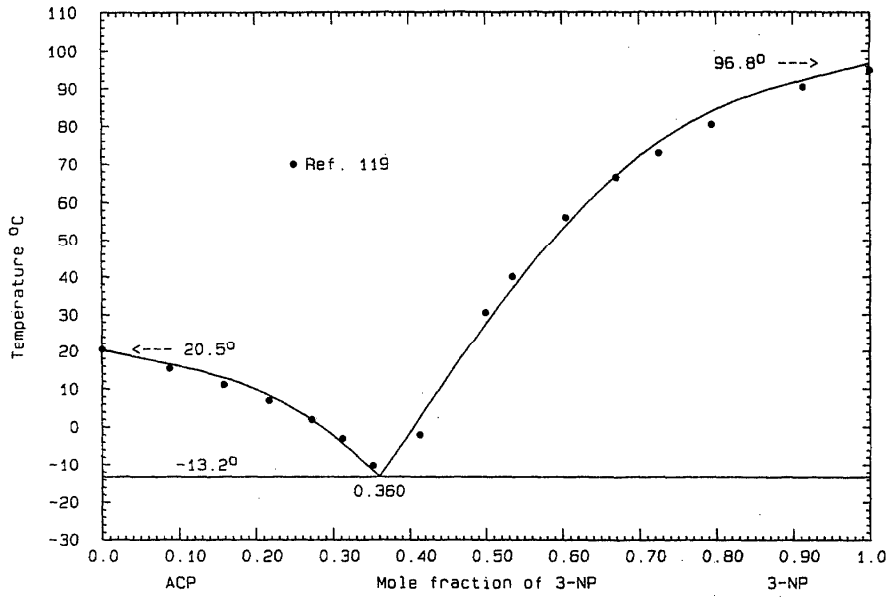

FIG. 129. The system ACP (A)+3-NP (B)

sideration. It also was apparent that, if E_1 were to be accepted, there would have to be a compound in the LHS of the diagram. The stoichiometry 4:1 was chosen as suitable for present purposes; such a stoichiometry, while unusual, is not unknown in these systems.[2] For the calculation of the phase diagram, therefore, the guiding assumptions were the observed[116] liquidus data at $0<x_B\leq 0.5$, the experimental E_1 data, 4:1 and 1:1 congruently melting compounds, and the observed 1:1 compound melting point. For the liquid, an estimated quantity

$$G^E(l) = -5000 x_A x_B \text{ J mol}^{-1} \quad (235)$$

was used. For the compound $(A_4B)/5$, the quantities

$$\Delta_{fus}G^0 = 19\,729 - 57.6603T \text{ J mol}^{-1}, \quad (236)$$

$$\Delta_f G^0 = -20\,529 + 53.5000T \text{ J mol}^{-1}, \quad (237)$$

and for the compound (AB)/2,

$$\Delta_{fus}G^0 = 17\,877 - 50.7628T \text{ J mol}^{-1}, \quad (238)$$

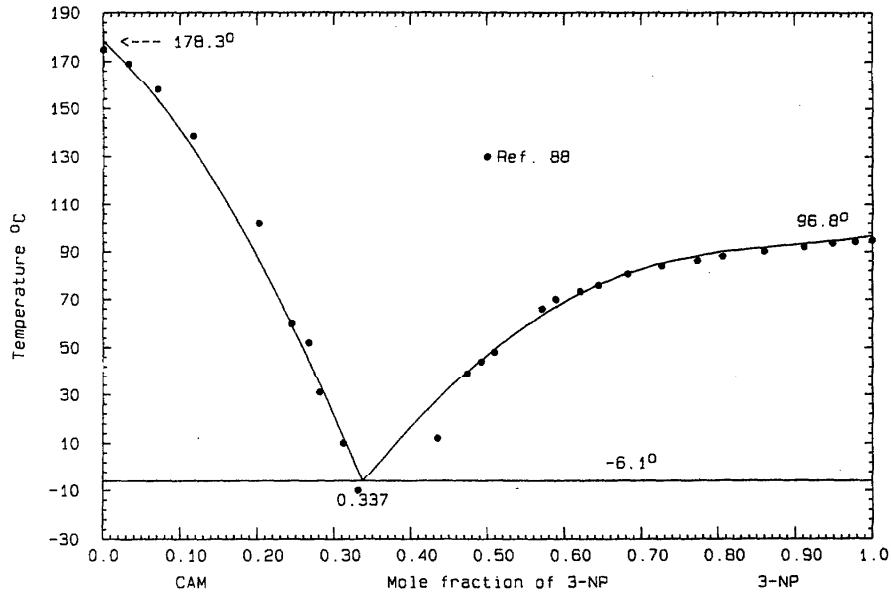

FIG. 130. The system CAM (A)+3-NP (B)

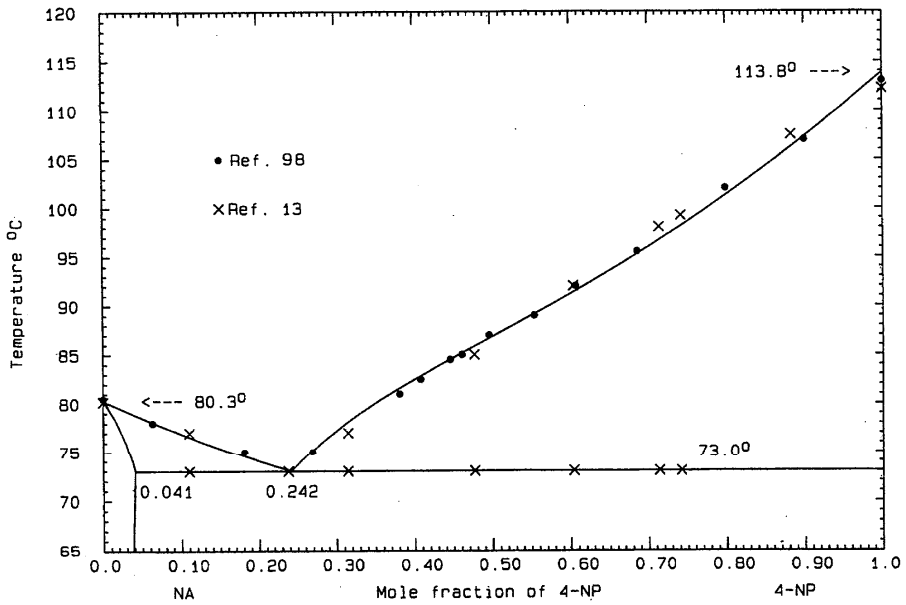

FIG. 131. The system NA (A)+4-NP (B)

$$\Delta_f G^0 = -19\,127 + 45.0000T \text{ J mol}^{-1}, \quad (239)$$

were used. The phase diagram, calculated with the use of Eqs. (235), (237), and (239) is shown in Fig. 132 and the calculated eutectics are E_1=64.2 °C, x_B=0.79; E_2=67.8 °C, x_B=0.276; and E_3=74.2 °C, x_B=0.648. The 4:1 and 1:1 compounds melt at 69.0 and 79.0 °C, respectively. Since the original data[116] were poor and badly interpreted, the calculated phase diagram can be only tentative.

DPM (A)+4-NP (B)

Data were obtained by thermal analysis[120] and the reported eutectic is 23.0 °C, x_B<0.001. The experimental melting point of diphenylmethane[120] is low, and hence the eutectic temperature is also low. The observed liquidus, tending toward flatness, suggests incipient liquid immiscibility. This is not surprising in a system like the present one having a nonpolar component (diphenylmethane) and a very polar one. It

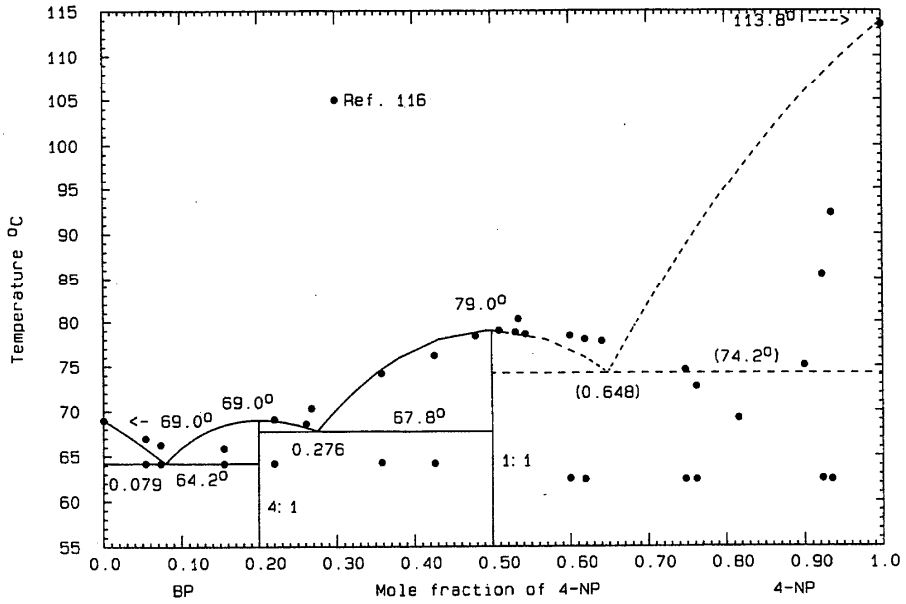

FIG. 132. The system BP (A)+4-NP (B)

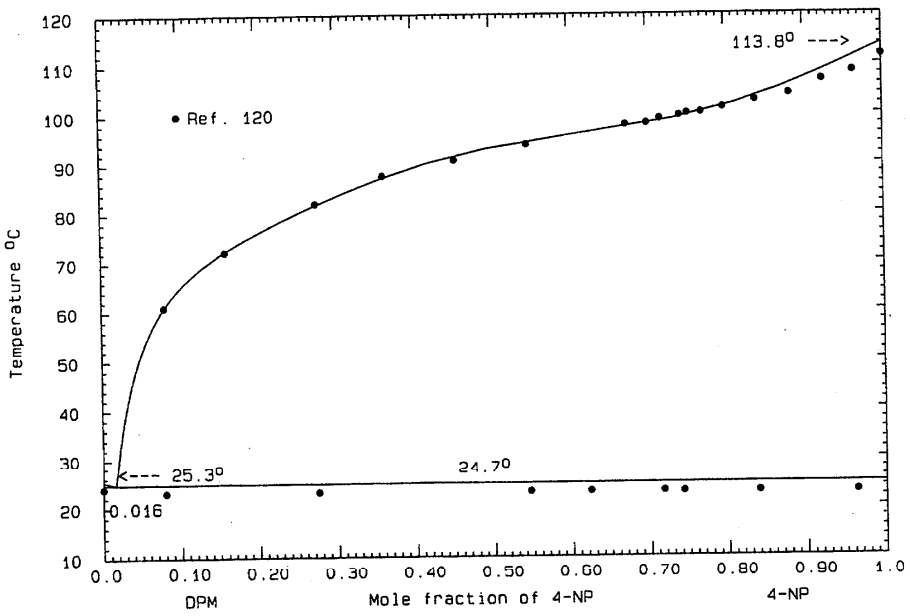

FIG. 133. The system DPM (A)+4-NP (B)

is also not surprising that four coefficients were necessary for the excess Gibbs energy of the liquid:

$$G^{E}(l)=x_A x_B(6414-8719x_B+15\,348x_B^2 - 9415x_B^3)\ \text{J mol}^{-1}. \quad (240)$$

The calculated phase diagram, Fig. 133, shows a eutectic 24.7 °C, $x_B=0.016$. The probable maximum inaccuracy in the calculated diagram is ±2°.

ANTH (A)+4-NP (B)

Data were obtained by thermal analysis[100] and the reported eutectic is 106.0 °C, $x_B=0.95$. The observed eutectic temperature is not consistent with the limiting liquidus slope for 4-nitrophenol. Data in the range $0.3<x_B<1$ were optimized and the result

$$G^{E}(l)=3496x_A x_B\ \text{J mol}^{-1} \quad (241)$$

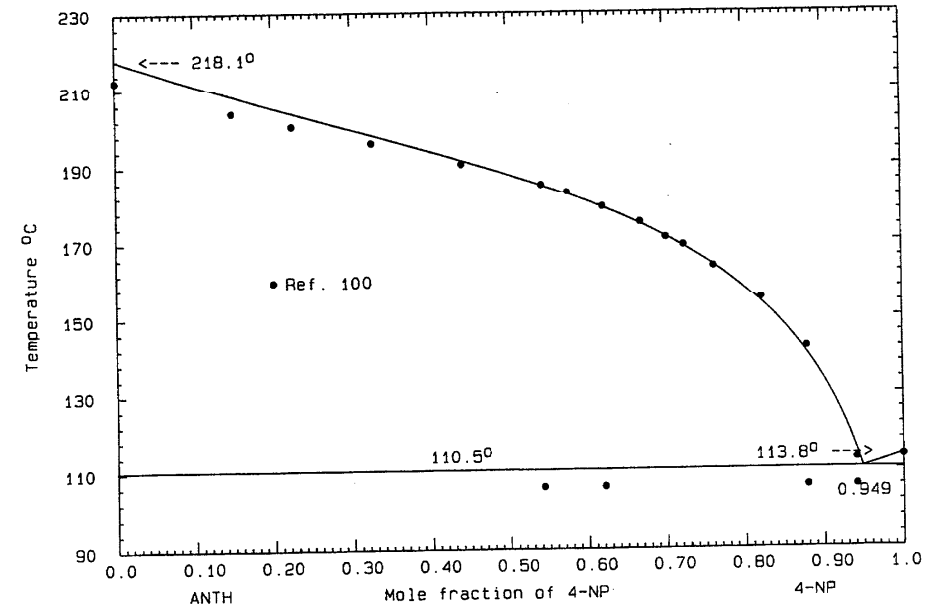

FIG. 134. The system ANTH (A)+4-NP (B)

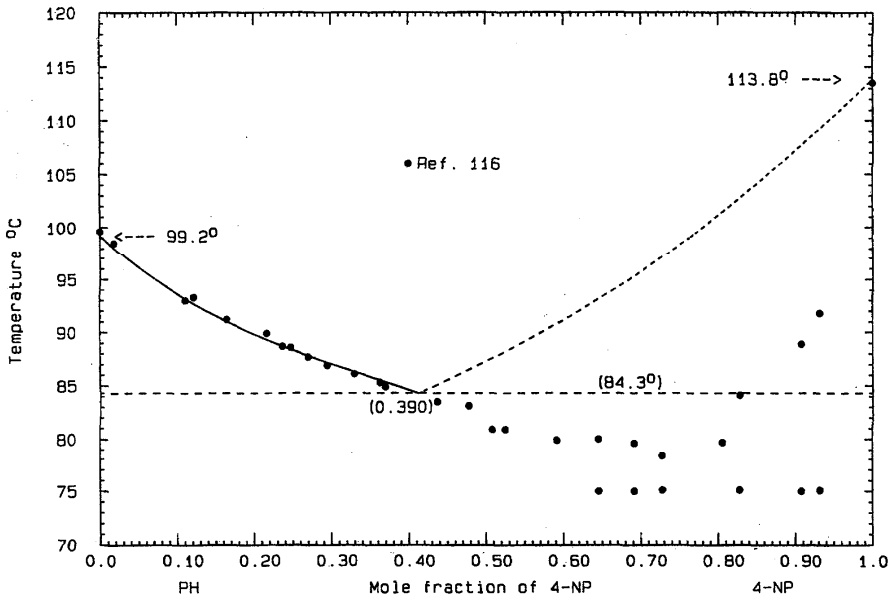

FIG. 135. The system PH (A)+4-NP (B)

was used to calculate the phase diagram, Fig. 134. The calculated eutectic is 110.5 °C, x_B=0.949. The probable maximum inaccuracy in the calculated diagram is ±3°.

PH (A)+4-NP (B)

Data were obtained by thermal analysis[116] and reported critical points are E=75.0 °C, x_B=0.77 and P=80.0 °C, x_B=0.56 (1:1 compound). Preliminary calculations showed that the data at x_B>0.5 are erroneous and hence were ignored in further consideration. Also, no compound of whatever stoichiometry could be thermodynamically stable in this system. For calculation of the phase diagram, the LHS liquidus was taken as guide, and the expression

$$G^E(l)=x_A x_B(4905-1611x_B)\ \text{J mol}^{-1} \quad (242)$$

was deduced for the liquid. The calculated phase diagram, Fig. 135, shows a eutectic 84.7 °C, x_B=0.413. Since the original data[116] were poor and badly interpreted, the calculated phase diagram can be only tentative.

TPM (A)+4-NP (B)

Data were obtained by thermal analysis[87] and the reported eutectic is 86.0 °C, x_B=0.13. Preliminary calculations showed that the temperature of reported eutectic arrests[87] were incompatible with the observed liquidus. Four coefficients were required in the quantity

$$G^E(l)=x_A x_B(8348-10\,466x_B+16\,178x_B^2 - 8381x_B^3)\ \text{J mol}^{-1} \quad (243)$$

in order that the experimental liquidus be reproduced satisfactorily. The calculated phase diagram is shown in Fig. 136 with a eutectic 88.4 °C, x_B=0.161. The probable maximum inaccuracy in the calculated diagram is ±2°.

MA (A)+4-NP (B)

Data were obtained by thermal analysis.[101] Two incongruently melting compounds were postulated (1:1 and 1:2) and reported invariant data are E=20.0 °C, x_B=0.25; P_1=24.5 °C, x_B=0.38; and P_2=58.0 °C, x_B=0.60. In the optimization, these invariant temperatures were given priority. For the liquid, the expression

$$G^E(l)=-8209x_A x_B\ \text{J mol}^{-1} \quad (244)$$

was used and optimization yielded, for the compound $(AB_2)/3$

$$\Delta_{fus}G^0=11\,132-33.4996T\ \text{J mol}^{-1}, \quad (245)$$

$$\Delta_f G^0=-12\,956+28.2093T\ \text{J mol}^{-1}. \quad (246)$$

The corresponding properties for the compound (AB)/2

$$\Delta_{fus}G^0=37\,653-125.7628T\ \text{J mol}^{-1}, \quad (247)$$

$$\Delta_f G^0=-39\,705+120.0000T\ \text{J mol}^{-1} \quad (248)$$

were not obtained from optimization but rather were assigned. These quantities are nominal and are probably in error. The calculated phase diagram, Fig. 137, was obtained with the use of Eqs. (244), (246), and (248). The calculated invariant points are E=20.0 °C, x_B=0.262; P_1=24.5 °C, x_B=0.371; P_2=57.6 °C, x_B=0.606. The probable maximum inaccuracy in the calculated diagram is ±3°.

1-AN (A)+4-NP (B)

Data were obtained by thermal analysis[102] and the reported eutectic is E=33.5 °C, x_B=0.16. No second eutectic was reported[102] but, from inspection of the tabulated data,[102] it would be approximately 66 °C, x_B=0.6. The 1:1 compound melts congruently at 68.2 °C. In preliminary calculations it

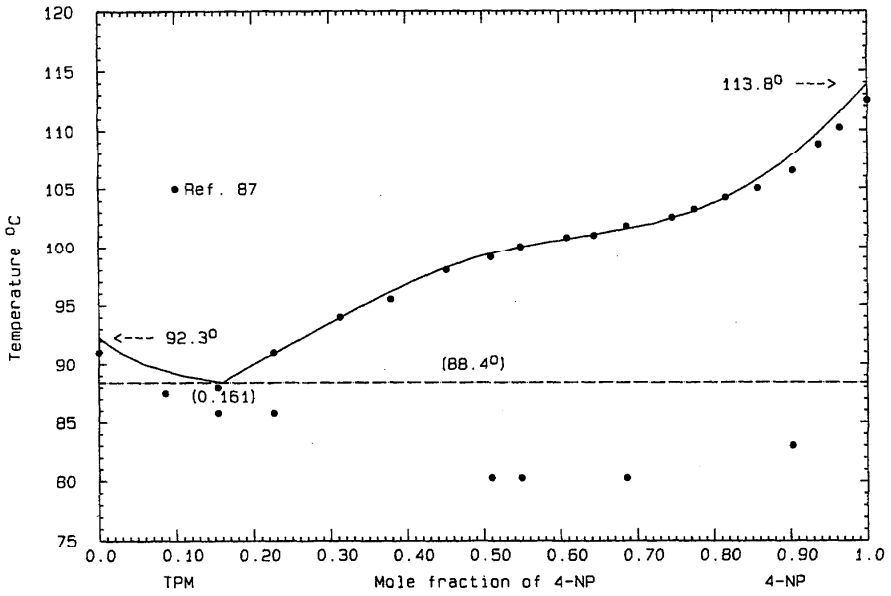

FIG. 136. The system TPM (A)+4-NP (B)

was found that the eutectic temperatures were not thermodynamically consistent with the liquidus data for the compound ($0.2<x_B<0.45$); in the final optimization, the eutectic temperatures were given greater weight. For the liquid,

$$G^E(l)=x_A x_B(-6010+2273x_B)\ \text{J mol}^{-1}, \quad (249)$$

and for the compound (AB)/2

$$\Delta_{fus}G^0=15\,271-44.8065T\ \text{J mol}^{-1}, \quad (250)$$

$$\Delta_f G^0=-16\,490+39.0453T\ \text{J mol}^{-1}. \quad (251)$$

The calculated phase diagram is shown in Fig. 138. Other calculated data are $E_1=34.4$ °C, $x_B=0.164$ and $E_2=66.6$ °C, $x_B=0.569$, and the compound melts at 67.7 °C. The probable maximum inaccuracy in the calculated diagram is ±2°.

2-AN (A)+4-NP (B)

Data were obtained by thermal analysis[102] and the reported eutectics are $E_1=78.0$ °C, $x_B=0.35$ and $E_2=78.0$ °C, $x_B=0.66$. The 1:1 compound melts congruently at 81.5 °C. The experimental melting points[102] of both pure components

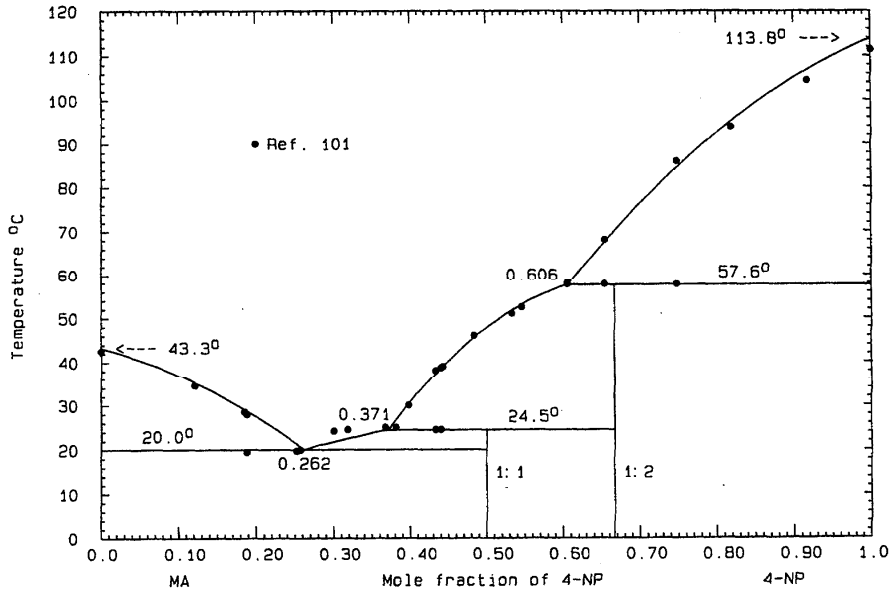

FIG. 137. The system MA (A)+4-NP (B)

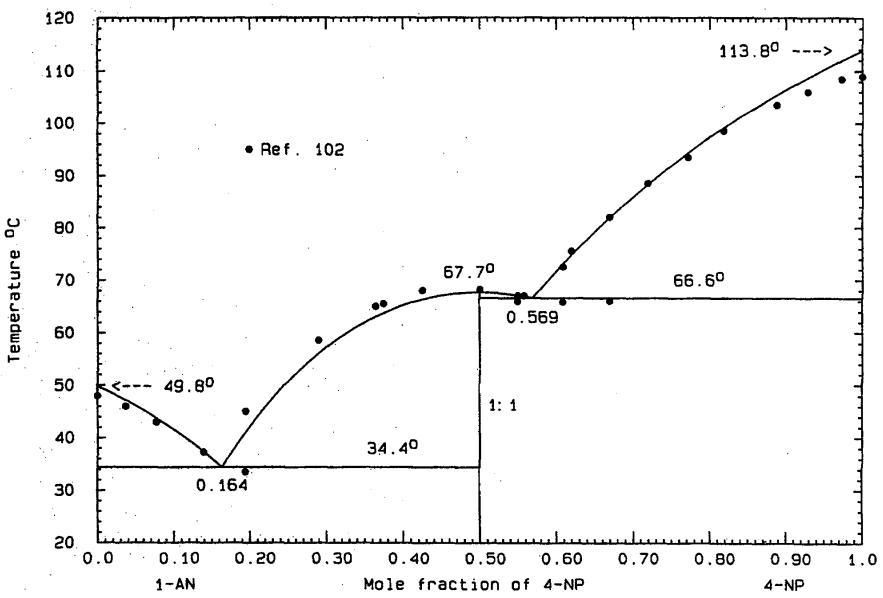

FIG. 138. The system 1-AN (A)+4-NP (B)

are low and hence the entire phase diagram may lie too low by a few degrees. Data in the range $0.2<x_B<0.8$ were optimized to give

$$G^E(l)=x_A x_B(-6164+9778x_B-7940x_B^2)\ \text{J mol}^{-1}, \quad (252)$$

and for the compound (AB)/2,

$$\Delta_{fus}G^0=19\,637-55.4244T\ \text{J mol}^{-1}, \quad (253)$$

$$\Delta_f G^0=-20\,452+49.6632T\ \text{J mol}^{-1}. \quad (254)$$

In the calculated phase diagram, Fig. 139, the chosen liquidus data are well reproduced. Other calculated data are $E_1=78.3$ °C, $x_B=0.361$; $E_2=78.1$ °C, $x_B=0.651$. The compound melts at 81.1 °C. The probable maximum inaccuracy in the calculated diagram is ±2°.

CAR (A)+4-NP (B)

Data were obtained by thermal analysis[117] and the reported eutectic is 106.7 °C, $x_B=0.95$. The experimental melting

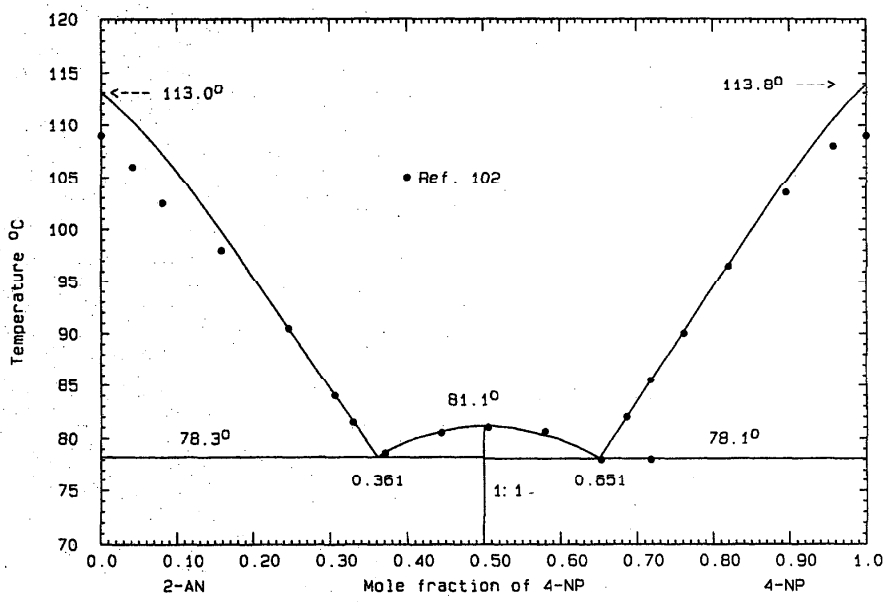

FIG. 139. The system 2-AN (A)+4-NP (B)

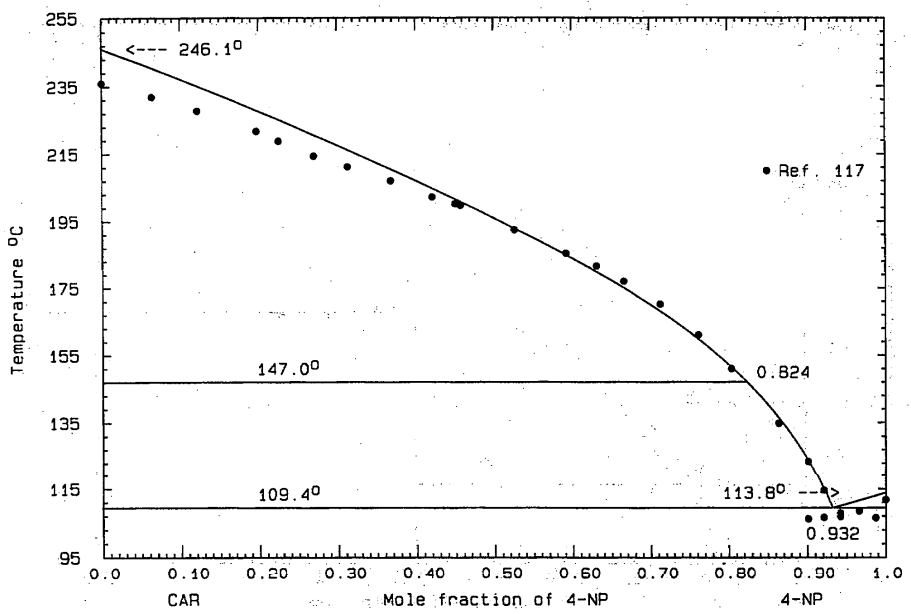

FIG. 140. The system CAR (A)+4-NP (B)

point[117] of carbazole is inaccurate and the limiting liquidus slope of 4-nitrophenol is not correct. Data in the range $0.35<x_B<1$ were optimized, and the equation

$$G^E(l)=x_A x_B(618+1398x_B)\ \text{J mol}^{-1} \quad (255)$$

was used to calculate the phase diagram, Fig. 140. The calculated eutectic is 109.4 °C, $x_B=0.932$, and the carbazole transition appears at $x_B=0.824$ on the calculated liquidus. The probable maximum inaccuracy in the calculated diagram is ±3°.

DMA (A)+4-NP (B)

Liquidus data were obtained by the visual-polythermal method[95] and the reported eutectics are $E_1=-36.0$ °C, $x_B=0.13$ and $E_2=15.0$ °C, $x_B=0.58$. The 1:1 compound melts congruently at 21.5 °C. The data were optimized to give

$$G^E(l)=x_A x_B(-11\,711-17\,916x_B+13\,660x_B^2)\ \text{J mol}^{-1} \quad (256)$$

for the liquid and

$$\Delta_{fus}G^0=14\,438-48.9089T\ \text{J mol}^{-1}, \quad (257)$$

$$\Delta_f G^0=-18\,752+43.1477T\ \text{J mol}^{-1} \quad (258)$$

for the compound (AB)/2. The calculated phase diagram, Fig. 141, shows eutectics $E_1=-32.2$ °C, $x_B=0.108$ and $E_2=18.2$ °C, $x_B=0.585$. The compound melts at 22.0 °C. The probable maximum inaccuracy in the calculated diagram is ±2°.

BENZ (A)+4-NP (B)

Liquidus data were obtained by the visual-polythermal method[118] and the reported eutectics are $E_1=94.5$ °C, $x_B=0.33$ and $E_2=85.5$ °C, $x_B=0.74$. The 1:1 compound melts congruently at 99.5 °C. The experimental[118] melting point of benzamide is 4° too low, so data in the range $0.2<x_B<1$ were optimized to give

$$G^E(l)=x_A x_B(-3471-1676x_B)\ \text{J mol}^{-1} \quad (259)$$

for the liquid and

$$\Delta_{fus}G^0=17\,111-46.0028T\ \text{J mol}^{-1}, \quad (260)$$

$$\Delta_f G^0=-18\,188+40.2416T\ \text{J mol}^{-1} \quad (261)$$

for the compound (AB)/2. The calculated phase diagram, Fig. 142, shows calculated eutectics $E_1=93.7$ °C, $x_B=0.349$ and $E_2=85.1$ °C, $x_B=0.732$. The compound melts at 98.8 °C. The probable maximum inaccuracy in the calculated diagram is ±1°.

HB (A)+4-NP (B)

Data were obtained by thermal analysis[104] and the reported eutectic is 65.8 °C, $x_B=0.48$. The experimental melting point[104] of 3-hydroxybenzaldehyde is 3° too low and in preliminary calculations it was found that if the experimental eutectic temperature were adopted as correct, the calculated liquidus would lie everywhere above the experimental data. Data in the range $0.25<x_B<1$ were optimized to give

$$G^E(l)=-1536x_A x_B\ \text{J mol}^{-1}, \quad (262)$$

and the calculated phase diagram, Fig. 143, shows a eutectic 64.2 °C, $x_B=0.497$. The probable maximum inaccuracy in the calculated diagram is ±2°.

ACP (A)+4-NP (B)

Data were obtained by thermal analysis[119] and the reported eutectic is −4.0 °C, $x_B=0.35$. In preliminary calculations, it was found that the data in the range $0.3<x_B<0.45$ were in-

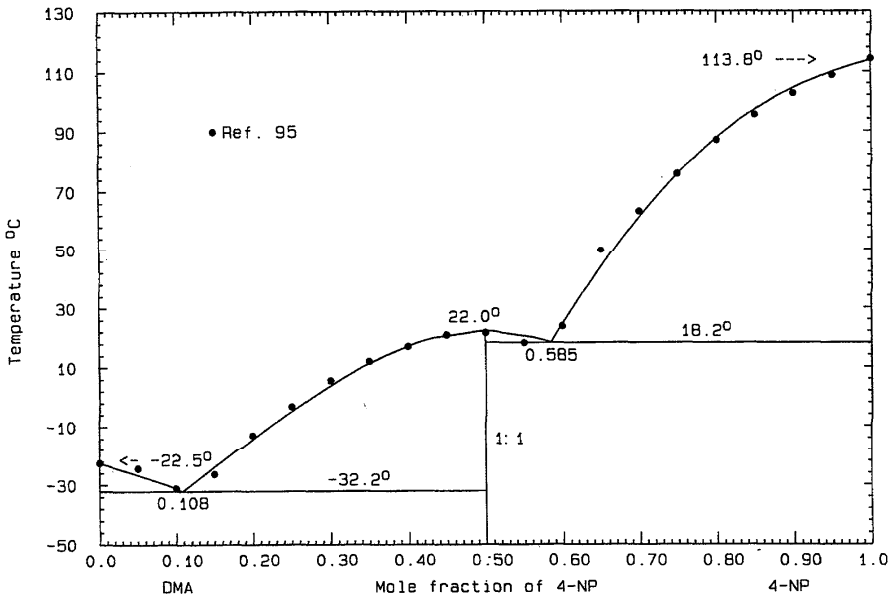

FIG. 141. The system DMA (A)+4-NP (B)

consistent with the remaining data and so these four data were omitted from the optimization, which yielded the expression

$$G^{E}(l)=x_A x_D(-3158-8586x_D+7733x_B^2)\ \text{J mol}^{-1}. \quad (263)$$

The calculated phase diagram, Fig. 144, shows a eutectic of −4.0 °C, x_B=0.313. The probable maximum inaccuracy in the calculated diagram is ±2°.

CAM (A)+4-NP (B)

Data were obtained by thermal analysis[88]; no eutectic data were reported. In preliminary calculations, it was found that data in the range $0.3<x_B<0.5$ did not fit well with the remaining liquidus data and so these were omitted in the optimization. The phase diagram, Fig. 145, was calculated with the use of the quantity

$$G^{E}(l)=x_A x_B(-8369+2500x_B)\ \text{J mol}^{-1}, \quad (264)$$

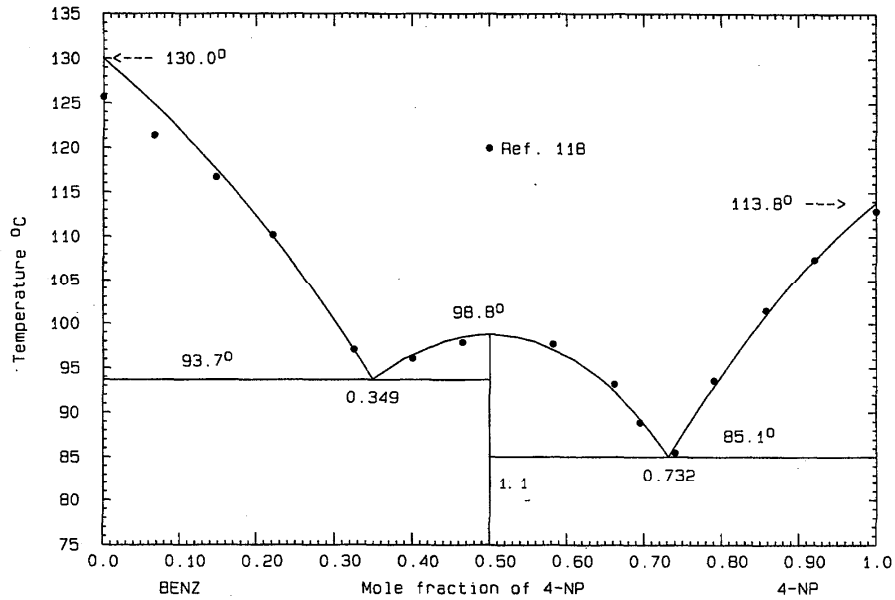

FIG. 142. The system BENZ (A)+4-NP (B)

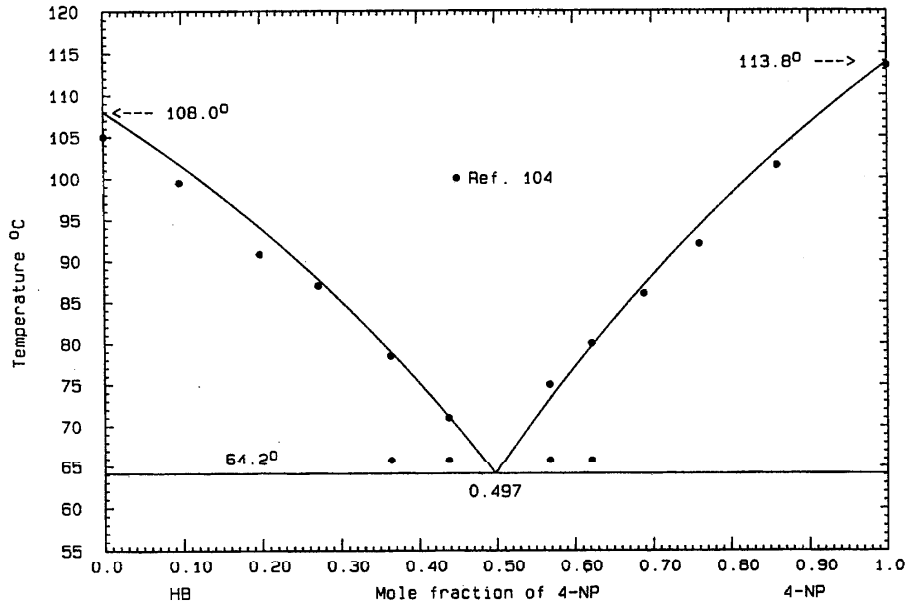

FIG. 143. The system HB (A)+4-NP (B)

and the calculated eutectic is 5.4 °C, x_B=0.357. The true eutectic temperature of this system remains uncertain. The probable maximum inaccuracy in the calculated diagram is ±10°.

2.5.16. Systems Based on 2-Nitroaniline

4-HBP (A)+2-NA (B)

Data were obtained by thermal analysis[72] and the reported eutectic is 64.6 °C, x_B=0.75. All liquidus data were included in the optimization, which yielded the expression

$$G^E(l)=x_A x_B(3950-9425x_B+7430x_B^2)\ \text{J mol}^{-1}. \quad (265)$$

The phase diagram calculated with the use of Eq. (265) is shown in Fig. 146 and the calculated eutectic is 64.6 °C, x_B=0.858. The probable maximum inaccuracy in the calculated diagram is ±2°.

ABA (A)+2-NA (B)

Data were obtained by the thaw–melt method,[56] using the "fused preparation" of sample mixtures (judged by the authors themselves to give the most reliable results). No eutec-

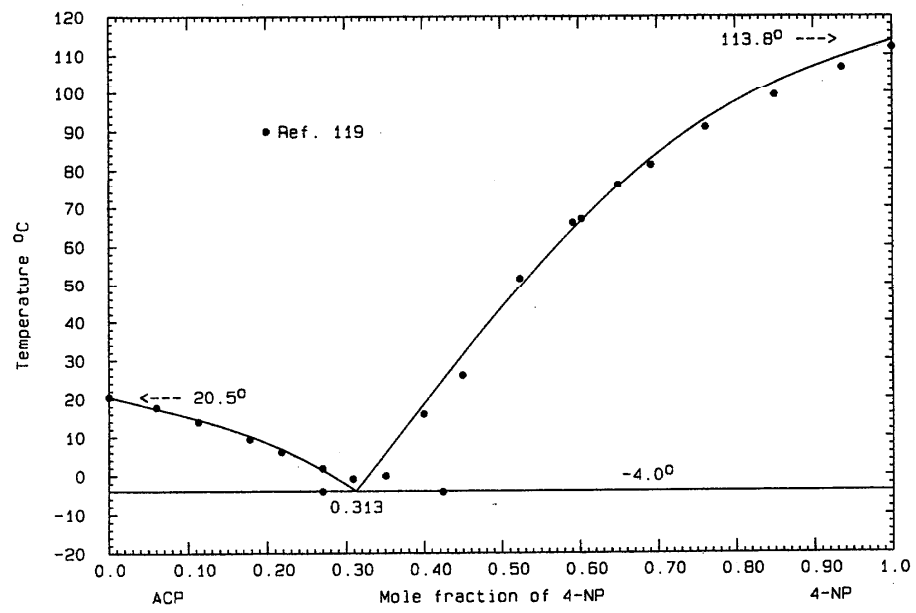

FIG. 144. The system ACP (A)+4-NP (B)

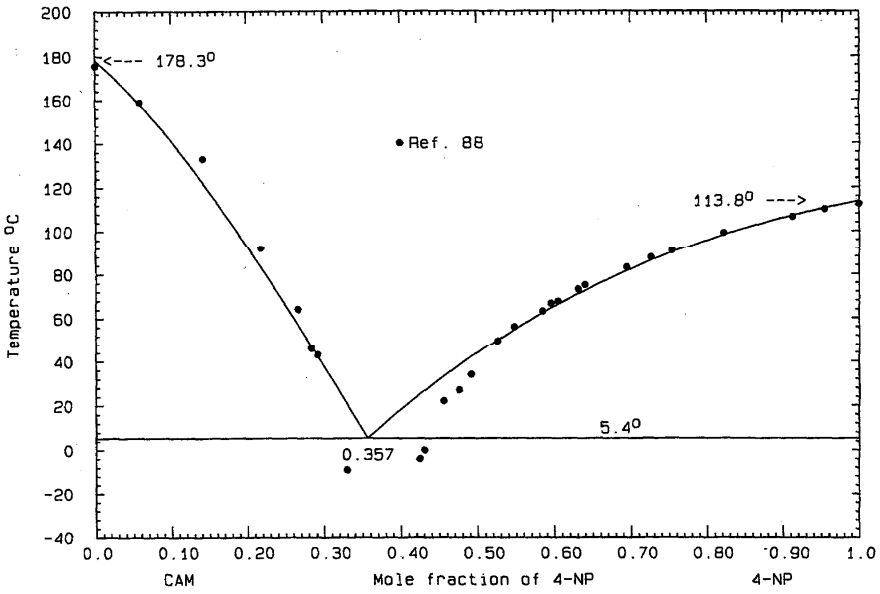

FIG. 145. The system CAM (A)+4-NP (B)

tic was reported, but from the tabulated data[56] the eutectic is close to 69.5 °C, x_B=0.95. The experimental phase diagram[56] shows a large amount of solid solubility based on 4-aminobenzoic acid, but preliminary calculations showed that the reported solidus data must be artefactual; no solid solubility is necessary to reproduce the experimental liquidus. The liquidus data were optimized and the result

$$G^E(l)=x_A x_B(3440-3019x_B+3150x_B^2)\ \text{J mol}^{-1} \quad (266)$$

was used to calculate the phase diagram, Fig. 147. The calculated eutectic is 69.4 °C, x_B=0.954. The probable maximum inaccuracy in the calculated diagram is ±2°.

2.5.17. Systems Based on 3-Nitroaniline

HQ (A)+3-NA (B)

Data were obtained by thermal analysis[72] and the reported eutectic is 100.1 °C, x_B=0.70. There is some small scatter in

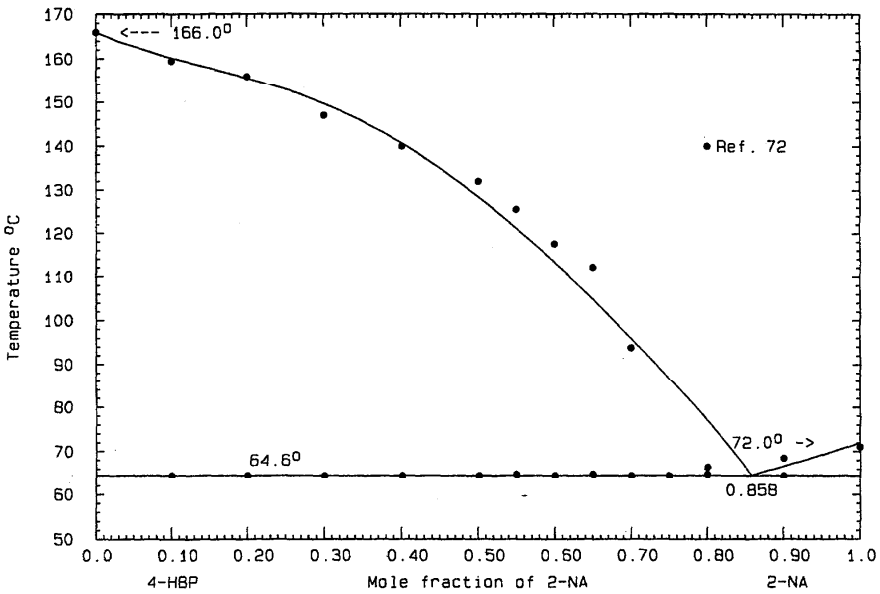

FIG. 146. The system 4-HBP (A)+2-NA (B)

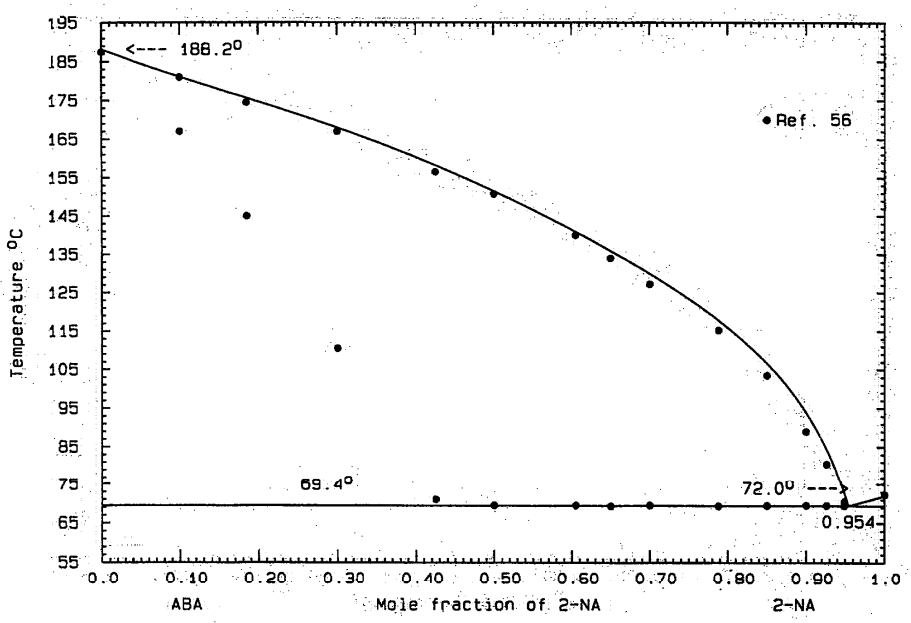

FIG. 147. The system ABA (A)+2-NA (B)

the liquidus data but all were included in the optimization to give

$$G^{E}(l)=x_A x_B(2145-9463x_B+9200x_B^2)\ \text{J mol}^{-1} \qquad (267)$$

on which the calculated phase diagram, Fig. 148, was based. The eutectic shown is 100.1 °C, $x_B=0.716$. The probable maximum inaccuracy in the calculated diagram is ±2°.

4-HBP (A)+3-NA (B)

Data were obtained by thermal analysis[72] and the reported eutectic is 97.0 °C, $x_B=0.70$. The LHS liquidus displays strong positive deviations from ideality, while the RHS arm shows negative deviations. The liquidus data were optimized to give the expression

$$G^{E}(l)=x_A x_B(2611-6261x_B+5450x_B^2)\ \text{J mol}^{-1} \qquad (268)$$

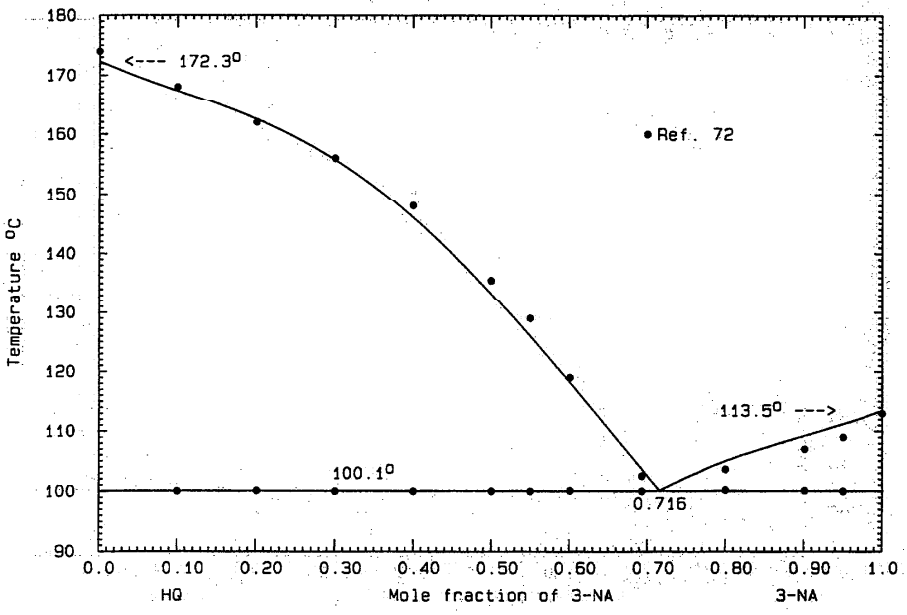

FIG. 148. The system HQ (A)+3-NA (B)

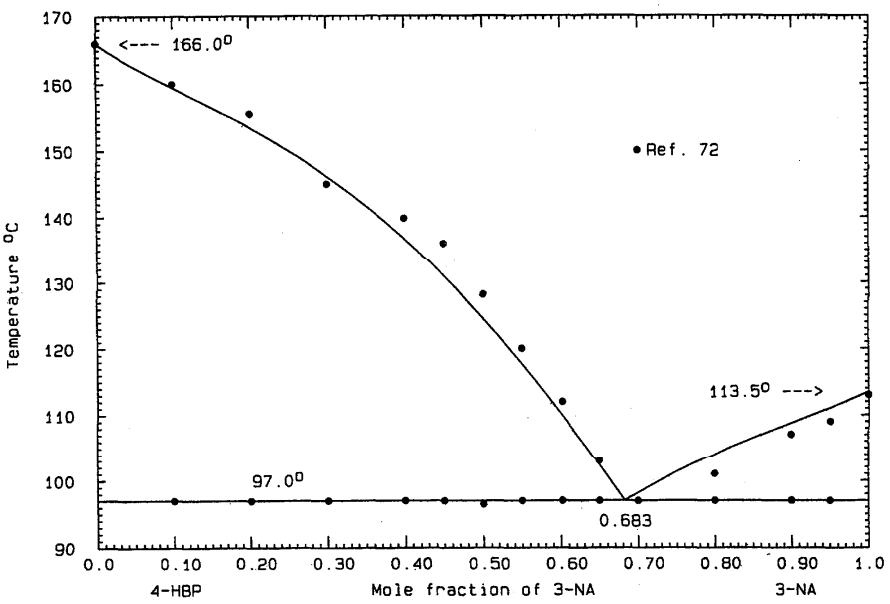

FIG. 149. The system 4-HBP (A)+3-NA (B)

on which the calculated phase diagram, Fig. 149, is based. The calculated eutectic is 97.0 °C, x_B=0.683. The probable maximum inaccuracy in the calculated diagram is ±2°.

2.5.18. Systems Based on 4-Nitroaniline

HQ (A)+4-NA (B)

Data were obtained by thermal analysis[58] and the reported eutectic is 120.5 °C, x_B=0.60. The LHS liquidus data may be high due to a high experimental melting point of hydroquinone.[58] The data were optimized to give the expression

$$G^E(l)=x_A x_B(325+605x_B)\ \text{J mol}^{-1}, \qquad (269)$$

and the calculated phase diagram, Fig. 150, shows a eutectic 121.0 °C, x_B=0.638. The probable maximum inaccuracy in the calculated diagram is ±2°.

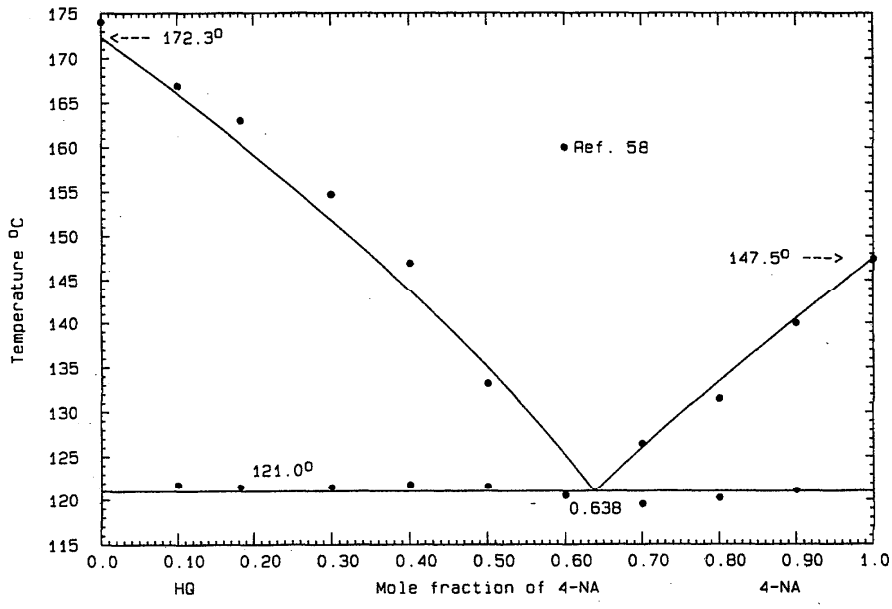

FIG. 150. The system HQ (A)+4-NA (B)

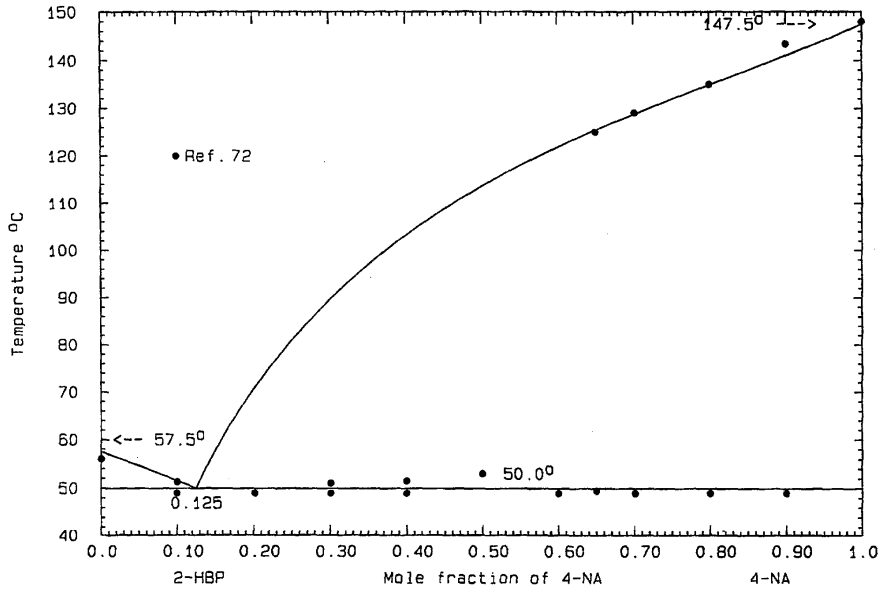

FIG. 151. The system 2 HBP (A)+4-NA (B)

2-HBP (A)+4-NA (B)

Data were obtained by thermal analysis[72] and the reported eutectics are E_1=49.0 °C, x_B=0.18 and E_2=49.0 °C, x_B=0.60; a congruently melting 1:1 compound is claimed (53.0 °C). The shape of the RHS liquidus does not at all suggest the presence of such a compound. The observed data[72] can equally well be accounted for by a simple eutectic system based on the quantity

$$G^E(l)=x_Ax_B(504+1606x_B) \text{ J mol}^{-1}. \quad (270)$$

The calculated phase diagram, Fig. 151, displays a eutectic of 50.0 °C, x_B=0.125. The probable maximum inaccuracy in the calculated diagram is ±3°.

4-HBP (A)+4-NA (B)

The data were obtained by thermal analysis[72] and the reported eutectic is 117.5 °C, x_B=0.62. All the liquidus data were optimized to deduce the equation

$$G^E(l)=x_Ax_B(3300-5752x_B+4547x_B^2) \text{ J mol}^{-1} \quad (271)$$

upon which the calculated phase diagram, Fig. 152, is based. The calculated eutectic is 117.5 °C, x_B=0.589. The probable maximum inaccuracy in the calculated diagram is ±1°.

2.5.19. System Based on 3-Nitrobenzoic Acid

PH (A)+NBA (B)

Data were obtained by the thaw–melt method[39] and the reported eutectics are E_1=94.5 °C, x_B=0.085 and E_2=125.0 °C, x_B=0.80. The 1:2 compound melts congruently at 129.5 °C. The heat of fusion of the compound[39] is 21 250 J mol^{-1}. All the liquidus data were optimized, and the eutectic temperatures were given preponderant weighting in the optimization to give

$$G^E(l)=x_Ax_B(5176-4244x_B) \text{ J mol}^{-1}. \quad (272)$$

The calculated phase diagram, Fig. 153, was based on Eq. (272) and the properties

$$\Delta_{fus}G^0=10\,590-26.2708T \text{ J mol}^{-1}, \quad (273)$$

$$\Delta_fG^0=-10\,069+20.9806T \text{ J mol}^{-1} \quad (274)$$

for the compound $(AB_2)/3$. The calculated eutectics are E_1=93.9 °C, x_B=0.106 and E_2=124.9 °C, x_B=0.788. The 1:2 compound melts at 129.9 °C. The probable maximum inaccuracy in the calculated diagram is ±1°.

2.5.20. Systems Based on 2,4-Dinitrophenol

NA (A)+DNP (B)

Data were obtained by thermal analysis[98,115] and the reported eutectics[98] are E_1=72.0 °C, x_B=0.15 and E_2=88.0 °C, x_B=0.64. No eutectic arrests were recorded in the two studies. The 1:1 compound melts congruently[98] at 91.5 °C. The two sets of liquidus data agree within 1°, although the RHS liquidus is low, due to the low experimental melting point of 2,4-dinitrophenol.[98,115] Optimization of liquidus data yielded the expression

$$G^E(l)=-3536x_Ax_B \text{ J mol}^{-1} \quad (275)$$

and the properties of the compound (AB)/2 are

$$\Delta_{fus}G^0=25\,739-70.4045T \text{ J mol}^{-1}, \quad (276)$$

$$\Delta_fG^0=-26\,623+64.6433T \text{ J mol}^{-1}. \quad (277)$$

The phase diagram, calculated with the use of Eqs. (275) and (277), is shown in Fig. 154. The calculated eutectics are E_1=71.0 °C, x_B=0.140 and E_2=88.7 °C, x_B=0.664; the compound melts at 92.4 °C. The probable maximum inaccuracy in the calculated diagram is ±1°.

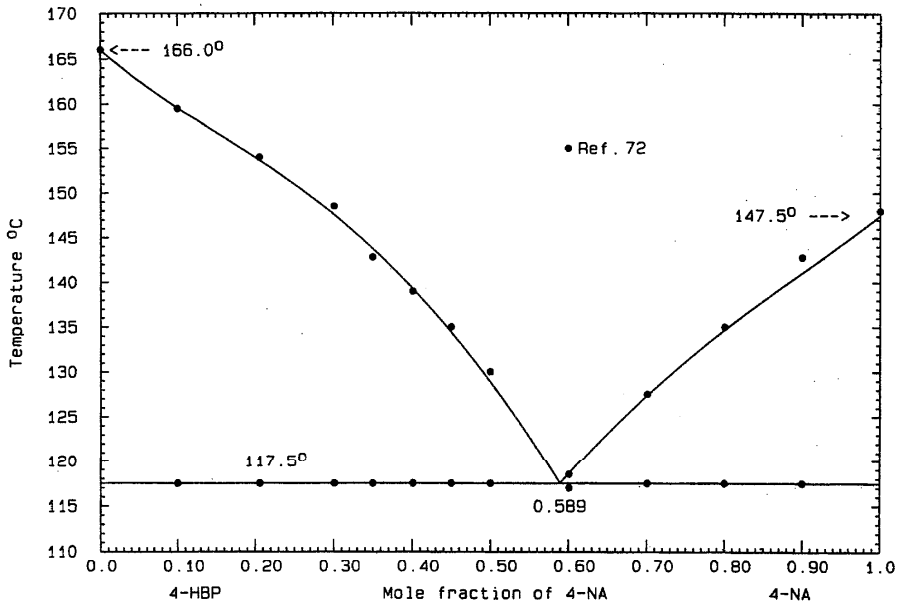

FIG. 152. The system 4-HBP (B)+4-NA (B)

FLN (A)+DNP (B)

Data were obtained by thermal analysis[99] and the reported eutectic is 74.0 °C, x_B=0.45. No eutectic arrests were recorded. Upon optimization of data in the range $0<x_B<0.7$, the expression

$$G^E(l)=x_A x_B(-1468+454x_B)\ \text{J mol}^{-1} \quad (278)$$

was obtained. The calculated phase diagram, Fig. 155, shows a eutectic of 73.7 °C, x_B=0.458. The probable maximum inaccuracy in the calculated diagram is ±1°.

ANTH (A)+DNP (B)

Data were obtained by thermal analysis[100] and the reported eutectic is 101.0 °C, x_B=0.84. The experimental melting points[100] of both end components are low and the observed eutectic temperature is probably 3°–4° low in consequence. Liquidus data in the range $0.3<x_B<0.85$ were optimized to give

$$G^E(l)=x_A x_B(-2457+1063x_B)\ \text{J mol}^{-1}. \quad (279)$$

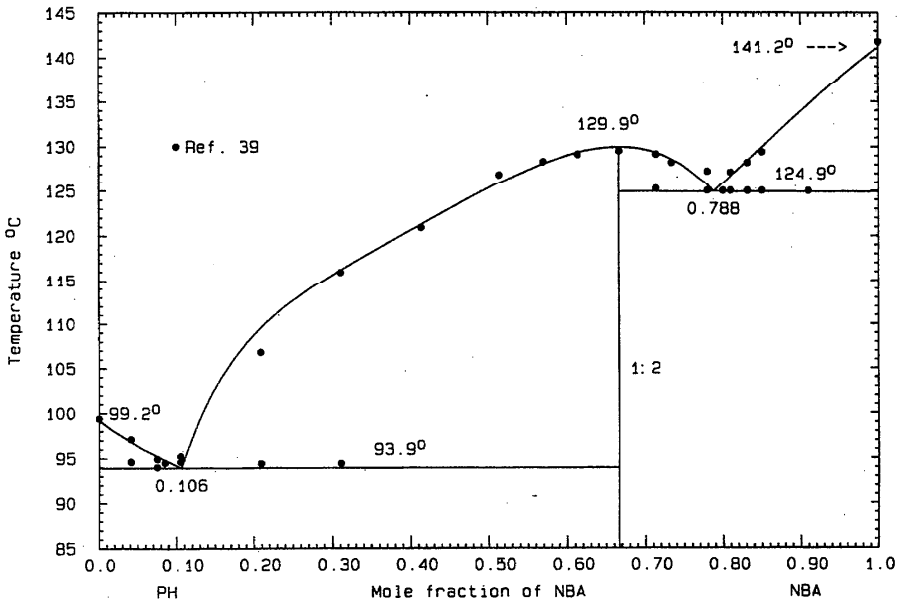

FIG. 153. The system PH (A)+NBA (B)

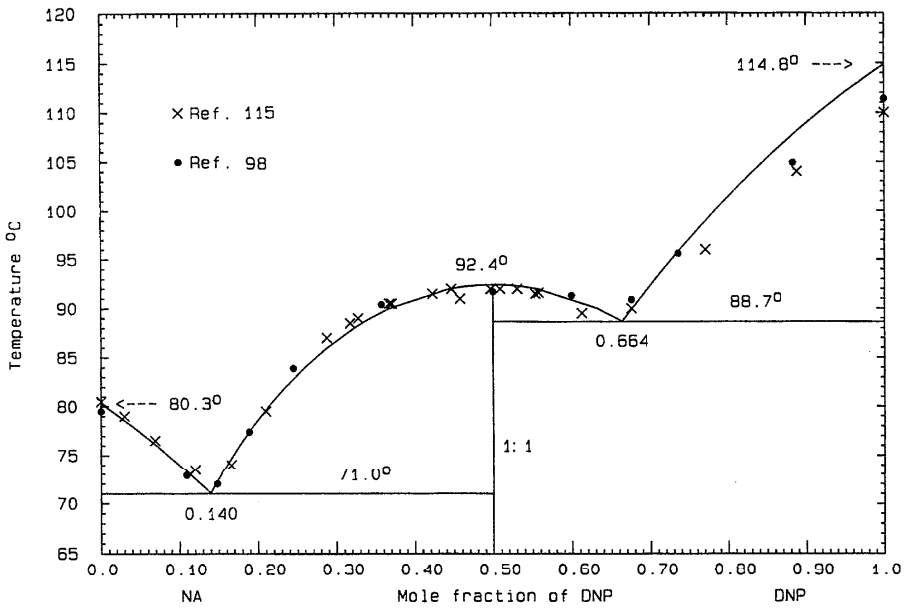

FIG. 154. The system NA (A)+DNP (B)

The phase diagram, Fig. 156, shows a eutectic of 104.7 °C, $x_B=0.824$. The probable maximum inaccuracy in the calculated diagram is ±2°.

PH (A)+DNP (B)

Liquidus data were obtained by thermal analysis[121] and the reported eutectics are $E_1=120.0$ °C, $x_B=0.264$ and $E_2=101.0$ °C, $x_B=0.844$. The 1:1 compound melts congruently at 146.3 °C. The eutectic temperatures were given preponderant weight in the optimization, which gave the quantity

$$G^E(l)=x_A x_B(-5600-620x_B)\ \text{J mol}^{-1} \quad (280)$$

and for the compound (AB)/2

$$\Delta_{fus}G^0=13\,077-31.1772T\ \text{J mol}^{-1}, \quad (281)$$

$$\Delta_f G^0=-14\,555+25.4144T\ \text{J mol}^{-1}. \quad (282)$$

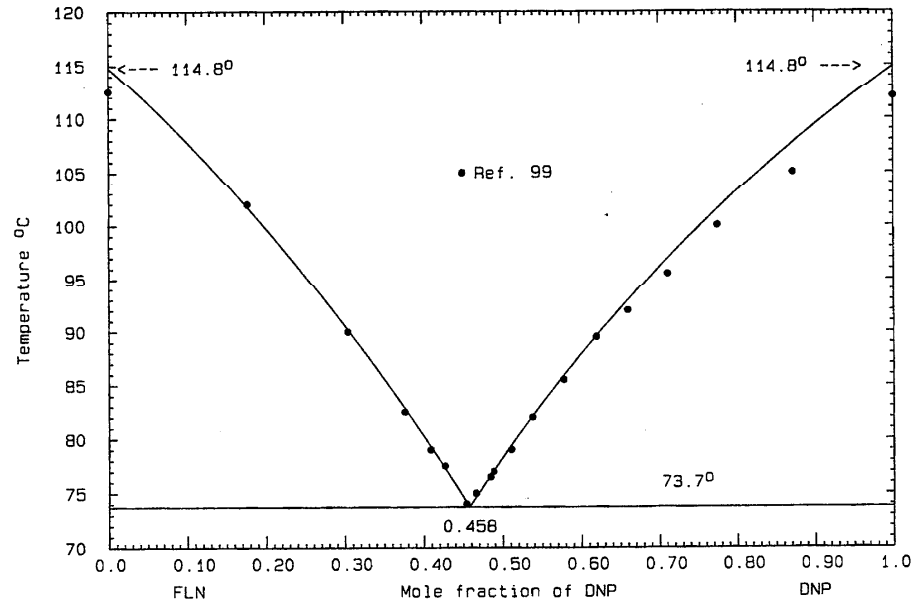

FIG. 155. The system FLN (A)+DNP (B)

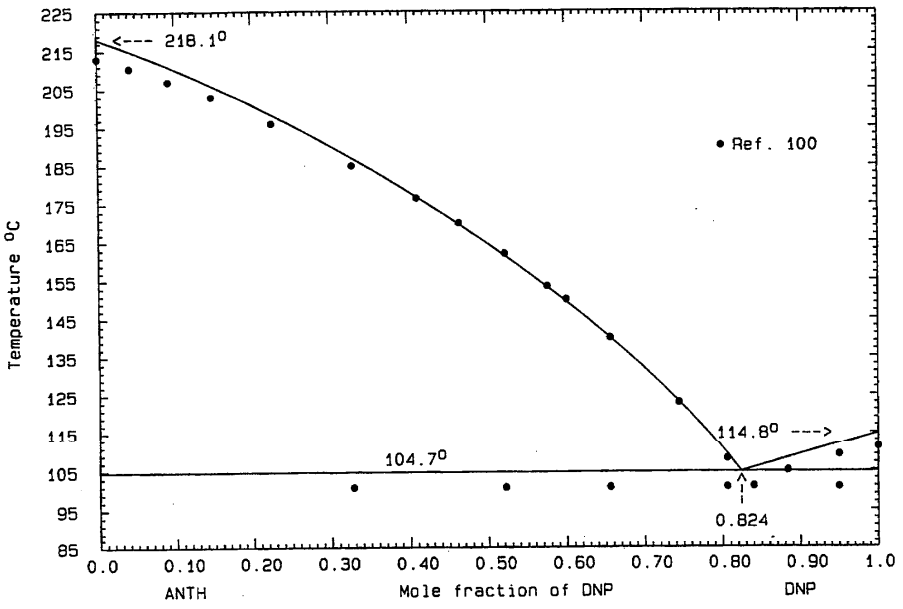

FIG. 156. The system ANTH (A)+DNP (B)

The calculated phase diagram, Fig. 157, shows calculated eutectics $E_1=120.0$ °C, $x_B=0.250$ and $E_2=101.0$ °C, $x_B=0.815$. The compound melts at 146.3 °C. The probable maximum inaccuracy in the calculated diagram is ±1°.

PY (A) + DNP (B)

Data were obtained by the thaw-melt method[43] and the reported eutectics are $E_1=120.0$ °C, $x_B=0.264$ and $E_2=101.0$ °C, $x_B=0.844$. The 1:1 compound melts congruently at 146.3 °C. The principal features of the system were reproduced with the use of

$$G^E(1)=x_A x_B(-5600-620\ x_B)\ \text{J mol}^{-1} \quad (283)$$

for the liquid and

$$\Delta_{fus}G^0=13\ 077-31.1772T\ \text{J mol}^{-1} \quad (284)$$

$$\Delta_f G^0=-14\ 555+25.4144T\ \text{J mol}^{-1} \quad (285)$$

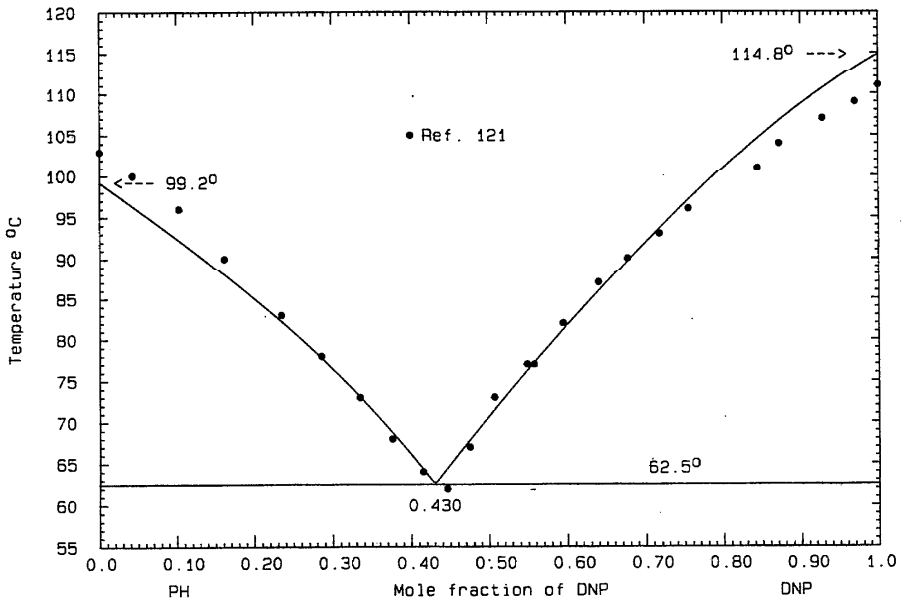

FIG. 157. The system PH (A)+DNP (B)

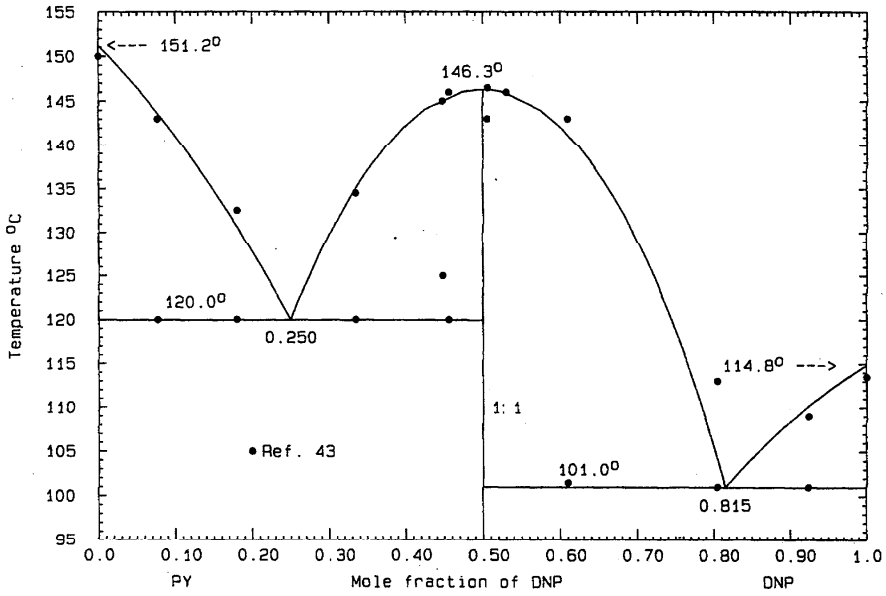

FIG. 158. The system PY (A)+DNP (B)

for the compound (AB)/2. The calculated phase diagram appears in Fig. 158, with calculated eutectics $E_1=120$ °C, $x_B=0.250$ and $E_2=101.0$ °C, $x_B=0.815$. The compound melts at 146.3 °C. The probable maximum inaccuracy in the calculated diagram is ±1°.

FTHN (A)+DNP (B)

Data were obtained by the thaw–melt method[43] and the reported eutectics are $E_1=75.0$ °C, $x_B=0.312$ and $E_2=85.0$ °C, $x_B=0.612$. The 1:1 compound melts congruently at 92.0 °C. In the optimization, the eutectic and compound melting temperatures were given preponderant weight, with the result

$$G^E(l)=x_A x_B(-5000+1500x_B)\ \text{J mol}^{-1} \quad (286)$$

for the liquid and for the compound (AB)/2

$$\Delta_{fus}G^0=7836-21.4610T\ \text{J mol}^{-1}, \quad (287)$$

$$\Delta_f G^0=-8899+15.6982T\ \text{J mol}^{-1}. \quad (288)$$

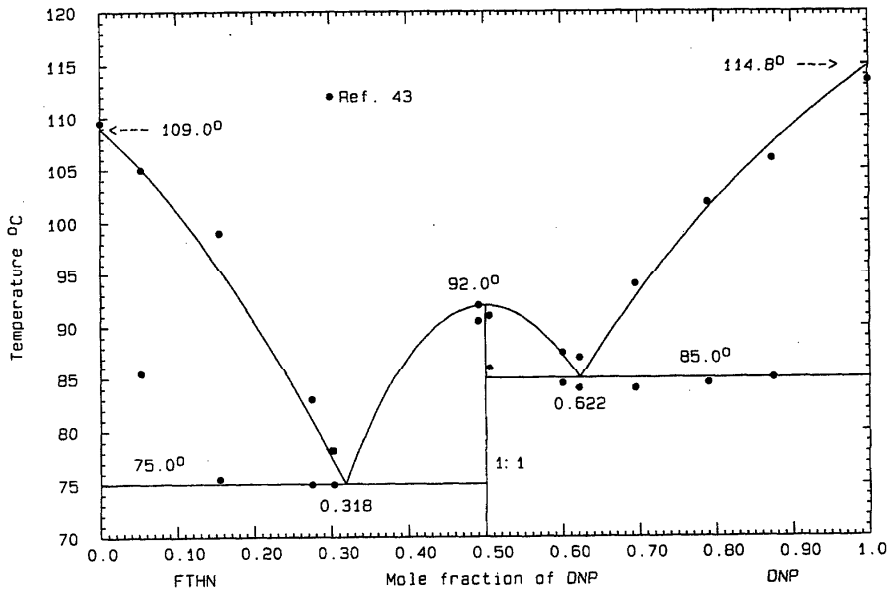

FIG. 159. The system FTHN (A)+DNP (B)

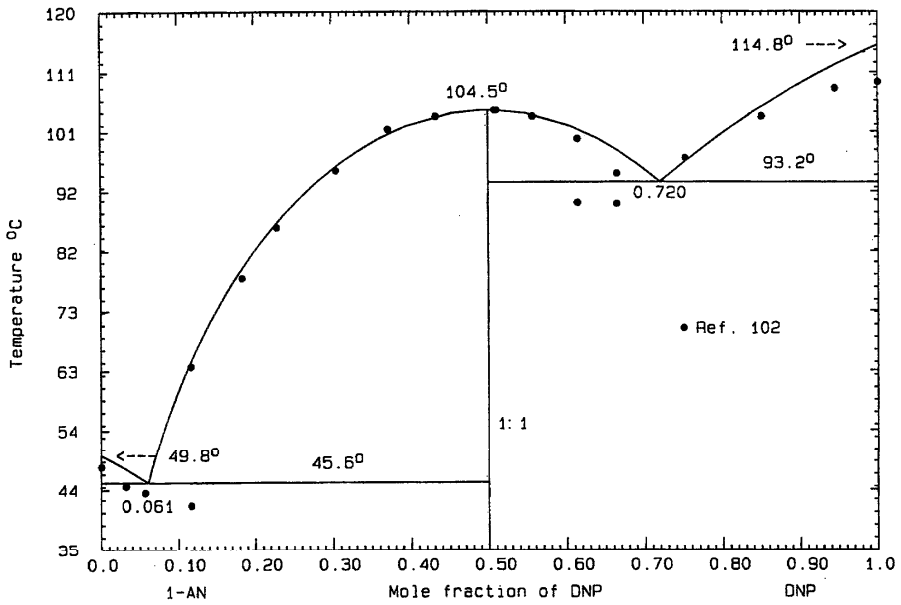

FIG. 160. The system 1-AN (A)+DNP (B)

The calculated phase diagram, Fig. 159, shows calculated eutectics E_1=75.0 °C, x_B=0.318 and E_2=85.0 °C, x_B=0.622; the compound melts at 92.0 °C. The probable maximum inaccuracy in the calculated diagram is ±1°.

1-AN (A)+DNP (B)

Data were obtained by thermal analysis[102] and the reported eutectics are E_1=42.0 °C, x_B=0.05 and E_2=90.0 °C, x_B=0.70. The 1:1 compound melts congruently at 104.5 °C. The experimental E_1 temperature is erroneous because the melting point and limiting liquidus slope for one-aminonaphthalene are both in error; the same is true also for 2,4-dinitrophenol.[102] In such a case, the observed compound liquidus and melting point data were given greater weight than the eutectic temperatures. For the liquid,

$$G^E(l) = -4439 x_A x_B \text{ J mol}^{-1}, \quad (289)$$

and for the compound (AB)/2,

$$\Delta_{fus}G^0 = 17\,999 - 47.6546T \text{ J mol}^{-1}, \quad (290)$$

$$\Delta_f G^0 = -19\,109 + 41.8934T \text{ J mol}^{-1}. \quad (291)$$

The calculated phase diagram, Fig. 160, shows calculated eutectics E_1=45.6 °C, x_B=0.061 and E_2=93.2 °C, x_B=0.720; the compound melts at 104.5 °C. The probable maximum inaccuracy in the calculated diagram is ±2°.

2-AN (A)+DNP (B)

Data were obtained by thermal analysis[102] and the reported eutectics are E_1=72.0 °C, x_B=0.44 and E_2=72.0 °C, x_B=0.54. The 1:1 compound melts at 72.3 °C. The experimental melting points of both end components[102] are low, and there are not enough compound liquidus data for a proper optimization. First, the LHS and RHS liquidus data in the interval $0.3<x_B<0.8$ were fitted by trial and error to give

$$G^E(l) = -5000 x_A x_B \text{ J mol}^{-1}, \quad (292)$$

and then the properties for the compound (AB)/2

$$\Delta_{fus}G^0 = 17\,310 - 50.0000T \text{ J mol}^{-1}, \quad (293)$$

$$\Delta_f G^0 = -18\,560 + 44.2372T \text{ J mol}^{-1} \quad (294)$$

were chosen to reproduce, as closely as possible, the experimental eutectics. The calculated phase diagram, Fig. 161, shows eutectics E_1=71.9 °C, x_B=0.427 and E_2=72.3 °C, x_B=0.558; the compound melts at 73.1 °C. The calculated phase diagram and the assigned thermodynamic properties, Eqs. (292)–(294), carry significant uncertainty. The probable maximum inaccuracy in the calculated diagram is ±4°.

CAR (A)+DNP (B)

Data were obtained by thermal analysis[117] and the reported eutectic is 98.6 °C, x_B=0.82. This temperature is almost certainly in error, since the experimental melting point of 2,4-dinitrophenol is 5° too low. Liquidus data in the interval $0.4<x_B<0.9$ were optimized to give

$$G^E(l) = x_A x_B(-2997 - 602x_B) \text{ J mol}^{-1} \quad (295)$$

and the calculated phase diagram, Fig. 162, shows a calculated eutectic 101.8 °C, x_B=0.808. The carbazole transition appears on the calculated liquidus at x_B=0.652. The probable maximum inaccuracy in the calculated diagram is ±3°.

HB (A)+DNP (B)

Data were obtained by thermal analysis[104] and the reported eutectics are E_1=78.0 °C, x_B=0.33 and E_2=78.5 °C, x_B=0.53. The central part of the liquidus appears almost flat and the authors[104] speculated that there might be a 1:1 compound melting congruently at a temperature close to the eutectic temperatures. Most of the LHS and RHS liquidus data

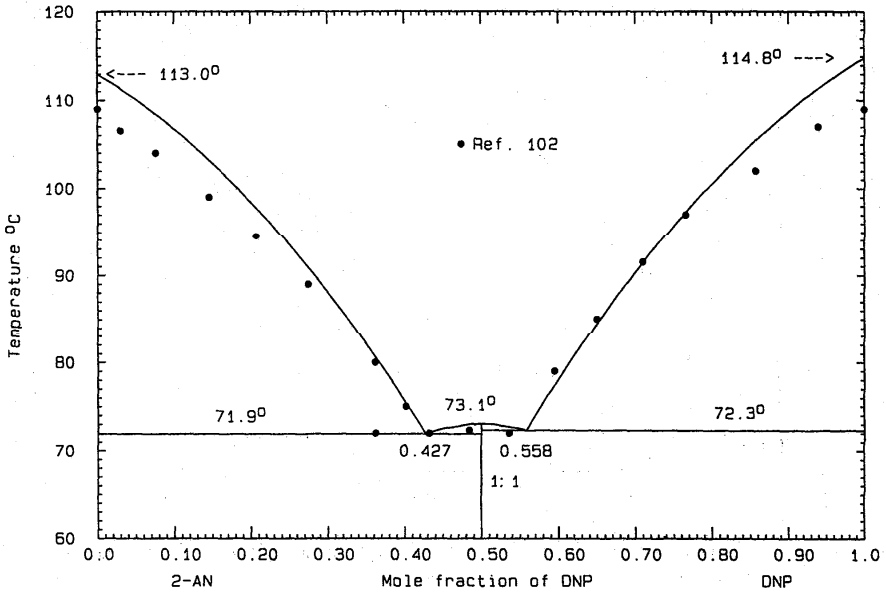

FIG. 161. The system 2-AN (A)+DNP (B)

are too low. In preliminary calculations, it was found that a congruent melting point for the compound was more consistent with the data than a peritectic. There were too few data on which to perform an optimization, so the quantities

$$G^{E}(l) = -2000 x_A x_B \text{ J mol}^{-1} \quad (296)$$

for the liquid and

$$\Delta_{fus} G^0 = 21\,500 - 60.7628T \text{ J mol}^{-1}, \quad (297)$$

$$\Delta_f G^0 = -22\,000 + 55.0000T \text{ J mol}^{-1} \quad (298)$$

for the compound (AB)/2 were assigned in order to reproduce as many experimental features of the system as possible. The calculated phase diagram, Fig. 163, shows eutectics E_1=78.1 °C, x_B=0.362 and E_2=80.3 °C, x_B=0.551; the compound melts at 80.7 °C. The calculated phase diagram and Eqs. (296)–(298) carry significant uncertainty. The probable maximum inaccuracy in the calculated diagram is ±4°

ACP (A)+DNP (B)

Data were obtained by thermal analysis[119] and the reported

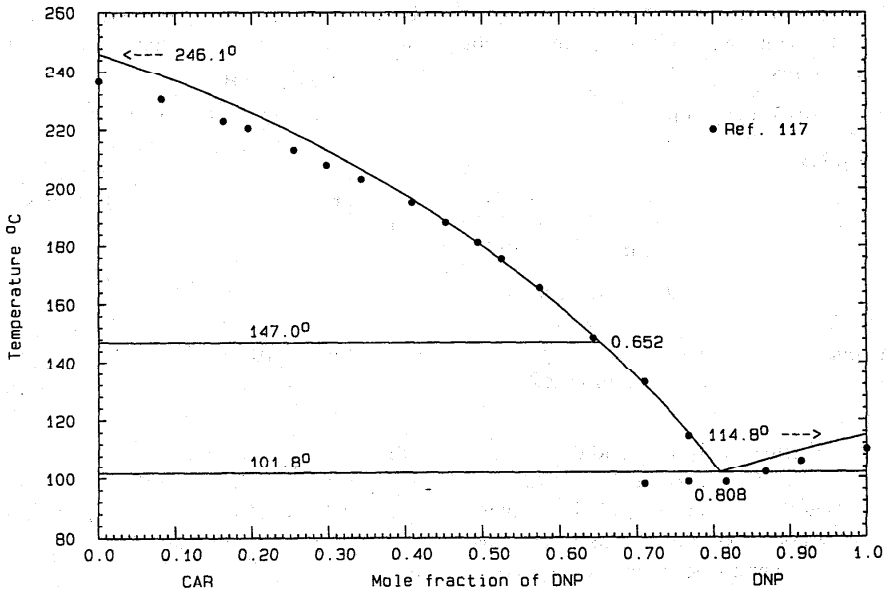

FIG. 162. The system CAR (A)+DNP (B)

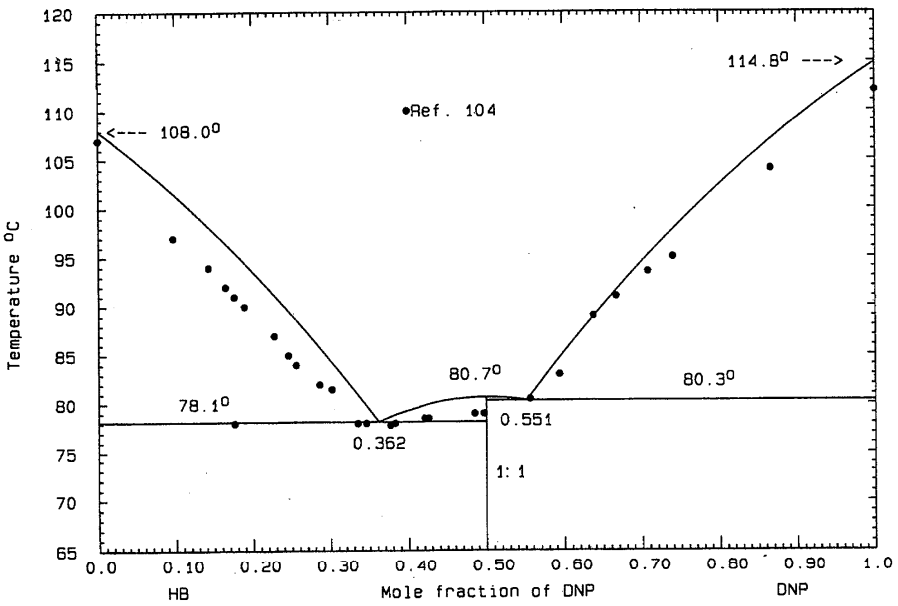

FIG. 163. The system HB (A)+DNP (B)

utectic is 12.0 °C, x_B=0.15. Data in the range $0<x_B<0.6$ vere optimized and the result

$$G^E(l) = -2732 x_A x_B \text{ J mol}^{-1} \quad (299)$$

was used to calculate the phase diagram, Fig. 164. The calculated eutectic is 10.6 °C, x_B=0.148. The probable maximum inaccuracy in the calculated diagram is ±2°.

CAM (A)+DNP (B)

Data were obtained by thermal analysis[88] and the reported eutectic is 67.0 °C, x_B=0.35. Data in the range $0<x_B<0.7$ were optimized to give

$$G^E(l) = x_A x_B(-1163+1778 x_B) \text{ J mol}^{-1}. \quad (300)$$

The calculated phase diagram, Fig. 165, shows a eutectic 67.0 °C, x_B=0.345. The probable maximum inaccuracy in the calculated diagram is ±2°.

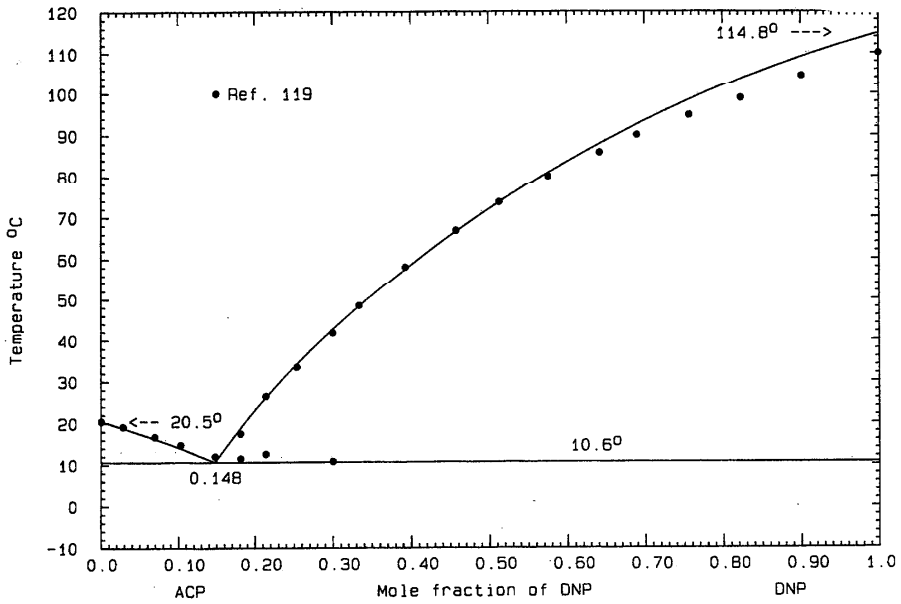

FIG. 164. The system ACP (A)+DNP (B)

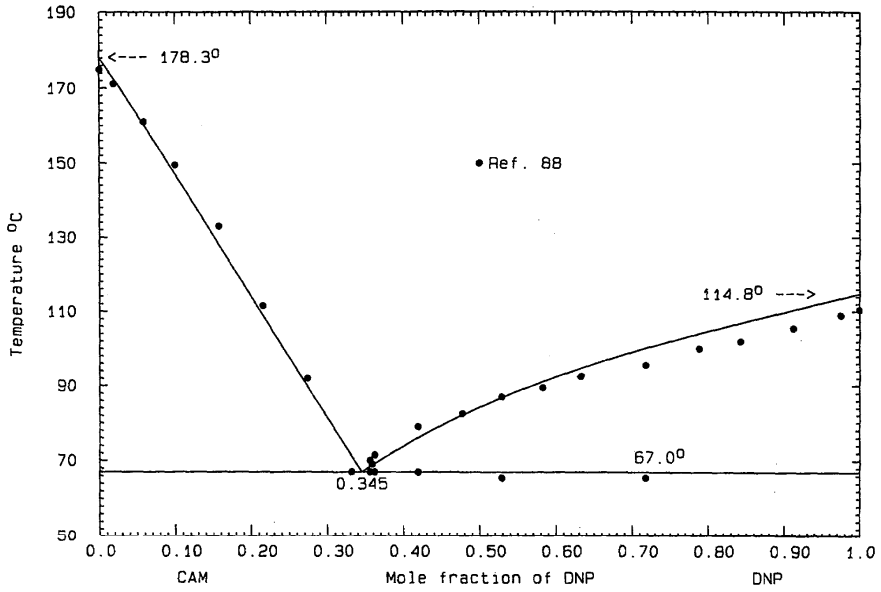

FIG. 165. The system CAM (A)+DNP (B)

BZP (A)+DNP (B)

Data were obtained by thermal analysis[119] and the reported eutectic is 35.0 °C, x_B=0.20. Data in the range $0<x_B<0.6$ were optimized, giving the quantity

$$G^E(l)=x_A x_B(-634-2209x_B)\ \text{J mol}^{-1}. \quad (301)$$

The calculated phase diagram is shown in Fig. 166, and the calculated eutectic is 37.0 °C, x_B=0.222. The probable maximum inaccuracy in the calculated diagram is ±2°.

2.5.21. Systems Based on Picric Acid

BZ (A)+PA (B)

Liquidus data were obtained by thermal analysis[122] and the reported eutectic is 4.2 °C, x_B=0.013. The 1:1 compound melts incongruently at 84.3 °C (no peritectic composition was stated). No eutectic or peritectic arrests were recorded. In preliminary calculations it was found that the liquidus data could be reproduced equally well with or without the pres-

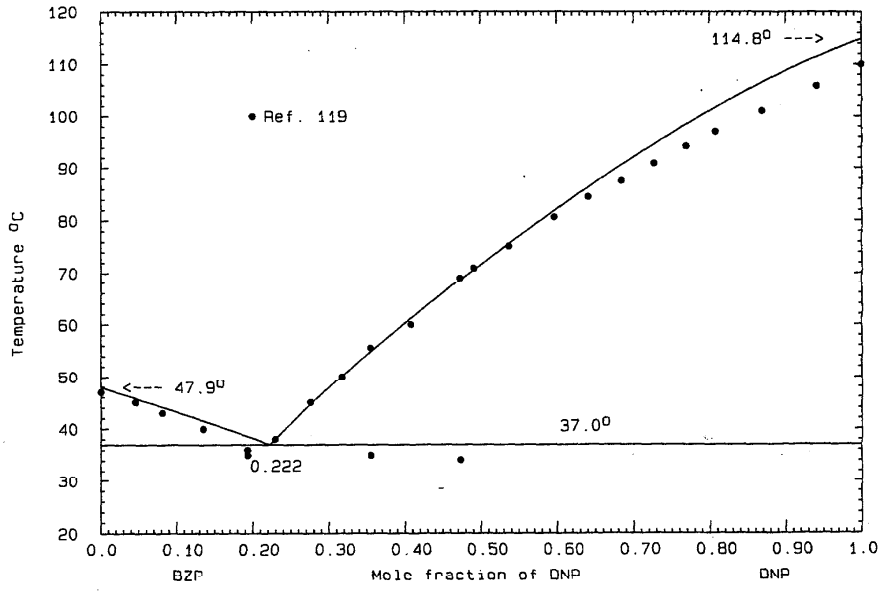

FIG. 166. The system BZP (A)+DNP (B)

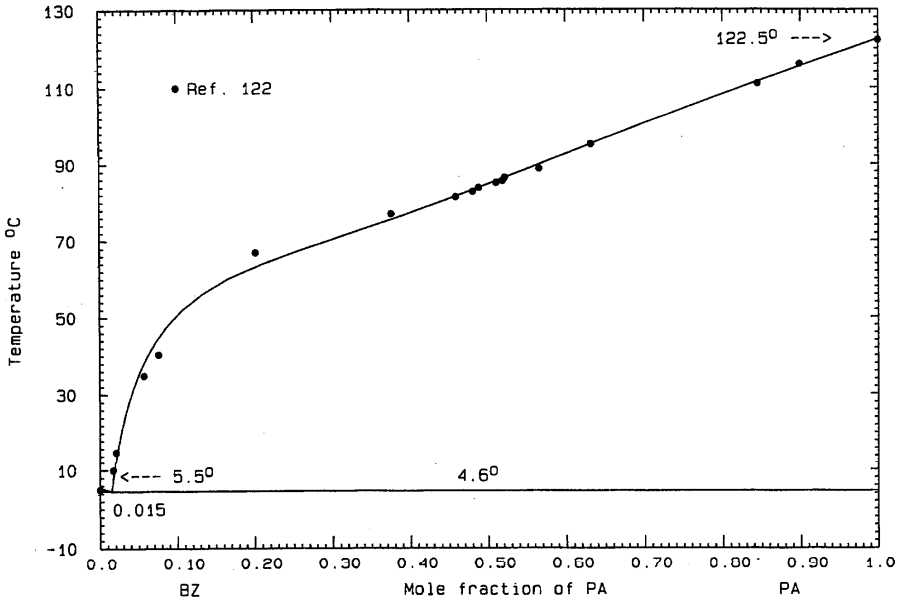

FIG. 167. The system BZ (A)+PA (B)

ence of a compound. All liquidus data were used in the optimization, with the result

$$G^{E}(l)=x_A x_B(4456-5184x_B+2520x_B^2)\ \text{J mol}^{-1}. \quad (302)$$

The calculated eutectic is 4.6 °C, $x_B=0.015$ (Fig. 167). The probable maximum inaccuracy in the calculated diagram is ±1°.

NA (A)+PA (B)

Data were obtained by thermal analysis[115,123,124] and the thaw–melt method.[13,32,33] Data in two sources[32,33] are identical. A eutectic summary is given in Table 14. Among all the reported liquidus data, there is disagreement to a maximum of 12°, although the two earliest reports[115,123] are quite concordant (≈2°). All the liquidus data were used in the optimization and were weighted equally. For the liquid, the result is

TABLE 14. Reported invariant data for the system NA (A)+PA (B)

	°C	x_B	Ref.
E_1	78.0	0.05	13
	78.0	0.04	123
	78.5	0.05	124
	73.5	0.06	32, 33
E_2	111.0	···	70
	111.0	0.92	13, 123
	114.0	0.90	124
	107.5	0.79	32, 33
1:1	150.5		70
	150.2		13
	149.5		115
	147.0		123
	155.0		33

$$G^{E}(l)=-4060x_B\ \text{J mol}^{-1} \quad (303)$$

and for the compound (AB)/2,

$$\Delta_{fus}G^0=20\,183-47.3982T\ \text{J mol}^{-1}, \quad (304)$$

$$\Delta_f G^0=-21\,198+41.6370T\ \text{J mol}^{-1}. \quad (305)$$

The phase diagram, Fig. 168, was calculated with the use of Eqs. (303) and (305). There is an apparent flattening of the liquidus at and near the compound melting point, according to the experimental data; this observation could also be accounted for by a solid transition a few degrees below the melting point that masks the higher thermal event. Other calculated data are $E_1=77.9$ °C, $x_B=0.041$ and $E_2=112.2$ °C, $x_B=0.877$; the compound melts at 152.7 °C. The probable maximum inaccuracy in the calculated diagram is ±5°.

ANTH (A)+PA (B)

Data were obtained by the thaw–melt method.[13,32,33] The liquidus data of these authors are in gross disagreement on the LHS of the phase diagram, but in good agreement on the RHS (1°–2°). The data in two reports[32,33] are identical. The limiting liquidus slope for anthracene[13] is steeper than thermodynamic expectation. The reported eutectic data are, for E_1 (Ref. 33)=130.0 °C, $x_B=0.38$; $E_2=110.0$ °C, $x_B=0.88$ or 109.5 °C, $x_B=0.90$ (Refs. 13 and 33, respectively). The 1:1 compound was claimed to melt incongruently[13,70] at 143.0 or 141.0 °C (peritectic composition $x_B=0.56$) respectively, whereas other investigators[33,102] report congruent melting at 140.0 or 152.7 °C. The unindexed x-ray diffraction spectrum of the compound was reported,[125] together with its heat of fusion (24 900 J mol^{-1}). It also reportedly has a solid

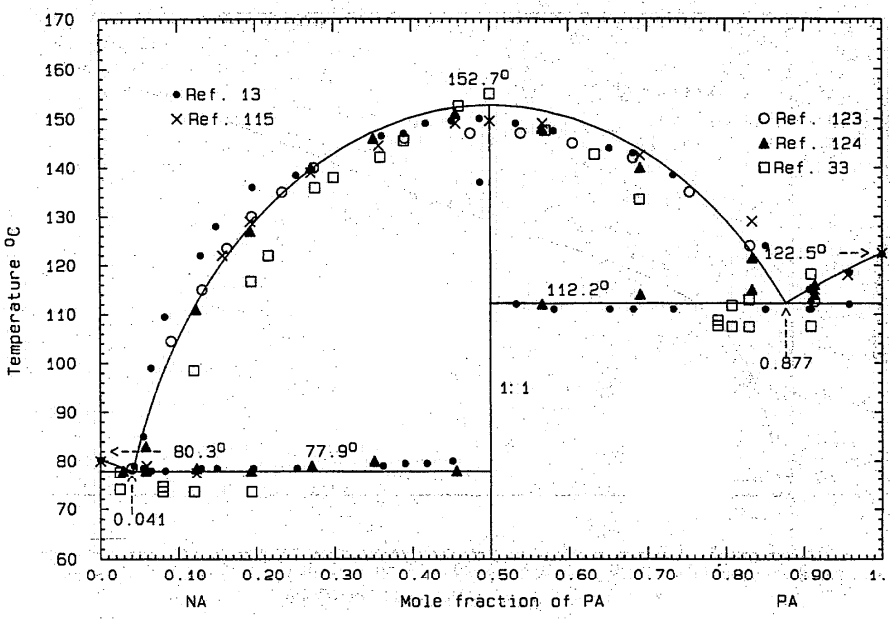

FIG. 168. The system NA (A)+PA (B)

transition[70] at 85 °C. For the optimization, in congruent melting was assumed and the diverging data[33] were omitted. For the liquid

$$G^{E}(l) = -5496 x_A x_B \text{ J mol}^{-1}, \quad (306)$$

and for the compound (AB)/2

$$\Delta_{fus} G^0 = 30\,443 - 73.7001 T \text{ J mol}^{-1}, \quad (307)$$

$$\Delta_f G^0 = -31\,817 + 67.9389 T \text{ J mol}^{-1}. \quad (308)$$

The calculated phase diagram, Fig. 169, indicates $E = 111.5$ °C, $x_B = 0.875$ and $P = 139.1$ °C, $x_B = 0.567$. The probable maximum inaccuracy in the calculated diagram is ±3°.

PH (A)+PA (B)

Liquidus data were obtained by the microthermal method[70] and thaw–melt method.[32,126] The data in two reports[32,126] are identical. A summary of invariant data is

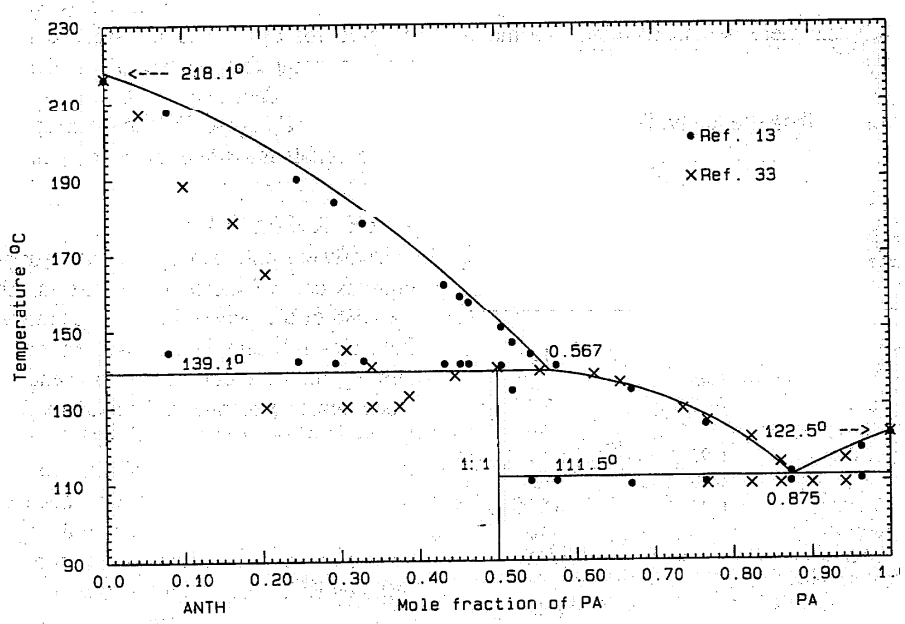

FIG. 169. The system ANTH (A)+PA (B)

TABLE 15. Reported invariant data for the system PH (A)+PA (B)

	°C	x_B	Ref.
E_1	86.0	0.15	70
	82.5	0.17	126
E_2	108.0	0.82	70
	103.0	0.79	126
1:1	146.0		70
	145.0		126

TABLE 16. Reported invariant data for the system FLN (A)+PA (B)

	°C	x_B	Ref.
E_1	80.5	0.37	99
	77.0	0.39	70
E_2	80.0	0.58	99
	79.0	0.53	70
1:1	84.0		99
	79.5		70

given in Table 15. Since no eutectic arrests were recorded, the reported eutectic temperatures are extrapolated data and there is evident disagreement in this respect.[70,126] The observed compound liquidus data are not thermodynamically consistent with the reported eutectic temperatures. In the optimization, all liquidus data were weighted equally, with the result

$$G^E(l) = -1175 x_A x_B \text{ J mol}^{-1} \quad (309)$$

for the liquid and

$$\Delta_{fus}G^0 = 5920 - 14.1569T \text{ J mol}^{-1}, \quad (310)$$

$$\Delta_f G^0 = -6214 + 8.3941T \text{ J mol}^{-1} \quad (311)$$

for the compound (AB)/2. Both the calculated heat and entropy of fusion of the compound are very low compared with the same quantities of the component compounds. The calculated phase diagram is shown in Fig. 170 and calculated data are E_1=85.1 °C, x_B=0.188 and E_2=103.1 °C, x_B=0.764; the compound melts at 145.0 °C. The probable maximum inaccuracy in the calculated diagram is ±4°.

FLN (A)+PA (B)

Liquidus data were obtained by the microthermal method[70] and thermal analysis[99] and a summary of reported invariant data is given in Table 16. The liquidus data are in good agreement (≈1°) except in the central region, where Kofler's data[70] were omitted from the optimization. Some liquidus data on the LHS are clearly faulty, but all were used in the optimization for the liquid,

$$G^E(l) = x_A x_B(-3488 + 1644 x_B) \text{ J mol}^{-1}, \quad (312)$$

and for the compound (AB)/2,

$$\Delta_{fus}G^0 = 8108 - 22.6576T \text{ J mol}^{-1}, \quad (313)$$

$$\Delta_f G^0 = -8774 + 16.8964T \text{ J mol}^{-1}. \quad (314)$$

The calculated phase diagram, Fig. 171, shows calculated eutectics E_1=77.8 °C, x_B=0.369 and E_2=82.3 °C, x_B=0.580; the compound melts at 84.7 °C. The probable maximum inaccuracy in the calculated diagram is ±2°.

DPM (A)+PA (B)

Data were obtained by thermal analysis[120] and the reported eutectic is 22.5 °C, x_B=0.05. There is a tendency for the liquidus to flatten in the central region, presumably due to incipient liquid immiscibility. The calculation of the phase diagram was determined by the picric acid liquidus since it covers 95% of the composition range:

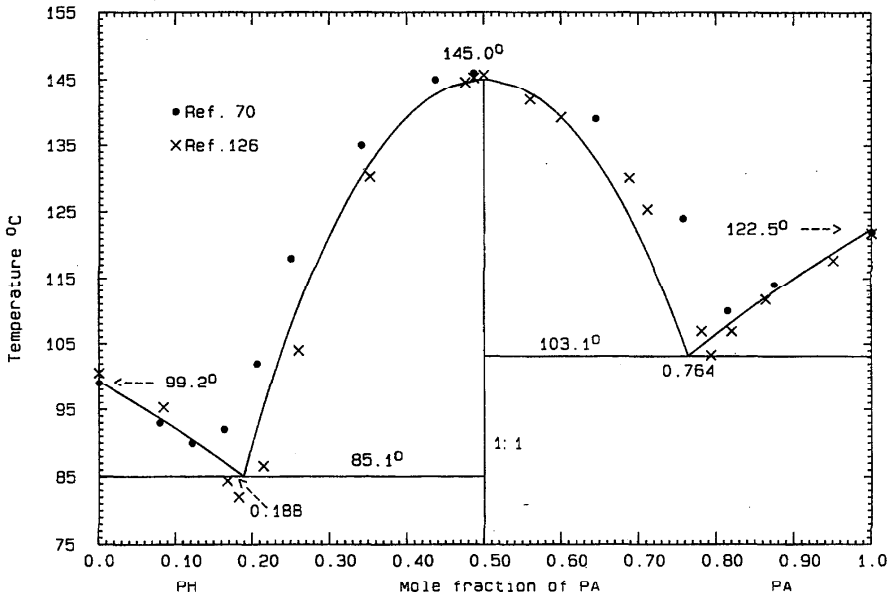

FIG. 170. The system PH (A)+PA (B)

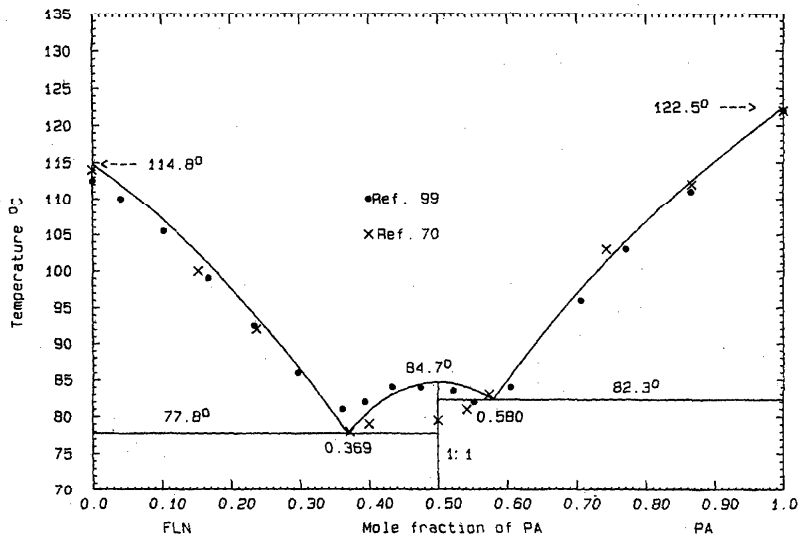

FIG. 171. The system FLN (A)+PA (B)

$$G^{E}(l)=x_A x_B(2621-2311x_B-2144x_B^2)\ \text{J mol}^{-1}. \quad (315)$$

The calculated phase diagram, Fig. 172, shows a calculated eutectic of 23.2 °C, $x_B=0.054$. The probable maximum inaccuracy in the calculated diagram is ±2°.

CAR (A)+PA (B)

Data were obtained by thermal analysis[117] and the reported eutectics are $E_1=181.5$ °C, $x_B=0.41$ and $E_2=113.0$ °C, $x_B=0.93$. The RHS liquidus is low and hence the reported E_2 temperature is probably low also. The 1:1 compound melts congruently at 183.0 °C. Data in the range $0.35<x_B<1$ were *optimized to give*

$$G^{E}(l)=-7262x_A x_B\ \text{J mol}^{-1} \quad (316$$

for the liquid and

$$\Delta_{fus}G^{0}=23\,071-50.6349T\ \text{J mol}^{-1}, \quad (317$$

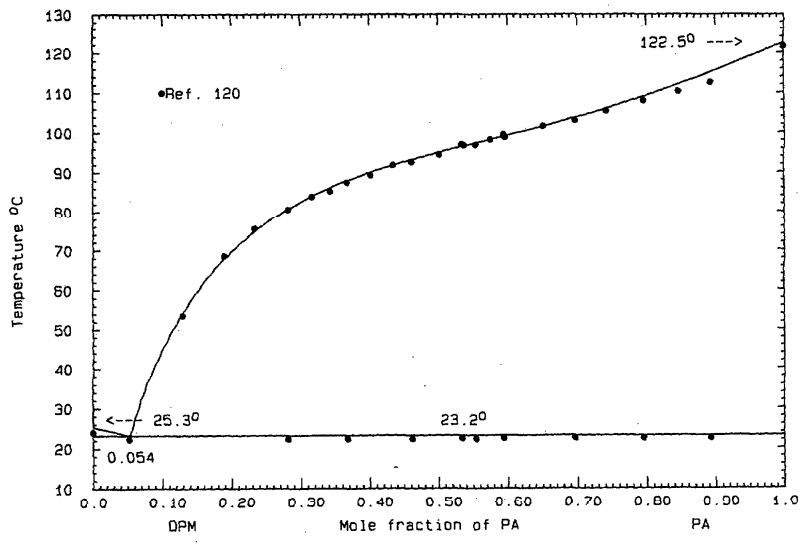

FIG. 172. The system DPM (A)+PA (B)

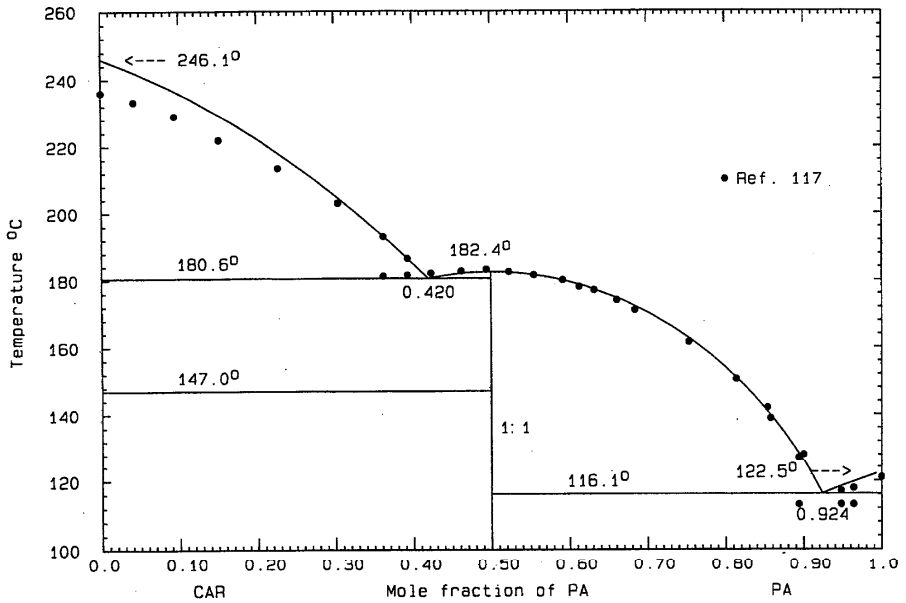

FIG. 173. The system CAR (A)+PA (B)

$$\Delta_f G^0 = -24\,886 + 44.8737T \text{ J mol}^{-1} \quad (318)$$

for the compound (AB)/2. The calculated phase diagram, Fig. 173, shows eutectics E_1=180.6 °C, x_B=0.420 and E_2=116.1 °C, x_B=0.924; the compound melts at 182.4 °C. The probable maximum inaccuracy in the calculated diagram is ±2°.

P (A)+PA (B)

Data were obtained by thermal analysis[123,127] and the thaw–melt method.[13] The liquid data of the three studies agree within 2°, and a summary of invariant points is given in Table 17. The agreement in the observed eutectic temperatures is very close, if not unanimous; however, in preliminary calculations it was found that the invariant temperatures were not precisely consistent with all the liquidus data. In the optimization, therefore, the invariant temperatures were—as far as possible—given more weight than liquidus data. For the liquid,

$$G^E(l) = x_A x_B(3000 - 5500x_B) \text{ J mol}^{-1}, \quad (319)$$

and for the compound (AB)/2,

$$\Delta_{fus}G^0 = 6405 - 17.8844T \text{ J mol}^{-1}, \quad (320)$$

TABLE 17. Reported invariant data for the system P (A)+PA (B)

	°C	x_B	Ref.
E_1	36.0	0.07	123
	36.0	0.06	13
E_2	80.0	0.59	123
	80.5	0.59	13
1:1	85.0		123
	80.5		13

$$\Delta_f G^0 = -6344 + 12.1233T \text{ J mol}^{-1}. \quad (321)$$

The calculated heat and entropy of fusion of the compound, Eq. (320), seem rather low; an alternative set of fusion properties more comparable to those of the components is possible, with a slightly poorer fit to the data.[13,123,127] Other calculated data of the phase diagram, Fig. 174, are E_1=37.1 °C, x_B=0.066 and E_2=80.0 °C, x_B=0.613; the compound melts at 85.0 °C. The probable maximum inaccuracy in the calculated diagram is ±2°.

2-N (A)+PA (B)

Data were obtained by thermal analysis[122] and the thaw–melt method.[128] The agreement in the liquidus data in these two reports is good (≈1°). Only Kuriloff[122] reported eutectic data: E_1=116.0 °C, x_B=0.06 and E_2=111.0 °C, x_B=0.91. The 1:1 compound melts at[122] 157.0 °C or[129] 155.0 °C. I preliminary calculations it was found that the liquidus poir of Kuriloff[122] at x_B=0.124 is quite false and is entirely out c line with the rest of the data defining the compound liquidu As a consequence, the observed E_1 temperature[122] is mis taken. Optimization of all liquidus data yielded

$$G^E(l) = -31\,327x_A x_B \text{ J mol}^{-1} \quad (322)$$

for the liquid and

$$\Delta_{fus}G^0 = 61\,542 - 143.1381T \text{ J mol}^{-1}, \quad (323)$$

$$\Delta_f G^0 = -69\,373 + 137.3769T \text{ J mol}^{-1} \quad (324)$$

for the compound (AB)/2. The calculated heat and entropy of the compound, Eq. (323), are much larger than the corresponding data for the two components; the fit to the experimental data[122,128] is, however, very good. Similarly the calculated excess Gibbs energy of the liquid, Eq. (322) is very

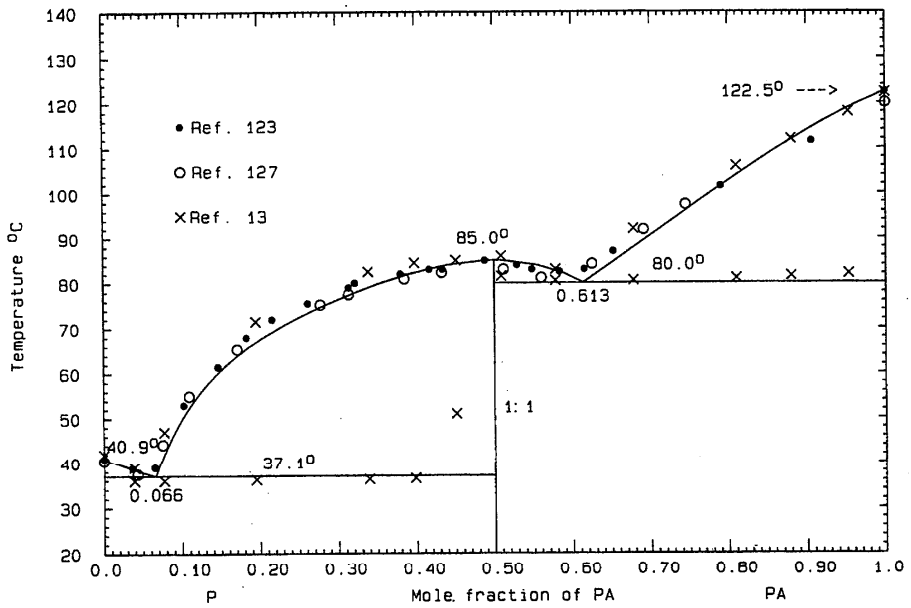

FIG. 174. The system P (A)+PA (B)

negative, compared to other systems analyzed in the present work. These findings are necessary consequences of the high eutectic and compound melting temperatures. Other calculated data of the phase diagram, Fig. 175, are E_1=110.1 °C, x_B=0.099 and E_2=109.4 °C, x_B=0.904; the compound melts at 156.8 °C. The probable maximum inaccuracy in the calculated diagram is ±1°.

DMA (A)+PA (B)

Liquidus data were obtained by the visual-polythermal method[95] and the reported eutectics are E_1=−29.0 °C, x_B=0.07 and E_2=57.0 °C, x_B=0.57. The 1:1 compound melts at 60.0 °C. All the liquidus data were used in the optimization to yield

$$G^E(l)=x_A x_B(-4300+3600x_B)\ \text{J mol}^{-1} \quad (325)$$

for the liquid and for the compound (AB)/2

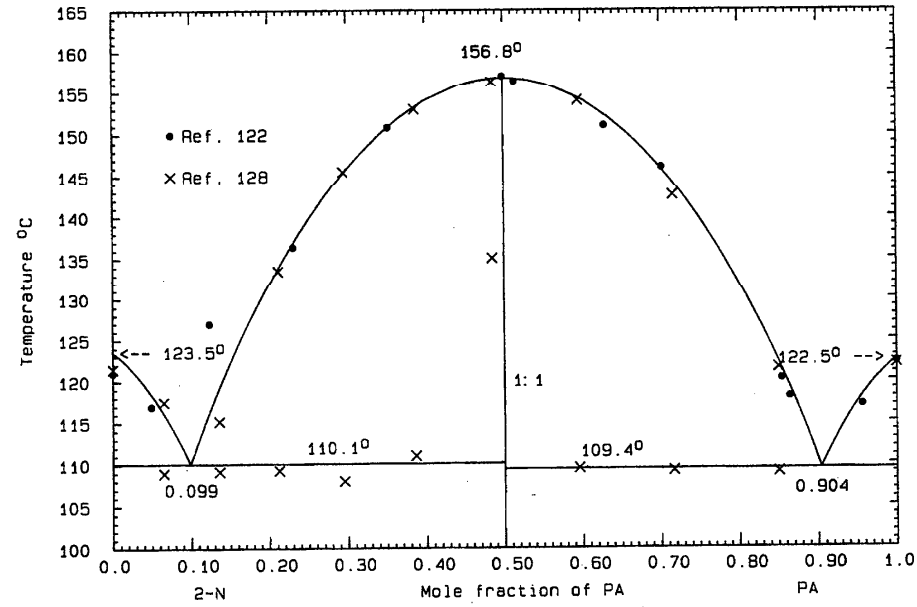

FIG. 175. The system 2-N (A)+PA (B)

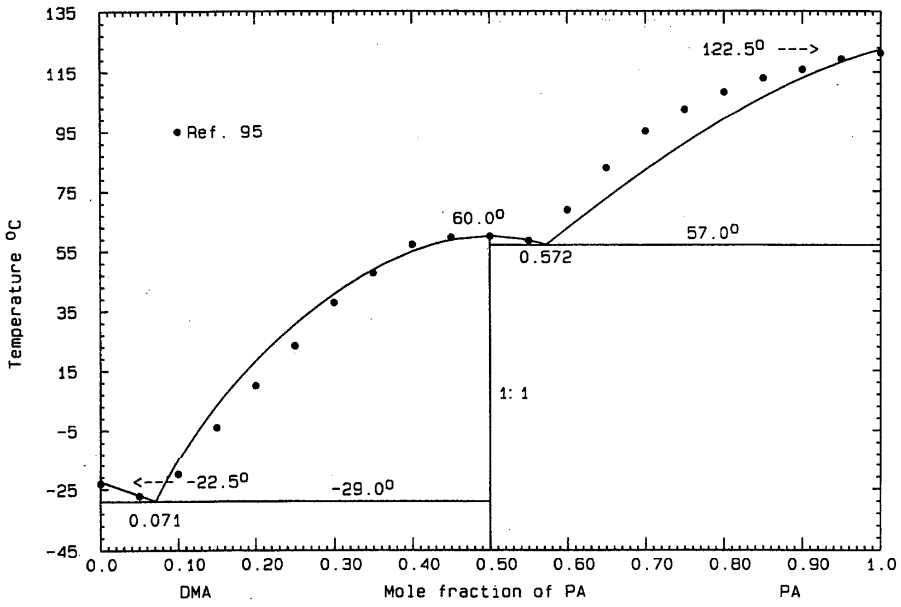

FIG. 176. The system DMA (A)+PA (B)

$$\Delta_{fus}G^0 = 7133 - 21.4113T \text{ J mol}^{-1}, \quad (326)$$

$$\Delta_f G^0 = -8659 + 15.6501T \text{ J mol}^{-1}. \quad (327)$$

The experimental RHS liquidus is evidently too high. The calculated phase diagram is shown in Fig. 176 and the calculated eutectics are $E_1 = -29.0$ °C, $x_B = 0.071$ and $E_2 = 57.0$ °C, $x_B = 0.572$; the compound melts at 60.0 °C. The probable maximum inaccuracy in the calculated diagram is ±5°.

BENZ (A)+PA (B)

Liquidus data were obtained by the visual-polythermal method[118] and the reported eutectics are $E_1 = 103.0$ °C, $x_B = 0.29$ and $E_2 = 103.0$ °C, $x_B = 0.73$; the 1:1 compound melts congruently at 110.5 °C. Data in the range $0.2 < x_B < 1$ were optimized to give

$$G^E(l) = x_A x_B(-843 + 1573x_B) \text{ J mol}^{-1} \quad (328)$$

for the liquid and

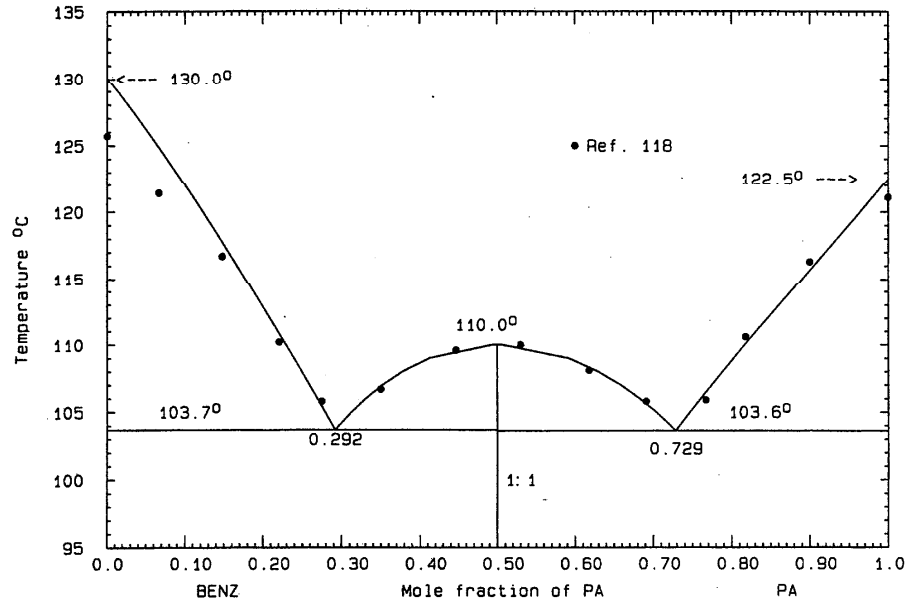

FIG. 177. The system BENZ (A)+PA (B)

TABLE 18. Reported invariant data for the system HB (A)+PA (B)

	°C	x_B	Ref.
E_1	88.9	0.25	105
	90.0	0.16	13
	88–89	0.16	104
E_2	90.0	0.54	105
	90.0	0.58	13
	88–89	0.59	104
1:1	90.5		105

$$\Delta_{fus}G^0 = 19\,961 - 52.0974T \text{ J mol}^{-1}, \quad (329)$$

$$\Delta_f G^0 = -19\,976 + 46.3363T \text{ J mol}^{-1} \quad (330)$$

for the compound (AB)/2. The calculated phase diagram, Fig. 177, shows eutectics E_1=103.7 °C, x_B=0.292 and E_2=103.6 °C, x_B=0.729; the compound melts at 110.0 °C. The probable maximum inaccuracy in the calculated diagram is ±1°.

HB (A)+PA (B)

Data were obtained by the thaw–melt method[13,105] and thermal analysis.[104] A summary of invariant data is given in Table 18. The apparently horizontal and parallel central liquidus and solidus puzzled early investigators[13,104]; such a construction is not thermodynamically permissible. The presence of a congruently melting 1:1 compound was suspected[104] and later reported.[105] The experimental LHS liquidus data are faulty because the reported melting points of 3-hydroxybenzaldehyde are low. Few reliable data remained for optimization; the calculated properties, Eqs. (331)–(333) were assigned to give the best fit to the RHS liquidus data[13,104,105] and the reported melting point of the compound. Thus

$$G^E(l) = 1000x_A x_B \text{ J mol}^{-1} \quad (331)$$

for the liquid and

$$\Delta_{fus}G^0 = 27\,188 - 74.7628T \text{ J mol}^{-1}, \quad (332)$$

$$\Delta_f G^0 = -26\,938 + 69.0000T \text{ J mol}^{-1} \quad (333)$$

for the compound (AB)/2. In the calculated phase diagram, Fig. 178, the eutectics are shown as E_1=88.1 °C, x_B=0.318 and E_2=90.2 °C, x_B=0.569; the compound melts at 90.5 °C. Considerable uncertainty remains concerning the calculated thermodynamic properties. The probable maximum inaccuracy in the calculated diagram is ±4°.

ACP (A)+PA (B)

Data were obtained by thermal analysis[119] and the reported invariant data are P=50.0 °C, x_B=0.42 (1:1 compound) and no eutectic data were given. All liquidus data were optimized to give

$$G^E(l) = -2802x_A x_B \text{ J mol}^{-1} \quad (334)$$

for the liquid and

$$\Delta_{fus}G^0 = 17\,304 - 53.1737T \text{ J mol}^{-1}, \quad (335)$$

$$\Delta_f G^0 = -18\,004 + 47.4125T \text{ J mol}^{-1} \quad (336)$$

for the compound (AB)/2. The calculated phase diagram, Fig. 179, shows calculated invariant points P=50.1 °C, x_B=0.412 and E=16.1 °C, x_B=0.081. The probable maximum inaccuracy in the calculated diagram is ±2°.

CA (A)+PA (B)

Data were obtained by the thaw–melt method[60] and the reported eutectics are E_1=107.0 °C, x_B=0.42 and E_2=104.0 °C, x_B=0.66; the 1:1 compound melts congruently at 109.0 °C. Its heat of fusion[60] is 28 560 J mol^{-1}. Pre-

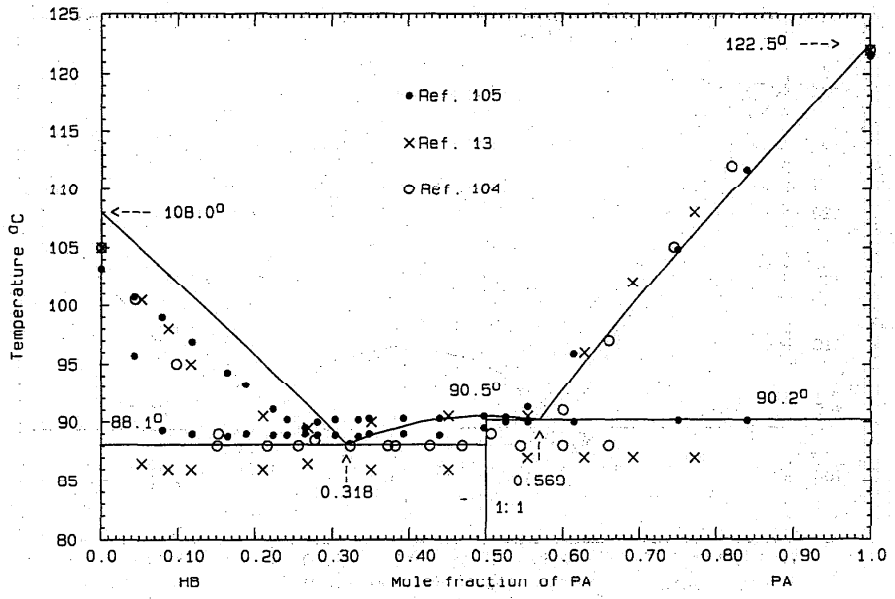

FIG. 178. The system HB (A)+PA (B)

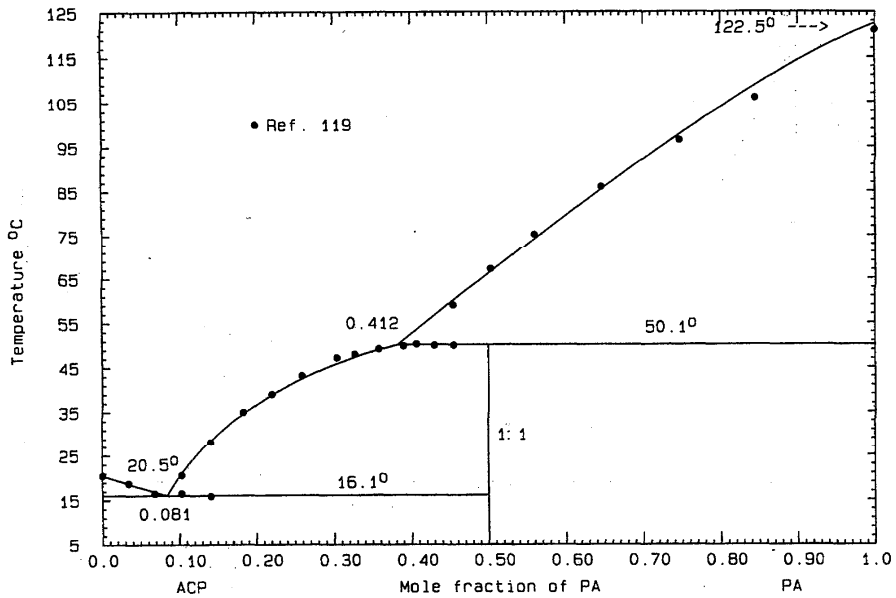

FIG. 179. The system ACP (A)+PA (B)

liminary calculations showed that both the LHS and RHS liquidus data are too high; taken at face value, they would imply solid solubility to an extent not at all consistent with the remainder of the phase diagram.[60] The calculations were therefore based on the reported eutectic temperatures and the compound melting point. For the liquid

$$G^{E}(l)=x_A x_B(-350+1000x_B)\ \text{J mol}^{-1} \qquad (337)$$

and for the compound (AB)/2

$$\Delta_{fus}G^0=28\,560-74.7350T\ \text{J mol}^{-1}, \qquad (338)$$

which, in the calculated phase diagram, Fig. 181, reproduces the slight inflection in the RHS liquidus; the calculated eutectic is 71.0 °C, $x_B=0.302$.

Probable maximum inaccuracy in calcualted diagram: ±1°

BZP(A)+PA(B).

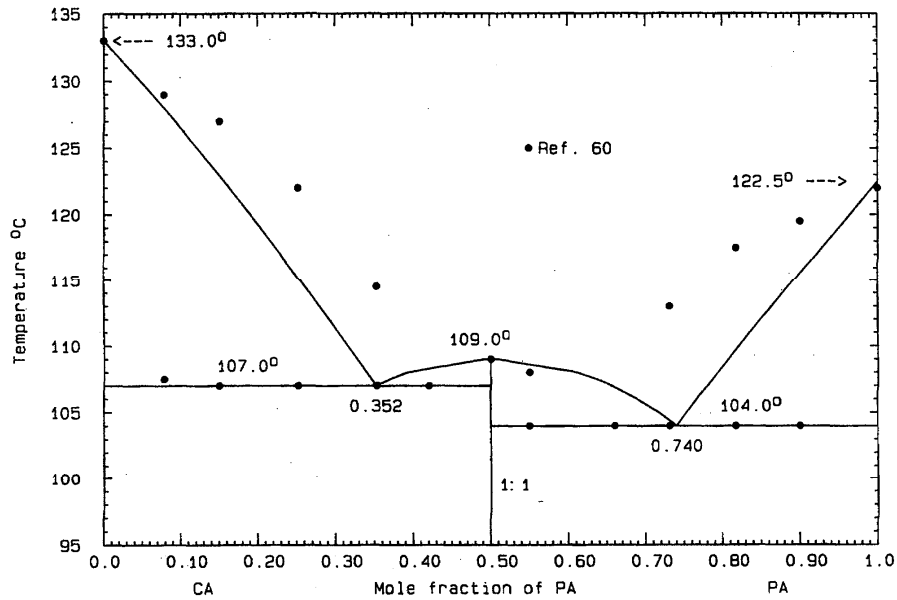

FIG. 180. The system CA (A)+PA (B)

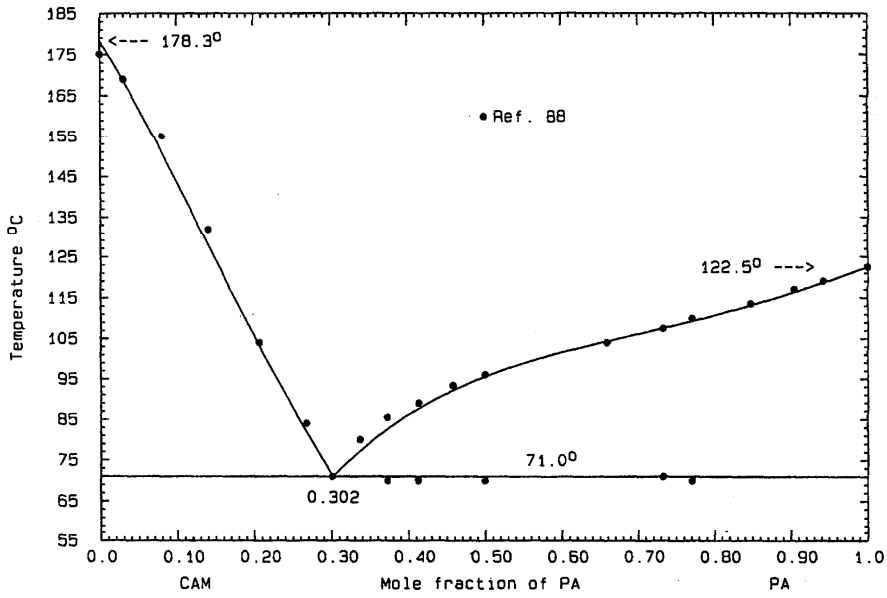

FIG. 181. The system CAM (A)+PA (B)

Data were obtained by thermal analysis[111,119] and the reported eutectic is[111] 28.5 °C, x_B=0.29 (no eutectic data appeared in the other report[119]). The two liquidus data sets are concordant within 2°. All liquidus data were optimized to give

$$G^E(1)=x_A x_B(-4035+2254x_B) \quad \text{J mol}^{-1} \quad (339)$$

and the calculated phase diagram, Fig. 182, shows a eutectic 26.0 °C, x_B=0.285.

Probable maximum inaccuracy in calculated diagram: ±2°

2.5.22. Systems Based on Picryl Chloride

PY(A)+PC(B)

Data were obtained by the thaw–melt method[43] and the reported eutectics are E_1=125.0 °C, x_B=0.23 and E_2=73.5 °C, x_B=0.92. The 1:1 compound melts congruently at 154.0 °C. The experimental liquidus data for the com-

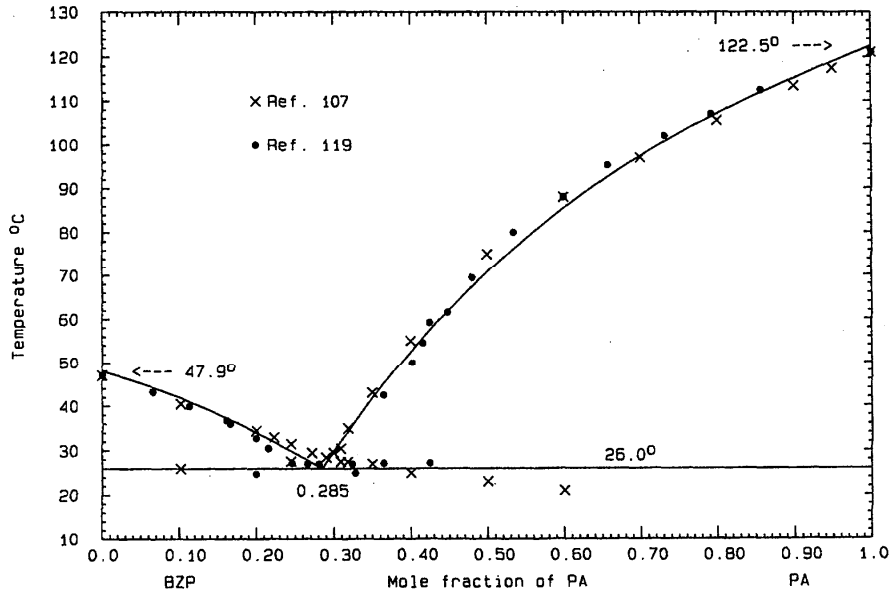

FIG. 182. The system BZP (A)+PA (B)

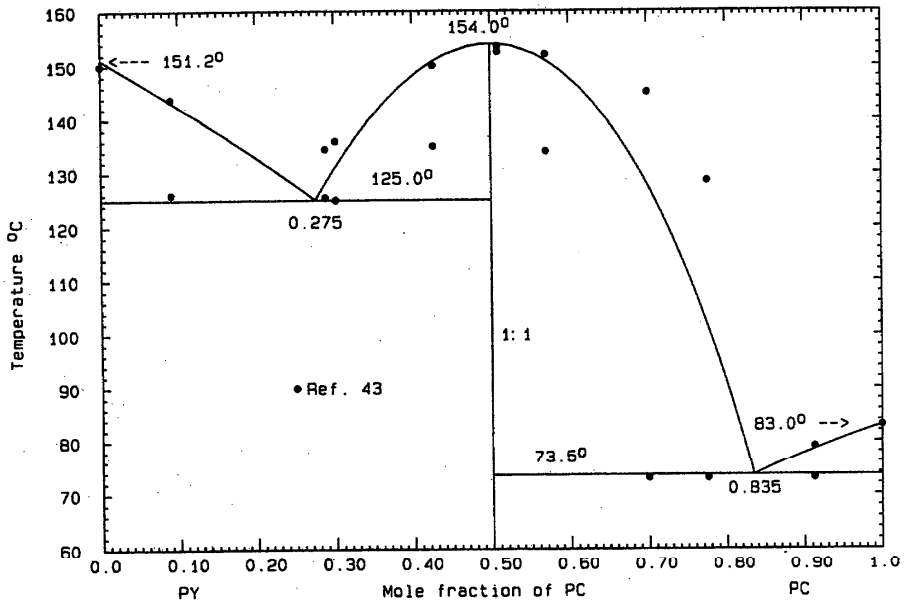

FIG. 183. The system PY (A)+PC (B)

pound define two unsymmetrical arms; few reliable liquidus data remained for optimization and so calculations were based on the reported eutectic temperatures and the compound melting point. Thus, for the liquid

$$G^{E}(1)=x_A x_B(-700-1600\,x_B) \quad \text{J mol}^{-1} \quad (340)$$

for the compound (AB)/2

$$\Delta_{fus}G^0=6088-14.2529T \quad \text{J mol}^{-1}, \quad (341)$$

$$\Delta_f G^0=-6463+8.4901T \quad \text{J mol}^{-1}. \quad (342)$$

The calculated heat and entropy of fusion of the compound, Eq. (341), are quite low. The calculated phase diagram, Fig. 183, shows calculated eutectics $E_1=125.0$ °C, x_B-0.275 and

$$\Delta_f G^0=-28\,523+68.9722T \quad \text{J mol}^{-1}. \quad (343)$$

The calculated phase diagram, Fig. 180, shows eutectics $E_1=107.0$ °C, $x_B=0.352$ and $E_2=104.0$ °C, $x_B=0.740$; the compound melts at 109.0 °C. The probable maximum inaccuracy in the calculated diagram is ±5°.

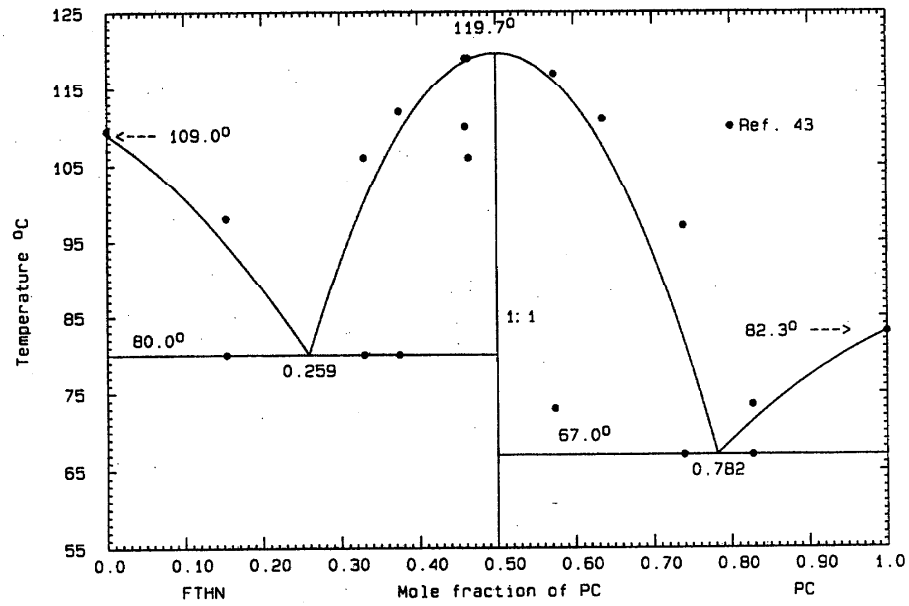

FIG. 184. The system FTHN (A)+PC (B)

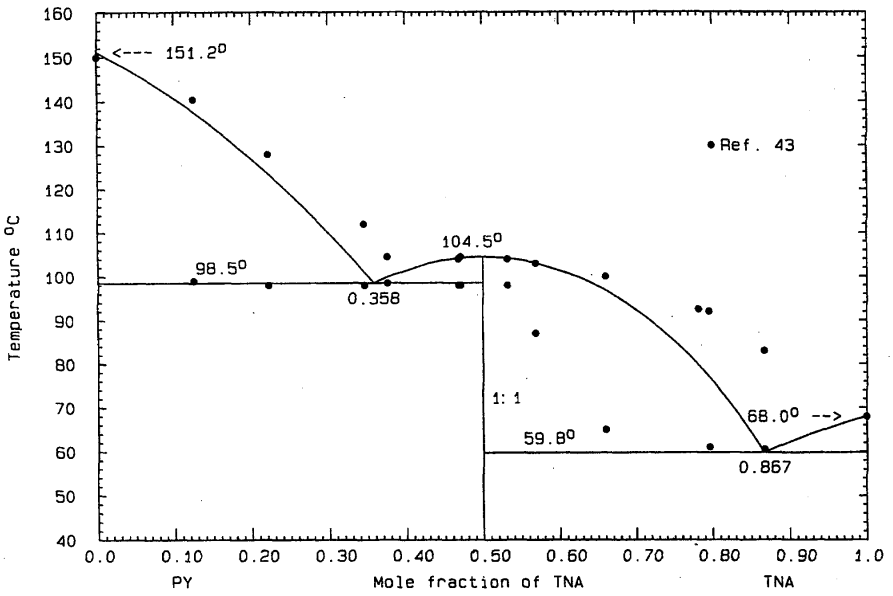

FIG. 185. The system PY (A)+TNA (B)

CAM (A)+PA (B)

Data were obtained by thermal analysis[88] and the reported eutectic is 71.0 °C, x_B=0.31. All the data were used in the optimization, with the result

$$G^E(l)=x_A x_B(-1638+7774x_B-3598x_B^2)\ \text{J mol}^{-1}, \quad (344)$$

E_2=73.5 °C, x_B=0.835; the compound melts at 154.0 °C. The probable maximum inaccuracy in the calculated diagram is ±2°.

FTHN (A)+PC (B)

Data were obtained by the thaw–melt method[43] and the reported eutectics are E_1=80.0 °C, x_B=0.262 and E_2=67.0 °C, x_B=0.844. The 1:1 compound melts congruently at 120.0 °C. There are not many liquidus data for optimization; some are not consistent with the observed[43] eutectic temperatures, which were taken as guides to calculations. Optimization of all the data yielded the expression

$$G^E(l)=x_A x_B(-7870+530x_B)\ \text{J mol}^{-1} \quad (345)$$

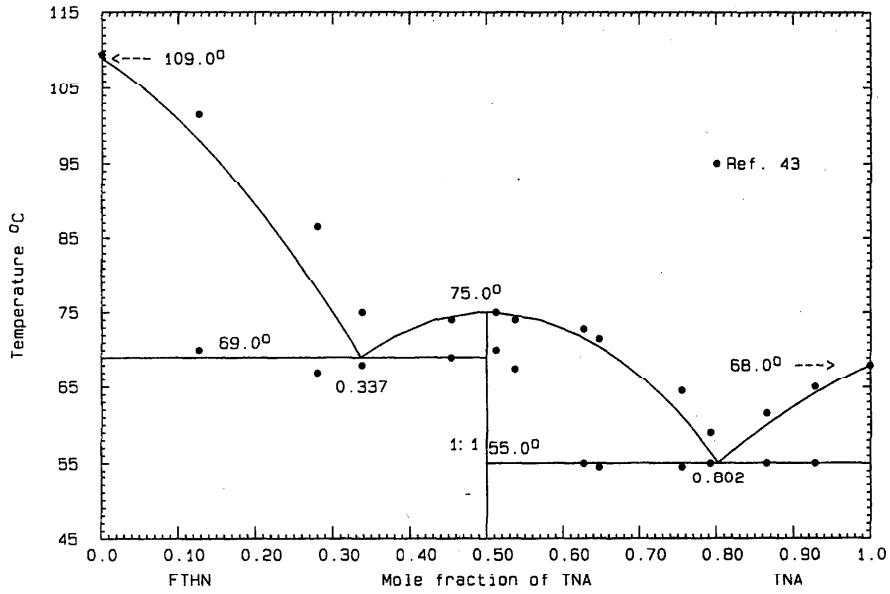

FIG. 186. The system FTHN (A)+TNA (B)

TABLE 19. Reported invariant data for the system NA (A)+TNF (B)

	°C	x_B	Ref.
E_1	77.4	0.025	34
	78.0	···	6
E_2	143.4	0.660	34
	143.5	···	6
1:1	153.2		34
	153.7		6

for the liquid and

$$\Delta_{fus}G^0 = 8350 - 21.2547T \text{ J mol}^{-1}, \quad (346)$$

$$\Delta_f G^0 = -10\,251 + 15.4919T \text{ J mol}^{-1} \quad (347)$$

for the compound (AB)/2. The calculated phase diagram, Fig. 184, displays calculated eutectics E_1=80.0 °C, x_B=0.259 and E_2=67.0 °C, x_B=0.782; the compound melts at 119.7 °C. The probable maximum inaccuracy in the calculated diagram is ±2°.

2.5.23. Systems Based on 2,4,6-Trinitroanisole

PY (A)+TNA (B)

Data were obtained by the thaw–melt method[43] and the reported eutectics are E_1=98.5 °C, x_B=0.40 and E_2=60.5 °C, x_B=0.97; the 1:1 compound melts congruently at 104.5 °C. The liquidus arms of the compound, according to the data,[43] are very unsymmetrical; as a consequence, the reported eutectic compositions are probably in error (that is, on the assumption that the eutectic temperatures are more reliable). There are very few good liquidus data for a proper optimization, so the quantity

$$G^E(l) = -6000x_A x_B \text{ J mol}^{-1} \quad (348)$$

was assigned to the liquid, based on the result for a similar system with fluoranthene, which follows. Taking the eutectic and compound melting temperatures as guides, the properties

$$\Delta_{fus}G^0 = 15\,790 - 41.8116T \text{ J mol}^{-1}, \quad (349)$$

$$\Delta_f G^0 = -17\,290 + 36.0504T \text{ J mol}^{-1} \quad (350)$$

were deduced for the compound (AB)/2. The calculated phase diagram, Fig. 185, shows calculated eutectics E_1=98.5 °C, x_B=0.358 and E_2=59.8 °C, x_B=0.867; the compound melts at 104.5 °C. The probable maximum inaccuracy in the calculated diagram is ±2°.

FTHN (A)+TNA (B)

Data were obtained by the thaw–melt method[43] and the reported eutectics are E_1=68.5 °C, x_B=0.370 and E_2=55.5 °C, x_B=0.815. The 1:1 compound melts congruently at 75.0 °C. Preliminary calculations showed that the LHS liquidus data are too high, and so these were excluded from the optimization, which yielded the expression

$$G^E(l) = x_A x_B(-6700 + 1100x_B) \text{ J mol}^{-1} \quad (351)$$

for the liquid and

$$\Delta_{fus}G^0 = 19\,509 - 56.0357T \text{ J mol}^{-1}, \quad (352)$$

$$\Delta_f G^0 = -21\,048 + 50.2745T \text{ J mol}^{-1} \quad (353)$$

for the compound (AB)/2. The calculated phase diagram, Fig. 186, shows eutectics E_1=69.0 °C, x_B=0.337 and E_2=55.0 °C, x_B=0.802; the compound melts at 75.0 °C. The probable maximum inaccuracy in the calculated diagram is ±1°.

2.5.24. Systems Based on 2,4,7-Trinitrofluoren-9-One

NA (A)+TNF (B)

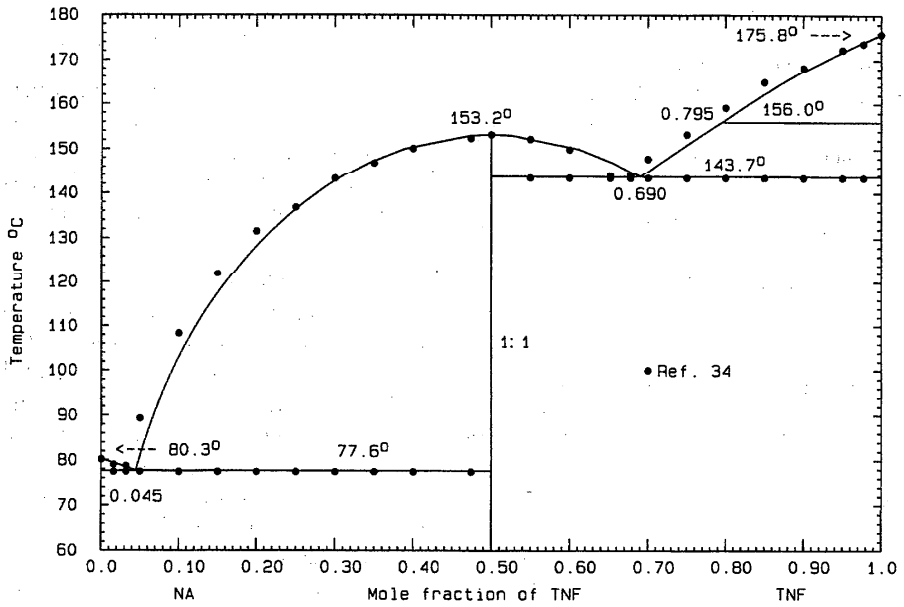

FIG. 187. The system NA (A)+TNF (B)

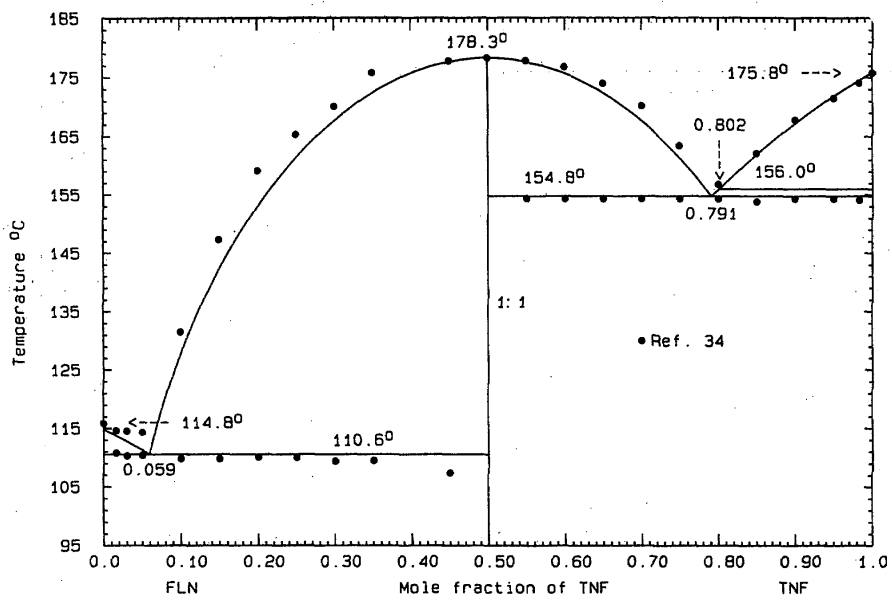

FIG. 188. The system FLN (A)+TNF (B)

Data were obtained by thermal analysis[34] and a summary of invariant points is given in Table 19. All liquidus data were used in the optimization, but the eutectic and compound melting temperatures were given more weight than individual data points. The result for the liquid was

$$G^{E}(l) = -5000 x_A x_B \text{ J mol}^{-1} \quad (354)$$

and for the compound (AB)/2

$$\Delta_{fus}G^0 = 20\,329 - 47.8607T \text{ J mol}^{-1}, \quad (355)$$

$$\Delta_f G^0 = -21\,655 + 42.0995T \text{ J mol}^{-1}. \quad (356)$$

The calculated phase diagram, Fig. 187, shows calculated eutectics E_1=77.6 °C, x_B=0.045 and E_2=143.7 °C, x_B=0.690. The trinitrofluorenone transition appears on the calculated liquidus at x_B=0.795. The calculated melting point of the compound is 153.2 °C. The probable maximum inaccuracy in the calculated diagram is ±2°.

FLN (A)+TNF (B)

Data were obtained by thermal analysis[34] and the reported eutectics are E_1=109.8 °C, x_B=0.046 and E_2=154.3 °C, x_B=0.790; the 1:1 compound melts congruently at 178.3 °C or[7] 179.0–179.4 °C. In preliminary calculations it was fou that the compound liquidus was consistent with eutectic te peratures somewhat higher than those actually reported.[34] liquidus data were used in the optimization, but the expe mental eutectic and compound melting temperatures we given more weight. For the calculation of the phase diagra Fig. 188,

$$G^{E}(l) = -6000 x_A x_B \text{ J mol}^{-1} \quad (35$$

was used for the liquid and the properties

$$\Delta_{fus}G^0 - 23\,750 - 52.6099T \text{ J mol}^{-1}, \quad (35$$

$$\Delta_f G^0 = -25\,252 + 46.8487T \text{ J mol}^{-1} \quad (35$$

for the compound (AB)/2. The calculated eutectics E_1=110.6 °C, x_B=0.059 and E_2=154.8 °C, x_B=0.791. T compound melts at 178.3 °C, and the trinitrofluorenone tr sition appears on the calculated liquidus at x_B=0.802. T probable maximum inaccuracy in the calculated diagram ±2°.

TABLE 20. Reported invariant data for the system ANTH (A)+TNF (B)

	°C	x_B	Ref.
E_1	181.4	0.315	34
	182.2	...	6
E_2	156.8	0.825	34
	159.2	...	6
1:1	193.8		34
	193.9		6
	193.3		8
	193.8–194.0		7

ANTH (A)+TNF (B)

Data were obtained by thermal analysis[34] and the repor invariant data are summarized in Table 20. The heat of sion of the compound is[8] 45 200 J mol^{-1}. A 1:2 compou melting incongruently, was also claimed[34] (P=161.2 x_B=0.81). In preliminary calculations, it was found that existence of a 1:2 compound was thermodynamically inc patible with a eutectic at 157 °C. It is probable that the t mal arrests[34] near 157 °C are due rather to the trinitrofl renone transition (156.0 °C), and were mistaken by investigators[34] as representing a eutectic. Thus, an E_2 t perature at or near 161 °C was assumed in the present o mization. For the liquid,

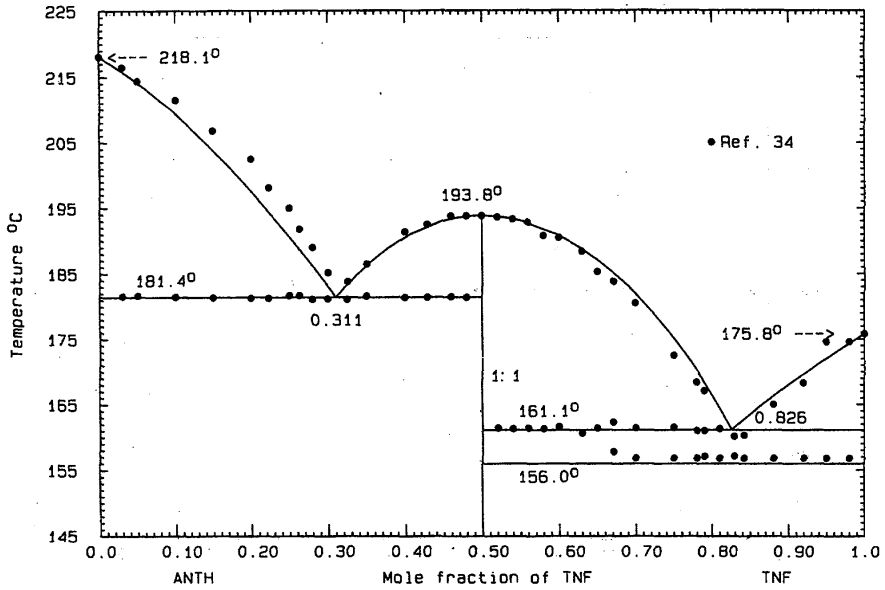

FIG. 189. The system ANTH (A)+TNF (B)

$$G^{E}(l)=x_A x_B(-6700+2700x_B)\ \text{J mol}^{-1}, \quad (360)$$

and for the compound (AB)/2,

$$\Delta_{fus}G^0=19\,643-42.0616T\ \text{J mol}^{-1}, \quad (361)$$

$$\Delta_f G^0=-20\,981+36.3004T\ \text{J mol}^{-1}. \quad (362)$$

The phase diagram, Fig. 189, was calculated with the use of Eqs. (360) and (362) and the calculated eutectics are E_1=181.4 °C, x_B=0.311 and E_2=161.1 °C, x_B=0.826; the compound melts at 193.8 °C. The probable maximum inaccuracy in the calculated diagram is ±1°.

PY (A)+TNF (B)

Data were obtained by thermal analysis[34] and the reported eutectics are E_1=145.8 °C, x_B=0.045 and E_2=170.8 °C, x_B=0.943. The 1:1 compound melts congruently[7,8,34] at

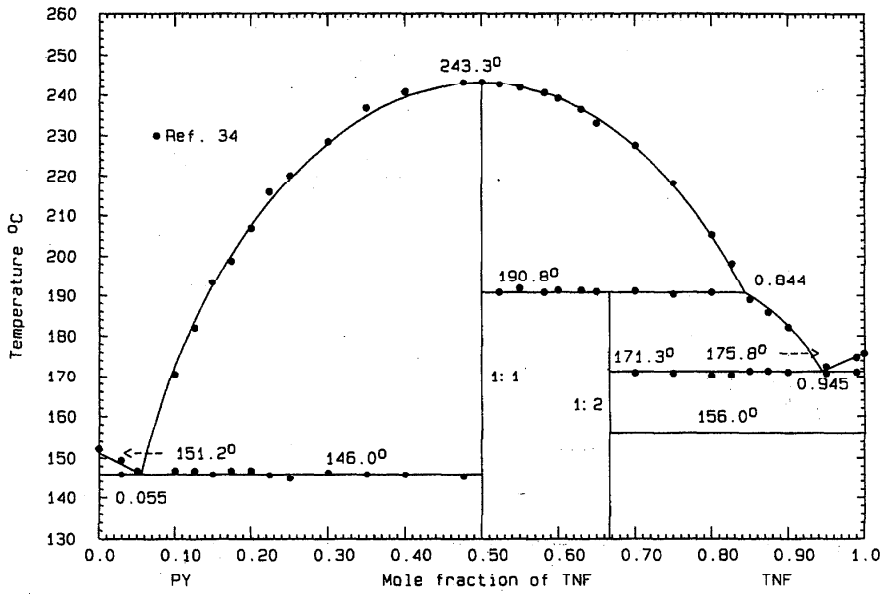

FIG. 190. The system PY (A)+TNF (B)

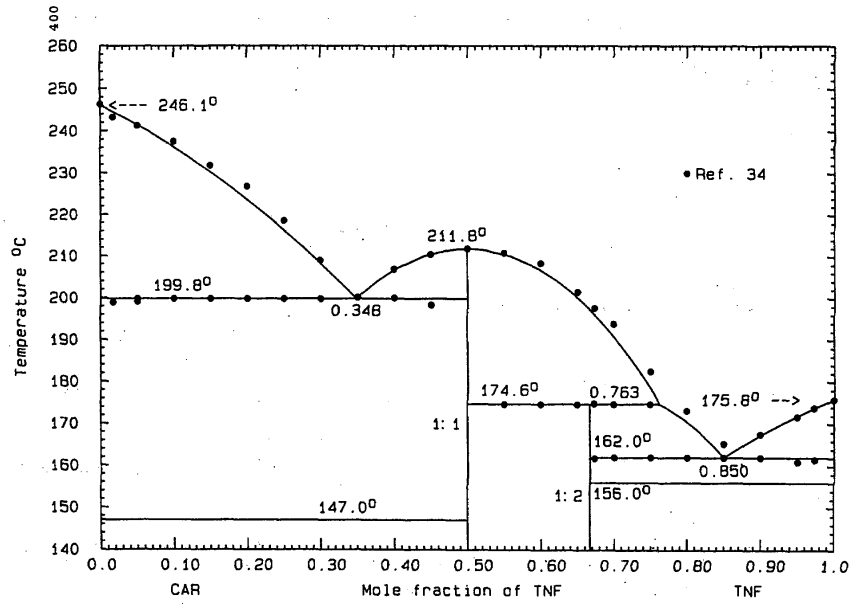

FIG. 191. The system CAR (A)+TNF (B)

242–243, 246.4, or 243.3 °C, respectively; its measured heat of fusion[8] is 43 900 J mol^{-1}. There is also a 1:2 compound melting incongruently[34] (P=190.8 °C, x_B=0.84). In this system, all liquidus data were used in the optimization and a good fit was obtained with

$$G^E(l)=x_A x_B(-5500-1000x_B)\ \text{J mol}^{-1} \quad (363)$$

for the liquid. For the compound (AB)/2

$$\Delta_{fus}G^0=19\,863-38.4604T\ \text{J mol}^{-1}, \quad (364)$$

$$\Delta_f G^0=-21\,365+32.6992T\ \text{J mol}^{-1} \quad (365)$$

and for $(AB_2)/3$

$$\Delta_{fus}G^0=31\,889-67.5906T\ \text{J mol}^{-1}, \quad (366)$$

$$\Delta_f G^0=-33\,310+62.3003T\ \text{J mol}^{-1}. \quad (367)$$

The phase diagram, Fig. 190, was calculated with the use of Eqs. (362), (364), and (366). The calculated eutectics are E_1=146.0 °C, x_B=0.055 and E_2=171.3 °C, x_B=0.945;

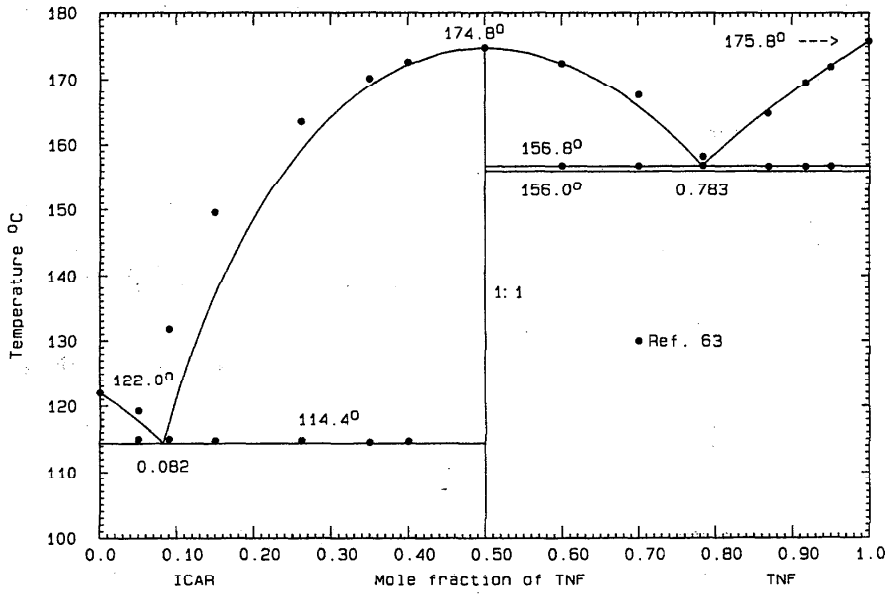

FIG. 192. The system ICAR (A)+TNF (B)

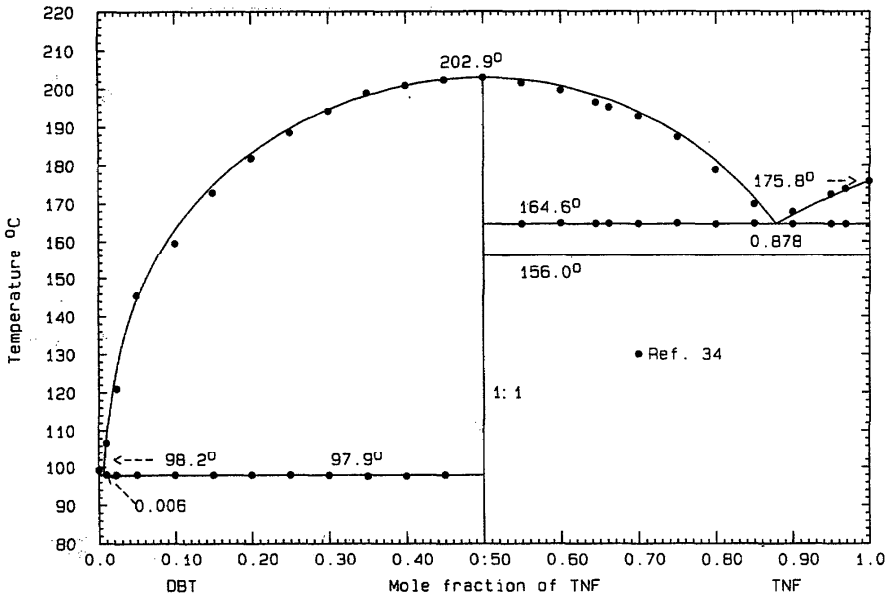

FIG. 193. The system DBT (A)+TNF (B)

P=190.8 °C, x_B=0.844. The 1:1 compound melts congruently at 243.3 °C. The probable maximum inaccuracy in the calculated diagram is ±1°.

CAR (A)+TNF (B)

Data were obtained by thermal analysis[34] and the reported eutectics are E_1=199.8 °C, x_B=0.349 and E_2=162.0 °C, x_B=0.855. The 1:1 compound melts congruently at 211.8 °C and a 1:2 compound melts incongruently with peritectic[34] 174.6 °C, x_B=0.77 or[7] 173.4–174.4 °C. All liquidus data were used in the optimization, but greater weight was given to the invariant temperatures. The result was

$$G^E(l) = -5500 x_A x_B \text{ J mol}^{-1} \quad (368)$$

for the liquid; for the compound (AB)/2

$$\Delta_{fus}G^0 = 12\,844 - 26.4861T \text{ J mol}^{-1}, \quad (369)$$

$$\Delta_f G^0 = -14\,220 + 20.7249T \text{ J mol}^{-1} \quad (370)$$

and for the compound $(AB_2)/3$

$$\Delta_{fus}G^0 = 15\,064 - 33.2671T \text{ J mol}^{-1}, \quad (371)$$

$$\Delta_f G^0 = -16\,258 + 27.9768T \text{ J mol}^{-1}. \quad (372)$$

The phase diagram, Fig. 191, was calculated with the use of Eqs. (368), (370), and (372). Other calculated data are E_1=199.8 °C, x_B=0.348; E_2=162.0 °C, x_B=0.850; P=174.6 °C, x_B=0.763. The 1:1 compound melts at 211.8 °C. The probable maximum inaccuracy in the calculated diagram is ±2°.

ICAR (A)+TNF (B)

Data were obtained by thermal analysis and by means of a hot-stage microscope.[63] The reported eutectics are E_1=114.8 °C, x_B=0.065 and E_2=156.8 °C, x_B=0.790; the 1:1 compound melts congruently at 174.8 °C. The compound LHS liquidus arm[63] lies too high to be compatible with the observed E_1 temperature, and so in the optimization greater weight was given to the invariant temperatures. For the liquid,

$$G^E(l) = x_A x_B(-7000 + 3000 x_B) \text{ J mol}^{-1}, \quad (373)$$

and for the compound (AB)/2,

$$\Delta_{fus}G^0 = 24\,686 - 55.1131T \text{ J mol}^{-1}, \quad (374)$$

$$\Delta_f G^0 = -26062 + 49.3519T \text{ J mol}^{-1}. \quad (375)$$

The calculated phase diagram, Fig. 192, shows calculated eutectics E_1=114.4 °C, x_B=0.082 and E_2=156.8 °C, x_B=0.783 (this eutectic temperature probably could not be distinguished from the transition temperature of trinitrofluorenone[63]). The compound melts at 174.8 °C. The probable maximum inaccuracy in the calculated diagram is ±2°.

DBT (A)+TNF (B)

Data were obtained by thermal analysis[34] and the reported eutectics are E_1=97.9 °C, x_B<0.005 and E_2=164.6 °C, x_B=0.855; the 1:1 compound melts at 202.9 °C. Since the crystallization field of the compound occupies more than 80% of the composition range, an excess Gibbs energy of the liquid was assigned rather than calculated:

$$G^E(l) = x_A x_B(-5000 - 1270 x_B) \text{ J mol}^{-1}. \quad (376)$$

For the compound (AB)/2, the calculated quantities are

$$\Delta_{fus}G^0 = 30\,938 - 64.9877T \text{ J mol}^{-1}, \quad (377)$$

$$\Delta_f G^0 = -32\,349 + 59.2265T \text{ J mol}^{-1}, \quad (378)$$

and the calculated phase diagram is shown in Fig. 193. Other

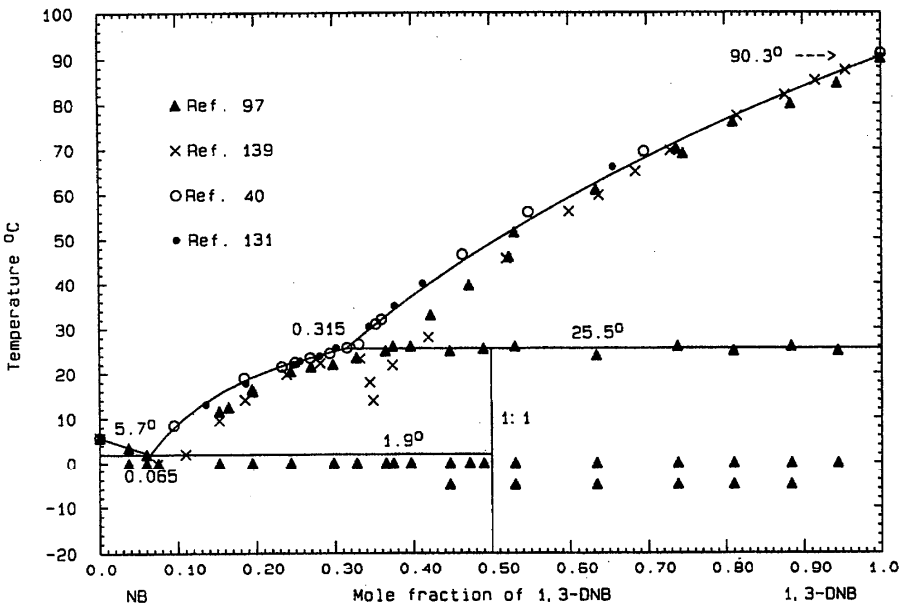

FIG. 194. The system NB (A)+1,3-DNB (B)

calculated data are E_1=97.9 °C, x_B=0.006 and E_2=164.6 °C, x_B=0.878; the compound melts at 202.9 °C. The probable maximum inaccuracy in the calculated diagram is ±1°.

2.5.25. Systems Containing Two Nitroaromatic Compounds

The systems in this section are ordered according to the simpler nitroaromatic compound in the sequence given in Table 1. Thus, for example, the three systems containing nitrobenzene come first and are ordered according to their second components, again referred to Table 1. Next come eight systems based on 1,3-dinitrobenzene, arranged in similar order, etc.

NB (A)+1,3-DNB (B)

Data were obtained by thermal analysis with stirring and the visual-polythermal method[97] and also by the conventional melting point method.[40,134,139] The liquidus data of Lehmstedt[139] and Ravich and Bogush[97] are lower than those

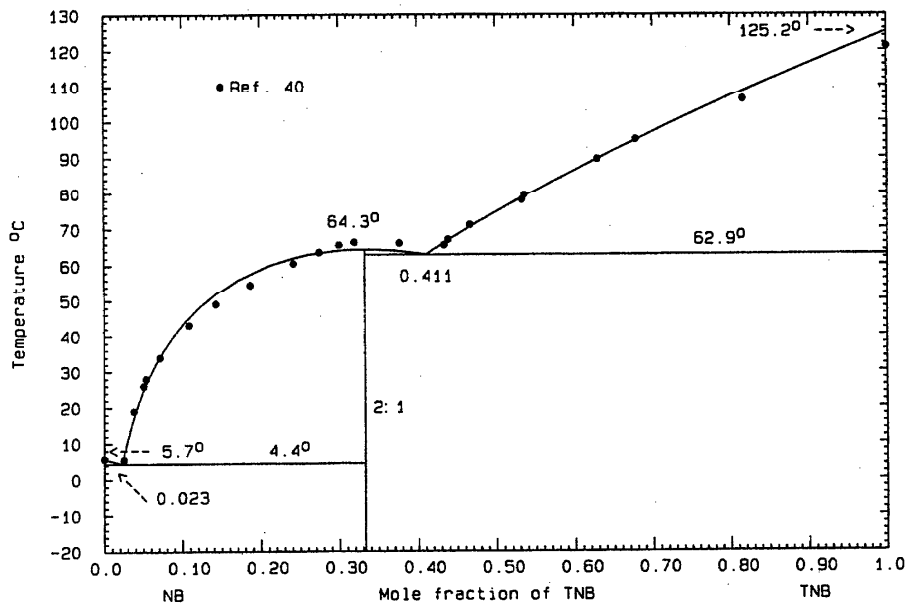

FIG. 195. The system NB (A)+TNB (B)

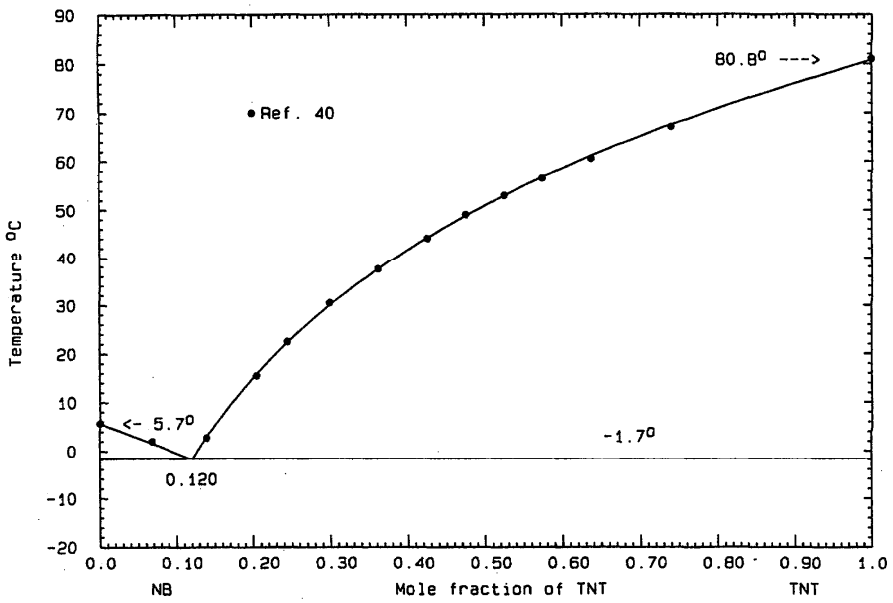

FIG. 196. The system NB (A)+TNT (B)

of Hammick and co-workers.[40,134] Only one author[97] reported a eutectic: 0.0 °C, x_B=0.075. The compound was stated by one author[139] to be of congruently melting 2:1 stoichiometry (23.3 °C), but others[40,97] indicated a 1:1 compound melting incongruently (P=25.0 °C, x_B=0.365 or ≈26 °C, x_B≈0.33). In preliminary calculations it was found that the liquidus data of Hammick and co-workers[40,131] were more thermodynamically self-consistent than the others. Only these data, therefore, were used in the optimization, which yielded

$$G^E(l) = -493 x_A x_B \text{ J mol}^{-1} \quad (379)$$

for the liquid and

$$\Delta_{fus}G^0 = 19\,381 - 64.2152T \text{ J mol}^{-1}, \quad (380)$$

$$\Delta_f G^0 = -19\,504 + 58.4540T \text{ J mol}^{-1} \quad (381)$$

for the compound (AB)/2. The calculated phase diagram,

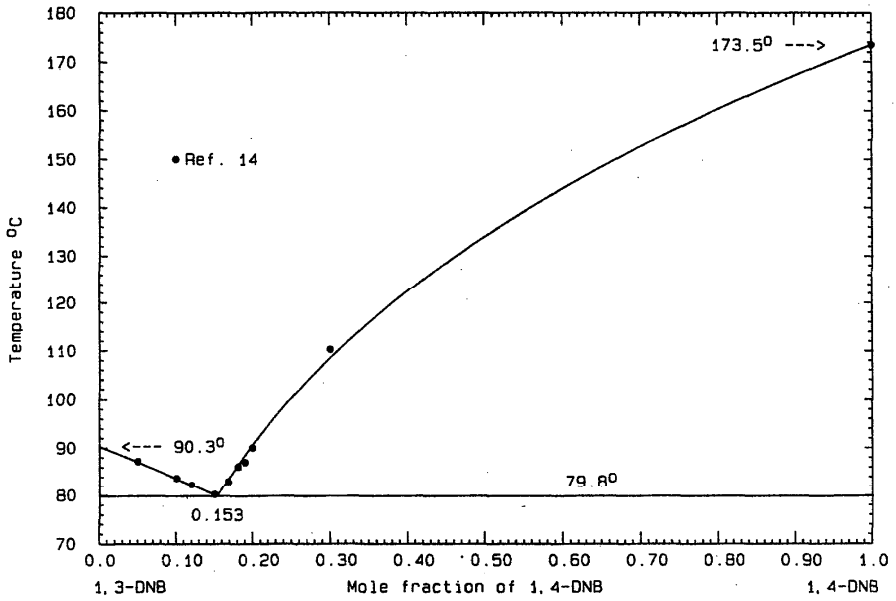

FIG. 197. The system 1,3-DNB (A)+1,4-DNB (B)

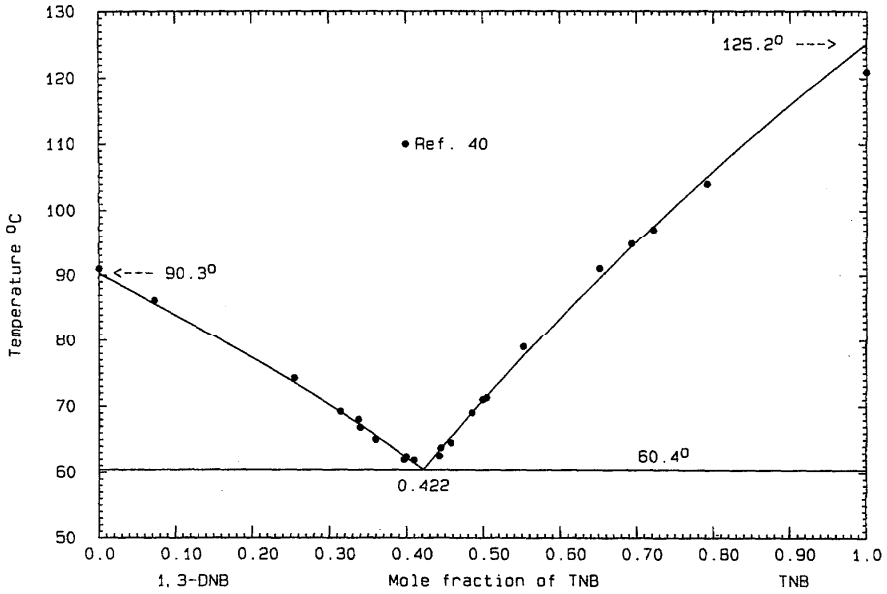

FIG. 198. The system 1,3-DNB (A)+TNB (B)

Fig. 194, shows invariant points $E=1.9$ °C, $x_B=0.065$ and $P=25.5$ °C, $x_B=0.315$. The probable maximum inaccuracy in the calculated diagram is ±2°.

NB (A)+TNB (B)

Liquidus data were obtained by the conventional melting point method.[40] No eutectic data were reported, but a 2:1 compound was claimed to melt congruently at ≈66 °C. In the optimization, all liquidus data were weighted equally, with the result

$$G^E(l)=402x_Ax_B \text{ J mol}^{-1} \quad (382)$$

for the liquid and

$$\Delta_{fus}G^0=8017-23.7562T \text{ J mol}^{-1}, \quad (383)$$

$$\Delta_fG^0=-7927+18.4676T \text{ J mol}^{-1} \quad (384)$$

for the compound $(A_2B)/3$. The calculated phase diagram is shown in Fig. 195. Other calculated data are $E_1=4.4$ °C,

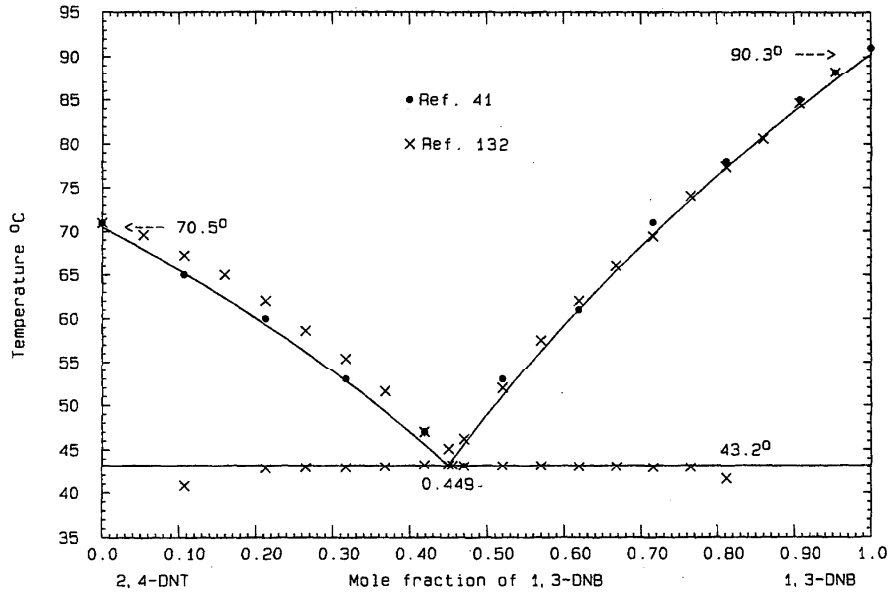

FIG. 199. The system 2,4-DNT (A)+1,3-DNB (B)

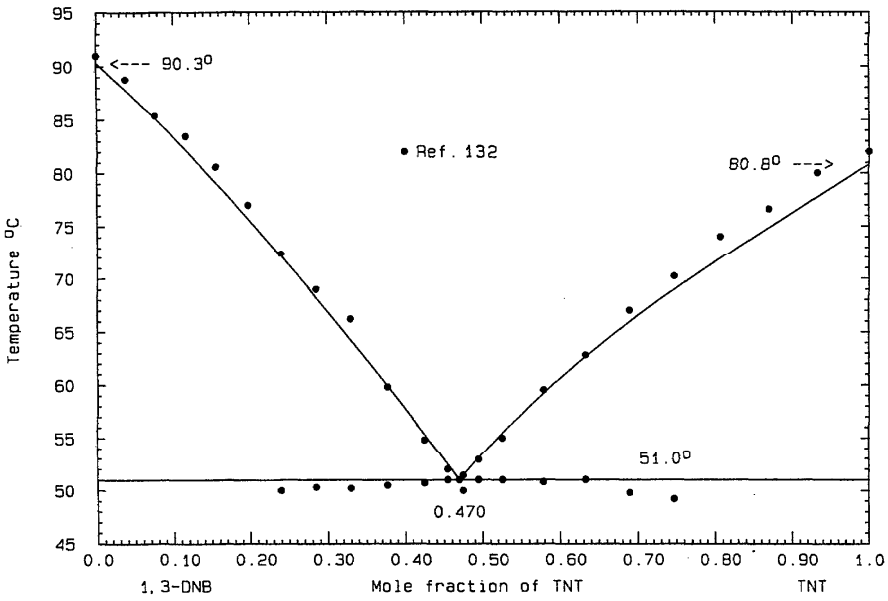

FIG. 200. The system 1,3-DNB (A)+TNT (B)

x_B=0.023 and E_2=62.9 °C, x_B=0.411; the compound melts at 64.3 °C. The probable maximum inaccuracy in the calculated diagram is ±2°.

NB (A)+TNT (B)

Liquidus data were obtained by the conventional melting point method[40] and no eutectic data were reported. All liquidus data were weighted equally in the optimization and the quantity

$$G^E(l)=x_Ax_B(-706+612x_B)\ \text{J mol}^{-1} \qquad (385)$$

was deduced. The calculated phase diagram, Fig. 196, shows a eutectic −1.7 °C, x_B=0.120. The probable maximum inaccuracy in the calculated diagram is ±1°.

1,3-DNB (A)+1,4-DNB (B)

The few liquidus points were obtained by the thaw–melt method,[14] and the reported eutectic is 79.9 °C, x_B=0.155. Optimization of the data gave the result

$$G^E(l)=-549x_Ax_B\ \text{J mol}^{-1}, \qquad (386)$$

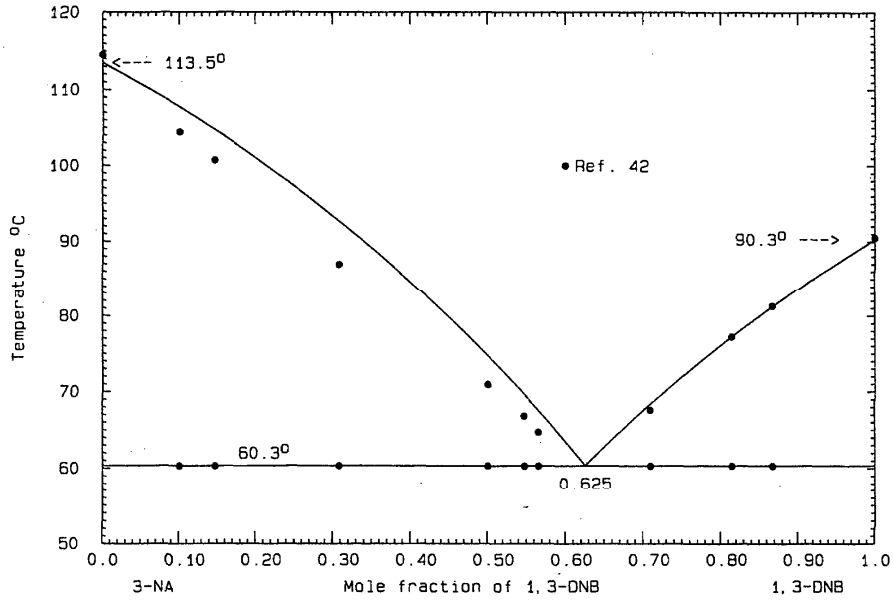

FIG. 201. The system 3-NA (A)+1,3-DNB (B)

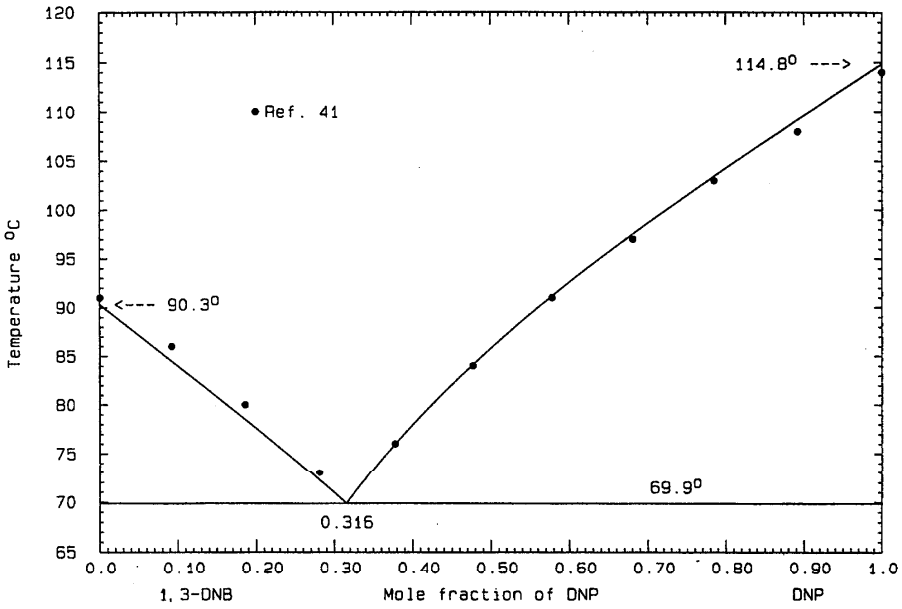

FIG. 202. The system 1,3-DNB (A)+DNP (B)

and the calculated phase diagram, Fig. 197, shows a eutectic 79.8 °C, $x_B=0.153$. The probable maximum inaccuracy in the calculated diagram is ±1°.

1,3-DNB (A)+TNB (B)

Liquidus data were obtained by the conventional melting point method,[40] and no eutectic data were reported. Despite a low experimental melting point of trinitrobenzene,[40] the data were well fitted by the expression

$$G^E(l)=x_Ax_B(393-637x_B)\ \text{J mol}^{-1}. \quad (387)$$

The calculated phase diagram, Fig. 198, shows a calculated eutectic 60.4 °C, $x_B=0.422$. The probable maximum inaccuracy in the calculated diagram is ±1°.

2,4-DNT (A)+1,3-DNB (B)

Data were obtained by the microthermal method[41] and thermal analysis.[132] The reported eutectic is[41] 45.0 °C, $x_B=0.45$ or[132] 43.2 °C, $x_B=0.455$. About 41 mol % solid solubility at the RHS was claimed by Brandstätter,[41] but it proved unnecessary to include any in the final diagram. The LHS liquidus data[132] lie too high and are inconsistent with the RHS data. The optimization yielded the result

$$G^E(l)=-490x_Ax_B\ \text{J mol}^{-1}, \quad (388)$$

and the calculated eutectic is 43.2 °C, $x_B=0.449$ (Fig. 199). The probable maximum inaccuracy in the calculated diagram is ±1°.

1,3-DNB (A)+TNT (B)

Data were obtained by thermal analysis[132] and the reported eutectic is 51.0 °C, $x_B=0.47$. The experimental limiting liquidus slope at the RHS lies a little high and might indicate some solid solubility there. The experimental eutectic proved to be reproduced quite accurately without the assumption of solid solution, with the expression

$$G^E(l)=x_Ax_B(-696+1324x_B)\ \text{J mol}^{-1}, \quad (389)$$

as seen in the calculated phase diagram, Fig. 200. The probable maximum inaccuracy in the calculated diagram is ±2°.

3-NA (A)+1,3-DNB (B)

Data were obtained by the thaw–melt method[42] and the reported eutectic is 60.3 °C, $x_B=0.63$. The experimental limiting liquidus slope at the LHS is quite inaccurate, as are the LHS liquidus data. The optimization therefore used only the RHS liquidus data, together with the observed eutectic temperature as guide. The phase diagram, Fig. 201, was calculated with the use of

$$G^E(l)=x_Ax_B(-1448+412x_B)\ \text{J mol}^{-1}, \quad (390)$$

and the calculated eutectic is 60.3 °C, $x_B=0.625$. The probable maximum inaccuracy in the calculated diagram is ±1°.

1,3-DNB (A)+DNP (B)

Liquidus data were obtained by the microthermal method,[41] and the reported eutectic is 70.0 °C, $x_B=0.32$. A solid solubility of 16 mol % at the LHS and 23 mol % at the RHS was claimed by the investigator,[41] but the limiting liquidus slopes at either end do not support this claim. Zero solid solubility was therefore assumed in the optimization, which gave the expression

$$G^E(l)=1038x_Ax_B\ \text{J mol}^{-1}, \quad (391)$$

and the calculated phase diagram, Fig. 202, shows a eutectic 69.9 °C, $x_B=0.316$. The probable maximum inaccuracy in the calculated diagram is ±1°.

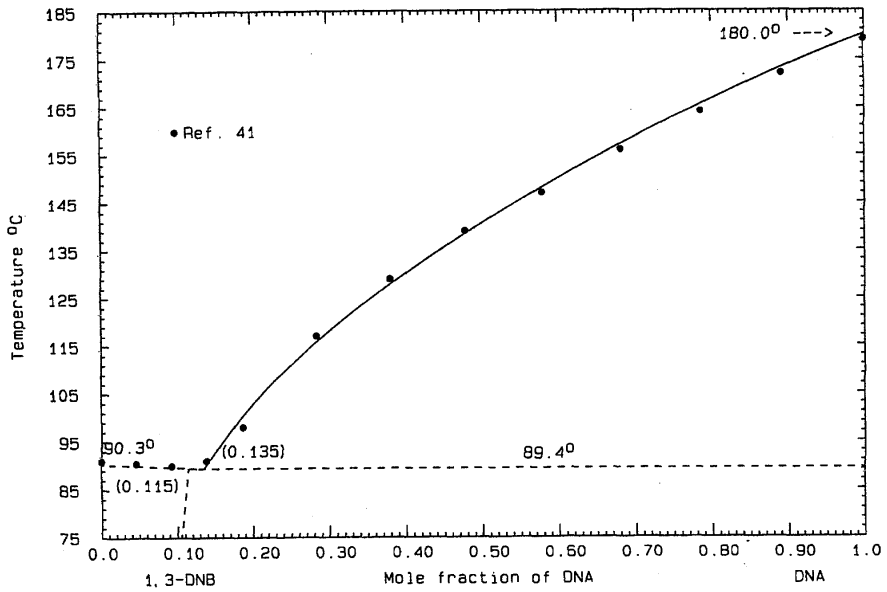

FIG. 203. The system 1,3-DNB (A)+DNA (B)

1,3-DNB (A)+DNA (B)

Liquidus data were obtained by the microthermal method.[41] The liquidus appears horizontal in the range $0<x_B<0.15$, which makes the interpretation of the data rather ambiguous. The author[41] confusedly claims three simultaneous features of the phase diagram: peritectic at 92.0 °C, $x_B=0.17$, minimum at 90.0 °C, $x_B=0.09$, and solid solubility up to 17 mol % at the LHS. If the LHS liquidus is taken as accurate, solid solubility is definitely indicated. The phase diagram, Fig. 203, was calculated with the use of the following equation for the liquid

$$G^E(l)=x_A x_B(451-1254x_B)\ \text{J mol}^{-1}, \quad (392)$$

and the solid solution was represented by a temperature-independent Henrian activity coefficient

$$RT\ \ln\ \gamma_B=6500\ \text{J mol}^{-1}. \quad (393)$$

The calculated eutectic is 89.4 °C, $x_B=0.135$, and there is 11.5 mol % solid solution at the eutectic temperature. The

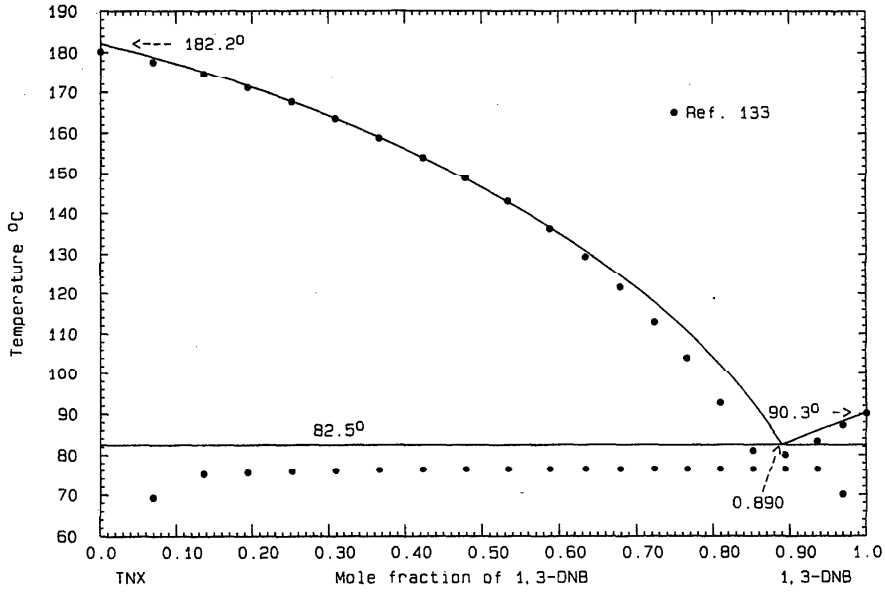

FIG. 204. The system TNX (A)+1,3-DNB (B)

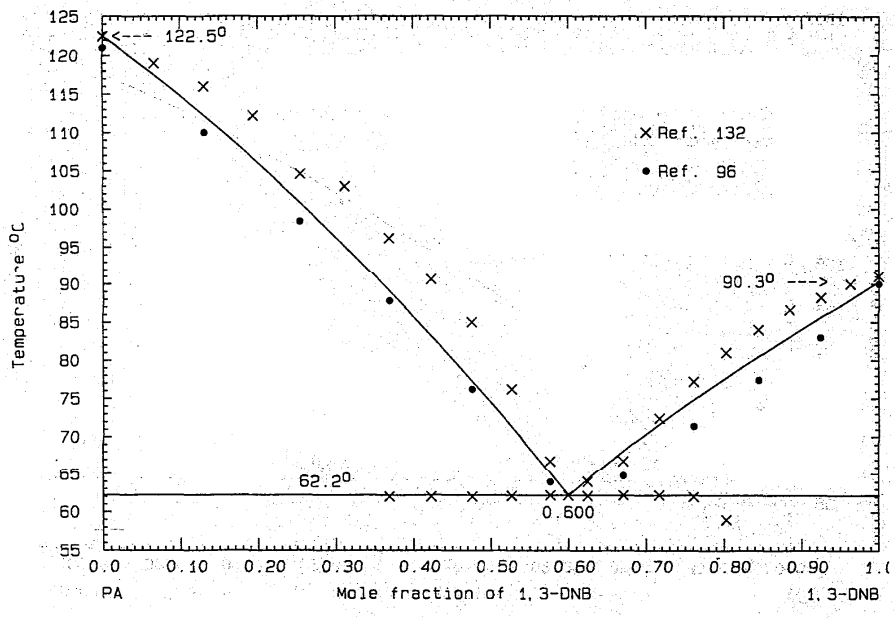

FIG. 205. The system PA (A)+1,3-DNB (B)

LHS liquidus remains speculative. The probable maximum inaccuracy in the calculated RHS liquidus is ±2°.

TNX (A)+1,3-DNB (B)

Data were obtained by the thaw–melt method[133] and the reported eutectic is 76.4 °C, x_B=0.87. Another determination of the eutectic[96] revealed 82.0 °C, x_B=0.93. It was evident that experimental liquidus data near the eutectic[133] are low, and hence the same author's reported eutectic is also too low. Optimization of the data yielded the result

$$G^E(l) = -2420 x_A x_B \text{ J mol}^{-1} \quad (394)$$

with which the phase diagram, Fig. 204, was calculated. The calculated eutectic is 82.5 °C, x_B=0.890, closer to the more recently reported value.[96] The probable maximum inaccuracy in the calculated diagram is ±2°.

PA (A)+1,3-DNB (B)

Data were obtained by thermal analysis[132] and the visual-polythermal method[96]; the reported eutectic[132] is 62.2 °C,

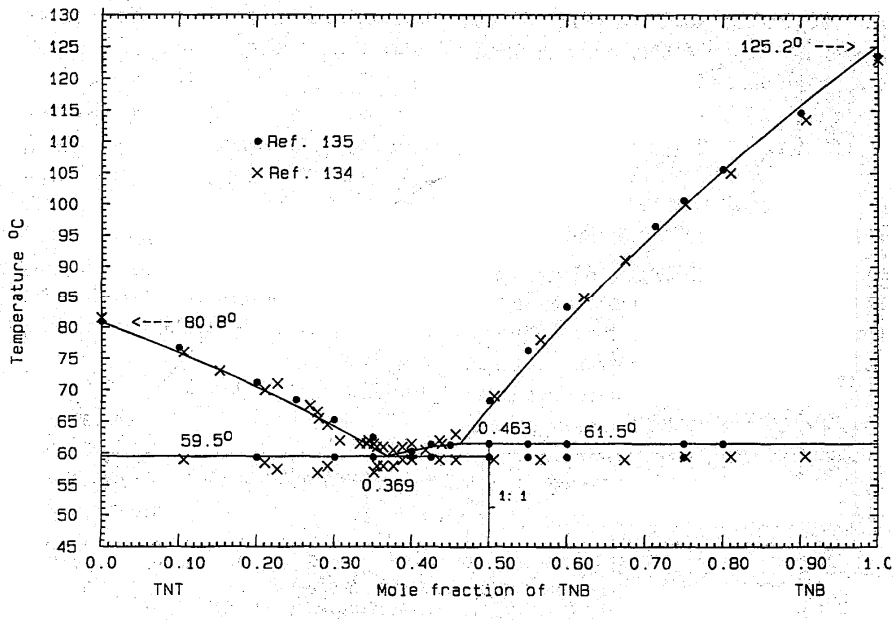

FIG. 206. The system TNT (A)+TNB (B)

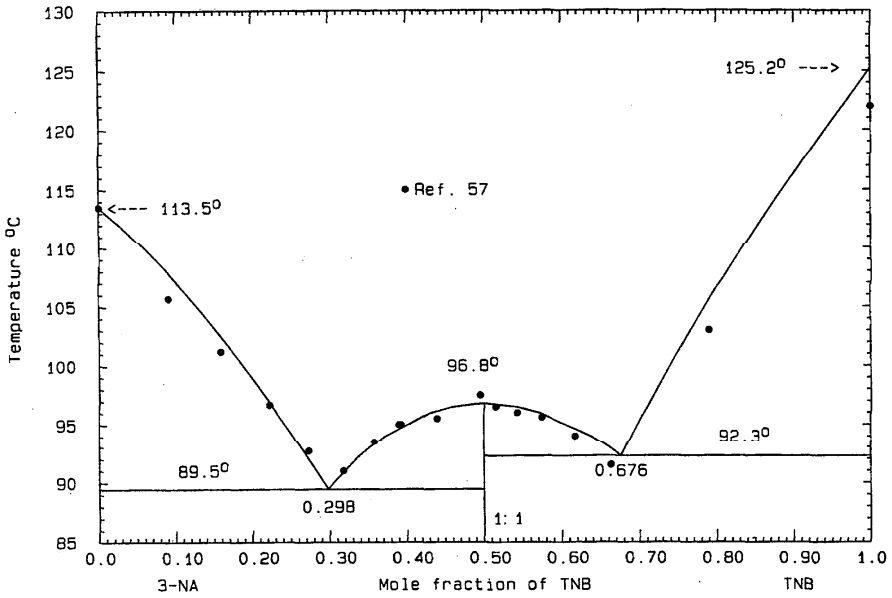

FIG. 207. The system 3-NA (A)+TNB (B)

x_B=0.60 or[96] 59.5 °C, x_B=0.625. The liquidus data of Hrynakowski and Kapuscinski[132] are much higher everywhere than those in the other set,[96] although the reported eutectics are in fair agreement. In this case, all liquidus data[96,132] were weighted equally, with the result

$$G^E(l)=x_A x_B(-1000+1227x_B)\ \text{J mol}^{-1} \quad (395)$$

from which the phase diagram, Fig. 205, was calculated. The calculated eutectic is 62.2 °C, x_B=0.600. The probable maximum inaccuracy in the calculated diagram is ±2°.

TNT (A)+TNB (B)

Data were obtained by the thaw–melt method[134] and by thermal analysis with stirring,[135] supplemented by optical transmission[135] (for locating the liquidus). The two liquidus data sets agree quite well (within 1°), but the region

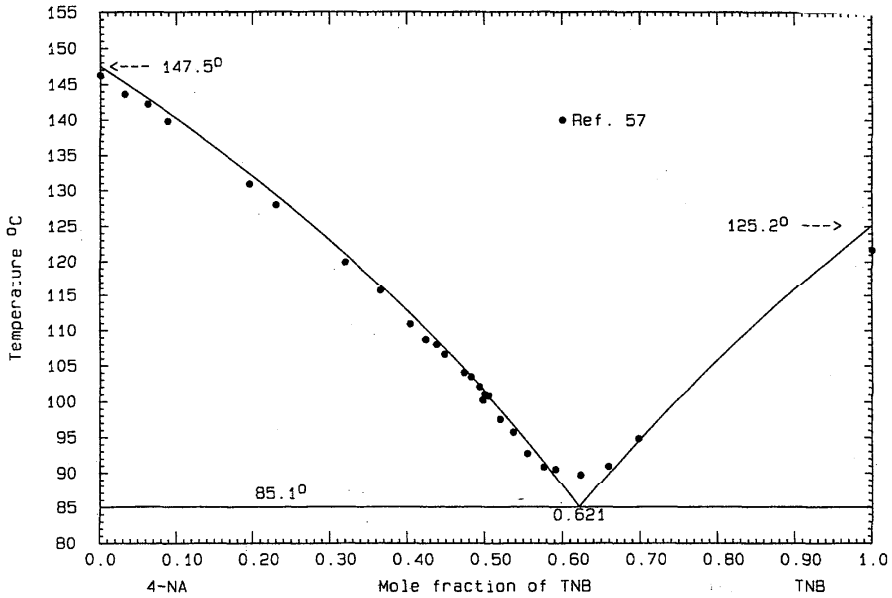

FIG. 208. The system 4-NA (A)+TNB (B)

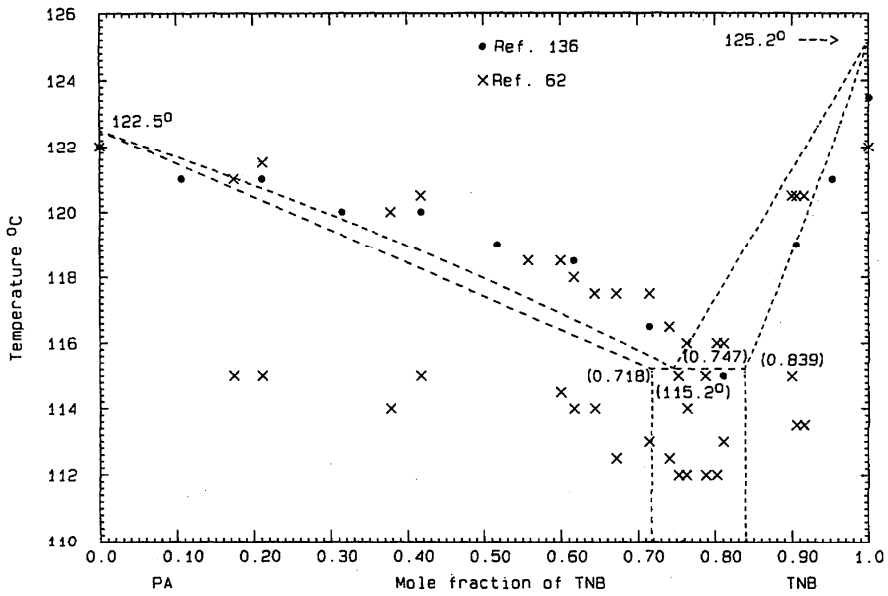

FIG. 209. The system PA (A)+TNB (B)

$0.3<x_B<0.45$ is very confused. In the early work[134] the apparently flat central liquidus was interpreted as indicating a liquid immiscibility gap, but the unquestionably better later data[135] rule this out. This very careful work[135] indicates a eutectic at 59.4 °C, $x_B=0.39$ and a peritectic 61.5 °C, $x_B=0.47$ (1:1 compound). The LHS and RHS liquidus data of both data sets were optimized to give the expression

$$G^E(l)=x_Ax_B(-600-300x_B)\ \text{J mol}^{-1}, \quad (396)$$

and, since the data defining the compound liquidus are so poor, the properties of the compound (AB)/2

$$\Delta_{fus}G^0=16\,998-50.7628T\ \text{J mol}^{-1}, \quad (397)$$

$$\Delta_fG^0=-17\,186+45.0000T\ \text{J mol}^{-1} \quad (398)$$

were assigned in order to reproduce the observed[135] eutectic and peritectic temperatures. The phase diagram, Fig. 206, was calculated with the use of Eqs. (396) and (398) and shows calculated invariant points $E=59.5$ °C, $x_B=0.369$ and $P=61.5$ °C, $x_B=0.463$. The probable maximum inaccuracy in the calculated diagram is ±1°.

3-NA (A)+TNB (B)

Liquidus data were obtained by the conventional melting point method[57] and no eutectic data were reported. The congruent melting point of the 1:1 compound was also not reported. Some liquidus data on the LHS and RHS lie too low; nevertheless, optimization of all the data yielded the quantity

$$G^E(l)=x_Ax_B(-3576+2292x_B)\ \text{J mol}^{-1} \quad (399)$$

for the liquid and

$$\Delta_{fus}G^0=20\,516-55.4609T\ \text{J mol}^{-1}, \quad (400)$$

$$\Delta_fG^0=-21\,124+49.6997T\ \text{J mol}^{-1} \quad (401)$$

for the compound (AB/2). The calculated eutectics of the phase diagram, Fig. 207, are $E_1=89.5$ °C, $x_B=0.298$ and $E_2=92.3$ °C, $x_B=0.676$; the compound melts at 96.8 °C. The probable maximum inaccuracy in the calculated diagram is ±2°.

4-NA (A)+TNB (B)

Liquidus data were obtained by the conventional melting point method[57] and no eutectic data were reported. The liquidus at its lowest point appears rounded, suggesting a minimum rather than a eutectic; the experimental limiting liquidus slopes[57] at both sides do not suggest the presence of any solid solution, and hence a minimum is ruled out. The liquidus data are almost all confined to the LHS arm; optimization yielded the expression

$$G^E(l)=-636x_Ax_B\ \text{J mol}^{-1} \quad (402)$$

and the calculated phase diagram, Fig. 208, shows a calculated eutectic 85.1 °C, $x_B=0.621$. The probable maximum inaccuracy in the calculated diagram is ±1°.

PA (A)+TNB (B)

Data were obtained by the *microthermal method*[136] and thaw–melt method.[62] The reported eutectic is[136] 115.0 °C, $x_B=0.811$ or[62] 114.0 °C, $x_B=0.764$. "Extensive solid solubility" was claimed[136] and the liquidus data[62,136] definitely support this conclusion. Apart from these observations, very little further can be deduced with any confidence about this system. A phase diagram was constructed, based on the reported eutectic data[62,136] as a general guide, together with extensive solid solutions at both sides. Since it was impossible to obtain excess properties of the liquid by optimization, the quantity

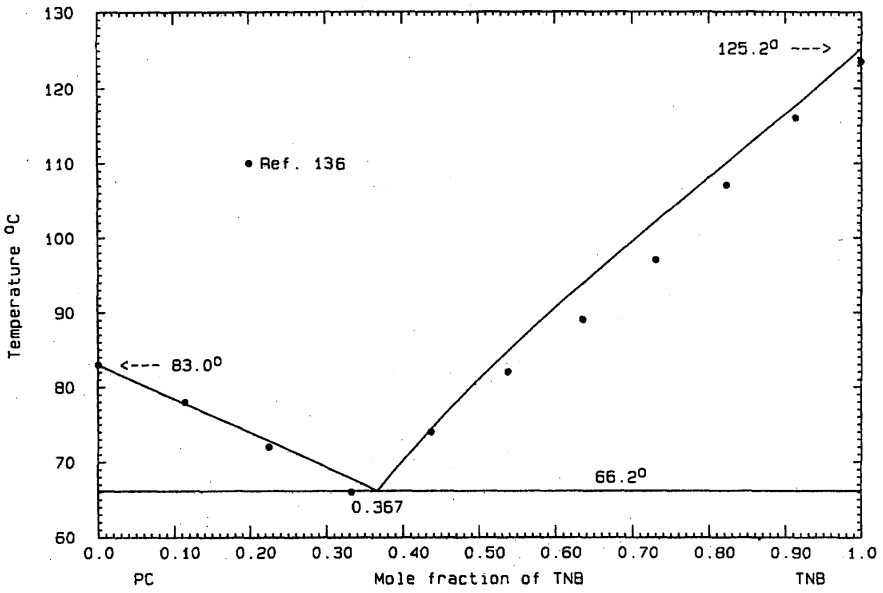

FIG. 210. The system PC (A)+TNB (B)

$$G^{E}(l)=0 \tag{403}$$

was arbitrarily assigned and two temperature-independent Henrian activity coefficients

$$RT \ln \gamma_B = 500 \text{ J mol}^{-1}, \tag{404}$$

$$RT \ln \gamma_A = 1800 \text{ J mol}^{-1} \tag{405}$$

were chosen to reproduce the observed eutectic as closely as possible. The calculated phase diagram, Fig. 209, is only tentative and shows a eutectic 115.2 °C, $x_B=0.747$, with 71.8 and 16.1 mol % solid solution at the LHS and RHS, respectively, at the eutectic temperature. The probable maximum inaccuracy in the calculated diagram is ±5°.

PC (A)+TNB (B)

Liquidus data were obtained by the microthermal method[136] and no eutectic data were stated. Optimization of the data yielded the expression

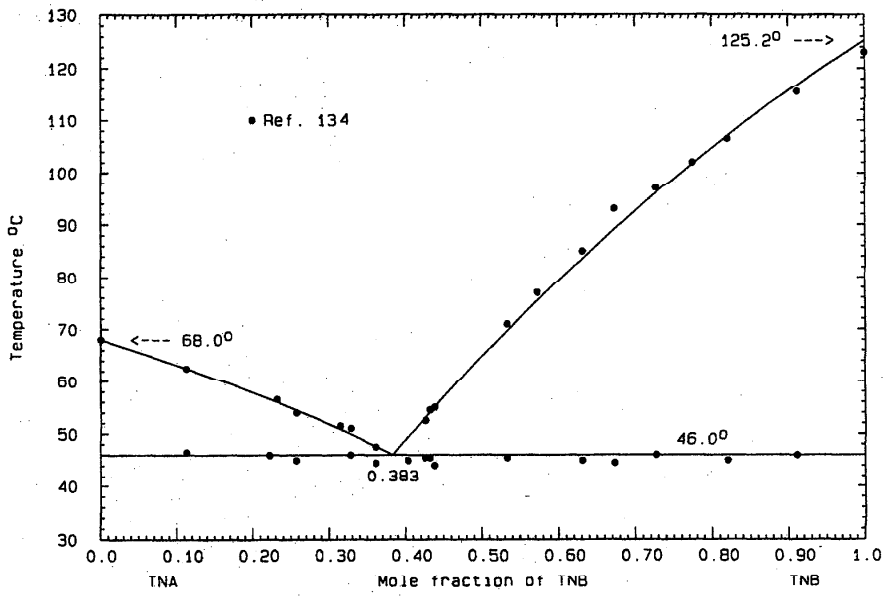

FIG. 211. The system TNA (A)+TNB (B)

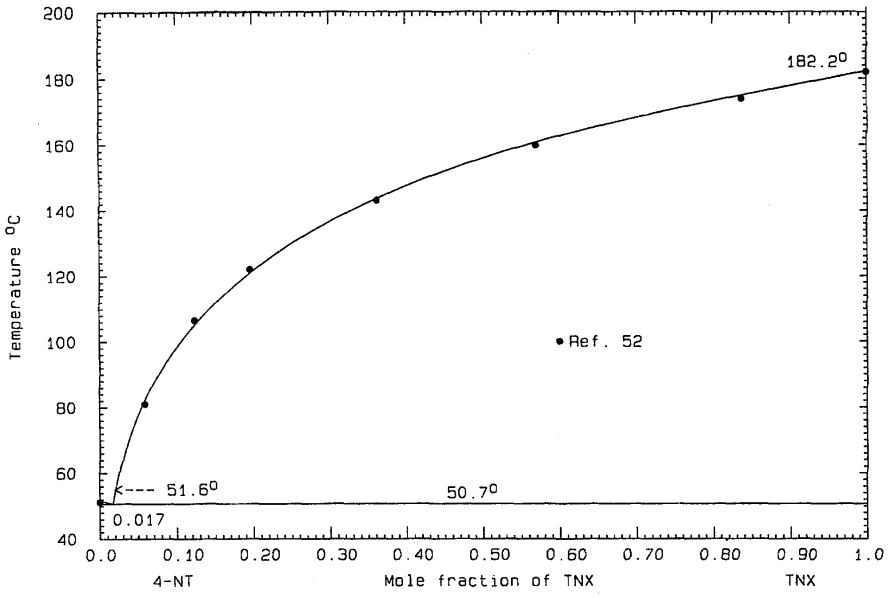

FIG. 212. The system 4-NT (A)+TNX (B)

$$G^{E}(l)=1505x_A x_B \text{ J mol}^{-1}, \quad (406)$$

and the calculated phase diagram, Fig. 210, shows a calculated eutectic 66.2 °C, $x_B=0.367$. The dip in the experimental RHS liquidus may be an artefact. The probable maximum inaccuracy in the calculated diagram is ±2°.

TNA (A)+TNB (B)

Data were obtained by the thaw–melt method[134] and no eutectic data were stated. Optimization of the data gave the result

$$G^{E}(l)=x_A x_B(-609-705x_B) \text{ J mol}^{-1}, \quad (407)$$

and the calculated phase diagram, Fig. 211, has a eutectic 46.0 °C, $x_B=0.383$. The probable maximum inaccuracy in the calculated diagram is ±2°.

4-NT (A)+TNX (B)

Liquidus data were obtained by thermal analysis[52] and the reported eutectic is 50.5 °C, $x_B=0.02$. The data, although sparse, appear to be of good quality and optimization gave the expression

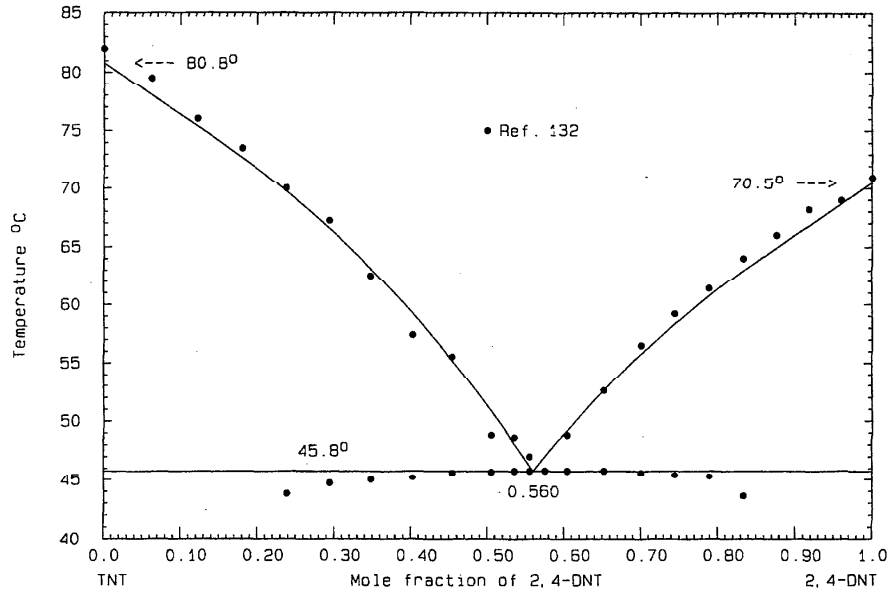

FIG. 213. The system TNT (A)+2,4-DNT (B)

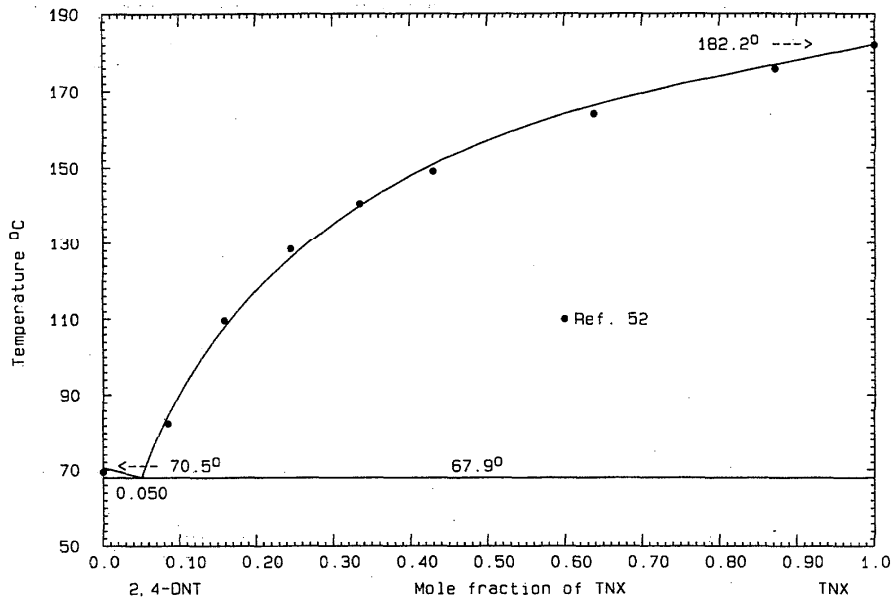

FIG. 214. The system 2,4-DNT (A)+TNX (B)

$$G^{E}(l)=x_A x_B(-223+1214x_B)\ \text{J mol}^{-1}. \quad (408)$$

The calculated phase diagram, Fig. 212, shows a calculated eutectic 50.7 °C, $x_B=0.017$. The probable maximum inaccuracy in the calculated diagram is ±1°.

TNT (A)+2,4-DNT (B)

Data were obtained by thermal analysis[132] and the reported eutectic is 45.8 °C, $x_B=0.58$. There is some scatter in the data but optimization yielded the quantity

$$G^{E}(l)=x_A x_B(715-2808x_B+2749x_B^2)\ \text{J mol}^{-1} \quad (409)$$

with which the phase diagram, Fig. 213, was calculated. The calculated eutectic is 45.8 °C, $x_B=0.560$. The probable maximum inaccuracy in the calculated diagram is ±1°.

2,4-DNT (A)+TNX (B)

Liquidus data were obtained by thermal analysis,[52] and the

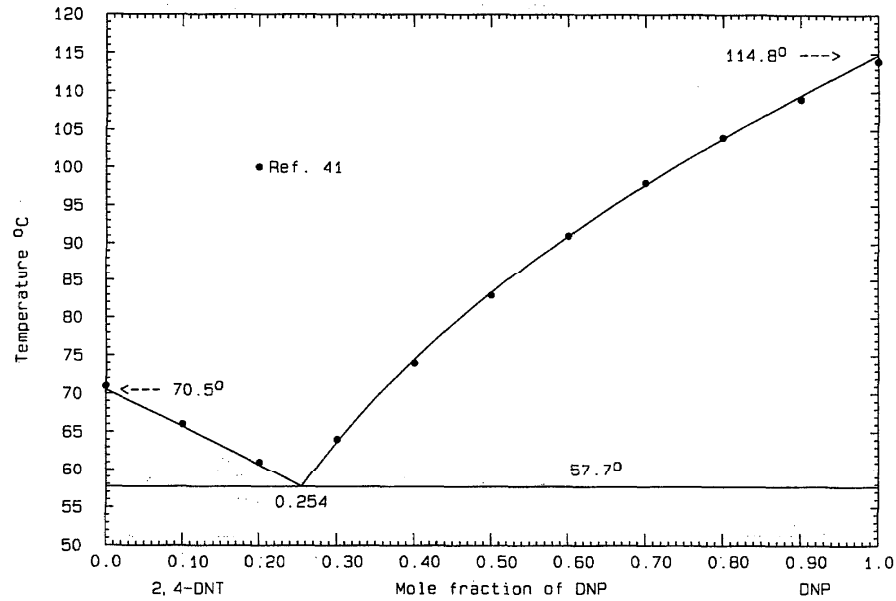

FIG. 215. The system 2,4-DNT (A)+DNP (B)

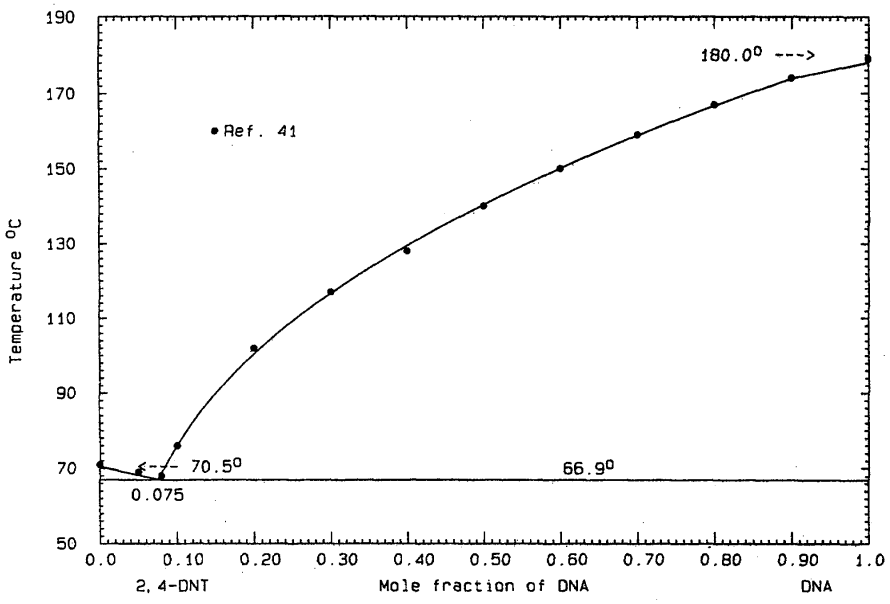

FIG. 216. The system 2,4-DNT (A)+DNA (B)

reported eutectic is 67.7 °C, x_B=0.06. Optimization of the data gave the result

$$G^E(l)=x_A x_B(-1609+3042x_B)\ \text{J mol}^{-1}, \quad (410)$$

and the calculated phase diagram, Fig. 214, shows a eutectic 67.9 °C, x_B=0.050. The probable maximum inaccuracy in the calculated diagram is ±1°.

2,4-DNT (A)+DNP (B)

Liquidus data were obtained by the microthermal method,[41] and the reported eutectic is 56.0 °C, x_B=0.26. The author[41] claimed the presence of about 12 mol % solid solubility at the RHS, but the experimental limiting liquidus slope of dinitrophenol does not suggest any solid solution there, and none was assumed in the calculations. All liquidus data could be reproduced quite well with the use of

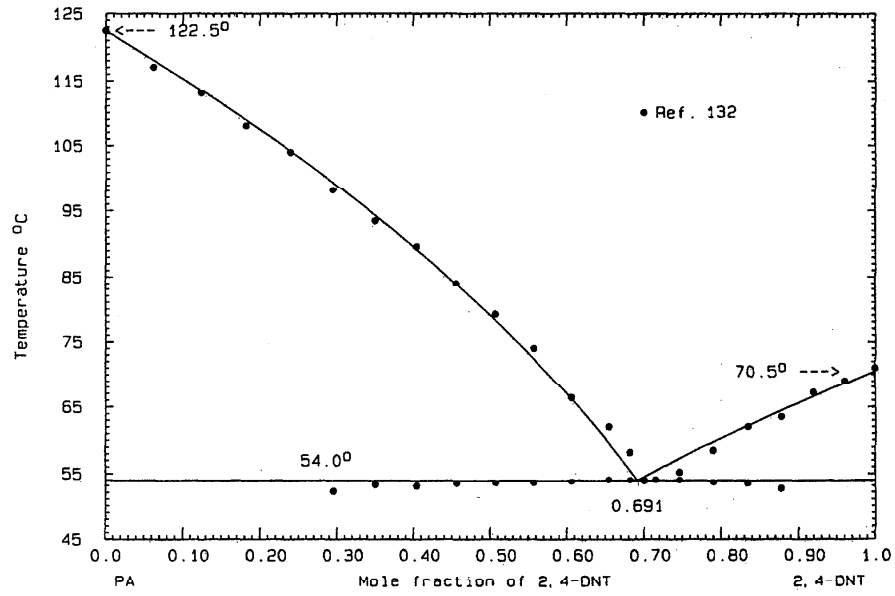

FIG. 217. The system PA (A)+2,4-DNT (B)

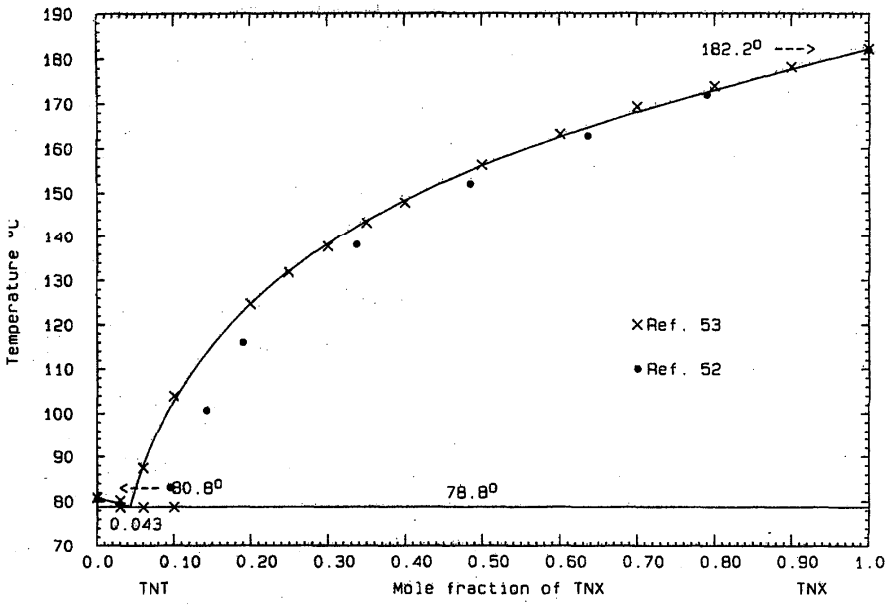

FIG. 218. The system TNT (A)+TNX (B)

$$G^{E}(l)=372x_Ax_B \text{ J mol}^{-1} \quad (411)$$

as seen on the calculated phase diagram, Fig. 215. The calculated eutectic is 57.7 °C, $x_B=0.254$. The probable maximum inaccuracy in the calculated diagram is ±1°.

2,4-DNT (A)+DNA (B)

Liquidus data were obtained by the microthermal method,[41] and the reported eutectic is 68.0 °C, $x_B=0.08$. All liquidus data could be reproduced quite well with the use of

$$G^{E}(l)=x_Ax_B(18-871x_B) \text{ J mol}^{-1} \quad (412)$$

as seen in the calculated phase diagram, Fig. 216. The calculated eutectic is 66.9 °C, $x_B=0.075$. The probable maximum inaccuracy in the calculated diagram is ±1°.

PA (A)+2,4-DNT (B)

Data were obtained by thermal analysis[132] and the reported eutectic is 54.0 °C, $x_B=0.71$. The data appear to be of good quality, and optimization gave the result

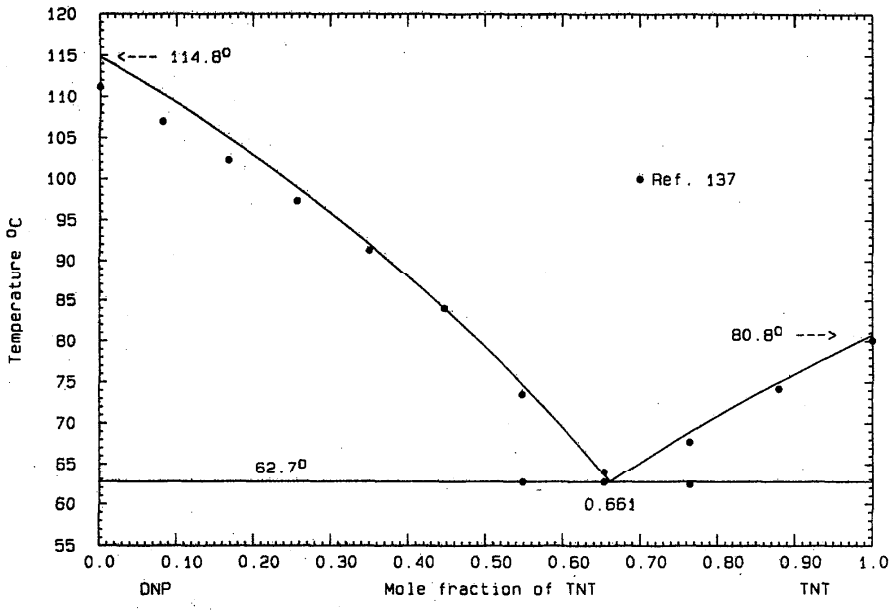

FIG. 219. The system DNP (A)+TNT (B)

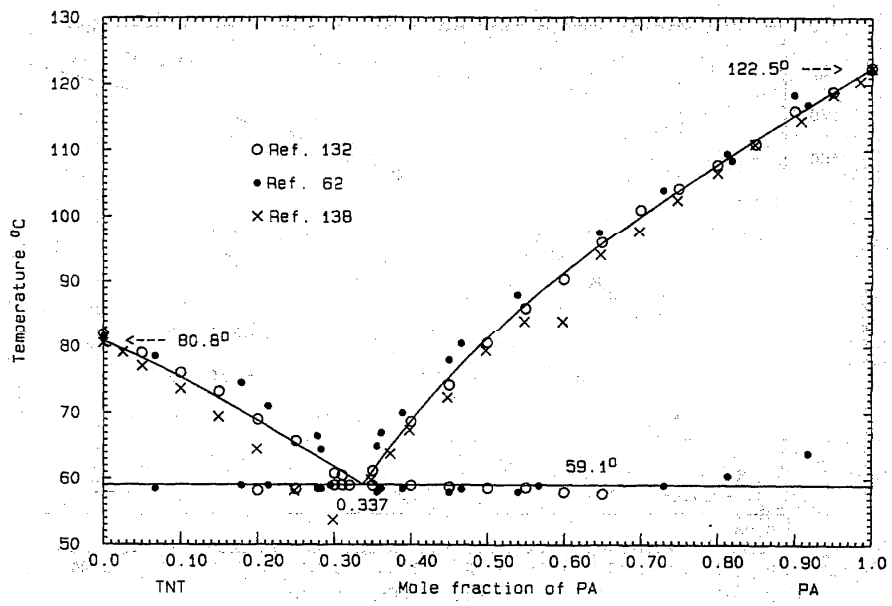

FIG. 220. The system TNT (A)+PA (B)

$$G^E(l) = -35x_A x_B \text{ J mol}^{-1}. \quad (413)$$

The calculated phase diagram, Fig. 217, shows a eutectic 54.0 °C, x_B=0.691. The probable maximum inaccuracy in the calculated diagram is ±1°.

TNT (A)+TNX (B)

Data were obtained by thermal analysis[52,53] and the reported eutectics are not in good agreement: the earlier work[52] states 74.8 °C, x_B=0.08; the later[53] 78.7 °C, x_B=0.046. It is evident by inspection that the two sets of data diverge as they approach the LHS of the diagram. In the later work[53] the liquidus was also located by measurement of optical transmission through the samples; thus the optimization was based on these data[53] only. The result is

$$G^E(l) = x_A x_B(479 + 604x_B) \text{ J mol}^{-1}, \quad (414)$$

and the calculated phase diagram, Fig. 218, shows a calculated eutectic 78.8 °C, x_B=0.043. The probable maximum inaccuracy in the calculated diagram is ±1°.

DNP (A)+TNT (B)

Data were obtained by thermal analysis[137] and no eutectic data were stated. The optimization was performed on data in the range $0.3 < x_B < 1$ and the result

$$G^E(l) = x_A x_B(-744 + 675x_B) \text{ J mol}^{-1} \quad (415)$$

was used to calculate the phase diagram, Fig. 219, in which the eutectic is 62.7 °C, x_B=0.661. The probable maximum inaccuracy in the calculated diagram is ±1°.

TNT (A)+PA (B)

Data were obtained by thermal analysis[132,138] and the thaw–melt method.[62] The eutectic was reported by two investigators[132,138] as 59.0 °C, x_B=0.32 or 53.7 °C, x_B=0.298. The three sets of liquidus data lie on the phase diagram in the following order: high,[62] low,[138] and intermediate,[132] consistently over the whole composition range. The LHS liquidus data of Efremov and co-workers[138] were omitted from the optimization, and the result

$$G^E(l) = x_A x_B(-1542 + 3190x_B - 1606x_B^2) \text{ J mol}^{-1} \quad (416)$$

was used to calculate the phase diagram, Fig. 220. Evidently the data of Hrynakowski and Kapuscinski[132] were the most consistent; the calculated eutectic is 59.1 °C, x_B=0.337. The probable maximum inaccuracy in the calculated diagram is ±2°.

PC (A)+TNT (B)

Data were obtained by thermal analysis[139] and the microthermal method.[140] No eutectic data were stated in either report, although the earlier data,[139] considered by themselves, suggest the presence of a congruently melting 1:1 compound. There is not much that can be deduced about the system from the very scattered data, except for two observations: the experimental limiting liquidus slopes indicate appreciable solid solubility at the RHS but none on the LHS. Since the central part of the diagram is confused, an approximate calculation was attempted, based on liquidus data in the two intervals $0 < x_B < 0.3$ and $0.6 < x_B < 1$. Since the two components are very similar is size and chemical nature, the approximation was made that

$$G^E(l) = 0 \quad (417)$$

and enough solid solubility was used at the RHS to make the RHS liquidus approximate as closely as possible the observed data.[140] The solid solution was represented by a temperature independent Henrian activity coefficient

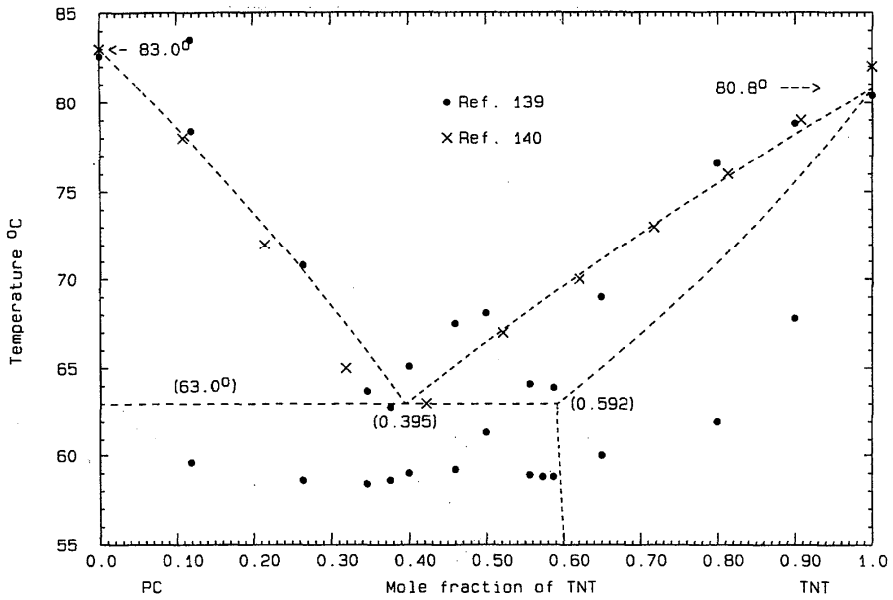

FIG. 221. The system PC (A)+TNT (B)

$$RT \ln \gamma_A = 2500 \text{ J mol}^{-1}. \quad (418)$$

The phase diagram, Fig. 221, was calculated with the use of Eqs. (416) and (417) and shows a calculated eutectic 63.0 °C, $x_B = 0.395$; there is a 40.8 mol % solid solution at the eutectic temperature at the RHS. This phase diagram is suggestive only.

TNA (A)+TNT (B)

Data were obtained by the thaw–melt method[134] and indicate a eutectic temperature ≈42.5 °C. In preliminary calculations it was found that the liquidus data were thermodynamically consistent only with a somewhat higher temperature. The quantity

$$G^E(l) = -500 x_A x_B \text{ J mol}^{-1} \quad (419)$$

defines a calculated liquidus (Fig. 222) that respects the eu-

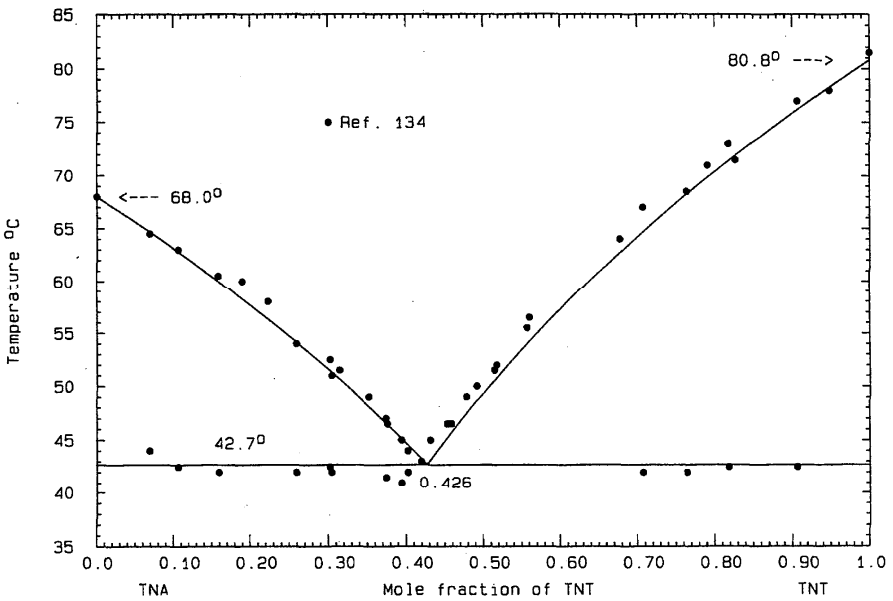

FIG. 222. The system TNA (A)+TNT (B)

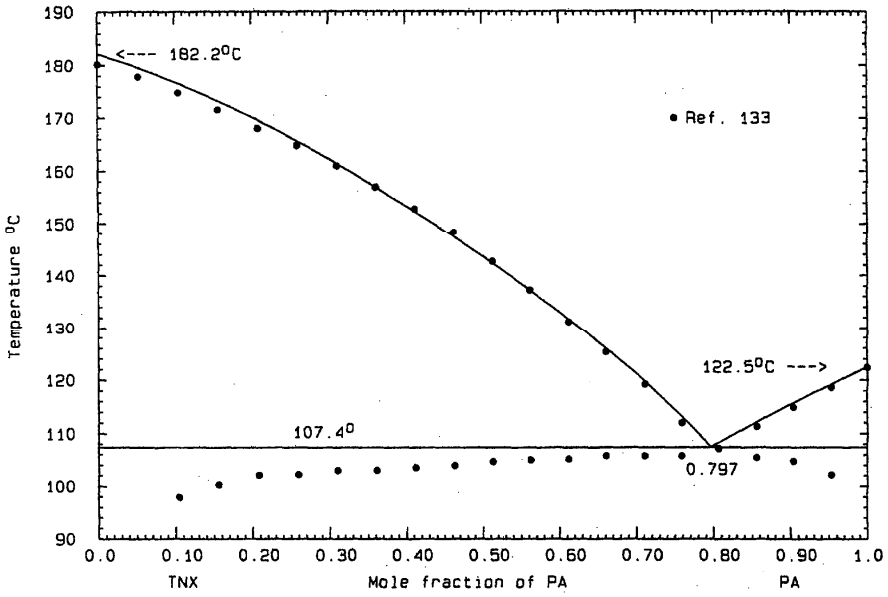

FIG. 223. The system TNX (A)+PA (B)

tectic data more than individual liquidus measurements.[134] The calculated eutectic is 42.7 °C, x_B=0.426. The discrepancy between low eutectic temperature and high liquidus data remains, even if solid solubility is included (this is contraindicated by the limiting liquidus slopes at both sides[134]). The probable maximum inaccuracy in the calculated diagram is ±2°.

TNX (A)+PA (B)

Data were obtained by the thaw–melt method,[133] and the reported eutectic is 105.8 °C, x_B=0.79; another determination[96] was 107.5 °C, x_B=0.86. In preliminary calculations, it was evident that the reported liquidus[133] is not consistent with a eutectic of 105.8 °C, but rather with the higher reported temperature.[96] Data in the range $0.2<x_B<1$ were optimized, with the result

$$G^E(l)=x_A x_B(-3422+2368x_B)\ \text{J mol}^{-1}. \quad (420)$$

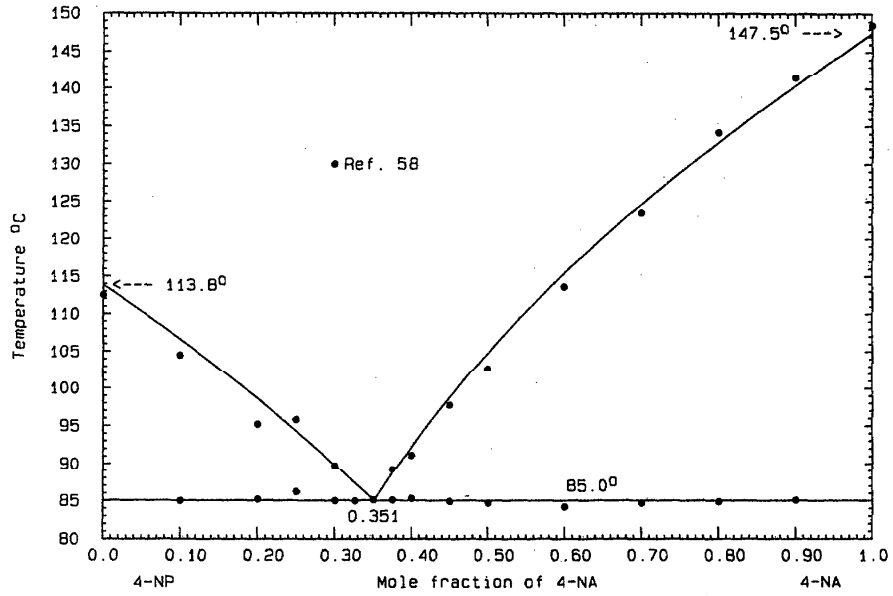

FIG. 224. The system 4-NP (A)+4-NA (B)

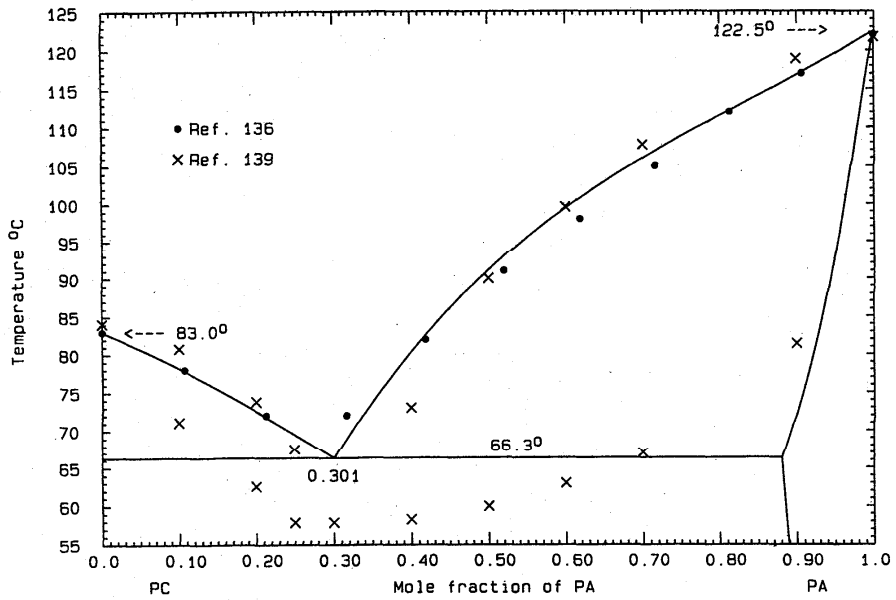

FIG. 225. The system PC (A)+PA (B)

The calculated phase diagram, Fig. 223, shows a calculated eutectic 107.4 °C, x_B=0.797. The probable maximum inaccuracy in the calculated diagram is ±2°.

4-NP (A)+4-NA (B)

Data were obtained by thermal analysis[58] and the stated eutectic is 85.0 °C, x_B=0.326. Data in the range $0.25<x_B<1$ were optimized and the result

$$G^E(l)=x_A x_B(-430+556x_B) \text{ J mol}^{-1} \quad (421)$$

was used to calculate the phase diagram, Fig. 224. The calculated eutectic is 85.0 °C, x_B=0.351. The probable maximum inaccuracy in the calculated diagram is ±1°.

PC (A)+PA (B)

Data were obtained by thermal analysis[139] and the microthermal method.[136] No eutectic data were stated in either report; "extensive solid solubility" was said to be present.[132] The data of Kofler and Brandstätter[132] were taken to be more

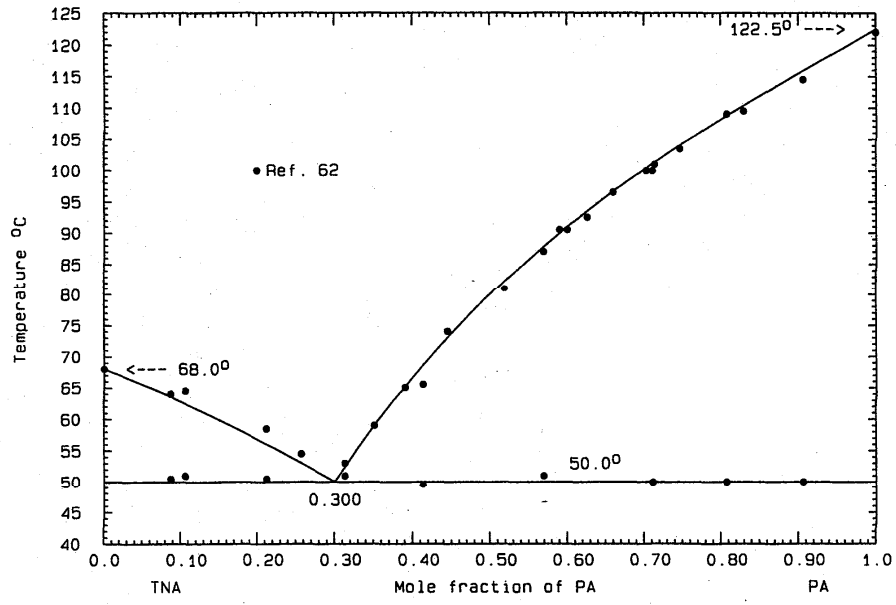

FIG. 226. The system TNA (A)+PA (B)

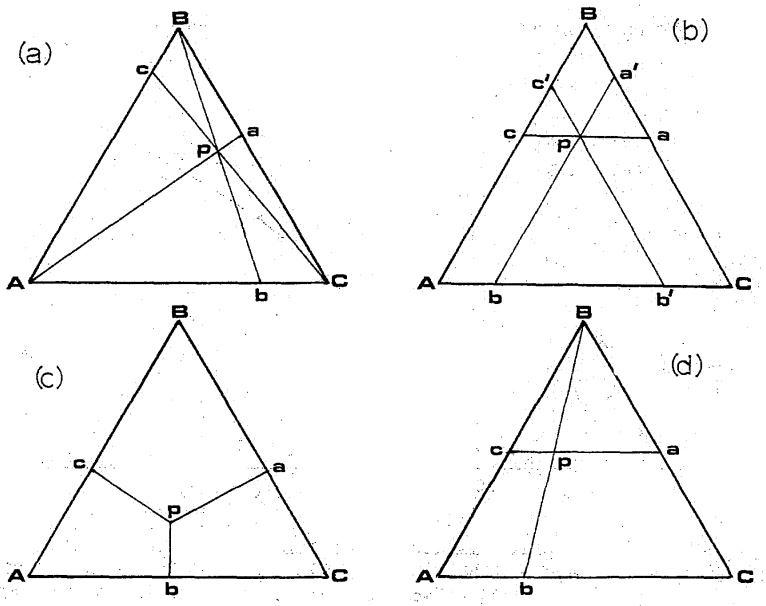

FIG. 227. Models for predicting ternary solution properties from binary properties

reliable, but the experimental limiting liquidus slope at the LHS does not suggest solid solution there; at the RHS a solid solution is consistent with the data.[136,139] In preliminary calculations, it was found that the RHS liquidus could be fitted equally well with or without the assumption of solid solubility; somewhat arbitrarily, it was decided to include it. The calculated phase diagram, Fig. 225, was based on

$$G^{E}(l)=x_A x_B(-751+2586x_B)\ \text{J mol}^{-1}, \quad (422)$$

and for the solid solution, a Henrian activity coefficient, assumed to be temperature independent,

$$RT\ \ln\ \gamma_A=6000\ \text{J mol}^{-1}. \quad (423)$$

The calculated eutectic is 66.3 °C, $x_B=0.301$ and there is 11.9 mol % solid solubility at the eutectic temperature. The probable maximum inaccuracy in the calculated diagram is ±4°.

TNA (A)+PA (B)

Data were obtained by the thaw–melt method.[62] There is no stated eutectic in the report, but from the tabulated data[62] the eutectic temperature is approximately 50 °C. In the optimization, all liquidus data were included, but greater weight was given to the observed eutectic temperature. The phase diagram, Fig. 226, was calculated with the use of

$$G^{E}(l)=x_A x_B(-1085+1249x_B)\ \text{J mol}^{-1} \quad (424)$$

and shows a calculated eutectic 50.0 °C, $x_B=0.300$. The probable maximum inaccuracy in the calculated diagram is ±2°.

3. Evaluation of Ternary Systems

The liquidus surface of a three-component system is investigated experimentally in the same way as a binary system (thermal analysis, thaw–melt method, etc.). One or both of liquidus datum and univariant datum may be obtained for a given composition depending upon the method used. The same strengths and weaknesses of the methods for investigating binary systems, described in Sec. 2.1, apply also to the study of ternary systems.

Following the procedure used in the analysis of binary data (Sec. 2.2), ternary phase diagram data could, in principle, be optimized in the same way. The excess Gibbs energy of the liquid could be fitted to a suitable analytical expression using, for example, mole fractions of the three components. In practice, however, this would require a large number of accurately measured data, together with a knowledge of the identity of the equilibrium solid in each case.

It has proved to be much easier to use thermodynamic models for the ternary system based upon the thermodynamic data for the three constituent binaries.[141] The experimental phase diagrams and thermodynamic data for the three binary subsystems are critically analyzed and mathematical expressions for the Gibbs energies of the binary phases are obtained, as was done in Sec. 2 of the present work. Then interpolation procedures, based on solution models, are used to estimate the Gibbs energies of the ternary phases from the Gibbs energies of the binary phases. Once these quantities for the ternary system have been found, the ternary phase diagram may be calculated by computer in a manner similar to that used for binary systems. An interactive program[17] was used for these calculations and generation of the ternary phase diagram; it has been used successfully for ternary systems composed of alloys, molten salts, or organic compounds.[142–144]

3.1. Models for Estimating Ternary Solution Properties

In the case of relatively simple ternary solutions in which the excess Gibbs energies of the binaries can be well represented by simple polynomial expansions, Eq. (1), certain "geometric" models, based on regular solution theory, proved successful in estimating ternary properties from binaries. Four of these are illustrated in Fig. 227. In each case, G^E of the ternary liquid solution at point "p" is related to the quantities of the binary systems at compositions a,a′,b,b′, etc. These models are discussed by Acree.[145]

In the symmetric Kohler model [Fig. 227(a)], the expression for interpolation is

$$G_p^E = G_c^E(1-X_c)^2 + G_a^E(1-X_a)^2 + G_b^E(1-X_b)^2 \qquad (425)$$

where X (upper case) indicates mole fraction of a component in the ternary solution ($X_A+X_B+X_C=1$). The three binary G^E contributions in Eq. (425) are evaluated at binary mole fractions given by $X_B/(X_A+X_B)$, $X_C/(X_B+X_C)$, and $X_C/(X_A+X_C)$, respectively. The Colinet and Jacob-Fitzner models in Fig. 227 are also symmetrical interpolations, while for the asymmetric Toop model (Fig. 227d)

$$G_p^E = G_c^E X_A/(X_A+X_C) + G_a^E X_c/(X_A+X_C) + G_b^E(1-X_b)^2. \qquad (426)$$

In this case both G_c^E and G_a^E are evaluated at a binary mole fraction identical to X_B and G_b^E at binary mole fraction $X_C/(X_A+X_C)$. In Eq. (426) component B is treated as chemically "different" in some degree than A and C: A and C could be hydrocarbons and B an alcohol, etc. The theoretical adequacy of these models has been discussed at some length;[144–146] in the present work, the excess Gibbs energies of the binary systems are all quite small and the solutions display regular or subregular behaviour for the most part. Under these conditions, all the models yield generally similar results and the Kohler model, Eq. (425), was used for the ternary calculations in the present instance.

3.2. Presentation of Ternary Phase Diagrams

Experimental and calculated ternary phase diagrams are conventionally of the equilateral "composition triangle" type. The diagrams usually display liquidus isothermal contours at regular temperature intervals, together with univariant loci and invariant points for both the ternary system and binary subsystems. In the evaluations of the present work, the reported experimental ternary data are summarized and compared with the calculated values. Experimental and calculated phase diagrams are presented side by side for overall comparison.

When experimental ternary data of sufficient accuracy are available, these can be used to refine the calculations through the addition of a ternary correction term $\varphi X_A X_B X_C$ to the excess Gibbs energy expression in Eq. (425); φ is an adjustable parameter. This term is necessarily zero in any binary subsystem.

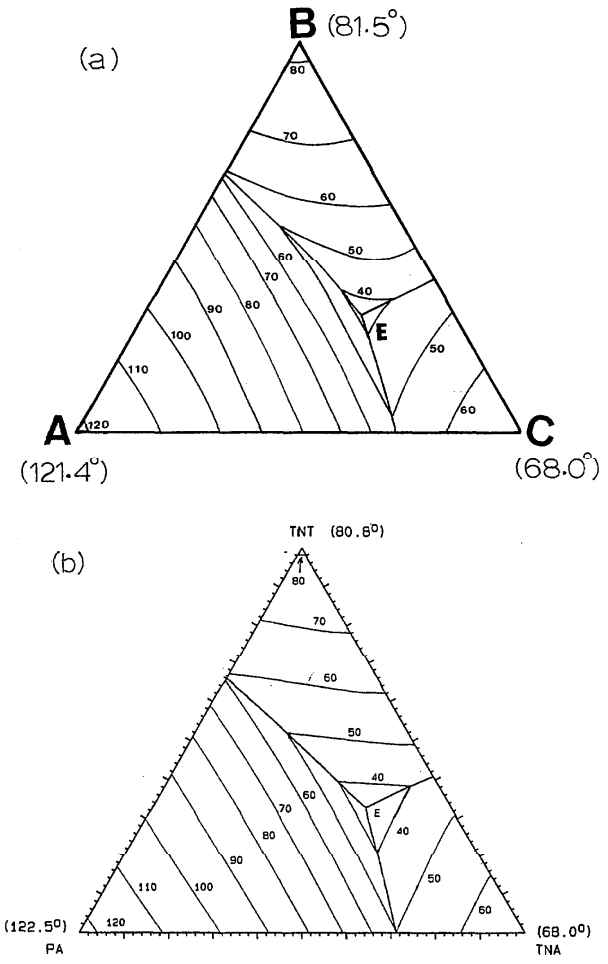

FIG. 228. Experimental and calculated phase diagrams of the system PA (A)+TNT (B)+TNA (C)

Melting points of the pure components and invariant points of the limiting binary systems on the calculated ternary diagrams are taken from Sec. 2 of the present work. In addition, solid bars exist on some of the binary edges of the triangular diagrams. These indicate the extent of solid solubility in the binary subsystems, as determined in Sec. 2.

TABLE 21. Experimental and calculated ternary eutectic data of the system PA (A)+TNT (B)+TNA (C). The ternary interaction term used in the calculation is $\varphi X_A X_B X_C$ J mol^{-1}

	Expt. (Ref. 62)	Calculated	
		$\varphi=0$	$\varphi=8000$
°C	37.0	33.3	36.7
Weight fraction A	0.21	0.19	0.15
Weight fraction B	0.30	0.33	0.33
Weight fraction C	0.49	0.48	0.52

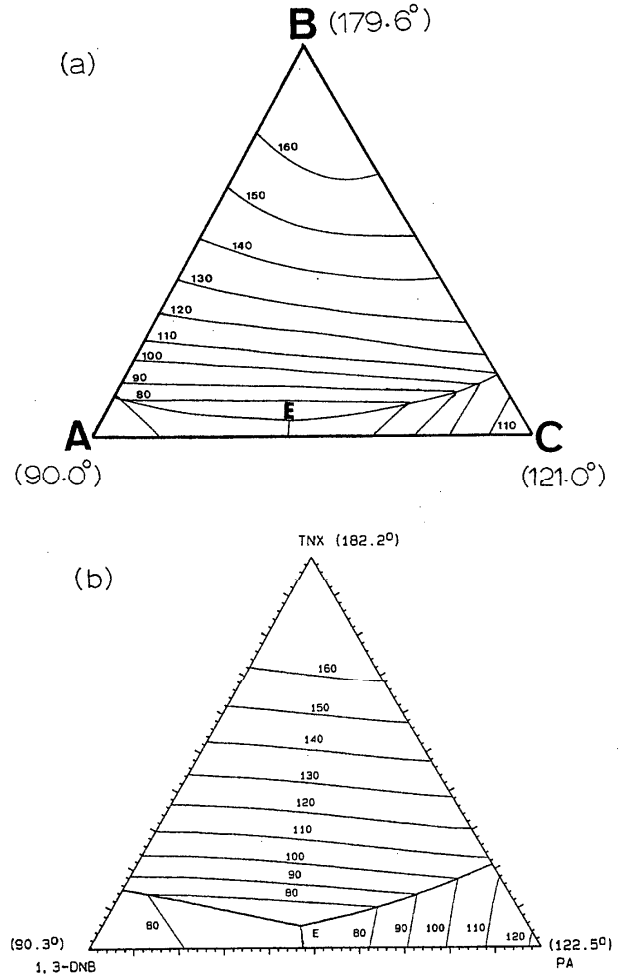

FIG. 229. Experimental and calculated phase diagrams of the system 1,3-DNB (A)+TNX (B)+PA (C)

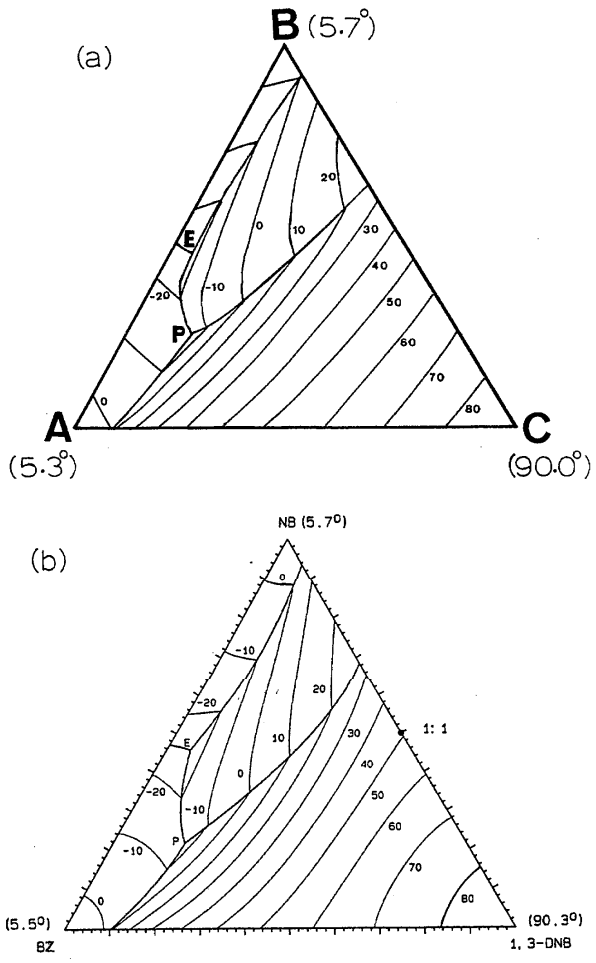

FIG. 230. Experimental and calculated phase diagrams of the system BZ (A)+NB (B)+1,3-DNB (C)

3.3. The Evaluations

3.3.1. PA (A)+TNT (B)+TNA (C)

The liquidus surface was investigated by the thaw–melt method in ten sections through the composition triangle.[62] The system has a simple ternary eutectic. The thermal arrests were tabulated.[62] The experimental melting points of the pure substances are within 1° of accepted values, while the experimental eutectic temperatures of the three limiting binary systems are also within 1° of evaluated data. The ternary phase diagram was calculated from the evaluated data of the three binary systems, using the Kohler method (zero ternary term) and is shown in Fig. 228. Experimental and calculated ternary eutectic data are given in Table 21. The calculated ternary eutectic temperature is about 4° below the experimental datum, although the calculated eutectic composition is close to the experimental. Another calculation was done, in which a ternary term $8000X_AX_BX_C$ J mol^{-1} was used. Thus, the calculated eutectic temperature can be brought more into line with the experimental value, but the calculated eutectic composition deviates (in the wrong direction) from experiment. The calculated isotherms are in general much less curved than experiment indicates. The probable maximum inaccuracy in the calculated diagram is ±3°.

TABLE 22. Experimental and calculated ternary invariant data for the system 1,3-DNB (A)+TNX (B)+PA (C). The ternary interaction term used in the calculation is $\varphi X_AX_BX_C$ J mol^{-1}

	Expt. (Ref. 96)	Calculated	
		$\varphi=0$	$\varphi=-12\,250$
°C	57.0	59.9	57.0
Weight fraction A	0.52	0.50	0.47
Weight fraction B	0.05	0.06	0.10
Weight fraction C	0.43	0.44	0.43

3.3.2. 1,3-DNB (A)+TNX (B)+PA (C)

The liquidus surface was investigated by the visual-polythermal method[96] in nine sections; only a summary of the data was tabulated.[96] The system has a single ternary eutectic. The experimental melting points of the pure com-

TABLE 23. Experimental and calculated invariant ternary data for the system BZ (A)+NB (B)+1,3-DNB (C). The ternary interaction term used in the calculation is $\varphi X_A X_B X_C$ J mol^{-1}

	Expt. (Ref. 97)		Calculated					
			$\varphi=0$		$\varphi=-15\,000$		$\varphi=-22\,000$	
	E	*P*	*E*	*P*	*E*	*P*	*E*	*P*
°C	−31.0	−19.0	−25.8	−10.1	−28.0	−14.9	−30.3	−18.2
Weight fraction A	0.49	0.60	0.52	0.75	0.49	0.62	0.47	0.57
Weight fraction B	0.46	0.25	0.47	0.16	0.45	0.22	0.45	0.25
Weight fraction C	0.05	0.15	0.01	0.09	0.05	0.16	0.08	0.18

ponents are within 2.6° of the accepted values, and the experimental eutectic temperatures of the three limiting binaries are with in 2.5° of evaluated data. The ternary phase diagram, Fig. 229, was calculated from the evaluated thermodynamic properties of the three constituent binaries (Kohler method). The results are given in Table 22. Two calculations were done, one with a zero ternary term and the other with a correction term of $-12250X_AX_BX_C$ J mol^{-1}, the latter of which brought experimental and calculated eutectic temperatures into exact agreement, but with some deviation of calculated compositions. Since the ternary eutectic is very close to the 1,3-DNB+PA binary edge, both calculated and experimental values are sensitive to uncertainties in the data for this binary system. (The observed eutectic temperatures of this binary are[96,132] 62.2 and 59.5 °C, respectively.) Although the experimental isotherms tend to be curved toward the TNX apex, the calculated isotherms are straighter. In the calculated phase diagram shown in Fig. 229 (negative ternary term) the calculated isotherms actually tend to curve away from the TNX apex. The probable maximum inaccuracy in the calculated diagram is ±3 °C.

3.3.3. BZ (A)+NB (B)+1,3-DNB (C)

The liquidus surface was studied by thermal analysis[97] in 25 sections; data were summarized in tabular form.[97] The experimental melting points of the pure substances were within 0.2° and the experimental eutectic and peritectic temperatures of the three limiting binaries are within 2° of evaluated data. The ternary phase diagram was calculated from the evaluated data of the three substituent binaries using the Kohler method. Three different ternary interaction terms were used in the calculations ($\varphi=0$, $-15\,000$ and $-22\,000$ J mol^{-1}). Experimental and calculated phase diagrams are shown in Fig. 230, and the corresponding invariant data are given in Table 23. In this case, it was evident that a negative ternary term was needed to harmonize calculated and experimental diagrams. The calculated diagram shown in Fig. 230 was derived with a ternary term of $-15\,000X_AX_BX_C$ J mol^{-1}. The calculated phase diagram with $\varphi=-22\,000$ J mol^{-1} was rejected because the isotherms became too distorted, compared with experiment.

The 1:1 compound compound formed in the NB+1,3-

TABLE 24. Experimental and calculated ternary eutectic data for the system TNB (A)+PA (B)+TNA (C). The ternary interaction term used in the calculation is $\varphi X_A X_B X_C$ J mol^{-1}

	Expt. (Ref. 62)	Calculated $\varphi=0$
°C	37.5	44.8
Weight fraction A	0.34	0.29
Weight fraction B	0.04	0.08
Weight fraction C	0.62	0.63

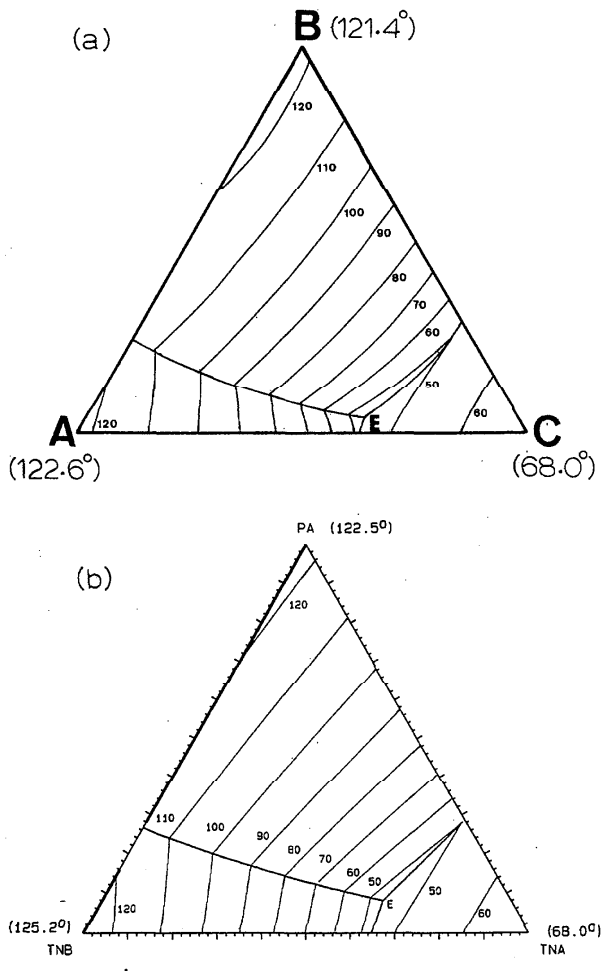

FIG. 231. Experimental and calculated phase diagrams of the system TNB (A)+PA (B)+TNA (C)

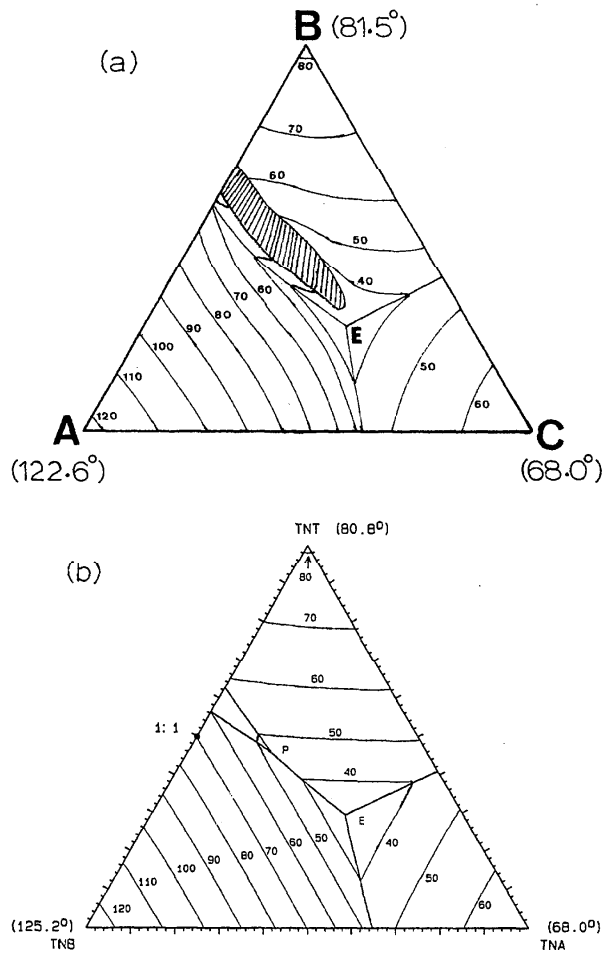

FIG. 232. Experimental and calculated phase diagrams of the system TNB (A)+TNT (B)+PA(C)

DNB binary is evidently quite stable over an appreciable temperature range, and its crystallization field extends practically to the other side of the triangle. Thus the calculated peritectic and eutectic temperatures, being much below 0 °C, will undoubtedly be sensitive to the (extrapolated) Gibbs energy of the 1:1 compound. The probable maximum inaccuracy in the calculated diagram is ±4°.

TABLE 25. Experimental and calculated ternary invariant data for the system TNB (A)+TNT (B)+TNA (C). The ternary interaction term used in the calculation is $\varphi X_A X_B X_C$ J mol^{-1}

	Expt. (Ref. 134)		Calculated φ=0	
	E	*P*	*E*	*P*
°C	30.0	···	30.0	46.3
Weight fraction A	0.28	···	0.27	0.35
Weight fraction B	0.27	···	0.30	0.46
Weight fraction C	0.45	···	0.43	0.19

3.3.4. TNB (A)+PA B+TNA (C)

The liquidus surface was studied by the thaw–melt method[62] in five sections; the data were tabulated. The experimental melting points of the pure components[62] are within 3° of accepted values, and the experimental eutectic temperatures of the three edge binaries are within 1° of evaluated data. The ternary system has a single ternary eutectic and there is extensive solid solubility in the TNB+PA binary. The ternary diagram was calculated from the evaluated data of the three constituent binaries (Kohler method) with zero ternary term. The results are given in Table 24 and Fig. 231.

The calculation does not reproduce at all the low temperature of the eutectic. The experimental isotherms in the TNA corner are widely spaced, suggesting that the ternary eutectic temperature should be higher than 37.5 °C. Also, from the spacing of the isotherms along the LHS univariant line, the eutectic temperature is expected to be *greater*, not less, than 40 °C. Furthermore, the exact nature of the TNB+PA binary system is somewhat conjectural, which may add some uncer-

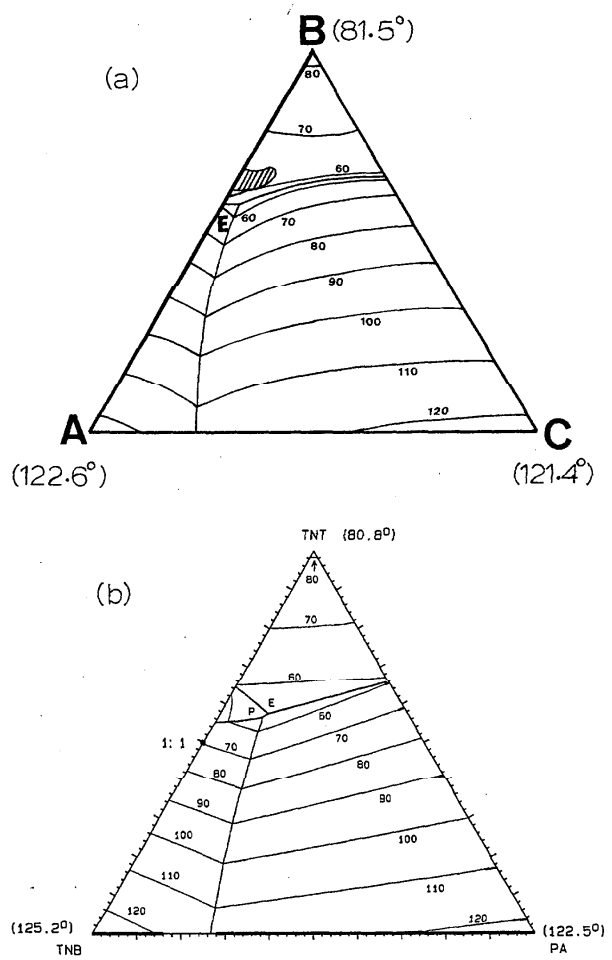

FIG. 233. Experimental and calculated phase diagrams of the system TNB (A)+TNT (B)+PA (C)

TABLE 26. Experimental and calculated ternary invariant data of the system TNB (A)+TNT (B)+PA (C). The ternary interaction term used in the calculation is $\varphi X_A X_B X_C$ J mol^{-1}

	Expt. (Ref. 62)		Calculated $\varphi=0$	
	E	*P*	*E*	*P*
°C	54.0	···	53.7	55.3
Weight fraction A	0.36	···	0.32	0.34
Weight fraction B	0.60	···	0.58	0.56
Weight fraction C	0.04	···	0.10	0.10

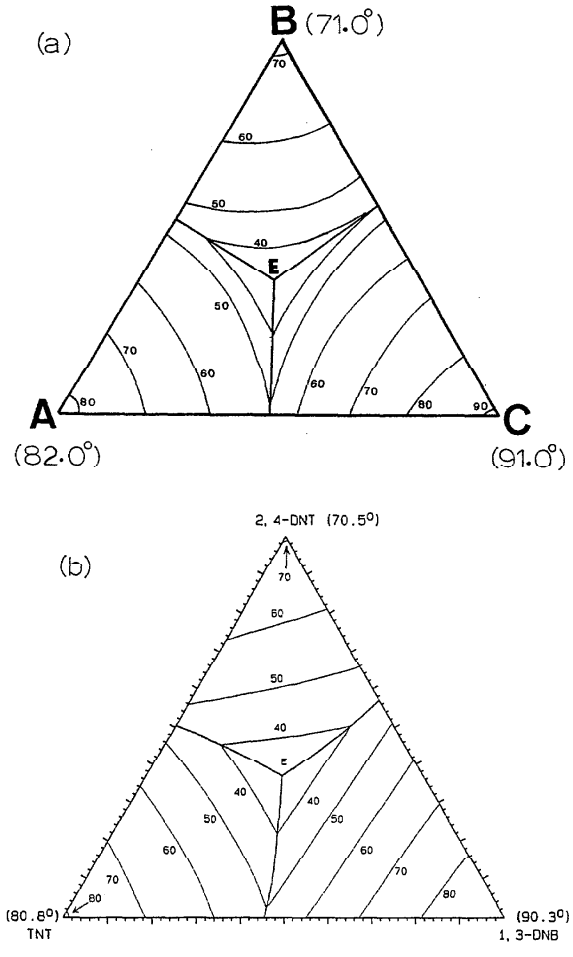

FIG. 234. Experimental and calculated phase diagrams of the system TNT (A)+2,4-DNT (B)+1,3-DNB (C)

tainty to the calculated diagram. In view of these unresolved matters, calculation of the ternary diagram with a very negative ternary correction term is not justified. The probable maximum inaccuracy in the calculated diagram is ±5°.

3.3.5. TNB (A)+TNT (B)+TNA (C)

The liquidus surface was studied by the thaw–melt method[134] in 16 sections; the data were tabulated. The experimental melting points of the pure compounds[134] are within 2.2° of accepted values, and the experimental eutectic temperatures of the three constituent binaries are within 1° of evaluated data. According to the authors,[134] the system has a ternary eutectic and a liquid miscibility gap extending far into the ternary triangle (the miscibility supposedly originating in the TNT+TNB binary system). As was discovered in the evaluation of the TNT+TNB binary, there is in fact no miscibility gap, but rather a 1:1 compound and peritectic. The calculated ternary phase diagram was calculated from the evaluated properties of the three binaries (Kohler method) with a zero ternary correction term. The experimental and calculated phase diagrams are shown in Fig. 232 and the invariant data in Table 25.

The ternary eutectic is well reproduced in the calculated diagram, and there is no miscibility gap but rather a ternary peritectic for reasons stated above. The (at times strong) curvature of the experimental isotherms[134] is not reproduced in the calculated diagram. The probable maximum inaccuracy in the calculated diagram is ±3°.

3.3.6. TNB (A)+TNT (B)+PA (C)

The liquidus surface was investigated by the thaw–melt method[62] in nine sections; the data were tabulated. The experimental melting points of the pure substances[62] were within 3° of accepted values, and the reported eutectic temperatures of the three edge binaries are within 1.2° of evaluated data. As in the previous case, this system is reported[62]—mistakenly—to display a liquid miscibility gap, originating in the TNB+TNT binary. The ternary phase diagram was calculated from the evaluated data of the three constituent binaries (Kohler method) with a zero ternary correction term. The experimental and calculated phase diagrams appear in Fig. 233, and invariant data are given in Table 26.

The experimental ternary eutectic temperature is reproduced well in the calculation, but not so the composition,

TABLE 27. Experimental and calculated ternary eutectic data for the system TNT (A)+2,4-DNT (B)+1,3-DNB (C). The ternary interaction term used in the calculation is $\varphi X_A X_B X_C$ J mol^{-1}

	Expt. (Ref. 132)	Calculated $\varphi=0$
°C	29.0	30.2
Weight fraction A	0.34	0.32
Weight fraction B	0.35	0.37
Weight fraction C	0.31	0.31

TABLE 28. Excess Gibbs energies[a] of the liquid phase of binary systems A+B. $G^E = x_A x_B(g_0 + g_1 x_B + g_2 x_B^2 + g_3 x_B^3)$ J mol^{-1}

A	B	g_0 / g_2	g_1 / g_3
	Systems with nitrobenzene		
BZ	NB	951	0
NA	NB	2	0
AN	NB	639	0
	Systems with 1,2-dinitrobenzene		
BZ	1,2-DNB	3 757	−5 848
		6 355	0
FLN	1,2-DNB	−78	0
ANTH	1,2-DNB	547	0
PH	1,2-DNB	1 028	0
MA	1,2-DNB	−957	0
1-AN	1,2-DNB	−3 025	1 583
2-AN	1,2-DNB	−2 889	1 613
CAR	1,2-DNB	−1 061	0
HB	1,2-DNB	1 262	0
	Systems with 1,3-dinitrobenzene		
BZ	1,3-DNB	959	0
NA	1,3-DNB	−791	1 161
FLN	1,3-DNB	−2 264	696
ANTH	1,3-DNB	1 188	−2 425
PH	1,3-DNB	−1 137	0
PY	1,3-DNB	−5 136	−2 475
FTHN	1,3-DNB	−4 100	2 675
AN	1,3-DNB	−3 608	2 696
1,2-DAB	1,3-DNB	−550	66
1,3-DAB	1,3-DNB	−633	1 427
MA	1,3-DNB	−3 391	965
1-AN	1,3-DNB	−5 510	1 100
2-AN	1,3-DNB	−5 309	1 816
CAR	1,3-DNB	−2 578	−1 508
1-N	1,3-DNB	90	475
HB	1,3-DNB	99	862
	Systems with 1,4-dinitrobenzene		
BZ	1,4-DNB	1 594	0
FLN	1,4-DNB	−3 394	1 875
ANTH	1,4-DNB	−1 487	0
PH	1,4-DNB	−6 683	3 724
PY	1,4-DNB	−2 748	−1 258
MA	1,4-DNB	−5 253	7 761
		−6 242	0
1-AN	1,4-DNB	−5 144	0
2-AN	1,4-DNB	−5 824	1 880
CAR	1,4-DNB	−2 550	−2 103
HB	1,4-DNB	1 434	−3 447
		4 264	0
	Systems with 1,3,5-trinitrobenzene		
BZ	TNB	−1 987	2 849
NA	TNB	−9 000	1 400
ACN	TNB	(−4 400)[b]	(0)
FLN	TNB	−1 989	1 376
ANTH	TNB	−4 379	0
PH	TNB	(−4 400)	(0)
PY	TNB	(−4 400)	(0)
FTHN	TNB	(−4 400)	(0)
AN	TNB	(−5 000)	(0)
DP	TNB	11 688	3 134
2-AN	TNB	(−5 000)	(2 500)
CAR	TNB	(−5 000)	(0)
	Systems with 1,2,3,5-tetranitrobenzene		
ACN	TENB	−7 200	1 400
FLN	TENB	−7 409	−3 268
ANTH	TENB	−12 400	4 400
PH	TENB	−12 400	3 000
PY	TENB	−6 072	0
FTHN	TENB	−13 400	4 650
	Systems with 2-nitrotoluene		
BZ	2-NT	516	318
		−1 410	0
BA	1-NT	534	0
	Systems with 4-nitrotoluene		
BZ	4-NT	938	−783
NA	4-NT	−304	−1 915
		2 401	0
AN	4-NT	638	−558
BA	4-NT	550	0
SA	4-NT	888	0
	Systems with 3,4-dinitrotoluene		
BZ	3,4-DNT	−869	596
ACN	3,4-DNT	263	−1 527
FLN	3,4-DNT	−1 073	−1 795
ANTH	3,4-DNT	−1 037	0
PH	3,4-DNT	−155	−2 031
AN	3,4-DNT	−656	−1 096
MA	3,4-DNT	−2 150	−550
1-AN	3,4-DNT	−8 342	3 804
2-AN	3,4-DNT	−4 824	665
	Systems with 2,6-dinitrotoluene		
BZ	2,6-DNT	1 408	−2 779
ACN	2,6-DNT	−1 590	6 182
		−7 494	0
FLN	2,6-DNT	−2 378	4 049
		−3 798	0
ANTH	2,6-DNT	−3 996	0
PH	2,6-DNT	12	−2 925
MA	2,6-DNT	−3 060	3 216
		−3 476	0
1-AN	2,6-DNT	−6 229	7 737
		−7 374	0
2-AN	2,6-DNT	−4 754	8 345
		−6 775	0
	Systems with 2,4-dinitrotoluene		
BZ	2,4-DNT	855	0
NA	2,4-DNT	−820	0
FLN	2,4-DNT	−2 858	0
ANTH	2,4-DNT	−1 967	0
PH	2,4-DNT	−1 063	−5 280
		4 631	0
PY	2,4-DNT	−3 229	−2 246
FTHN	2,4-DNT	−7 200	2 425
AN	2,4-DNT	−894	−456
MA	2,4-DNT	−2 750	0
1-AN	2,4-DNT	−5 279	3 000
2-AN	2,4-DNT	−5 671	2 399
CAR	2,4-DNT	−3 940	0
BA	2,4-DNT	1 260	788
HB	2,4-DNT	−500	1 943
SA	2,4-DNT	1 059	0
	Systems with 2,4,6-trinitrotoluene		
NA	TNT	−186	0
ACN	TNT	−15 616	0
FLN	TNT	−4 893	0
ANTH	TNT	−3 437	1 253
PH	TNT	−2 800	200
PY	TNT	(−12 000)	(0)
FTHN	TNT	−4 950	1 267
AN	TNT	(−5 000)	(0)

TABLE 28. Excess Gibbs energies[a] of the liquid phase of binary systems A+B. $G^E = x_A x_B(g_0 + g_1 x_B + g_2 x_B^2 + g_3 x_B^3)$ J mol^{-1}—Continued

A	B	g_0	g_1
		g_2	g_3
CAR	TNT	−4 055	−5 000
BA	TNT	2 491	−2 036
HB	TNT	−1 000	8 095
		−5 723	0
SA	TNT	1 640	670
	Systems with 2-nitrophenol		
NA	2-NP	413	0
BP	2-NP	991	0
ANTH	2-NP	842	−793
TPM	2-NP	1 199	586
1-AN	2-NP	−116	0
2-AN	2-NP	−776	1 140
CAR	2-NP	−606	0
DMA	2-NP	−1 800	0
BENZ	2-NP	2 270	2 116
HB	2-NP	−129	3 447
ACP	2-NP	1 110	−1 590
CAM	2-NP	−1 076	−675
		2 540	0
	Systems with 3-nitrophenol		
BP	3-NP	4 950	−1 421
DPM	3-NP	4 601	−338
ANTH	3-NP	2 439	−1 621
MA	3-NP	−6 853	−2 106
1-AN	3-NP	−1 711	0
2-AN	3-NP	−3 784	1 291
CAR	3-NP	−52	2 545
DMA	3-NP	−15 650	−4 400
BENZ	3-NP	−3 993	−8 283
		639	0
ACP	3-NP	−3 435	−1 502
		14 635	0
CAM	3-NP	−9 423	−761
		9 583	0
	Systems with 4-nitrophenol		
NA	4-NP	4 276	−1 077
BP	4-NP	(−5 000)	(0)
DPM	4-NP	6 414	−8 719
		15 348	−9 415
ANTH	4-NP	3 496	0
PH	4-NP	4 905	−1 611
TPM	4-NP	8 348	−10 466
		16 178	−8 381
MA	4-NP	−8 209	0
1-AN	4-NP	−6 010	2 273
2-AN	4-NP	−6 164	9 778
		−7 940	0
CAR	4-NP	618	1 398
DMA	4-NP	−11 711	−17 916
		13 660	0
BENZ	4-NP	−3 471	−1 676
HB	4-NP	−1 536	0
ACP	4-NP	−3 158	−8 586
		7 733	0
CAM	4-NP	−8 369	2 500
	Systems with 2-nitroaniline		
4-HBP	2-NA	3 950	−9 425
		7 430	0
ABA	2-NA	3 440	−3 019
		3 150	0
	Systems with 3-nitroaniline		
HQ	3-NA	2 145	−9 463
		9 200	0
4-HBA	3-NA	2 611	−6 261

TABLE 28. Excess Gibbs energies[a] of the liquid phase of binary systems A+B. $G^E = x_A x_B(g_0 + g_1 x_B + g_2 x_B^2 + g_3 x_B^3)$ J mol^{-1}—Continued

A	B	g_0	g_1
		g_2	g_3
		5 450	0
	Systems with 4-nitroaniline		
HQ	4-NA	325	605
2-HBP	4-NA	504	1 606
4-HBP	4-NA	3 300	−5 752
		4 547	0
	System with 3-nitrobenzoic acid		
PH	NBA	5 176	−4 244
	Systems with 2,4-dinitrophenol		
NA	DNP	−3 536	0
FLN	DNP	−1 468	454
ANTH	DNP	−2 457	1 063
PH	DNP	−1 089	−1 979
PY	DNP	−5 600	−620
FTHN	DNP	−5 000	1 500
1-AN	DNP	−4 439	0
2-AN	DNP	(−5 000)	(0)
CAR	DNP	−2 997	−602
HB	DNP	(−2 000)	(0)
ACP	DNP	−2 732	0
CAM	DNP	−1 163	1 778
BZP	DNP	−634	−2 209
	Systems with picric acid		
BZ	PA	4 456	−5 184
		2 520	0
NA	PA	−4 060	0
ANTH	PA	−5 496	0
PH	PA	−1 175	0
FLN	PA	−3 488	1 644
DPM	PA	2 621	2 311
		−2 144	0
CAR	PA	−7 262	0
P	PA	3 000	−5 500
2-N	PA	−31 327	0
DMA	PA	−4 300	3 600
BENZ	PA	−843	1 573
HB	PA	1 000	0
ACP	PA	−2 802	0
CA	PA	−350	1 000
CAM	PA	−1 638	7 774
		−3 598	0
BZP	PA	−4 035	2 254
	Systems with picryl chloride		
PY	PC	−700	−1 600
FTHN	PC	−7 870	530
	Systems with 2,4,6-trinitroanisole		
PY	TNA	(−6 000)	(0)
FTHN	TNA	−6 700	1 100
	Systems with 2,4,7-trinitrofluoren-9-one		
NA	TNF	−5 000	0
FLN	TNF	−6 000	0
ANTH	TNF	−6 700	2 700
PY	TNF	−5 500	−1 000
CAR	TNF	−5 500	0
ICAR	TNF	−7 000	3 000
DBT	TNF	(−5 000)	(−1 270)
	Systems containing two nitroaromatic compounds		
NB	1,3-DNB	−493	0
NB	TNB	402	0
NB	TNT	−706	611
1,3-DNB	1,4-DNB	−549	0
1,3-DNB	TNB	393	611
2,4-DNT	1,3-DNB	−490	0

TABLE 28. Excess Gibbs energies[a] of the liquid phase of binary systems A+B. $G^E = x_A x_B(g_0 + g_1 x_B + g_2 x_B^2 + g_3 x_B^3)$ J mol^{-1}—Continued

A	B	g_0 g_2	g_1 g_3
1,3-DNB	TNT	−696	1 324
3-NA	1,3-DNB	−1 448	412
1,3-DNB	DNP	1 038	0
1,3-DNB	DNA	451	−1 254
TNX	1,3-DNB	−2 400	0
PA	1,3-DNB	−1 000	1 227
TNT	TNB	−600	−300
3-NA	TNB	−3 576	2 292
4-NA	TNB	−636	0
PA	TNB	(0)	(0)
PC	TNB	1 505	0
TNA	TNB	−609	−705
4-NT	TNX	−223	1 214
TNT	2,4-DNT	715	−2 808
		2 749	0
2,4-DNT	TNX	−1 609	3 042
2,4-DNT	DNP	372	0
2,4-DNT	DNA	18	−871
PA	2,4-DNT	−35	0
TNT	TNX	479	604
DNP	TNT	−744	675
TNT	PA	−1 542	3 190
		−1 606	0
PC	TNT	(0)	(0)
TNA	TNT	−500	0
TNX	PA	−3 422	2 368
4-NP	4-NA	−430	556
PC	PA	−751	2 586
TNA	PA	−1 085	1 249

[a]Where the coefficients of g_2 and g_3 are not given, they are to be assumed to be zero.

[b]Data in parentheses are approximate or were assigned, rather than derived from optimization.

TABLE 29. Henrian activity coefficients of solid solutions of binary systems A+B, $\mu^E(i) = RT \ln \gamma_i$ J mol^{-1} (i=A or B)

A	B	i	$RT \ln \gamma_i$
HB	1,2-DNB	A	5500
BA	4-NT	A	6000
BZ	3,4-DNT	B	4800
NA	4-NP	B	9200
1,3-DNB	DNA	B	6500
PA	TNB	A	1800
		B	500
PC	TNT	A	2500
PC	PA	A	6000

TABLE 30. Gibbs energies of fusion and formation (from the pure component liquids) of intermediate compounds.[a] $\Delta_{fus}G^0 = a + b[T\ (K)]$ J mol^{-1} $\Delta_f G^0 = a' + b'[T\ (K)]$ J mol^{-1}

			Fusion		Formation	
A	B	Stoichiometry	a	b	a′	b′
		Compounds with 1,3-dinitrobenzene				
NA	1,3-DNB	(AB)/2	14 965	−46.1250	−15 018	40.3620
PY	1,3-DNB	(AB)/2	11 148	−30.4700	−12 741	24.7072
		$(AB_2)/3$	26 189	−72.2560	−27 697	66.9640
FTHN	1,3-DNB	(AB)/2	11 644	−33.2510	−12 334	27.4882
AN	1,3-DNB	(AB)/2	18 607	−59.2793	−19 172	53.5181
1-AN	1,3-DNB	(AB)/2	13 322	−29.5359	−14 562	33.7731
2-AN	1,3-DNB	(AB)/2	20 688	−63.3858	−21 789	57.6246
1-N	1,3-DNB	(AB)/2	6 715	−17.9949	−6 634	12.2337
		Compounds with 1,4-dinitrobenzene				
PY	1,4-DNB	(AB)/2	8 156	−20.9873	−9 004	15.2245
1-AN	1,4-DNB	(AB)/2(?)	13 673	−37.4535	14 959	31.6923
2-AN	1,4-DNB	(AB)/2	27 496	−74.6878	28 717	68.9250
		Compounds with 1,3,5-trinitrobenzene				
BZ	TNB	$(A_3B_2)/5(?)$	8 000	−23.0647	−8 203	17.4693
NA	TNB	(AB)/2	25 313	−58.8638	−27 388	53.1010
ACN	TNB	(AB)/2	18 538	−42.5712	−19 638	36.8100
FLN	TNB	$(A_2B_3)/5(?)$	14 680	−38.6990	−14 959	33.1052
ANTH	TNB	(AB)/2	27 537	−62.9177	−28 631	57.1565
PH	TNB	(AB)/2	18 333	−41.9165	−19 433	36.1537
PY	TNB	(AB)/2	(12 325	−23.7628	−13 425	18.0000)
FTHN	TNB	(AB)/2	(8 733	−18.2628	−9 833	12.5000)
AN	TNB	(AB)/2	16 574	−41.3683	−17 824	35.6071
DP	TNB	(AB)/2	32 174	−83.7141	−34 704	77.9529
2-AN	TNB	(AB)/2	13 853	−31.9215	−14 791	26.1603
CAR	TNB	(AB)/2	(20 384	−42.7628	−21 634	37.0000)
		Compounds with 1,2,3,5-tetranitrobenzene				
ACN	TENB	(AB)/2	(13 721	−35.7628	−15 346	30.0000)
FLN	TENB	$(AB_2)/3$	(26 367	−65.2920	−28 498	60.0000)
ANTH	TENB	(AB)/2	21 880	−49.2628	−24 430	43.5000
PH	TENB	$(A_2B_3)/5(?)$	31 951	−80.2459	−34 495	74.6505
PY	TENB	(AB)/2	13 244	−29.9742	−14 762	24.2131
FTHN	TENB	(AB)/2	16 555	−40.6607	−19 324	34.8988
		Compounds with 2,4-dinitrotoluene				
NA	2,4-DNT	(AB)/2	18 378	−55.1213	−18 583	49.3602
PY	2,4-DNT	(AB)/2	14 322	−39.2229	−15 410	33.4617
FTHN	2,4-DNT	(AB)/2	17 082	−48.9948	−18 578	43.2336
1-AN	2,4-DNT	(AB)/2	13 507	−40.2893	−14 608	34.5282
		Compounds with 2,4,6-trinitrotoluene				
NA	TNT	(AB)/2	13 973	−37.7542	−14 019	31.9930
ACN	TNT	(AB)/2	37 761	98.4569	−41 665	92.6957
FLN	TNT	(AB)/2	27 978	−78.1250	−29 201	72.3638
PH	TNT	(AB)/2	16 525	−45.8180	−17 201	40.0568
PY	TNT	(AB)/2	24 922	−56.9458	−27 925	51.1846
FTHN	TNT	(AB)/2	9 145	−22.4609	−10 226	16.6997
AN	TNT	(AB)/2	16 084	−44.9084	−17 335	39.1472
CAR	TNT	(AB)/2	20 288	−48.8929	−22 062	43.1317
		Compound with 2-nitrophenol				
DMA	2-NP	(AB)/2	6 571	−23.7967	−7 022	18.0355
		Compounds with 3-nitrophenol				
ANTH	3-NP	(AB)/2	16 232	−35.3345	−15 825	29.5717
MA	3-NP	(AB)/2	12 925	−41.7099	−14 901	35.9487
1-AN	3-NP	(AB)/2	11 387	−34.5597	−11 815	28.7985
2-AN	3-NP	(AB)/2	(11 768	−35.0000	−12 553	29.2372)
DMA	3-NP	(AB)/2	7 415	−25.7341	−11 879	19.9730
		Compounds with 4-nitrophenol				
BP	4-NP	$(A_4B)/5(?)$	(19 729	−57.6603	−20 529	53.5000)
		(AB)/2	(17 877	−50.7628	−19 127	45.0000)
MA	4-NP	$(AB_2/3$	11 132	−33.4996	−12 956	28.2093
		(AB)/2	(37 653	−125.7628	−39 705	120.0000)
1-AN	4-NP	(AB)/2	15 271	−44.8065	−16 490	39.0453
2-AN	4-NP	(AB)/2	19 637	−55.4244	−20 452	49.6632
DMA	4-NP	(AB)/2	14 438	−48.9089	−18 752	43.1477
BENZ	4-NP	(AB)/2	17 111	−46.0028	−18 188	40.2416

TABLE 30. Gibbs energies of fusion and formation (from the pure component liquids) of intermediate compounds.[a] $\Delta_{fus}G^0 = a + b[T\ (K)]$ J mol^{-1} $\Delta_f G^0 = a' + b'[T\ (K)]$ J mol^{-1}—Continued

			Fusion		Formation	
A	B	Stoichiometry	a	b	a′	b′
		Compound with 3-nitrobenzoic acid				
PH	NBA	$(AB_2)/3$	10 590	−26.2708	−10 069	20.9806
		Compounds with 2,4-dinitrophenol				
NA	DNP	(AB)/2	25 739	−70.4045	−26 623	64.6433
PY	DNP	(AB)/2	13 077	−31.1772	−14 555	25.4144
FTHN	DNP	(AB)/2	7 836	−21.4610	−8 899	15.6982
1-AN	DNP	(AB)/2	17 999	−47.6546	−19 109	41.8934
2-AN	DNP	(AB)/2	(17 310	−50.0000	−18 560	44.2372)
HB	DNP	(AB)/2	(21 500	−60.7628	−22 000	55.0000)
		Compounds with picric acid				
NA	PA	(AB)/2	20 183	−47.3982	−21 198	41.6370
ANTH	PA	(AB)/2	30 443	−73.7001	−31 817	67.9389
PH	PA	(AB)/2	5 920	−14.1569	−6 214	8.3941
FLN	PA	(AB)/2	8 108	−22.6576	−8 774	16.8964
CAR	PA	(AB)/2	23 071	−50.6349	−24 886	44.8737
P	PA	(AB)/2	6 405	−17.8844	−6 344	12.1233
2-N	PA	(AB)/2	(61 542	−143.1381	−69 373	137.3769)
DMA	PA	(AB)/2	7 133	−21.4113	−8 659	15.6501)
BENZ	PA	(AB)/2	19 961	−52.0974	−19 976	46.3363
HB	PA	(AB)/2	(27 188	−74.7628	−26 938	69.0000)
ACP	PA	(AB)/2	17 304	−53.1737	−18 004	47.4125
CA	PA	(AB)/2	28 560	−74.7350	−28 523	68.9722
		Compounds with picrylchloride				
PY	PC	(AB)/2	6 088	−14.2529	−6 463	8.4901
FTHN	PC	(AB)/2	8 350	−21.2547	−10 251	15.4919
		Compounds with 2,4,6-trinitroanisole				
PY	TNA	(AB)/2	15 790	−41.8116	−17 290	36.0504
FTHN	TNA	(AB)/2	19 509	−56.0357	−21 048	50.2745
		Compounds with 2,4,7-trinitrofluoren-9-one				
NA	TNF	(AB)/2	20 329	−47.8607	−21 655	42.0995
FLN	TNF	(AB)/2	23 750	−52.6099	−25 252	46.8487
ANTH	TNF	(AB)/2	19 643	−42.0616	−20 981	36.3004
PY	TNF	(AB)/2	19 683	−38.4604	−21 365	32.6992
		$(AB_2)/3$	31 889	−67.5906	−33 310	62.3003
CAR	TNF	(AB)/2	12 844	−26.4861	−14 220	20.7249
		$(AB_2)/3$	15 064	−33.2671	−16 258	27.9768
ICAR	TNF	(AB)/2	24 686	−55.1131	−26 062	49.3519
DBT	TNF	(AB)/2	30 938	−64.9877	−32 349	59.2265
		Compounds containing two nitroaromatic compounds				
NB	1,3-DNB	(AB)/2	19 381	−64.2152	−19 504	58.4540
NB	TNB	$(A_2B)/3$	8 017	−23.7562	−7 927	18.4676
TNT	TNB	(AB)/2	(16 998	−50.7628	−17 186	45.0000)
3-NA	TNB	(AB)/2	20 516	−55.4609	−21 124	49.6997

[a]Data between parentheses are approximate or assigned values, not obtained by optimization. A question mark (?) after an indicated stoichiometry means that the information is tentative and needs confirmation.

perhaps because of the nearness of the ternary invariant points to the misinterpreted TNT+TNB binary system. The calculated isotherms intersecting the lower univariant locus are much less curved than experiment indicates. The probable maximum inaccuracy in the calculated diagram is ±3°.

3.3.7. TNT (A)+2,4-DNT (B)+1,3-DNB (C)

The liquidus surface was studied by thermal analysis.[132] No detailed data were tabulated in the article, and the number of sections examined was not stated.[132] The system has a ternary eutectic. The experimental melting points of the pure substances[132] are within 1.5° of accepted values and the experimental eutectic temperatures of the three limiting binaries agree with evaluated data. The ternary phase diagram was calculated from the evaluated properties of the three binaries (Kohler method) with zero ternary correction term. The experimental and calculated phase diagrams appear in Fig. 234, and eutectic data in Table 27. The probable maximum inaccuracy in the calculated diagram is ±1°.

4. Acknowledgments

Thanks are due to Professor C. W. Bale and Professor A. D. Pelton, Center for Research in Computational Thermochemistry, Ecole Polytechnique, for use of computing facilities.

5. Appendix

The data presented here summarize thermodynamic information derived from the evaluation of the 226 binary systems in Sec. 2. They are placed in the Appendix rather than in the body of the text simply for reasons of convenience. The data in Tables 1, 28, 29, and 30 enable any of the 226 phase diagrams to be reproduced, with the use of appropriate algorithm or software. The data in Tables 28–30 are thus given without further comment: analysis or interpretation of these data in further depth is not among the purposes of the present article.

6. References

[1] R. P. Rastogi, Pure Appl. Chem. **66**, 441 (1994).
[2] J. Sangster, J. Phys. Chem. Ref. Data **23**, 295 (1994).
[3] V. E. Kampar, Russ. Chem. Rev. **51**, 107 (1982).
[4] R. Foster, *Organic Charge Transfer Complexes* (Academic, New York, 1969).
[5] N. B. Singh and K. D. Dwivedi, J. Sci. Ind. Res. **41**, 98 (1982).
[6] D. E. Laskowski, D. G. Grabar, and W. C. McCrone, Ind. Eng. Chem. **25**, 1400 (1953).
[7] M. Orchin and E. O. Woolfolk, J. Am. Chem. Soc. **68**, 1729 (1946).
[8] F. Casellato, C. Vecchi, A. Girelli, and P. G. Farrell, Thermochimica Acta **13**, 37 (1975).
[9] J. R. Goates, J. B. Ott, and A. H. Budge, J. Phys. Chem. **65**, 2162 (1961).
[10] Z. Bugajewski and A. Bylicki, J. Chem. Thermodyn. **20**, 1191 (1988).
[11] A. Stock, Ber. Deutsch. Chem. Gesell. **42**, 2059 (1909).
[12] R. P. Rastogi and P. S. Bassi, J. Phys. Chem. **68**, 2398 (1964).
[13] H. Rheinboldt, J. Prakt. Chem. (Neue Folge) **111**, 242 (1925).
[14] F. E. Pounder and I. Masson, J. Chem. Soc. **1934**, 1357.
[15] R. P. Rastogi and K. T. R. Varma, J. Chem. Soc. **1956**, 2097.
[16] L. Kofler and A. Kofler, Angew. Chem. **53**, 434 (1940).
[17] W. T. Thompson, C. W. Bale, and A. D. Pelton, F*A*C*T (Facility for the Analysis of Chemical Thermodynamics), Programs FITBIN, POTCOMP, and TERNFIG (Ecole Polytechnique/McGill University, Montreal, Canada, 1985).
[18] J. Sangster and A. D. Pelton, J. Phys. Chem. Ref. Data **16**, 509 (1987).
[19] J. Sangster, P. K. Talley, C. W. Bale, and A. D. Pelton, Can. J. Chem. Eng. **66**, 881 (1988).
[20] J. Buckingham, ed., *Dictionary of Organic Compounds*, 5th ed. (Chapman and Hall, New York, 1982).
[21] E. S. Domalski, W. H. Evans, and E. D. Hearing, J. Phys. Chem. Ref. Data **13** (Suppl. No. 1), 1 (1984).
[22] R. C. Weast and J. G. Grasselli, eds., *Handbook of Data on Organic Compounds*, 2nd ed. (CRC, Boca Raton, 1989).
[23] E. S. Domalski and E. D. Hearing, J. Phys. Chem. Ref. Data **19**, 881 (1990).
[24] J. R. Donnelly, L. A. Drewes, R. L. Johnson, W. D. Munslow, K. K. Knapp, and G. W. Sovocol, Thermochimica Acta **167**, 155 (1990).
[25] W. E. Acree, Thermochimica Acta **189**, 37 (1991).
[26] W. E. Acree, in *Handbook of Chemistry and Physics*, 73rd ed., edited by D. R. Lide (CRC, Boca Raton, 1992).
[27] M. W. Babich, S. W. Hwang, and R. D. Mounts, Thermochimica Acta **210**, 77 (1992).
[28] W. E. Acree, Thermochimica Acta **219**, 97 (1993).
[29] M. W. Babich, S. Hwang, and R. D. Mounts, Thermochimica Acta **226**, 163 (1993).
[30] M. W. Babich, R. Benrashid, and R. D. Mounts, Thermochimica Acta **243**, 193 (1994).
[31] A. Das, M. Frenkel, N. A. M. Gadalla, S. Kudchadker, K. N. Marsh, A. S. Rodgers, and R. C. Wilhoit, J. Phys. Chem. Ref. Data **22**, 659 (1993).
[32] U. S. Rai, K. D. Mandal, and N. P. Singh, J. Therm. Anal. **35**, 1687 (1989).
[33] B. M. Shukla, N. P. Singh, and N. B. Singh, Mol. Cryst. Liq. Cryst. **104**, 265 (1984).
[34] A. Krajewska and K. Pigon, Thermochimica Acta **41**, 187 (1980).
[35] M. Radomska and R. Radomski, Thermochimica Acta **40**, 405 (1980).
[36] F. Casellato, C. Vecchi, A. Girelli, and B. Casu, Thermochimica Acta **6**, 361 (1973).
[37] B. L. Sharma, N. K. Sharma, and M. Rambal, Thermochimica Acta **206**, 71 (1992).
[38] P. M. Robinson and H. G. Scott, Mol. Cryst. Liq. Cryst. **5**, 387 (1969).
[39] U. S. Rai and H. Shekhar, Mol. Cryst. Liq. Cryst. **220**, 217 (1992).
[40] D. L. Hammick, L. W. Andrew, and J. Hampson, J. Chem. Soc. **1932**, 171.
[41] M. Brandstätter, Monatsh. Chem. **77**, 7 (1947).
[42] R. P. Rastogi and K. T. R. Varma, J. Phys. Chem. **62**, 641 (1958).
[43] C. Shinomiya, Bull. Chem. Soc. Jpn. **15**, 259 (1940).
[44] R. Kremann, Monatsh. Chem. **29**, 863 (1908).
[45] M. Radomska, R. Radomski, and R. Klos, J. Chem. Soc., Perkin Trans. **2** (11), 1563 (1987).
[46] D. R. Lide, Editor, *Handbook of Chemistry and Physics*, 73rd ed. (CRC, Boca Raton, 1992).
[47] H. D. Crockford and A. E. Hughes, J. Phys. Chem. **34**, 2117 (1930).
[48] H. D. Crockford and N. L. Simmons, J. Phys. Chem. **37**, 259 (1933).
[49] R. Kremann, E. Hönigsberg, and O. Mauermann, Monatsh. Chem. **44**, 65 (1923).
[50] S. Zeman, J. Therm. Anal. **17**, 19 (1979).
[51] R. B. Cundall, T. F. Palmer, and C. E. C. Wood, J. Chem. Soc. Faraday Trans. I **78**, 1339 (1978).
[52] J. M. Bell and J. P. Sawyer, J. Ind. Eng. Chem. **11**, 1025 (1919).
[53] L. A. Burkardt, J. Phys. Chem. **61**, 502 (1957).
[54] R. Sabbah and M. Gouali, Aust. J. Chem. **47**, 1651 (1994).
[55] N. G. Buckman, J. O. Hill, and R. J. Magee, J. Therm. Anal. **37**, 95 (1991).
[56] K. Sekiguchi, Y. Ueda, and Y. Nakamori, Chem. Pharm. Bull. **11**, 1108 (1963).
[57] J. J. Sudborough and S. H. Beard, J. Chem. Soc. **97**, 773 (1910).
[58] R. Palepu and L. Moore, Thermochimica Acta **30**, 384 (1979).
[59] U. S. Rai and K. D. Mandal, Bull. Chem. Soc. Jpn. **63**, 1496 (1990).
[60] N. B. Singh and P. Kumar, J. Chem. Eng. Data **34**, 145 (1989).
[61] S. Zeman, J. Therm. Anal. **19**, 99 (1980).
[62] T. Asahina and C. Shinomiya, J. Chem. Soc. Jpn. **58**, 119 (1937).
[63] A. Krajewska-Cizio, Thermochimica Acta **158**, 317 (1990).
[64] P. Bret-Dibat and A. Lichanot, Thermochimica Acta **147**, 261 (1989).
[65] R. P. Rastogi, N. B. Singh, and K. D. Dwivedi, Ber. Bunsenges. Phys. Chem. **85**, 85 (1981).
[66] M. S. Dhillon, Z. Naturforsch. A **32**, 98 (1977).
[67] L. M. Meva'a and A. Lichanot, Thermochimica Acta **158**, 335 (1990).
[68] S. Budavari, Editor, *The Merck Index*, 11th ed. (Merck, Rahway, NJ, 1989).
[69] C. R. Smith, J. Am. Chem. Soc. **46**, 414 (1924).
[70] A. Kofler, Z. Elektrochem. **50**, 200 (1944).
[71] M. S. Dhillon and G. S. Dhillon, Thermochimica Acta **19**, 69 (1977).
[72] R. Palepu and L. Moore, Thermochimica Acta **37**, 109 (1980).
[73] N. G. Buckman, J. O. Hill, and R. J. Magee, J. Therm. Anal. **37**, 95 (1991).
[74] U. S. Rai and K. D. Mandal, Mol. Cryst. Liq. Cryst. B **182**, 387 (1990).
[75] M. S. Dhillon and S. P. Singh, Thermochimica Acta **15**, 248 (1976).
[76] Kh. I. Geidarov, K. A. Karasharli, and O. I. Dzafarov, Azerb. Khim. Zh. (5), 112 (1977).
[77] V. F. Chesnokov and I. M. Bokhovkin, J. Gen. Chem. USSR (Engl. Transl.) **39**, 1161 (1969).
[78] J. A. Harris, A. V. Bailey, and E. L. Skau, J. Am. Oil Chem. Soc. **45**, 183 (1968).
[79] G. P. Bettinetti, C. Caramella, F. Giordano, A. LaManna, C. Margheritis, and C. Sinistri, J. Therm. Anal. **28**, 285 (1983).
[80] U. S. Rai and K. D. Mandal, Can. J. Chem. **67**, 239 (1989).
[81] M. S. Dhillon and G. S. Dhillon, J. Chem. Thermodyn. **9**, 400 (1977).

[82] J. Kendall, J. Am. Chem. Soc. **36**, 1222 (1914).
[83] H. D. Crockford and F. W. Zurburg, J. Phys. Chem. **34**, 214 (1930).
[84] M. M. Mayer, W. J. Howell, D. L. Tomasko, and C. A. Eckert, J. Chem. Eng. Data **35**, 446 (1990).
[85] R. Sabbah and T. H. D. Le, Can. J. Chem. **71**, 1378 (1993).
[86] H.-M. Lin and R. A. Nash, J. Pharm. Sci. **82**, 1018 (1993).
[87] R. Kremann, F. Odelga, and O. Zawodsky, Monatsh. Chem. **42**, 117 (1921).
[88] R. Kremann and F. Odelga, Monatsh. Chem. **42**, 147 (1921).
[89] E. B. McCall, A. J. Neale, and T. J. Rawlings, J. Chem. Soc. 4900 (1962).
[90] H. H. Lee and J. C. Warner, J. Am. Chem. Soc. **55**, 209 (1933).
[91] K. G. Joback and R. C. Reid, Chem. Eng. Commun. **57**, 233 (1987).
[92] Z. Tingli, Proc. 17th Int. Pyrotech. Semin. **1**, 531 (1991).
[93] P. Simamora, A. H. Miller, and S. H. Yalkowsky, J. Chem. Inf. Comput. Sci. **33**, 437 (1993).
[94] P. Simamora and S. H. Yalkowsky (unpublished).
[95] V. F. Chesnokov and I. M. Bokhovkin, J. Gen. Chem. USSR (Engl. Transl.) **39**, 915 (1969).
[96] O. F. Bogush, Izv. Akad. Nauk SSSR (5), 940 (1966).
[97] G. B. Ravich and O. F. Bogush, J. Gen. Chem. USSR (Engl. Transl.) **31**, 656 (1961).
[98] R. Kremann, Monatsh. Chem. **25**, 1271 (1904).
[99] R. Kremann, Monatsh. Chem. **32**, 609 (1911).
[100] R. Kremann and R. Müller, Monatsh. Chem. **42**, 181 (1921).
[101] R. Kremann and B. Petritschek, Monatsh. Chem. **38**, 385 (1917).
[102] R. Kremann and G. Grasser, Monatsh. Chem. **37**, 723 (1916).
[103] R. Kremann and H. Strzelba, Monatsh. Chem. **42**, 167 (1921).
[104] R. Kremann and K. Pogantsch, Monatsh. Chem. **44**, 163 (1923).
[105] K. Sekiguchi, E. Suzuki, Y. Tsuda, K.-I. Shirotani, and K. Okamoto, Chem. Pharm. Bull. **32**, 658 (1984).
[106] N. A. Puschin, Z. Phys. Chem. **124**, 16 (1926).
[107] N. A. Puschin and I. I. Rikovski, Z. Phys. Chem. A **151**, 257 (1930).
[108] M. Radomska and R. Radomski, Thermochimica Acta **40**, 415 (1980).
[109] J. J. Sudborough, Trans. Chem. Soc. **109**, 1339 (1916).
[110] E. Hertl and G. H. Römer, Z. Phys. Chem. B **11**, 77 (1931).
[111] H. Rheinboldt and M. Kirscheisen, J. Prakt. Chem. (Neue Folge) **113**, 348 (1926).
[112] J. J. Sudborough, Trans. Chem. Soc. **79**, 522 (1901).
[113] R. Ciusa and L. Vecchiotti, Gazz. Chim. Ital. **43**(II), 91 (1913).
[114] H. D. Crockford and E. C. Powell, J. Elisha Mitchell Sci. Soc. **51**, 143 (1935).
[115] A. Saposchnikow, Z. Phys. Chem. Stöch. Verwandt. **49**, 688 (1904).
[116] K. T. R. Varma, M. K. Kumaran, P. Narayanan, and T. S. Seetharaman, J. Chem. Thermodyn. **12**, 615 (1980).
[117] R. Kremann and F. Slovak, Monatsh. Chem. **41**, 23 (1920).
[118] L. V. Gusakov, V. F. Chesnokov, I. M. Bokhovkin, N. N. Ermolina, and G. P. Ivanko, Zh. Obshch. Khim. **48**, 1225 (1978).
[119] R. Kremann and H. Marktl, Monatsh. Chem. **41**, 43 (1920).
[120] R. Kremann and J. Fritsch, Monatsh. Chem. **41**, 631 (1920).
[121] R. Kremann and F. Hofmeier, Monatsh. Chem. **31**, 201 (1910).
[122] B. Kuriloff, Z. Phys. Chem. Stöch. Verwandt. **23**, 673 (1897).
[123] R. Kremann, Monatsh. Chem. **25**, 1215 (1904).
[124] E. Rudolfi, Z. Phys. Chem. Stöch. Verwandt. **66**, 705 (1909).
[125] N. P. Singh and B. M. Shukla, Cryst. Res. Technol. **20**, 345 (1985).
[126] N. P. Singh, N. Singh, and N. B. Singh, J. Chem. Eng. Data **30**, 49 (1985).
[127] J. C. Philip, J. Chem. Soc. **83**, 814 (1903).
[128] T. Asahina and K. Yokoyama, J. Chem. Soc. Jpn. **56**, 415 (1935).
[129] C. Marchetti, Gazz. Chim. Ital. **12**, 502 (1882).
[130] K. Lehmstedt, Ber. Deutsch. Chem. Gesell. B **56**, 1218 (1932).
[131] D. L. Hammick and T. K. Hanson, J. Chem. Soc. **1933**, 669.
[132] K. Hrynakowski and Z. Kapuscinski, Rocz. Chem. **14**, 115 (1934).
[133] N. N. Efremov and A. M. Tikhomirova, Izv. Inst. Fiz.-Khim. Anal. Akad. Nauk SSSR **4**, 65 (1928).
[134] C. Shinomiya and T. Asahina, J. Chem. Soc. Jpn. **57**, 732 (1936).
[135] L. A. Burkardt, J. Phys. Chem. **66**, 1196 (1962).
[136] A. Kofler and M. Brandstätter, Monatsh. Chem. **78**, 65 (1948).
[137] A. N. Campbell and E. J. Pritchard, Can. J. Res. B **25**, 183 (1947).
[138] N. N. Efremov, O. K. Khaishbashev, and A. A. Frolova, Izv. Sekt. Fiz.-Khim. Anal., Inst. Obshch. Neorg. Khim. **17**, 149 (1949).
[139] H. G. Grimm, M. Günther, and H. Tittus, Z. Phys. Chem. B **14**, 169 (1931).
[140] A. Kofler and M. Brandstätter, Z. Phys. Chem. **192**, 60 (1943).
[141] A. D. Pelton, in *Physical Metallurgy*, 3rd ed., edited by R. W. Cahn and P. Haasen (North-Holland Elsevier, Amsterdam, 1983), Chap. 7.
[142] A. D. Pelton, C. W. Bale, and P. L. Lin, Can. J. Chem. **62**, 457 (1984).
[143] P. L. Lin, A. D. Pelton, and C. W. Bale, CALPHAD J. **4**, 47 (1980).
[144] J. Sangster and A. D. Pelton, J. Phase Equil. **12**, 511 (1991).
[145] W. E. Acree, in *Thermodynamic Properties of Nonelectrolyte Solutions* (Academic, New York, 1984), Chap. 4.
[146] M. Hillert, CALPHAD J. **4**, 1 (1980).